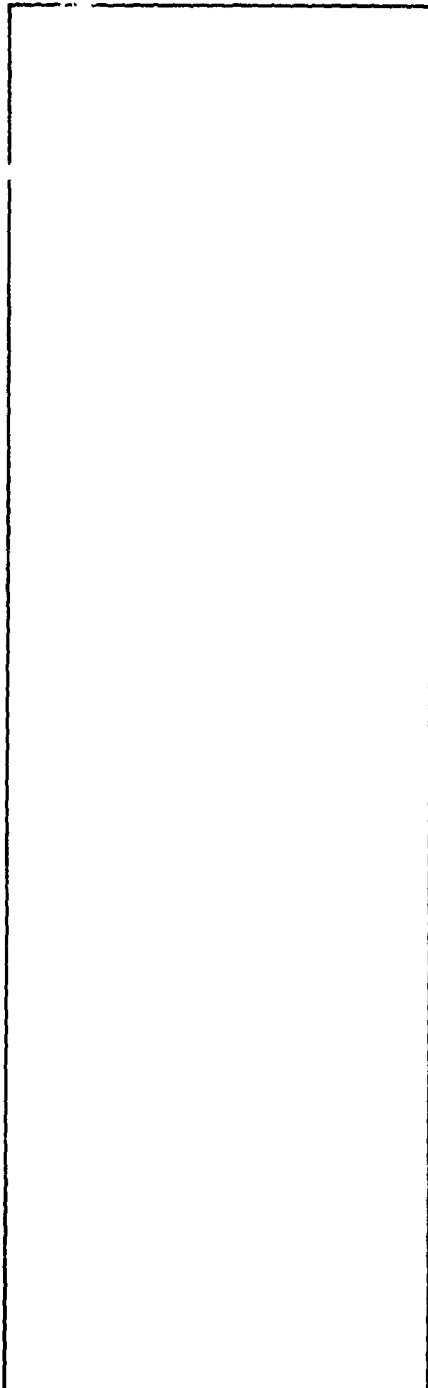


(NASA-CR-144069) DESIGN, DEVELOPMENT AND  
MANUFACTURE OF A FREIBOARD RADIC FREQUENCY  
MASS GAUGING SYSTEM Final Report (Bendix  
Corp.) 263 p HC \$9.00

CSCI 17E

N76-12232

Unclass  
G3/32 G4123



Instruments &  
Life Support  
Division



**The  
Bendix  
Corporation**

**Instruments & Life  
Support Division  
Davenport, IA 52808**

**Design, Development And  
Manufacture of a Breadboard  
Radio Frequency Mass Gauging  
System**

**Phase C Final Report**

**Contract NAS 8-30160**

**Prepared For**

**National Aeronautics And Space  
Administration  
George C. Marshall  
Space Flight Center  
Huntsville, Alabama**



## FOREWORD

This report covers the work performed under Phase C of Contract NAS 8-30160. It reports all RF Gauging work performed by the Instruments & Life Support Division of The Bendix Corporation for the NASA Marshall Space Flight Center during the contract period.

## APPROVED:

The Bendix Corporation  
Instruments & Life Support Division

William M. Ott  
Project Engineer

Carl Moseman  
Engineering Mgr.

Craig Bassi  
Director of Engineering

NASA/MSFC

Harold E. Thompson



## TABLE OF CONTENTS

Section		Page
1.0	Introduction . . . . .	1
2.0	Cryogenic Testing . . . . .	2
2.1	Test Hardware . . . . .	2
2.2	Liquid Hydrogen Tests – March 1974 . . . . .	7
2.2.1	LH <sub>2</sub> Test Procedure . . . . .	7
2.2.2	LH <sub>2</sub> Test Results . . . . .	10
2.3	Liquid Hydrogen Tests – January 1975 . . . . .	10
2.3.1	LH <sub>2</sub> Test Procedures . . . . .	14
2.3.2	LH <sub>2</sub> Test Results . . . . .	14
2.3.2.1	Weight Determination . . . . .	14
2.3.2.2	Linear Regression Curve (Static) . . . . .	15
2.3.2.3	Mass Error (Static) . . . . .	21
2.3.2.4	Linear Regression Curve (Dynamic) . . . . .	26
2.3.2.5	Mass Error (Dynamic) . . . . .	27
2.3.2.6	Mode Count Variance And Standard Deviation . . . . .	29
2.3.2.7	Data Distribution Test . . . . .	30
2.3.2.8	Computer Generated Plots . . . . .	30
2.3.3	Summary – LH <sub>2</sub> Test Results, January 1975 . . . . .	30
2.4	Liquid Oxygen Tests – February 3, 1975 . . . . .	34
2.4.1	LOX Test Procedures . . . . .	34
2.4.2	LOX Test Results . . . . .	34
2.4.2.1	Weight Determination . . . . .	34
2.4.2.2	Orientation Data – Dynamic . . . . .	35
2.4.2.3	Multi-Segment Non-Linear Regression Fit . . . . .	37
2.4.2.4	Single-Segment Non-Linear Regression Fit . . . . .	40
2.4.2.5	Mass Error – Statistical Analysis . . . . .	41
2.4.2.6	Data Distribution Test . . . . .	45
2.4.2.7	Computer Generated Plots . . . . .	48
2.4.2.8	Summary – LOX Test Results, February 3, 1975 . . . . .	48
2.5	Liquid Oxygen Tests – February 10, 1975 . . . . .	49



## TABLE OF CONTENTS (Continued)

Section		Page
2.5.1	LOX Test Procedures . . . . .	49
2.5.2	LOX Test Results . . . . .	49
2.5.2.1	Weight Determination . . . . .	49
2.5.2.2	Orientation Data – Dynamic . . . . .	50
2.5.2.3	Multi-Segment Non-Linear Regression Fit . . . . .	52
2.5.2.4	Single-Segment Non-Linear Regression Fit . . . . .	55
2.5.2.5	Summary – LOX Test Results, February 10, 1975 . . . . .	55
3.0	Empty Tank Orientation Sensitivity . . . . .	56
3.1	Cause Of Empty Tank Orientation Sensitivity . . . . .	56
3.2	Cryogenic Tank Re-Work . . . . .	68
3.3	Summary of Empty Tank Orientation Sensitivity Evaluation . . . . .	71
4.0	Configuration And Multiple Probe Evaluations . . . . .	77
4.1	Cylindrical Tank Evaluations . . . . .	77
4.1.1	Strip Chart Data . . . . .	79
4.1.2	Q Measurements . . . . .	83
4.1.2.1	Q Measurement Technique . . . . .	83
4.1.2.2	Q Measurement Results . . . . .	86
4.1.3	VSWR Data . . . . .	89
4.1.4	RP-1 Fuel Properties . . . . .	89
4.1.5	RP-1 Test Results . . . . .	93
4.2	Spherical Tank Evaluations . . . . .	109
4.2.1	Strip Chart Data . . . . .	109
4.2.2	RP-1 Test Results . . . . .	112
4.2.3	RP-1 Pressurization Tests . . . . .	116
4.2.3.1	Volume Change With Pressure . . . . .	116
4.2.3.2	Proof Pressure Testing . . . . .	118
4.2.3.3	RP-1 Pressurization Tests . . . . .	118
4.3	Summary Of Configuration, Multiple Probe, And Pressurization Evaluations . . . . .	142

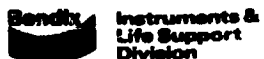


## TABLE OF CONTENTS (Continued)

Section	Page
5.0      Analog Processing Electronics . . . . .	144
6.0      Digital Processing Electronics . . . . .	151
7.0      Conclusions . . . . .	156
Appendix A — Computer Generated Plots of LH <sub>2</sub> Tests . . . . .	
Appendix B — Computer Generated Plots of LOX Tests . . . . .	



## 1.0 INTRODUCTION

The Instruments & Life Support Division of the Bendix Corporation submits this final report to the Marshall Space Flight Center (MSFC) to document the progress made during Phase C of NASA Contract NAS 8-30160 for "Design, Development and Manufacture of a Breadboard Radio Frequency Mass Gauging System."

The objectives of Phase C were as follows:

- Conduct and evaluate gauging performance tests using liquid hydrogen in the Phase B cryogenic test tank.
- Conduct and evaluate gauging performance tests using liquid oxygen in the Phase B cryogenic test tank.
- Evaluations of the multiple probe approach in conjunction with perturbations in tanks using RP-1 as a test fluid.
- Evaluations of the effects on gauging performance of perturbations in tanks using RP-1 as a test fluid.
- Conduct a pressurization test to determine system sensitivity to pressure using RP-1 as a test fluid.
- To improve analog and digital processing electronics.
- To investigate a non-linear sweep generator whose sweep rate would vary with frequency; and incorporate a solid state 1.0 - 2.0 GHz RF oscillator.

The following sections detail the accomplishments and conclusions which can be made from the work performed during Phase C.



## 2.0 CRYOGENIC TESTING

As a further evaluation of the RF gauging technique, additional tests were performed using the cryogens liquid hydrogen ( $LH_2$ ) and liquid oxygen (LOX). The test tank used in these tests was the dual-walled, vacuum-insulated test vessel which was designed, fabricated, and used in Phase B under NASA Contract NAS 8-30160. During March 1974  $LH_2$  tests were performed; after modifications to the test tank, additional  $LH_2$  tests were performed in January 1975. LOX tests were performed in February 1975. The following sections define the test hardware, procedures, and test results obtained in the course of these cryogenic gauging tests.

### 2.1 TEST HARDWARE

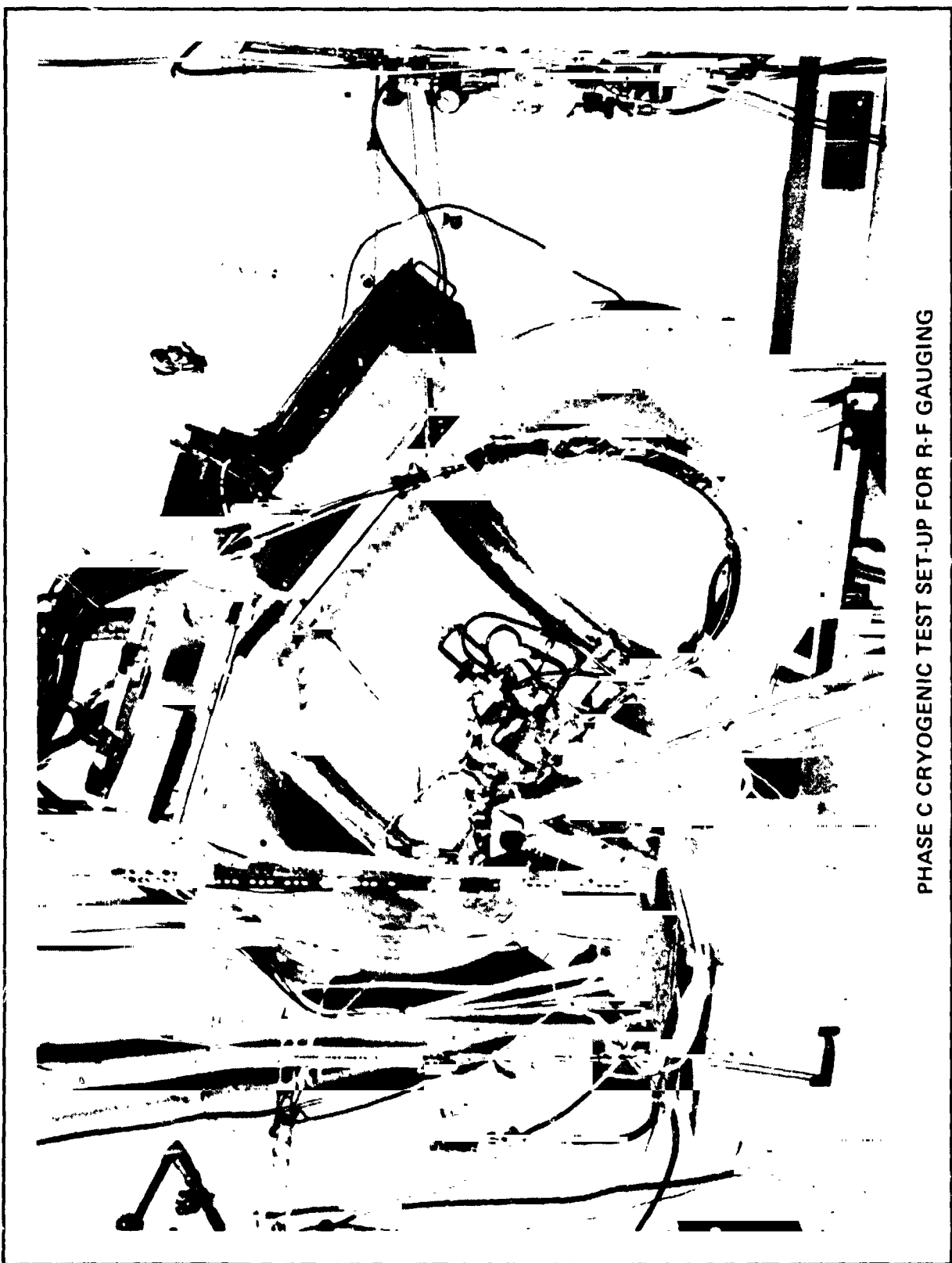
The test tank fabricated in Phase B consists of an inner pressure vessel and an outer vacuum shield vessel. The pressure vessel is wrapped with sheets of aluminized mylar and suspended in the outer vacuum shield. The space between the inner and outer vessels is evacuated to provide appropriate thermal insulation. (For complete details of tank construction refer to the Phase B Final Report, Volume I, Design, Development And Manufacture of a Breadboard Radio Frequency Mass Gauging System, Bendix I&LSD Publication Number 7246, November 15, 1974). Figures 2-1 thru 2-3 show the test tank mounted in a gimbaling fixture. This fixture contains a remotely controlled gimbaling mechanism which is capable of rotating the test tank, when filled with either test cryogen,  $180^\circ$  in either direction from a horizontal position about the minor axis of the dewar. Rotation of the test tank is accomplished by means of a reversible electric motor with a chain and sprocket drive.

Figure 2-4 shows the access hatch end of the test tank with the outer and inner hatch covers removed. Figure 2-5 shows the RF probe assembly used in the test tank. This probe assembly is a multi-element assembly, where each element is a short E-field probe covered with a teflon radome. This assembly mates with the pressure vessel at the access hatch and is sealed by welding at the outer lip of the access hatch.

Due to the inherent hazards associated with  $LH_2$  and LOX, the test tank, orientation fixture, and RF gauging processing electronics were positioned in a concrete hazard-test-cell during testing. Liquid transfer and tank orientation tests were remotely controlled from an instrumentation building that contained all control and monitoring

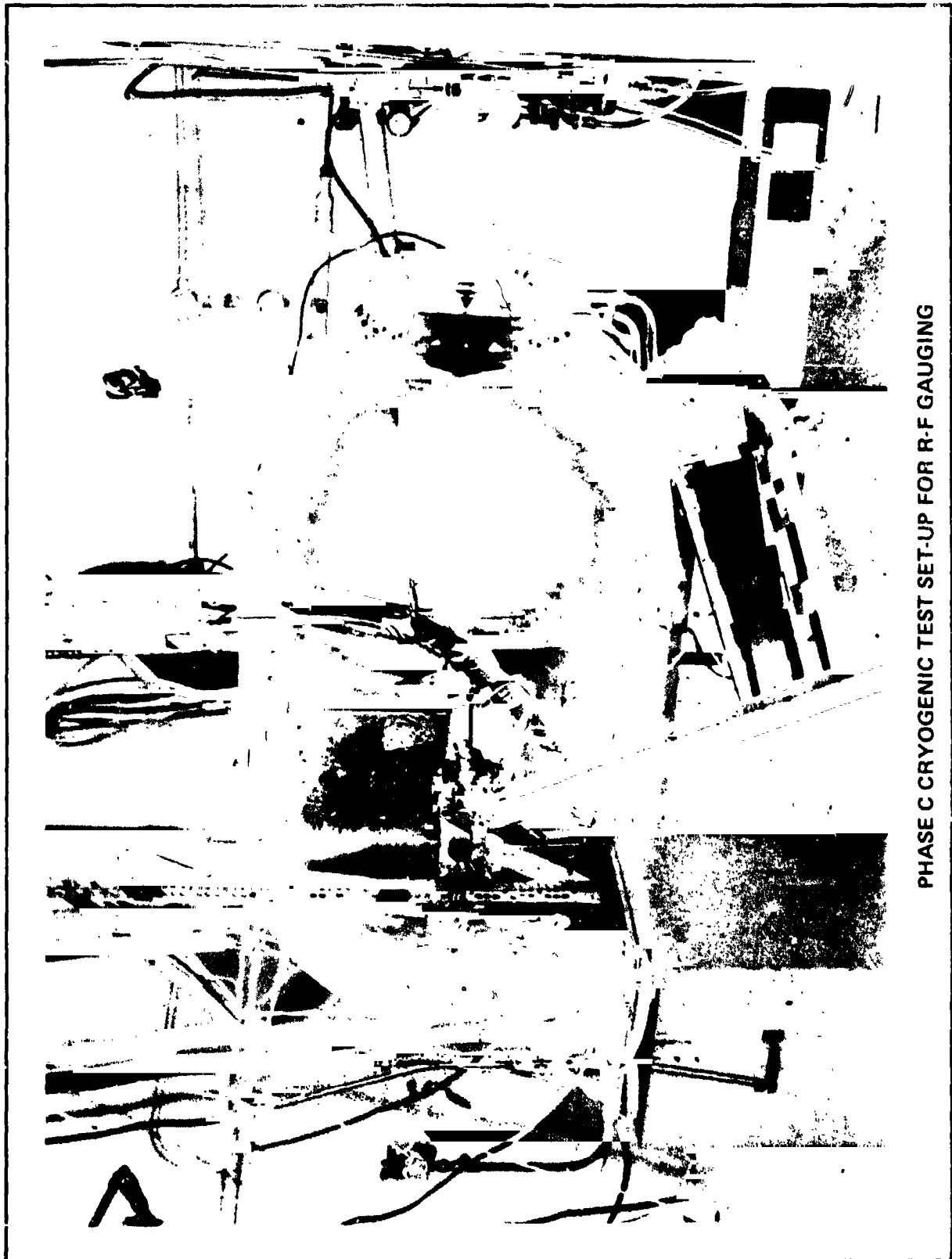


Figure 2-1



PHASE C CRYOGENIC TEST SET-UP FOR R-F GAUGING

Figure 2-2



PHASE C CRYOGENIC TEST SET-UP FOR R-F GAUGING

Figure 2-3

**Bendix** Instruments &  
Life Support  
Division

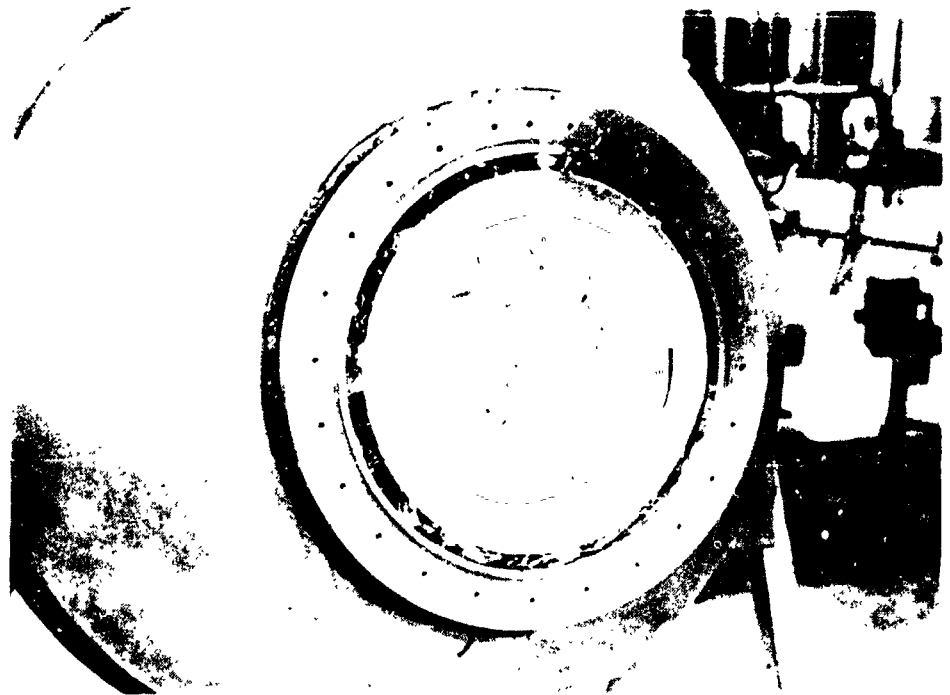


**Figure 2-4**  
**ACCESS HATCH-INNER AND OUTER VESSEL**



**Figure 2-5**  
**RF PROBE ASSEMBLY**



equipment. Figure 2-6 illustrates the physical arrangement of the test configuration. To facilitate the acquisition of a large quantity of data, an automatic data acquisition system provided the appropriate interface between data outputs and an IBM Model 026 modified keypunch. Figure 2-7 shows a block diagram of the basic test instrumentation setup which was used to record all test data. The RF gauging processing electronics designed for and used in Phase B was again used for the cryogenic tests after minor modifications.

## 2.2 LIQUID HYDROGEN TESTS - MARCH 1974

To augment the Phase B LH<sub>2</sub> loading and orientation test data, additional LH<sub>2</sub> tests were performed in Phase C. Problems that had been noted during the Phase B tests with the data acquisition system and the RF sweep oscillator were corrected prior to testing. The data acquisition system had been set up so that the RF sweep oscillator would provide system sequencing. This arrangement caused noise to feedback into the system from the IBM keypunch, causing errors in card punching. To alleviate this source of errors, the system was changed so that the IBM machine on automatic cycling would initiate the sequencing for the data acquisition.

### 2.2.1 LH<sub>2</sub> TEST PROCEDURE

After a systems checkout, the test tank was pre-chilled with LN<sub>2</sub>, emptied, then filled to approximately 100% of capacity with LH<sub>2</sub>. Both static and dynamic orientation testing was performed at approximately 10% intervals of mass. Static and dynamic orientations involved the following conditions.

#### A. STATIC ORIENTATION TESTS

- Tank positioned and fluid allowed to come to rest at each position prior to taking data.
- Mass held constant.
- Data recorded at each 15° increment of orientation.

#### B. DYNAMIC ORIENTATION TESTS

- Continuous orientation of test tank back and forth (360°).
- Rate of rotation of tank approximately 6° per second.

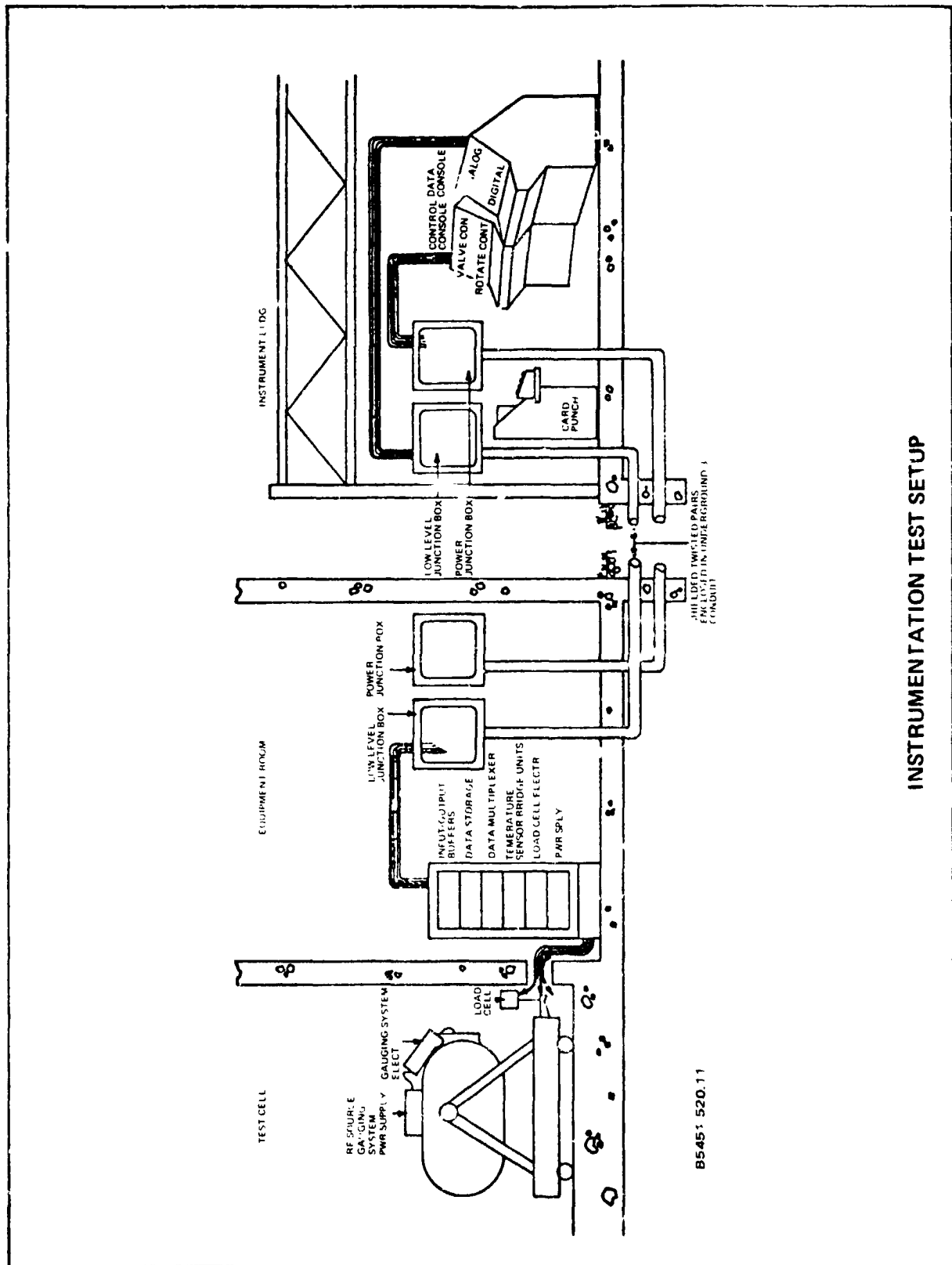
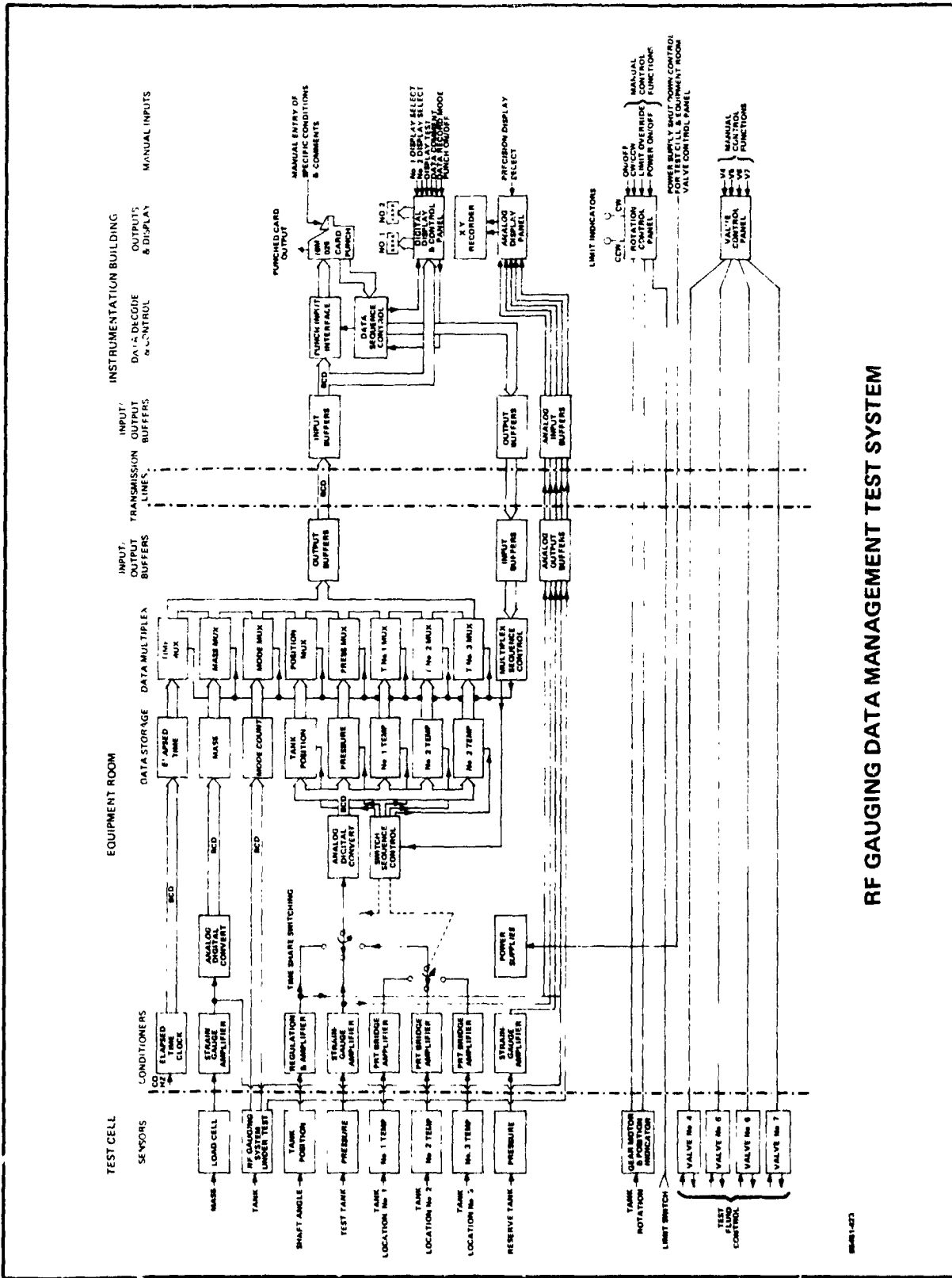


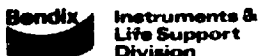
Figure 2-6

### INSTRUMENTATION TEST SETUP



RF GAUGING DATA MANAGEMENT TEST SYSTEM

Figure 2-7



- Mass held constant.
- Data recorded continuously.

### 2.2.2 LH<sub>2</sub> TEST RESULTS

At the beginning of the LH<sub>2</sub> tests (during LH<sub>2</sub> loading) the system had high sensitivity. However, a failure occurred during the testing which greatly reduced the system sensitivity, consequently causing the mass percent error to be large. This change or loss in sensitivity has been traced to a failure in the mode processing electronics where the cause of loss of sensitivity was due to damage of the crystal detector. However, the testing was continued. Figure 2-8 shows an error matrix for these LH<sub>2</sub> tests. Figures 2-9 and 2-10 show frequency distribution and cumulative error distribution curves for this data.

From these results it was clear that the reduced system sensitivity with the March 3, 1974 LH<sub>2</sub> tests caused the mass percent error to be larger than that obtained with the Phase B, January 9, 1974 LH<sub>2</sub> test data. As a result, total error analysis breakdown of the March LH<sub>2</sub> test data was not attempted. However, it was noted that for these tests errors due to the data acquisition system were reduced and the mode count variance was smaller than that seen in the Phase B tests.

### 2.3 LIQUID HYDROGEN TESTS - JANUARY 1975

Additional testing with LH<sub>2</sub> was performed in January, 1975. For these tests several changes were incorporated in the test tank and data acquisition system to improve the test system. These changes included the following:

- Add temperature control to the RF sweep oscillator test box.
- Add temperature control to the RF signal processing test box.
- Add N<sub>2</sub> cooling purge to solenoid valves in test tank.
- Improve performance of data acquisition interface with IBM keypunch.
- Modification of test tank to minimize variations in RF system output with empty tank orientation. (See Section 3.0 for details of the tank modifications).

DEGREE	0	5	15	20	35	45	55	65	75	85	90	100
+180	2.71	4.14	-4.23	9.05	-0.94	3.26	1.63	-1.95	-1.90	2.18	6.37	1.19
+165	1.69	1.67	-0.54	8.85	-2.29	-0.79	2.97	0.83	-1.10	-6.40	4.29	5.10
+150	0.31	-2.72	-3.44	5.98	-2.21	-3.49	1.95	-1.45	-2.18	-1.00	0.37	1.03
+135	0.25	-0.80	-0.80	6.55	-5.19	-5.78	-4.88	-5.86	-7.89	-1.84	1.13	-3.63
+120	1.10	5.98	-3.72	7.20	-3.11	-3.01	-0.90	-2.67	-4.27	-2.29	1.81	6.99
+105	1.26	2.69	-4.34	6.19	-1.31	.82	-2.70	-6.70	-8.26	-0.15	3.06	3.82
+90	1.29	3.03	-1.72	6.94	-0.42	-4.76	-5.36	-3.62	-7.28	1.49	2.97	5.48
+75	0.03	5.94	-1.56	5.53	-5.17	1.61	-4.23	-1.15	-7.73	-1.36	-2.80	1.58
+60	-0.86	1.33	-5.24	1.17	-4.93	-1.69	-4.22	-6.69	-7.73	-2.14	-1.49	-4.20
+45	-1.86	1.15	-1.55	4.42	-4.60	-4.08	-4.08	-3.91	-4.58	-1.87	0.43	-1.24
+30	-1.88	2.61	0.59	7.23	-3.40	-3.43	-2.46	0.83	-3.86	-1.98	-1.03	2.23
+15	-2.42	-0.51	2.37	5.87	-1.83	1.51	0.61	-1.12	-1.77	-0.61	-2.46	3.62
<0	-1.22	-0.65	-1.82	5.84	-1.49	-2.10	-2.03	0.78	-2.35	0.10	4.24	5.09
-15	-0.95	0.00	-3.78	5.03	0.48	1.34	-3.34	1.00	0.66	2.90	3.34	-2.22
-30	-3.96	-1.25	-5.36	2.73	1.41	1.50	-4.49	-1.88	-0.27	3.17	6.41	-3.42
-45	-2.81	-3.39	-0.13	3.98	3.60	1.53	-1.91	1.78	0.00	-2.00	4.23	0.36
-60	-2.79	-0.65	-8.04	7.19	0.12	0.95	0.99	-5.57	-5.53	0.24	4.04	0.66
-75	-3.72	2.70	-1.27	4.05	-1.69	1.74	-0.86	-2.21	-1.10	-1.22	6.65	1.00
-90	-3.73	2.46	-5.60	1.18	-0.87	-0.51	-0.69	-1.13	-3.83	2.26	4.82	2.57
-105	-2.71	2.16	0.56	3.05	-0.55	-0.48	-3.18	-3.42	-4.08	0.97	6.65	-0.40
-120	-5.10	-0.45	0.00	1.47	-1.13	1.22	0.79	-7.39	-5.06	-2.39	4.46	0.56
-135	-3.10	2.77	-1.95	2.73	-0.05	0.38	6.37	-1.20	-0.44	-2.12	9.36	4.68
-150	-4.25	2.70	-0.91	2.80	3.93	2.98	0.47	-3.29	0.84	4.45	7.20	2.11
-165	-3.86	3.52	1.54	11.11	4.86	1.07	-3.45	-2.19	1.47	4.55	5.61	4.76
-180	-3.32	4.36	2.89	6.0	-1.67	3.57	0.82	-2.80	-4.01	0.25	5.21	0.00

MASS ERROR MATRIX LH<sup>2</sup>, MARCH 3, 1974

ORIGINAL PAGE IS  
OF POOR QUALITY

Figure 2-8

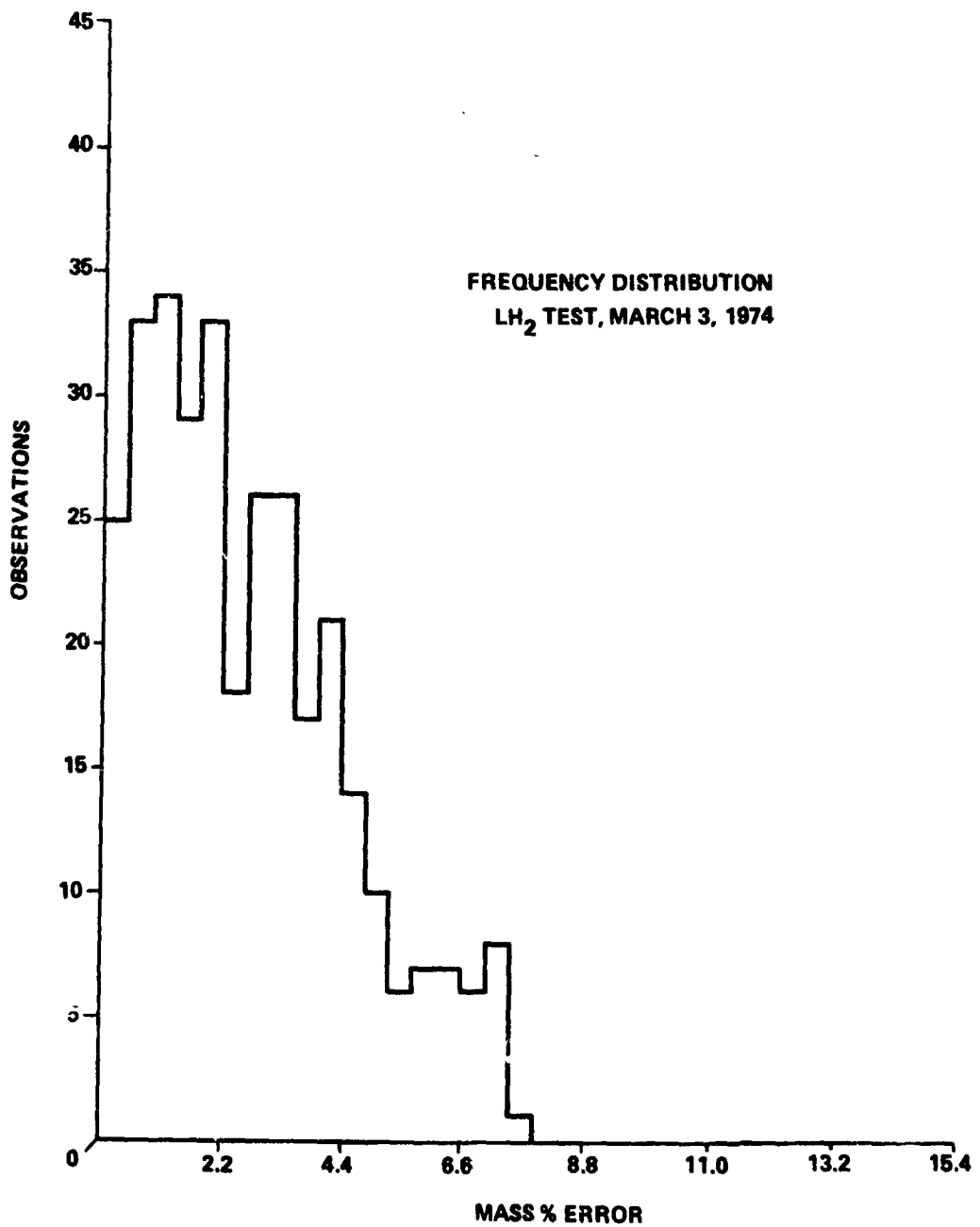


**Figure 2-9**

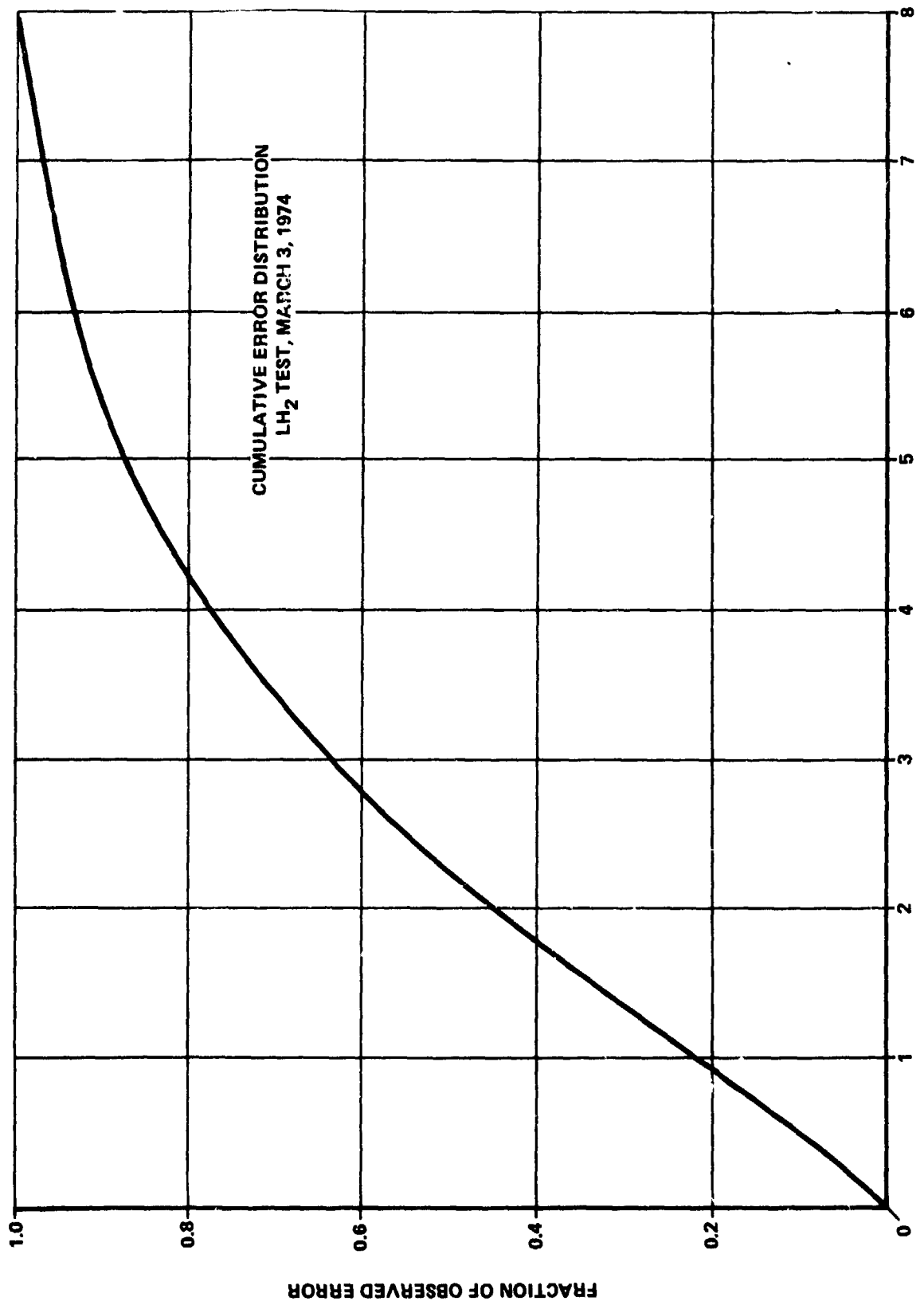


Figure 2-10



### 2.3.1 LH<sub>2</sub> TEST PROCEDURES

After the cryogenic test tank was modified to minimize the empty tank orientation sensitivity, it was returned to the hazard test cell and interfaced with the modified data acquisition and fluids handling hardware. Following a pre-test system checkout, the tank was pre-chilled with LN<sub>2</sub>, emptied, and then filled with LH<sub>2</sub> to approximately 95% of capacity (132.5 lbs of LH<sub>2</sub>). Static and dynamic orientation testing was then performed at each of the following incremental amounts of LH<sub>2</sub>: 95%, 90%, 80%, 70%, 60%, 50%, 40%, 30%, 20%, 10%, 5%, and 0%.

As in the previous LH<sub>2</sub> tests, the static and dynamic orientation tests involved the following conditions:

#### A. STATIC ORIENTATION TESTS

- Tank positioned and fluid allowed to come to rest at each position prior to taking data.
- Mass held constant.
- Data recorded at each 15° increment of orientation.
- 10 data frames recorded at each angular increment.

#### B. DYNAMIC ORIENTATION TESTS

- Continuous orientation of test tank back and forth (360°).
- Rate of rotation of tank approximately 6° per second.
- Mass held constant.
- Data recorded continuously.
- 100 Data frames recorded at each loading increment.

### 2.3.2 LH<sub>2</sub> TEST RESULTS

#### 2.3.2.1 WEIGHT DETERMINATION

To establish the mass of LH<sub>2</sub> in the tank during an incremental loading and orientation test, it was necessary to subtract out the tare



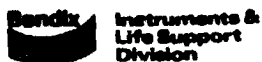
weight measured with the tank completely empty and the fill hose disconnected. At any given fill level where both dynamic and static orientation testing was performed, the tank fill and vent lines were closed. Hence, the actual mass for both dynamic and static orientation tests were the same. During orientation testing the fill hose was disconnected. The best indication of actual LH<sub>2</sub> mass in the tank at any given percent loading was determined from averaging the indicated mass on those IBM cards punched while the tank was in its normal upright position (same position as when tare weight of empty tank was acquired) and then subtracting that tare weight from it. Table 2-1 summarizes the actual LH<sub>2</sub> weight increments at which the orientation tests were performed. The volume of the tank is capable of containing 139.48 pounds of LH<sub>2</sub>.

TABLE 2-1  
ACTUAL MASS LOADING (LH<sub>2</sub>)

Approx. Percent Loading	Scale Indication of Mass (Avg.) In Pounds	Tare Weight In Pounds	Actual Weight of LH <sub>2</sub> In Pounds
95	137.51	5.35	132.16
90	132.08	"	126.73
80	116.81	"	111.46
70	103.16	"	97.81
60	89.69	"	84.34
50	74.24	"	68.89
40	61.95	"	56.60
30	48.37	"	43.02
20	33.91	"	28.56
10	20.50	"	15.15
5	12.50	"	7.15
0	5.33	"	0.0

### 2.3.2.2 LINEAR REGRESSION CURVE (STATIC)

The first step in analyzing the static orientation data was to calculate the average mode count for all of the static orientation positions for each respective incremental loading according to the equation:



$$\overline{\text{Mode}} = \frac{1}{N} \sum_{i=1}^N \text{Mode}(i). \quad (1)$$

Table 2-2 summarizes the average mode count for all orientations at each respective loading along with the actual mass.

It was noted that the temperature of the tank and the antenna structure had warmed up considerable by the time that the empty orientation data was acquired. As a result, the average mode count for the empty tank is lower than when the tank and probe structure is completely chilled.

This difference is primarily due to the change with temperature of the electrical and dimensional characteristics of the teflon associated with the antenna radomes and the teflon in the semi-rigid coax in the probe structure. Once the probe structure is completely chilled no further changes in these electrical and dimensional characteristics are seen. Alternate materials and design configurations can be used to limit this effect. As a result the empty tank mean mode count was not used in calculating the linear regression curve.

TABLE 2-2  
SUMMARY OF MEAN MODE COUNT AND ACTUAL  
MASS AT EACH INCREMENTAL LOADING  
(FROM STATIC ORIENTATION DATA)

Approx. Percent Loading	Mean Mode Count	Actual Mass (lbs)
95	2134.266	132.16
90	2108.818	126.73
80	2029.852	111.46
70	1976.824	97.81
60	1924.328	84.34
50	1871.388	68.89
40	1834.132	56.60
30	1756.292	43.02
20	1708.280	28.56
10	1648.752	15.15
5	1641.856	7.15
0	1539.394	0



Using the values from Table 2-2 for mass and average mode count (except for 0% loading), a linear regression curve of the form

$$Y = \beta_0 + \beta_1 X \quad (2)$$

was generated, where

$Y$  = mode count

$X$  = mass

$\beta_0$  = the  $Y$  intercept

$\beta_1$  = the slope of the line

The coefficients  $\beta_0$  and  $\beta_1$  can be determined from the simultaneous solution of the following equations

$$\beta_0 = \frac{1}{N} \left( \sum_{i=1}^N Y_i - \beta_1 \sum_{i=1}^N X_i \right) \quad (3)$$

$$\beta_1 = \frac{\sum_{i=1}^N X_i \sum_{i=1}^N Y_i - N \sum_{i=1}^N X_i Y_i}{\left( \sum_{i=1}^N X_i \right)^2 - N \sum_{i=1}^N X_i^2} \quad (4)$$

Solution of equations (3) and (4) provides values for  $\beta_0$  and  $\beta_1$  of the linear regression curve. They are

$$\beta_0 = 1596.64 \text{ (Empty tank mode count)}$$

$$\beta_1 = 3.9797 \text{ (Sensitivity - Modes/lbs)}$$

The regression curve then becomes

$$Y = 1596.64 + 3.9797X \quad (5)$$



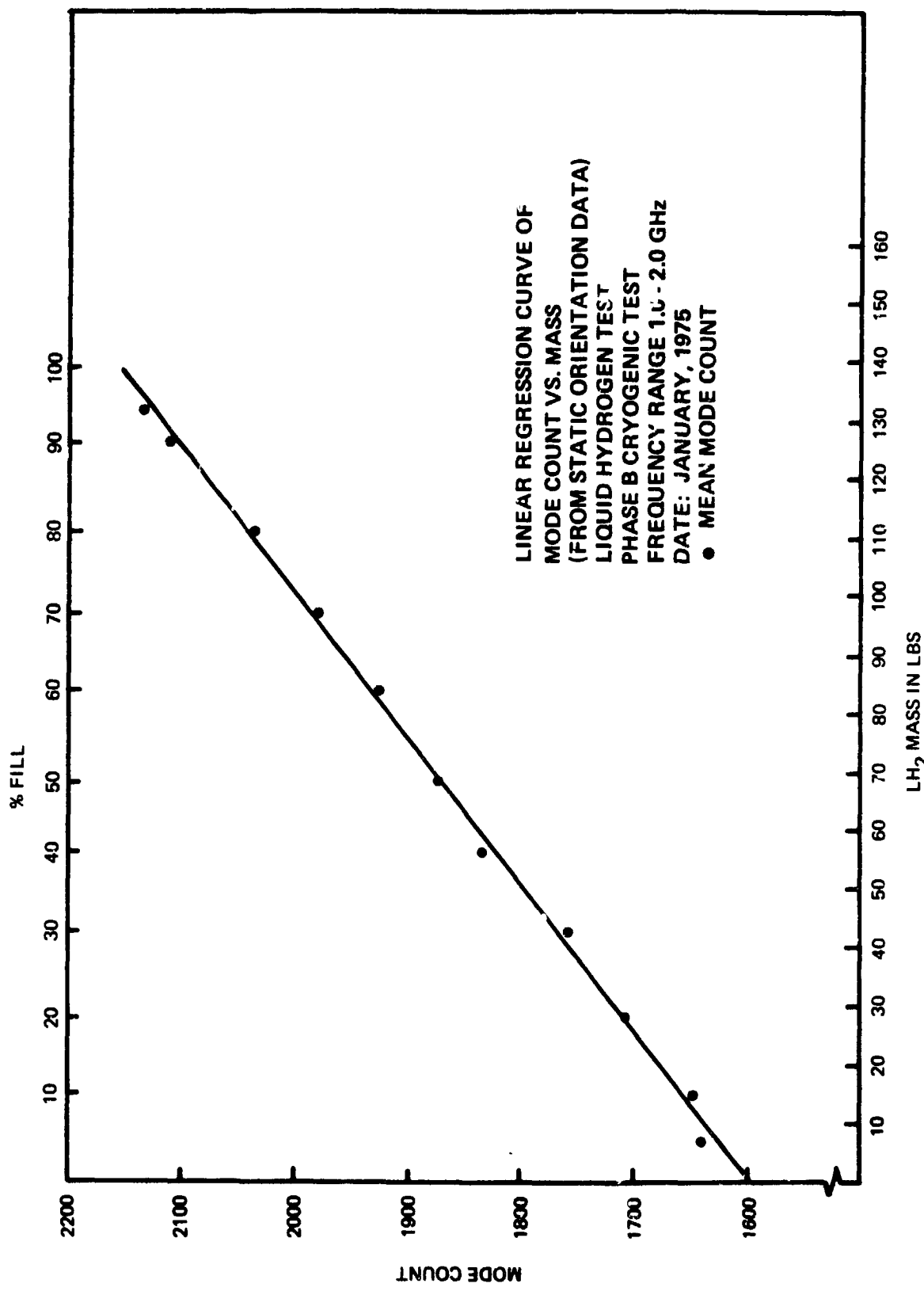
The regression curve is used as the basis for all error calculations relating to the static orientation tests. This curve is shown in Figure 2-11 along with the mean mode count for all orientations for each mass loading. The residuals of the measured mean mode count relative to the mode count calculated from the least squares regression curve as shown in Table 2-3. These residuals are calculated from

$$\% \text{ mode count error} = \frac{\left( \begin{array}{c} \text{mean mode} \\ \text{mode} \\ \text{count} \end{array} \right) - \left( \begin{array}{c} \text{calculated} \\ \text{mode} \\ \text{count} \end{array} \right)}{\left( \begin{array}{c} \text{calculated} \\ \text{mode} \\ \text{count} \end{array} \right)} \times 100 \quad (6)$$

Figure 2-12 shows the percent deviation in mean mode count from the linear regression curve; the average of these residuals is 0.48174% error of point.

TABLE 2-3  
% ERROR OF MODE COUNT FROM  
LINEAR REGRESSION CURVE (BASED  
ON MEAN OF DATA-STATIC ORIENTATION TEST)

Approx. Percent Loading	Actual Mass (Lbs.)	Actual Mode Count	Theoretical Mode Count	% Error Mode Count (of Point)
5	7.15	1641.9	1725.09	+1.0316
10	15.15	1648.7	1656.93	-0.4935
20	28.56	1708.3	1710.30	-0.1179
30	43.02	1756.3	1767.84	-0.6534
40	56.60	1834.1	1821.89	+0.6721
50	68.89	1871.4	1870.80	+0.0315
60	84.34	1924.3	1932.28	-0.4118
70	97.81	1976.8	1985.89	-0.4566
80	111.46	2029.8	2040.21	-0.5079
90	126.73	2108.8	2100.98	+0.3729
95	132.16	2134.3	2122.59	+0.5499
Average				0.4817



A5451-543A

Figure 2-11

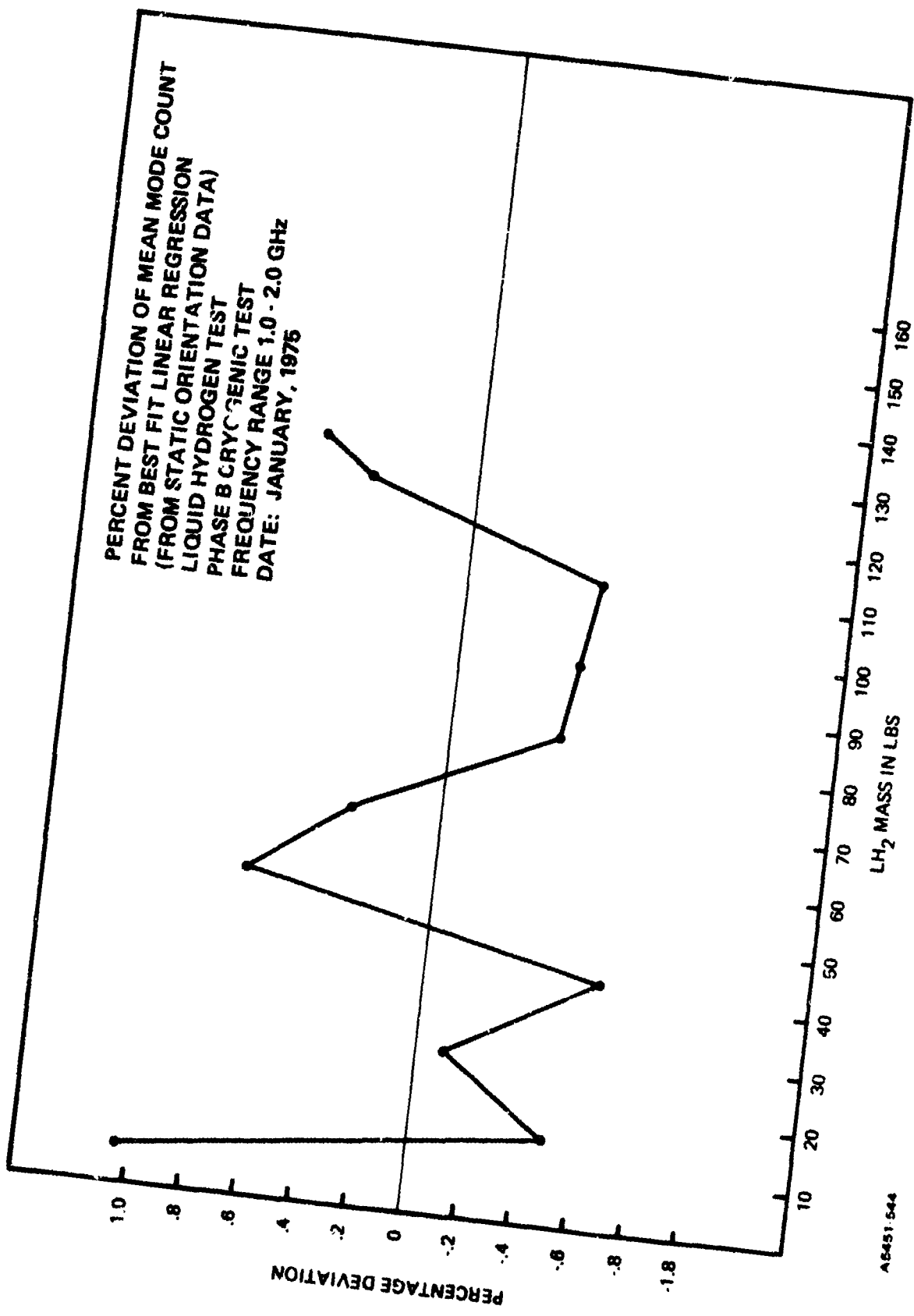


Figure 2-12



### 2.3.2.3 MASS ERROR (STATIC)

For each fill level and static orientation point the mean mass was calculated using the mean mode count for that orientation. The calculated mass for each orientation is arrived at by means of the equation

$$X = \frac{Y - 1596.64}{3.9797} \quad (7)$$

The % mass error of the system is then calculated as

$$\text{Percent Error} = \frac{\text{actual mass} - \text{calculated mass}}{\text{full tank mass}} \times 100\%. \quad (8)$$

A mass error matrix of percent fill and orientation angle can be constructed so as to present a summary of all system errors. This matrix is shown in Figure 2-13.

The error matrix can be analyzed to yield further insight into the behavior of the RF Gauging. One type of analysis available is to group the data so that its frequency distribution is apparent and the cumulative error distribution is calculated. Having the cumulative distribution, the probability function for the data can be arrived at by simply differentiating the cumulative distribution function. Figure 2-14 contains a plot of the mass error frequency of distribution in which the positive and negative mass errors are shown separately. Figure 2-15 contains a plot of the mass error frequency in which both the positive and negative mass errors are considered together (i.e. absolute values). Figure 2-16 contains the cumulative distribution plot obtained from the latter mass error frequency distribution data.



% FILL DEGREE	5	10	20	30	40	50	60	70	80	90	95
180	-4.5917	-1.0216	7.7460	5.4124	-1.7497	2.3236	4.7892	7.0243	0.1647	1.9067	1.1225
165	-3.6946	1.6446	3.6025	4.954	0.2860	2.8100	4.8811	6.8622	0.2007	-0.5924	-3.6942
150	1.8000	-1.7422	2.3053	-0.2805	-1.7317	3.7468	4.9153	2.0521	3.0290	4.2655	-1.0820
135	-1.5869	-2.0305	-0.3069	-1.2353	-4.3799	-1.5497	1.7443	0.1245	-0.0516	0.5536	-4.9013
120	-2.4336	-7.0026	-2.1984	-1.7397	-3.0108	-1.5857	3.4181	3.9797	2.7048	-0.0569	-5.1895
105	-6.8473	3.2299	-2.1804	-1.4875	-3.9475	-2.5405	-1.2098	-1.1006	-0.9523	-2.9033	-4.7751
90	-7.4959	-0.8415	-2.8830	-3.1088	-8.1612	-8.5936	-3.6239	-3.1002	-2.1394	-1.8044	3.9465
75	-4.1090	1.1222	-1.3697	-4.7482	-6.4697	-5.3328	0.899	-2.8857	-4.3752	-6.0920	-3.2979
60	-3.6046	0.1313	1.0623	-6.9210	-4.9564	2.3777	0.6397	-2.7940	0.2547	-5.8038	-6.1804
45	-4.2711	1.6986	-2.5767	-2.9647	-3.6953	-1.6037	0.6638	2.5025	5.0107	-4.2725	-6.8289
30	-5.2079	4.4910	-0.5771	1.2689	0.7364	1.9813	6.8970	3.1150	5.7493	-1.9125	-3.8564
15	-1.0645	5.3917	2.8738	4.4395	-0.7409	4.2152	3.3120	-2.8300	2.4526	-3.5699	-4.9733
0	-1.4608	5.7881	4.6113	4.8172	-7.3885	0.1978	-4.0048	-0.2899	0.9573	-0.1831	-2.0909
-15	-3.4795	1.7707	4.5212	0.8905	-2.5063	0.9365	-3.8941	2.8826	1.7320	-2.2007	-2.4692
-30	-4.7395	0.1673	-2.8650	0.9026	-1.7497	3.5847	-2.7051	0.3406	3.1191	-5.1192	-0.9379
-45	-5.3520	-6.2286	-2.9370	3.6469	-0.3004	1.9993	1.6366	-3.2984	0.8312	-2.7052	1.8544
-60	-2.6498	0.3420	-3.4595	5.7186	-2.7405	2.2516	-1.7863	0.3046	4.5964	3.0957	-3.6763
-75	-4.5774	2.0770	-1.4238	5.5564	-4.1817	2.9361	-4.1643	0.4425	0.4168	-0.3992	-3.1178
-90	-4.7755	0.5119	2.4687	2.6700	-3.6413	-5.3689	-1.5701	-1.9653	1.1375	-1.0117	-0.5776
-105	-3.9649	2.0904	0.6400	6.2050	-1.3534	0.0717	5.1855	4.9726	6.8482	-2.7231	1.0977
-120	-3.4654	6.164	2.1613	7.0444	2.7401	1.4589	4.7712	7.0963	6.4879	-1.5702	4.7008
-135	-1.0971	-1.1746	-2.593	2.89	2.4819	0.5761	-0.0929	6.6820	6.0916	0.1593	0.5394
-150	-4.543	6.273	-1.2156	4.9959	5.8527	0.2158	-0.8495	8.3754	2.1102	2.6034	-1.1361

ORIGINAL PAGE IS  
OF POOR QUALITY

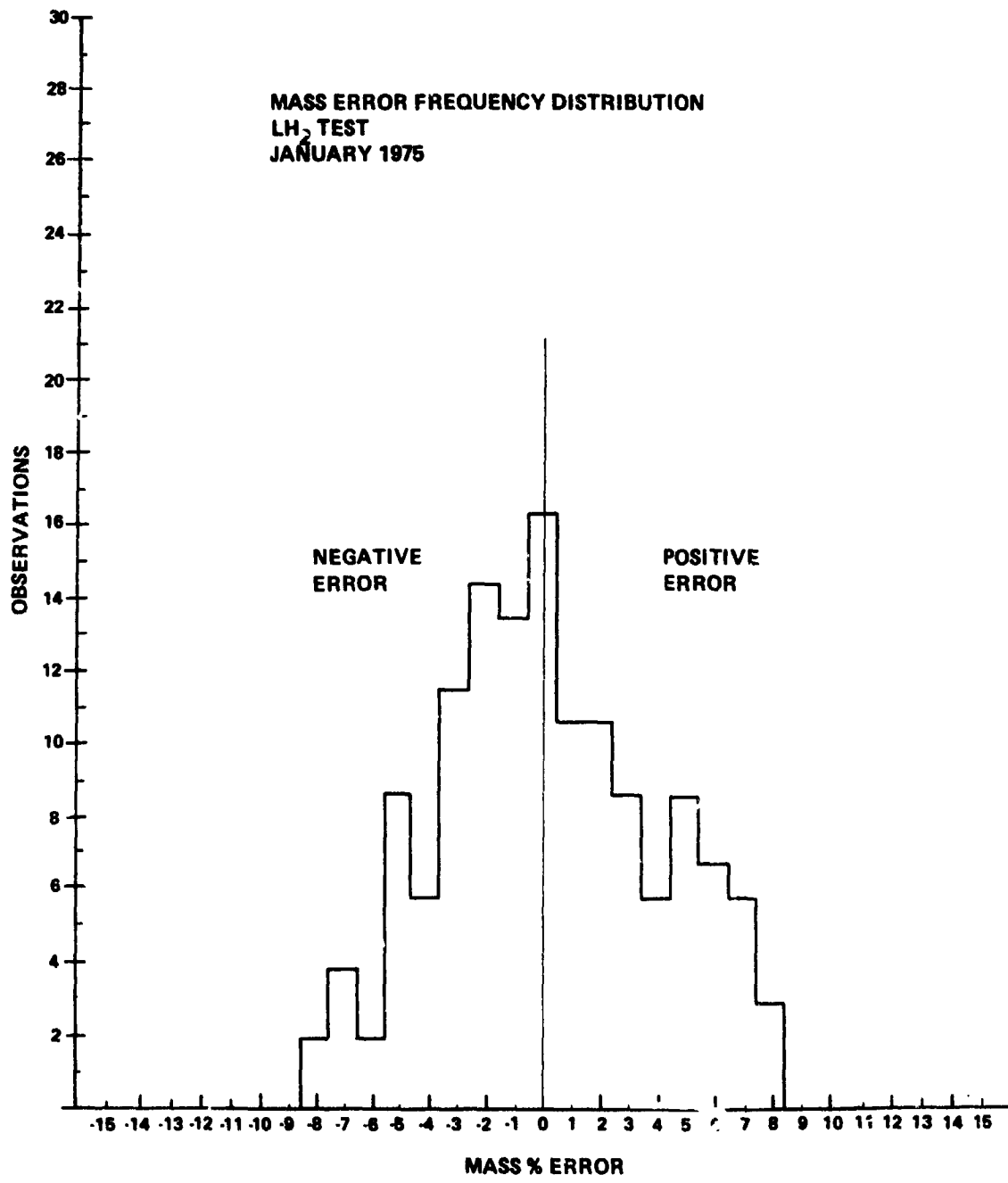
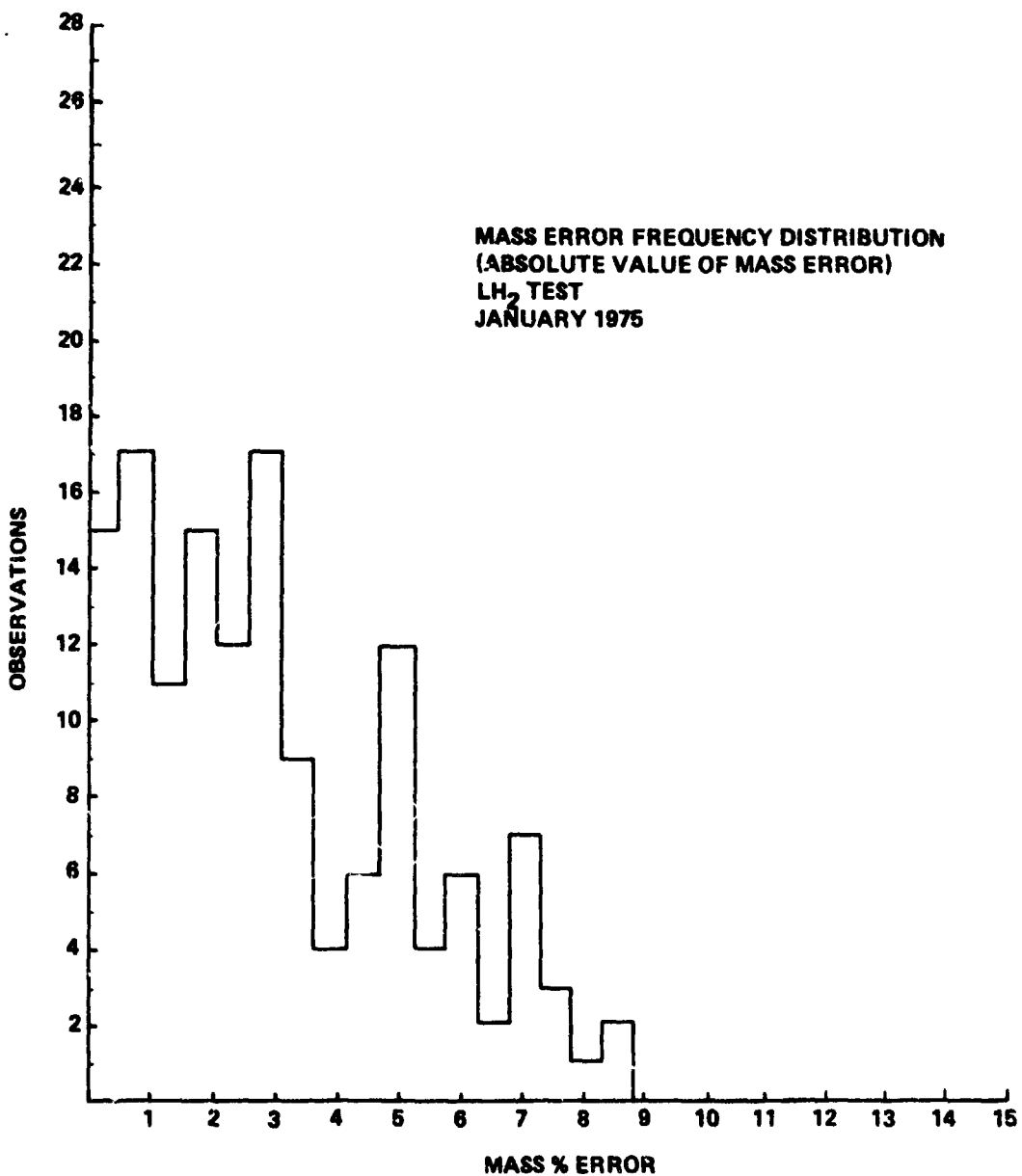
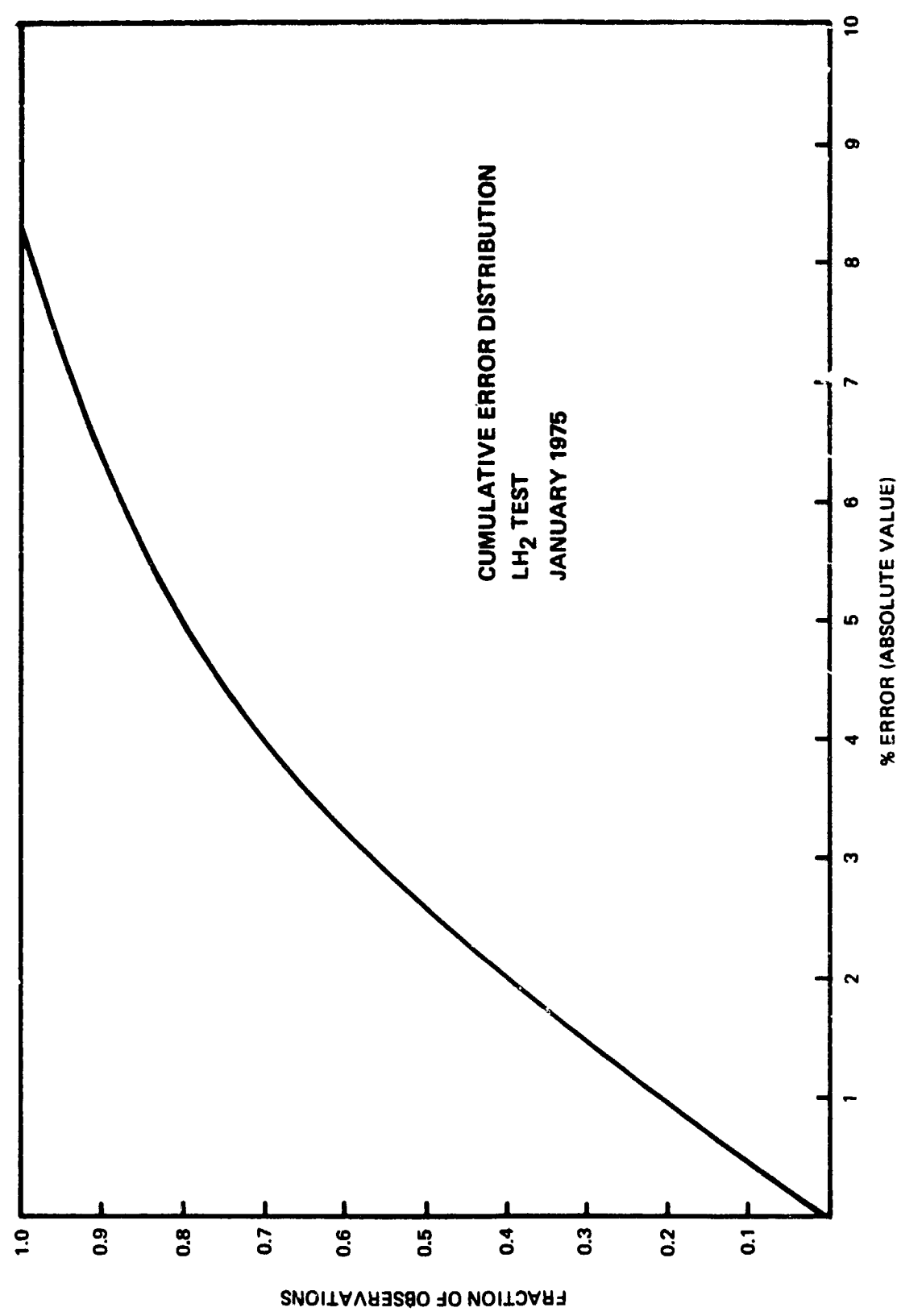


**Figure 2-14**



A5451 841

**Figure 2-15**



A5451-542

Figure 2-16



#### 2.3.2.4 LINEAR REGRESSION CURVE (DYNAMIC)

In examination of the dynamic orientation data, the first step was to calculate the average mode count for all of the data frames for each respective incremental loading according to the following equation:

$$\overline{\text{Mode}} = \frac{1}{N} \sum_{i=1}^N \text{Mode}(i). \quad (9)$$

Table 2-4 summarizes the average mode count for each respective loading along with the actual mass.

TABLE 2-4  
SUMMARY OF MEAN MODE COUNT AND ACTUAL MASS  
AT EACH INCREMENTAL LOADING (FROM DYNAMIC  
ORIENTATION DATA)

Approx. Percent Loading	Mean Mode Count	Actual Mass (lbs)
95	2133.336	132.16
90	2101.041	126.73
80	2041.980	111.46
70	1979.660	97.81
60	1919.510	84.34
50	1863.390	68.89
40	1833.600	56.60
30	1762.230	43.02
20	1698.950	28.56
10	1645.700	15.15
5	1630.340	7.15

Using the values from Table 2-4 for mass and average mode count, a linear regression curve can be established for the dynamic orientation test data. (Calculations based on same technique as described in section 2.3.2.2.) The regression curve for the dynamic orientation data is:

$$Y = 1590.18 + 4.0391X \quad (7)$$

where,

Y = mode count

X = mass.



It is noted that this curve agrees well with that calculated for the static orientation data (Equation 5). This dynamic linear regression curve is shown in Figure 2-17 along with the mean mode count for each mass loading (Dynamic test results).

#### 2.3.2.5 MASS ERROR (DYNAMIC)

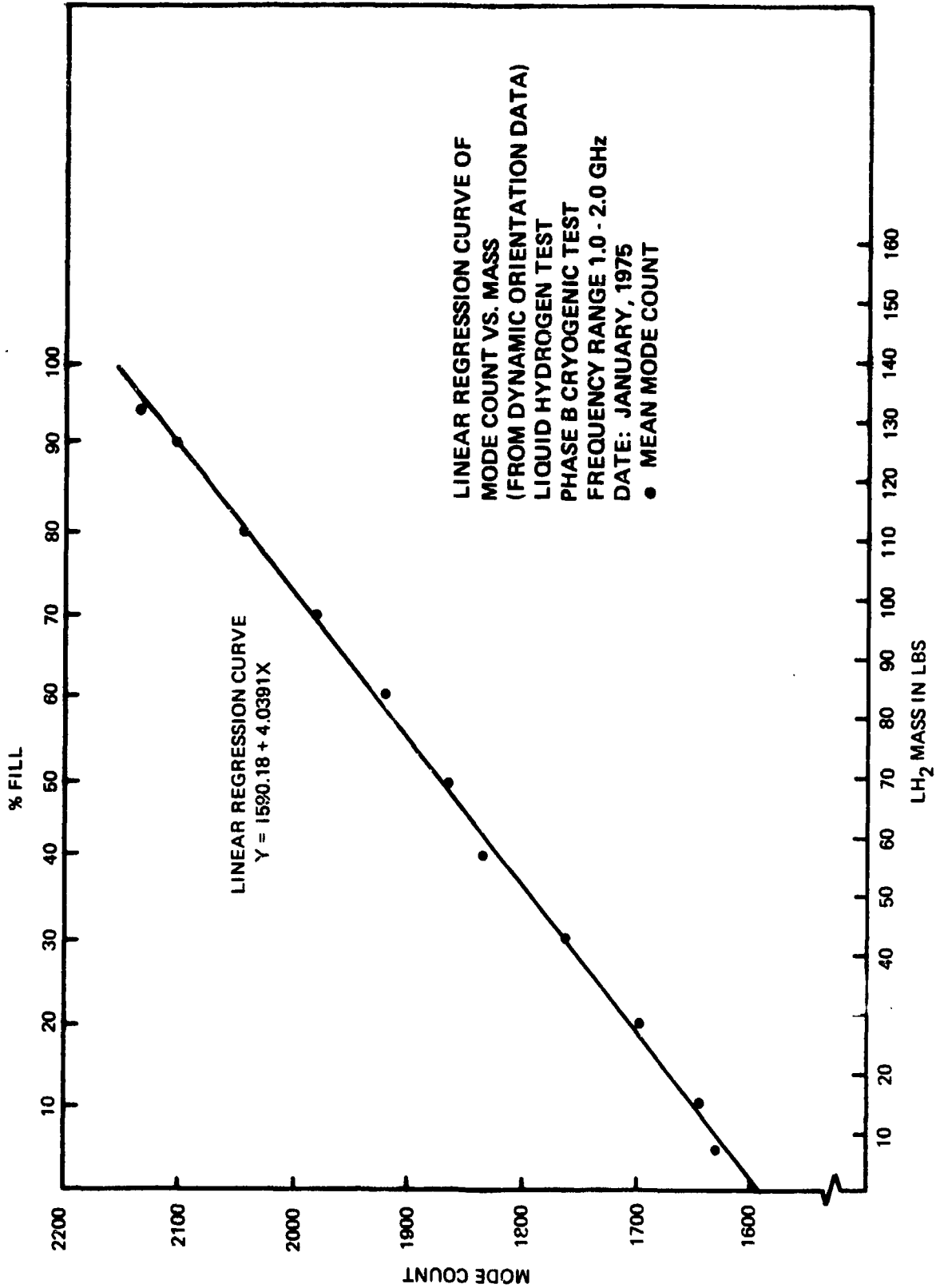
The residuals of the measured mean mode count relative to the mode count calculated from the least squares regression curve are shown in Table 2-5. As with the case of the static orientation data, these residuals are calculated from

$$\% \text{ mode count error} = \frac{\left( \begin{array}{c} \text{mean mode} \\ \text{mode} \\ \text{count} \end{array} \right) - \left( \begin{array}{c} \text{calculated} \\ \text{mode} \\ \text{count} \end{array} \right)}{\left( \begin{array}{c} \text{calculated} \\ \text{mode} \\ \text{count} \end{array} \right)} \times 100. \quad (11)$$

The average of these residuals is 0.36756% error of point, which is somewhat better than the residual mode % error calculated for the static orientation test data.

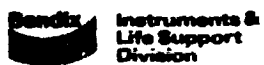
TABLE 2-5  
% ERROR OF MODE COUNT FROM  
LINEAR REGRESSION CURVE (BASED  
ON MEAN OF DATA – DYNAMIC ORIENTATION TEST)

Approx. Percent Loading	Actual Mass (Lbs)	Actual Mode Count	Theoretical Mode Count	% Error Mode Count (of Point)
5	7.15	1630.34	1619.06	0.6964
10	15.15	1645.70	1651.38	-0.3438
20	28.56	1698.95	1705.54	-0.3865
30	43.02	1762.23	1763.95	-0.0973
40	56.60	1833.60	1818.80	0.8138
50	68.89	1863.39	1868.44	-0.2702
60	84.34	1919.51	1930.84	-0.5869
70	97.81	1979.66	1985.25	-0.2816
80	111.46	2041.98	2040.38	0.0783
90	126.73	2101.04	2102.06	-0.0485
95	132.16	2133.34	2123.99	0.4399



A5451-639

Figure 2-17



For each fill level, the mean mass is calculated using the mean mode count for that fill level. The calculated mass is arrived at by means of the equation

$$X = \frac{Y - 1590.18}{4.0391} \quad (12)$$

The % mass error of the system is then calculated as

$$\text{Percent Error} = \frac{\text{actual mass} - \text{calculated mass}}{\text{full tank mass}} \times 100\%. \quad (13)$$

Table 2-6 summarizes the mass % error calculations obtained for the dynamic orientation test data. It is noted that the average mass % error for the dynamic orientation test data is 1.17336%.

TABLE 2-6  
DYNAMIC ORIENTATION MASS ERROR

Approx. Percent Loading	Actual Mass (Lbs)	% Error Mass
5	7.15	-2.0014
10	15.15	1.0078
20	28.56	1.1701
30	43.02	0.3048
40	56.60	-2.6273
50	68.89	0.8962
60	84.34	2.0116
70	97.81	0.9921
80	111.46	-0.2834
90	126.73	0.1810
95	132.16	-1.6585

**2.3.2.6 MODE COUNT VARIANCE AND STANDARD DEVIATION** Further insight into the results obtained with both the static and dynamic orientation data testing can be obtained by noting the typical spread in the raw data (mode count) at any given fill level.



Table 2-7 summarizes the variance and standard deviations in recorded mode count for both the static and dynamic data. For the static orientation testing the average standard deviation in mode count was 19.1 modes, whereas for the dynamic orientation testing the average standard deviation in mode count was 15.8 modes.

#### **2.3.2.7 DATA DISTRIBUTION TEST**

The question of the distribution of the raw mode count data at each fill level during the dynamic LH<sub>2</sub> orientation testing has been examined by application of the Kolmogorov-Smirnov tests for normal distribution and uniformity. Table 2-8 summarizes the results of the Kolmogorov-Smirnov tests for normal distribution and uniformity at each incremental level of LH<sub>2</sub>. It is significant to note that the data does approach a normal distribution. (Testing for a bivariate normal is not applicable, since mode count is a univariate statistic.) It is also noted that the distribution is not uniform in the statistical sense.

#### **2.3.2.8 COMPUTER GENERATED PLOTS**

Computer generated plots of the raw data from the January, 1975 LH<sub>2</sub> testing have been made of the following:

- Frequency of occurrence vs. mode count at each mass increment (static orientation data).
- Mode count vs. orientation angle at each mass increment (static orientation data).
- Frequency of occurrence vs. mode count at each mass increment (Dynamic orientation data).
- Mode count vs. orientation angle at each mass increment (Dynamic orientation data).

These plots are presented in Appendix A of this report.

#### **2.3.3 SUMMARY – LH<sub>2</sub> TEST RESULTS, JANUARY 1975**

From the data obtained with LH<sub>2</sub> using the Breadboard RF mode counting system, the following was observed:

##### **IN THE STATIC ORIENTATION TEST DATA –**

- The average percent error of mean mode count from the linear regression curve for all fill levels was 0.4817%.



**TABLE 2-7**  
**MEAN, VARIANCE, AND STANDARD DEVIATION IN MODE COUNT**  
**LH<sub>2</sub> TEST – JANUARY 1975**

Approx. Percent Loading	LH <sub>2</sub> Mass (Lbs)	Static Orientation			Dynamic Orientation		
		Mean Mode Count	Variance	Standard Deviation	Mean Mode Count	Variance	Standard Deviation
95	132.16	2134.3	287.2	16.9	2133.3	143.6	11.9
90	126.73	2108.8	/ 296.7	17.2	2101.0	170.9	13.1
80	111.46	2029.8	366.8	19.1	2042.0	219.3	14.8
70	97.81	1976.8	424.9	20.6	1979.7	202.4	14.2
60	84.34	1924.3	571.9	23.9	1919.5	265.9	16.3
50	68.89	1871.4	446.8	21.1	1863.4	242.4	15.6
40	56.60	1834.1	399.7	19.9	1833.6	347.4	18.6
30	43.02	1756.3	601.6	24.5	1762.2	313.1	17.7
20	28.56	1708.3	346.1	18.6	1698.9	384.4	19.6
10	15.15	1648.7	458.9	21.4	1645.7	485.9	22.0
5	7.15	1641.9	221.5	14.9	1630.3	288.7	17.0
0	0	1539.4	122.1	11.0	1547.0	74.0	8.6
				19.1 (AV)			15.8 (AV)



TABLE 2-8

KOLMOGOROV-SMIRNOV TEST FOR  
NORMAL DISTRIBUTION AND UNIFORMITY  
(DYNAMIC LH<sub>2</sub> ORIENTATION DATA)

% LOADING	TEST FOR NORMAL		TEST FOR UNIFORMITY	
	TEST STATISTIC	P(ACCEPT/NULL TRUE)	TEST STATISTIC	P(ACCEPT/NULL TRUE)
95	0.62390	0.8311E00	1.92548	0.1204E-02
90	0.66049	0.7756E00	2.25734	0.7498E-04
80	0.83026	0.4958E00	2.14590	0.2001E-03
70	1.12546	0.1587E00	1.9051	0.7835E-03
60	0.64473	0.8001E00	2.01008	0.6188E-03
50	0.86991	0.4356E00	2.4265	0.1562E-04
40	0.83134	0.4941E00	1.17265	1.278E+00
30	0.99856	0.2715E00	2.36667	0.2724E-04
20	1.18063	0.1231E00	2.06165	0.4066E-03
10	0.64882	0.7938E00	1.23276	0.9572E-01
5	1.15721	0.1373E00	2.87434	0.1192E-06
0	1.71130	0.5719E-02	3.47192	0.0000E00



- The average standard deviation in mode count distribution for all fill levels was 19.1 modes. For the empty tank the standard deviation in mode count was 11.0 modes. (See discussion on empty tank orientation sensitivity in section 3.0 of this report.)
- The average percent error of Mass from the linear regression curve for all fill levels and orientation angles was 3.02%.
- Based on cumulative distribution plot of mass errors for all fill levels and orientation angles, 75% of all points exhibited a mass error of less than 4.4% and 50% of all points exhibited a mass error of less than 2.6%.

#### IN THE DYNAMIC ORIENTATION TEST DATA –

- Average % of Error of Mode Count from linear regression curve for all fill levels was 0.3675%.
- The average standard deviation in mode count distribution for all fill levels was 15.8 modes. For the empty tank the standard deviation in mode count was 8.6 modes. (See discussion on empty tank orientation sensitivity in section 3.0 of this report.)
- Average % of Error of Mass from Linear Regression curve for all fill levels was 1.1734%.

#### BASED ON THESE RESULTS, THE FOLLOWING CAN BE CONCLUDED –

- The gauging response with LH<sub>2</sub> approaches a linear relationship as predicted.
- It is seen that under dynamic fluid conditions, in which the fluid assumes (with time) ever changing positions within the tank, the RF gauging technique on the average provides a very good indication of mass.



- The January 1975 LH<sub>2</sub> testing again demonstrated the credibility of the RF gauging technique as applied to LH<sub>2</sub>.

## 2.4 LIQUID OXYGEN TESTS – FEBRUARY 3, 1975

To augment the Phase B LOX loading and orientation test data, additional LOX tests were performed in Phase C. The RF sweep speed used in the February 3, 1975 LOX tests was 30 milliseconds, the same as that of the Phase B LOX test. The Phase B cryogenic tank was used as the test tank during testing.

### 2.4.1 LOX TEST PROCEDURES

The test procedures with LOX were similar to those used with LH<sub>2</sub> in that the test tank was filled to approximately 95% of capacity with LOX and then both static and dynamic orientation testing was performed at approximately 10% intervals of mass. Static and Dynamic orientations involved the following conditions:

#### A. STATIC ORIENTATION TESTS

- Tank positioned and fluid allowed to come to rest at each position prior to taking data.
- Mass held constant.
- Data recorded at each 15° increment of orientation.

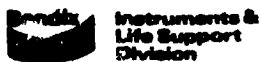
#### B. DYNAMIC ORIENTATION TESTS

- Continuous orientation of test tank back and forth (360°).
- Rate of rotation of tank approximately 6° per second.
- Mass held constant.
- Data recorded continuously.

### 2.4.2 LOX TEST RESULTS

#### 2.4.2.1 WEIGHT DETERMINATION

To establish the mass of LOX in the test tank during each incremental loading and orientation test, it was necessary to subtract out the tare weight measured with the tank completely empty and the fill hose disconnected. Although the majority of the tare weight



was nulled out during calibration, a residual tare weight had to be subtracted from the recorded data for weight. Table 2-9 summarizes the actual LOX weight increments at which the orientation tests were performed. Note that the volume of the test tank is capable of containing 2,243.16 pounds of LOX.

TABLE 2-9  
ACTUAL MASS LOADING (LOX)

Approx. Percent Loading	Scale Indication of Mass (Avg.) in Pounds	Tare Weight in Pounds	Actual Weight of LOX in Pounds
95	2124.90	5.87	2119.03
90	2022.72	"	2016.85
80	1801.42	"	1795.55
70	1577.10	"	1571.23
60	1349.60	"	1343.73
50	1125.00	"	1119.13
40	903.02	"	897.15
30	677.84	"	671.97
20	448.44	"	442.5
10	227.96	"	222.52
5	118.30	"	112.15
0	10.20	"	4.33

#### 2.4.2.2 ORIENTATION DATA -- DYNAMIC

The data from the dynamic orientation testing with LOX was first examined by calculating the mean mode count obtained for all orientations at each incremental mass loading. Table 2-10 summarizes the mean mode count obtained at each mass increment. Figure 2-18 contains a plot of the mean mode count versus percent loading of LOX, illustrating the characteristic non-linear loading curve.

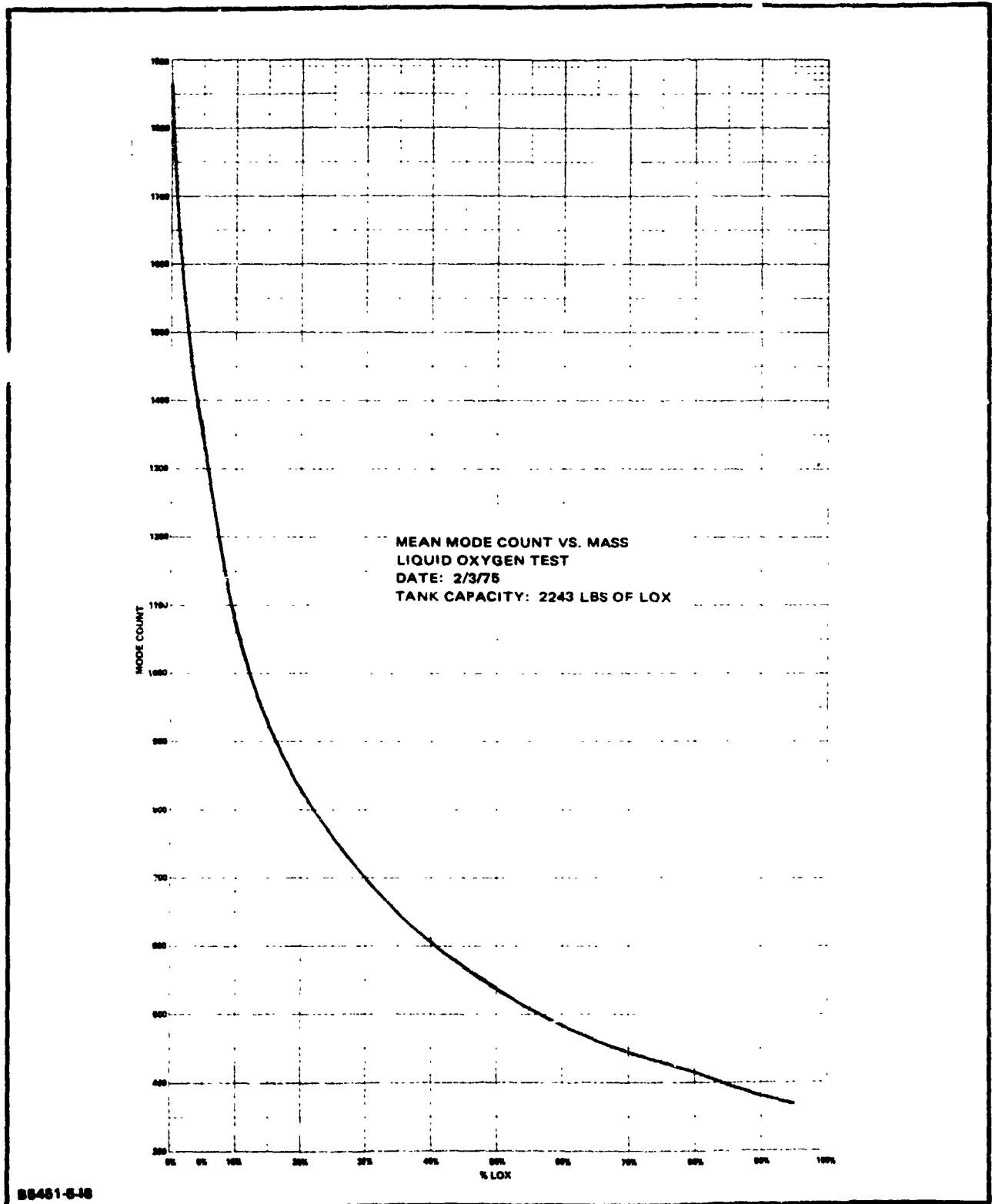


Figure 2-18

TABLE 2-10

MEAN MODE COUNT AND ACTUAL MASS  
AT INCREMENTAL LOADINGS OF LOX  
LOX TESTS - FEBRUARY 3, 1975

Approx. % Loading	Actual Mass (Pounds)	Mean Mode Count
95	2119.03	370.21
90	2016.85	378.43
80	1795.55	413.31
70	1571.23	456.36
60	1343.73	482.81
50	1119.13	541.91
40	1897.15	612.30
30	671.97	703.92
20	442.5	835.25
10	222.52	1070.34
5	112.15	1351.04
0	4.33	1863.45

#### 2.4.2.3 MULTI-SEGMENT NON-LINEAR REGRESSION FIT (DYNAMIC)

The data from the dynamic orientation testing with LOX has been examined to obtain a nonlinear regression curve of mean mode count. A polynomial fit of the curve was attempted. However, in order to make the fit as close as possible (thereby minimizing the residuals) the LOX curve was divided into three polynomial segments. (This permits a relative comparison to LOX tests conducted in 1974). The curves for each segment are of the form

$$Y = \beta_0 + \beta_1 X + \beta_2 X^2 + \beta_3 X^3 + \beta_4 X^4 \quad (14)$$

where

$Y$  = mass

$X$  = mode count

$\beta_0$  ..  $\beta_4$  are the coefficients of the regression polynomial.



Table 2-11 lists the coefficients for the three segments.

TABLE 2-11  
POLYNOMIAL COEFFICIENTS FOR LOX TEST  
(DYNAMIC DATA - FEB. 3-6, 1975 TEST)

Segment	Mass Range (lbs)	$\beta_0$	$\beta_1$	$\beta_2$	$\beta_3$	$\beta_4$
I	0-442.574	3126.64	-5.70493	0.364895E-02	-0.797773E-06	0.0
II	442.574-1343.73	4396.60	-7.97184	0.134261E-02	0.600516E-05	-0.355725E-08
III	1343.73-2119.03	24035.0	-112.53	0.932768E-01	0.297610E-03	-0.434190E-06

From the multi-segment polynomial, a percent of point mass error based on deviation of mean mode count from the polynomial can be calculated. Tables 2-12 thru 2-14 summarize the mass error.

TABLE 2-12  
SUMMARY OF POLYNOMIAL FIT-SEGMENT I  
(DYNAMIC DATA - FEB. 3-6, 1975 TEST)

Modes (Ave)	Actual Mass (lbs)	Calculated Mass (lbs)	% Error of Point
1863.45	4.334	4.38184	-1.09
1351.04	112.434	112.146	0.257
1070.34	222.094	222.521	-0.192
835.25	442.574	442.390	0.0415
Mean Error for estimate of mass = 0.335022 lbs			
Coefficient of correlation - 0.999999			



**TABLE 2-13**  
**SUMMARY OF POLYNOMINAL FIT - SEGMENT II**  
**(DYNAMIC DATA - FEB. 3-6, 1975 TEST)**

Modes (Ave)	Actual Mass (lbs)	Calculated Mass (lbs)	% Error of Point
835.25	442.5	442.699	-0.0282
703.92	671.974	671.515	0.0683
612.30	897.154	897.340	-0.0207
541.91	1119.13	1119.75	-0.0557
482.81	1343.73	1343.25	0.0356
Mean Error for estimate of mass = 0.483367 lbs Coefficient of correlation = 0.999999			

**TABLE 2-14**  
**SUMMARY OF POLYNOMINAL FIT - SEGMENT III**  
**(DYNAMIC DATA - FEB. 3-6, 1975 TEST)**

Modes (Ave)	Actual Mass (lbs)	Calculated Mass (lbs)	% Error of Point
482.81	1343.73	1349.07	-0.396
456.26	1571.23	1560.11	0.713
413.313	1795.55	1801.17	-0.312
378.43	2016.85	2032.28	-0.759
370.21	2119.03	2103.76	0.726
Mean Error for estimate of mass = 13.6271 lbs Coefficient of Correlation - 0.999190			

The percent mass error of full scale of the system can be arrived at for the dynamic testing by using the following:

$$\% \text{ Error (of full scale)} = \frac{\text{Actual Mass} - \text{Calculated Mass}}{\text{Full Tank Mass}} \times 100 \quad (15)$$

where full tank mass is 2,243.16 pounds of LOX, Table 2-15 summarizes the mass % error of full scale.

**TABLE 2-15**  
**SUMMARY OF MASS % ERROR OF FULL SCALE**  
**(DYNAMIC DATA - FEB. 3-6, 1975 TEST)**

Approximate % Loading	% Mass Error Of Full Scale
0	0.00213271
5	0.01283878
10	0.01903573
20	0.00557250
30	0.02046695
40	0.00829344
50	0.02764481
60	0.02139752
70	0.49573451
80	0.25054467
90	0.68786597
95	0.68073702
Average	0.18602205

#### 2.4.2.4 SINGLE-SEGMENT NON-LINEAR REGRESSION FIT

In addition to the multi-segment non-linear polynomial equation to fit the mean mode count versus mass data, a single-segment non-linear regression curve was also calculated for the dynamic orientation data. The single-segment non-linear regression curve is a four (4) degree polynomial of the form:

$$Y = \beta_0 + \beta_1 X + \beta_2 X^2 + \beta_3 X^3 + \beta_4 X^4 \quad (16)$$

where

$Y$  = mass

$X$  = mode count

$\beta_0 \dots \beta_4$  are the coefficients of the regression polynomial.



These coefficients are:

$$\beta_0 = 6762.44$$

$$\beta_1 = -19.3573$$

$$\beta_2 = 0.221144E-01$$

$$\beta_3 = -0.114314E-04$$

$$\beta_4 = 0.219705E-08$$

It is noted that the coefficient of correlation for the single-segment polynomial fit is 0.999401. A summary of the single-segment polynomial fit is shown in Table 2-16.

This single segment polynomial fit serves to illustrate one potential means of using the detected mode count to establish mass. It is noted that the multi-segment polynomial naturally provided a better correlation to actual mass. In either case, the mass errors are low.

#### 2.4.2.5 MASS ERROR – STATISTICAL ANALYSIS

A percent mass error of the gauging system can also be arrived at using the standard deviation of the mode count. This was done by using the  $\pm 1 \sigma$  distribution in mode count in conjunction with the calculated linear regression equations to calculate mass error. Recall that in calculating the best fit non-linear regression curve for LOX, two solutions were presented. These solutions were first, a multi-segment polynomial equation, and second, a single-segment polynomial equation. Using the coefficients for each of the equations, mass may be calculated from the  $\pm \sigma$  indications of mode count. From these results the percent mass error of full scale for the system is then calculated as:

$$\% \text{ error} = \frac{\text{Actual Mass} - \text{Calculated Mass}}{\text{Full Tank Mass}} \times 100\%. \quad (17)$$

Tables 2-17 and 2-18 show the mass error summaries of percent fill versus error for the multi-segment and the single-segment non-linear regression curves. It is noted that with the multi-segment non-linear



TABLE 2-16  
SUMMARY OF SINGLE SEGMENT POLYNOMIAL FIT  
(DYNAMIC DATA - FEB. 3-6, 1975)

MODES (AV)	ACTUAL MASS IN POUNDS	CALCULATED MASS IN POUNDS	DIFFERENCE IN POUNDS	% ERROR OF POINT	% ERROR OF FULL SCALE
1863.45	4.334	4.750	-0.416	-8.76	0.0185
1351.04	112.434	105.169	7.265	6.91	0.3238
1070.34	222.094	244.744	-22.650	-9.25	1.0097
835.25	442.574	430.427	12.147	2.82	0.5415
703.92	671.974	646.463	25.511	3.95	1.1373
612.30	897.154	885.576	11.578	1.31	0.5161
541.91	1119.13	1137.08	-17.946	-1.58	0.8002
482.81	1343.73	1404.38	-60.645	-4.32	2.7038
456.36	1571.23	1543.02	28.215	1.83	1.2576
413.31	1795.55	1796.58	-1.025	-0.06	0.0459
378.43	2016.85	2029.60	-12.471	-0.63	0.5684
370.21	2119.03	2088.33	30.699	1.47	1.3686
AVERAGE					0.8576



TABLE 2-17  
MASS ERROR BASED ON STANDARD DEVIATION OF MODE COUNT  
AS CALCULATED FROM MULT SEGMENT POLYNOMINAL EQUATIONS

POLYNOMIAL SEGMENT	APPROX % FILL	MEAN MODE COUNT	STANDARD DEVIATION	MODE COUNT $\pm \sigma$	ACTUAL MASS (LBS)	CALCULATED MASS	MASS % ERROR
I	0	1866.54	9.95	1876.49 1856.59	4.334	-1.173 7.212	0.245 -0.128
	5	1351.04	14.50	1365.54 1336.54	112.434	109.137 115.340	0.147 -0.129
	10	1070.34	10.88	1081.22 1059.46	222.094	215.737 229.569	0.283 -0.333
	20	835.25	9.42	844.67 825.83	442.57	430.490 454.588	0.538 -0.536
	30	703.92	8.89	712.81 695.03	671.94	652.951 690.613	0.846 0.197
	40	612.30	10.12	622.42 602.18	897.15	869.039 926.523	1.253 -1.308
II	50	541.78	11.70	553.48 530.08	1119.13	1080.007 1161.721	1.744 -1.899
	60	482.83	10.87	493.70 471.96	1343.73	1299.443 1388.081	1.974 -1.977
	70	456.36	14.19	470.55 442.17	1571.23	1458.020 1645.816	5.047 -3.325
	80	413.31	12.28	425.59 401.03	1795.55	1735.340 1872.695	2.684 -3.439
	90	378.43	11.37	389.80 367.06	2016.85	1946.293 2133.684	3.146 -5.209
	95	370.21	8.49	378.70 361.72	2119.03	2030.281 2187.270	3.957 -3.042



TABLE 2-18

MASS ERROR BASED ON STANDARD DEVIATION OF MODE COUNT  
AS CALCULATED FROM SINGLE SEGMENT POLYNOMINAL EQUATION

APPROX % FILL	MEAN MODE COUNT	STANDARD DEVIATION	MODE COUNT $\pm \sigma$	ACTUAL MASS (LBS)	CALCULATED MASS	MASS % ERROR
0	1866.54	9.95	1876.49 1856.59	4.334	16.059 -1.202	-0.523 0.246
5	1351.04	14.50	1365.54 1336.54	112.434	97.325 112.621	0.674 -0.008
10	1070.34	10.88	1081.22 1059.46	222.094	238.943 250.474	-0.751 -1.265
20	835.25	9.42	844.67 825.83	442.57	419.116 442.095	1.046 0.021
30	703.92	8.89	712.81 695.03	671.94	627.648 665.908	1.975 0.269
40	612.30	10.12	622.42 602.18	897.15	854.625 917.703	1.896 -0.916
50	541.78	11.70	553.48 530.08	1119.13	1091.038 1186.149	1.252 -2.988
60	482.83	10.87	493.70 471.96	1343.73	1350.831 1459.723	-0.316 -5.171
70	456.36	14.19	470.55 442.17	1571.23	1467.069 1622.636	4.644 -2.292
80	413.31	12.28	425.59 401.03	1795.55	1720.557 1875.680	3.343 -3.572
90	378.43	11.37	389.80 367.06	2016.85	1950.781 2111.229	2.945 -4.208
95	370.21	8.49	378.70 361.72	2119.03	2027.676 2150.582	4.073 -1.407



regression solution, the average mass % error based on standard deviation of mode count from the 0 thru 50% LOX loading is 0.685% and from the 0 thru 100% LOX loading it is 1.81%. Similarly, in the case of the single-segment non-linear regression solution, the average mass % error based on standard deviation of mode count from the 0 thru 50% LOX loading is 0.988% and from the 0 thru 100% LOX loading it is 1.91%. Plots of each respective  $\pm\sigma$  error are shown in Figures 2-19 and 2-20.

#### 2.4.2.6 DATA DISTRIBUTION TEST

The question of the distribution of the mode counts at each fill level during the dynamic LOX orientation testing has been examined by application of the Kolmogorov-Smirnov tests for normal distribution and uniformity. Table 2-19 summarizes the results of the Kolmogorov-Smirnov tests for normal distribution and uniformity at each incremental level of LOX. It is significant to note that the data does approach a normal distribution. (Testing for a bivariate normal is not applicable, since mode count is univariate statistic.) It is also noted that the distribution is not uniform in the statistical sense.

TABLE 2-19  
KOLMOGOROV-SMIRNOV TEST FOR  
NORMAL DISTRIBUTION AND UNIFORMITY  
(DYNAMIC LOX ORIENTATION DATA)

% LOADING	TEST FOR NORMAL		TEST FOR UNIFORMITY	
	TEST STATISTIC	P(ACCPT/NULL TRUE)	TEST STATISTIC	P(ACCPT/NULL TRUE)
95	0.68845	0.7304E00	1.35405	0.5111E-01
90	0.65102	0.7904E00	1.90000	0.1464E-02
80	0.61244	0.8474E00	2.30648	0.4786E-04
70	0.56843	0.9031E00	2.43134	0.1466E-04
60	0.55123	0.9216E00	2.29148	0.5496E-04
50	0.74718	0.6319E00	3.05324	0.0000E00
40	0.63296	0.8179E00	2.43019	0.1478E-04
30	1.05544	0.2152E00	1.20769	0.1082E00
20	0.74958	0.6279E00	3.10000	0.0000E00
10	0.82460	0.5047E00	2.03158	0.5201E-03
5	0.68440	0.7370E00	1.32295	0.6037E-01
0	0.67532	0.7518E00	1.72866	0.5075E-02

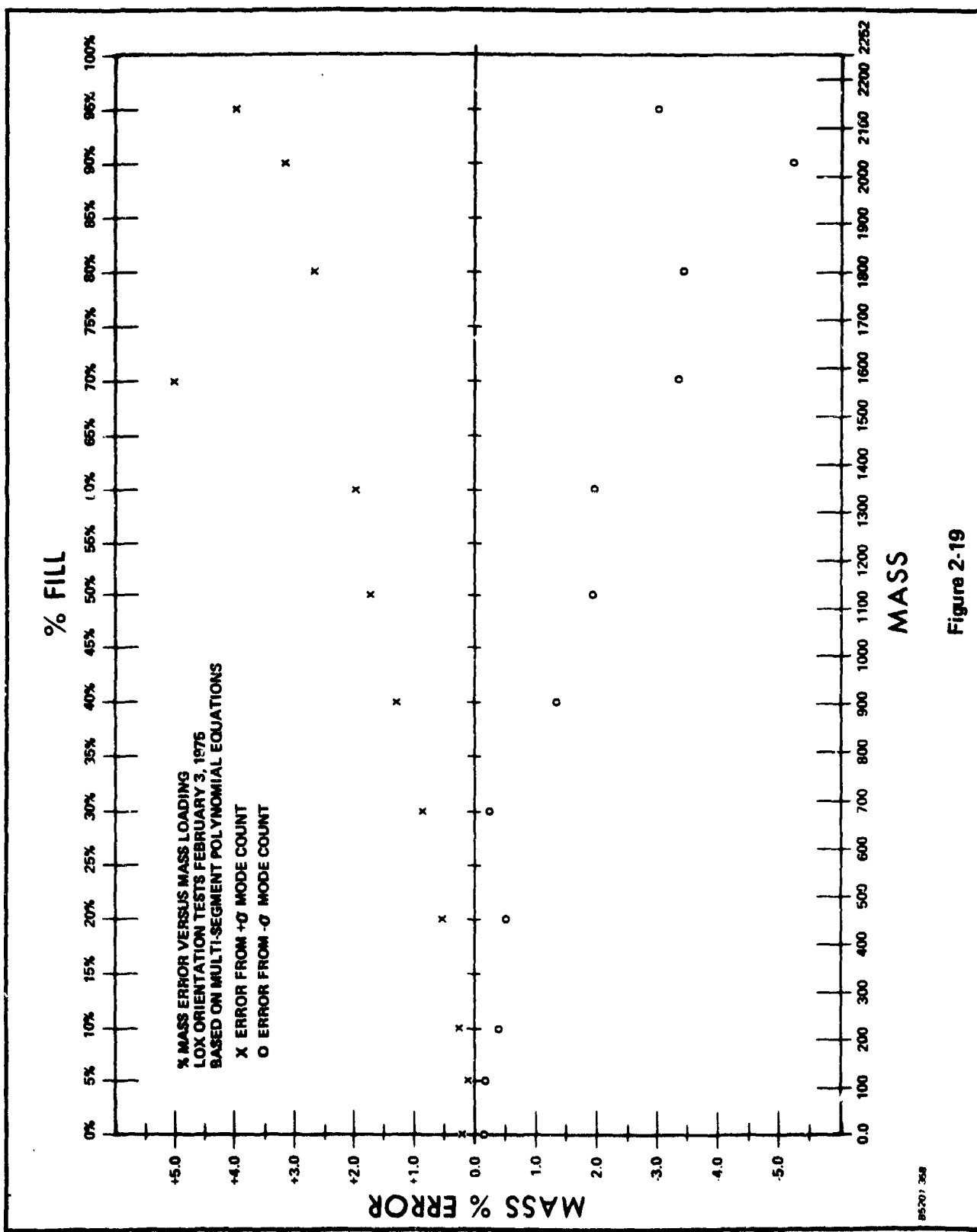


Figure 2-19

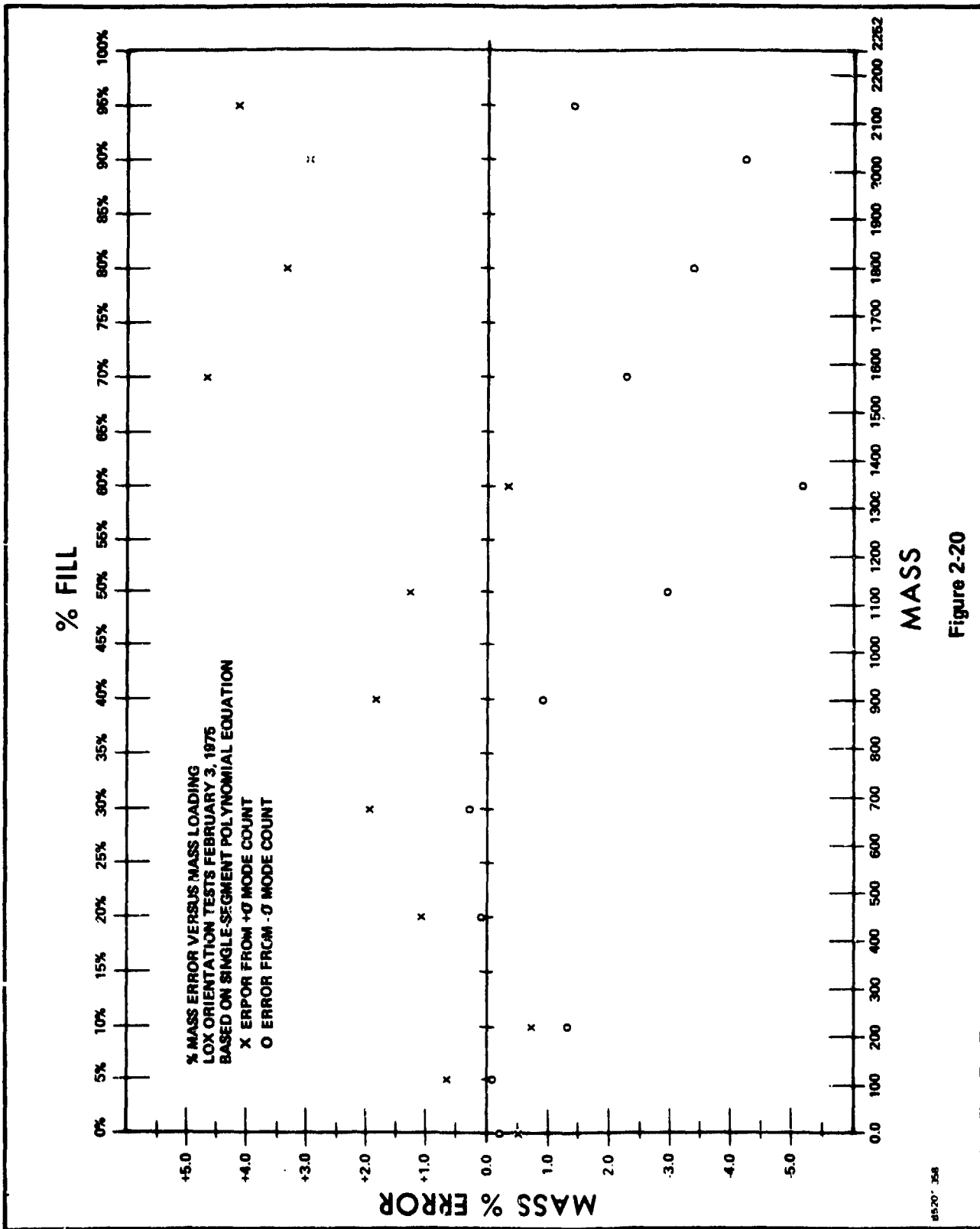


Figure 2-20

8520-358



#### 2.4.2.7 COMPUTER GENERATED PLOTS

Computer plots of the data from the February 3, 1975, LOX tests have been made of the following:

- Frequency of occurrence vs. mode count at each mass increment (DYNAMIC).
- Mode count vs. orientation angle at each mass increment (DYNAMIC).
- Frequency of occurrence vs. mode count at each mass increment (STATIC).
- Mode count vs. orientation angle at each mass increment (STATIC).

These plots are presented in Appendix B of this report.

#### 2.4.2.8 SUMMARY – LOX TEST RESULTS, FEBRUARY 3, 1975

From the data obtained with LOX using the Breadboard RF mode counting system, the following was observed:

- The mean mode count vs. mass loading response was the characteristic non-linear function anticipated with LOX.
- The average mass error using a multi-segment polynomial equation of calculated mass knowing mean mode count was 0.1860 percent of full scale.
- Calculations of mass error based on the standard deviation of mode count distribution at each increment of mass and using a multi-segment polynomial equation to calculate mass, resulted in an average mass percent error from 0 thru 50% LOX loadings of 0.685% and from 0 thru 100% LOX loading of 1.81%.
- A single-segment polynomial equation could be used to define the loading response curve. The average mass error using this polynomial equation to calculate mass knowing mean mode count was 0.8576 percent of full scale.
- Calculations of mass error based on the standard deviation of mode count distribution at each increment of mass, and using a single-segment polynomial to calculate mass, resulted in an average mass percent error from 0 thru 50% LOX loadings of 0.988% and from 0 thru 100% LOX loadings of 1.91%.



- It is significant to note that the distribution of the mode count data at each fill level during dynamic LOX orientation testing does approach a statistical normal distribution.

Based on these results, the following can be concluded:

- The gauging response with LOX fits a non-linear polynomial function as predicted.
- The February 3, 1975 LOX testing again demonstrated the credibility of the RF gauging technique as applied to LOX.

## 2.5 LIQUID OXYGEN TESTS – FEBRUARY 10, 1975

To supplement the February 3, 1975 LOX loading and orientation tests a second set of LOX tests were performed, wherein basic test parameter were left unchanged except for the RF sweep speed. This was slowed down from 30 milliseconds to 300 milliseconds. The R-C time constants in the RF mode-counting processor were adjusted to permit the processing of the resulting lower frequency mode pattern.

### 2.5.1 LOX TEST PROCEDURES

Test procedures for the February 10, 1975 LOX testing were identical to those of February 3, 1975, as defined in section 2.4.1. It included a loading to approximately 95% and both static and dynamic orientation testing at incremental LOX mass loading.

### 2.5.2 LOX TEST RESULTS

#### 2.5.2.1 WEIGHT DETERMINATION

As in the previous tests, to establish the mass of LOX in the test tank during each incremental loading and orientation test, it was necessary to subtract out the tare weight measured with the tank completely empty and the fill hose disconnected. Table 2-20 summarizes the actual LOX weight increments at which the orientation tests were performed.

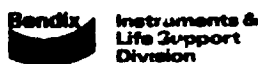
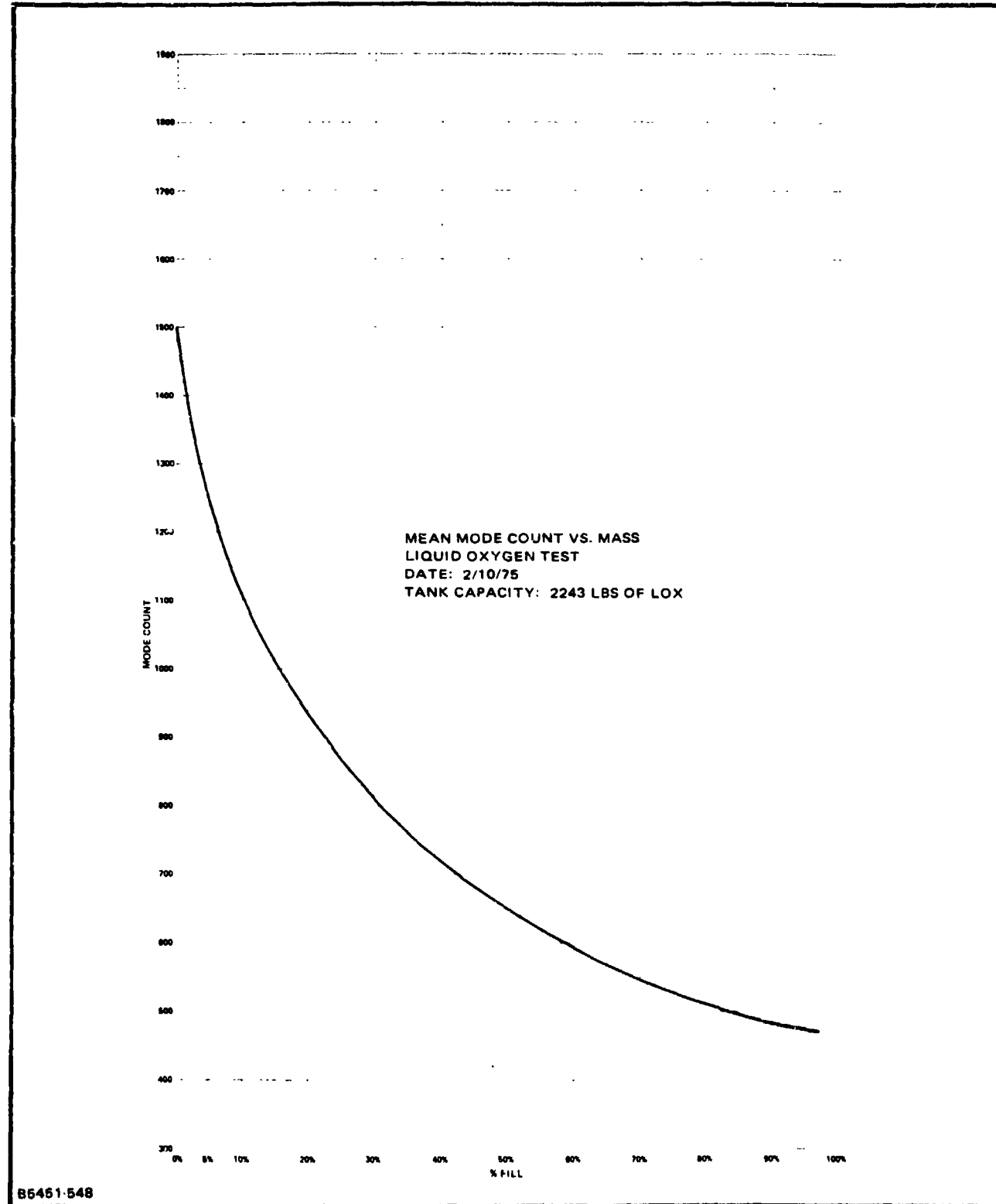


TABLE 2-20  
ACTUAL MASS LOADING (LOX)

Approx. Percent Loading	Scale Indication of Mass (Avg) in pounds	Tare Weight in Pounds	Actual Weight of LOX in Pounds
95	2173.74	6.6	2167.14
90	1982.28	"	1975.68
80	1800.22	"	1793.62
70	1579.34	"	1572.74
60	1353.18	"	1346.58
50	1128.32	"	1121.72
40	901.60	"	895.00
30	677.52	"	670.92
20	450.92	"	444.32
10	231.26	"	224.66
5	119.04	"	112.44
0	9.90	"	3.30

#### 2.5.2.2 ORIENTATION DATA - DYNAMIC

The mean mode count obtained for all orientations at each incremental mass loading is summarized in Table 2-21. Figure 2-21 contains a plot of the mean mode count versus percent loading of LOX. It is noted when compared to Figure 2-18, that the detected mode count is lower at the empty and low LOX quantities since a majority of the mode ringing was eliminated by going to a slower sweep speed. However, with the readjustment of the R-C time constants in the mode processor, a higher detected mode count was obtained as the LOX mass loading approached the full tank. The net result was a loading curve whose sensitivity ( $\Delta$  modes/ $\Delta$  mass) was smaller than that of the February 3, 1975 LOX tests.



**Figure 2-21**

TABLE 2-21  
MEAN MODE COUNT AND ACTUAL MASS  
AT INCREMENTAL LOADINGS OF LOX  
LOX TESTS - FEBRUARY 10, 1975

APPROX. % LOADING	ACTUAL MASS (POUNDS)	MEAN MODE COUNT
95	473.20	2167.14
90	487.70	1975.68
80	514.87	1793.62
70	555.42	1572.74
60	599.49	1346.58
50	655.22	1121.72
40	720.20	895.00
30	811.90	670.92
20	941.03	444.32
10	1119.66	224.66
5	1257.54	112.44
0	1501.82	3.30

#### 2.5.2.3 MULTI-SEGMENT NON-LINEAR REGRESSION FIT (DYNAMIC)

Using the average mode count data obtained during the dynamic orientation testing in conjunction with the measured actual mass figures for each incremental loading of LOX, a best fit non-linear regression curve was calculated. For comparative purposes, the data was first fitted to a multi-segmented non-linear regression curve. Table 2-22 lists the polynominal coefficients for each respective segment, and Table 2-23 contains a summary of this segmented polynomial fit, illustrating mass error based on use of the polynomial.



TABLE 2-22

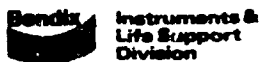
POLYNOMIAL COEFFICIENTS FOR SEGMENTED FIT  
TO LOX DYNAMIC TEST DATA – FEBRUARY 10-12, 1975

Segment	Mass Range (Lbs)	$\beta_0$	$\beta_1$	$\beta_2$	$\beta_3$	$\beta_4$
I	0 - 670.92	3667.25	- 5.48169	0.2169E-02	0.2088E-06	0.0703E-09
II	670.92-1572.74	6825.79	-14.1089	0.906E-02	-0.125E-05	---
III	1572.74-2167.14	20455.2	-70.2051	0.748E-01	-0.1729E-04	---

TABLE 2-23

SUMMARY OF MULTI-SEGMENT POLYNOMIAL FIT  
(DYNAMIC LOX DATA – FEB. 10-12, 1975)

SEGMENT	MODES (AVG)	ACTUAL MASS (LBS)	CALCULATED MASS (LBS)	% ERROR OF POINT	% ERROR OF FULL SCALE
I	1501.82	3.3	3.27393	0.796	0.0012
	1257.54	112.44	112.785	-0.306	0.0154
	1119.66	224.66	223.890	0.344	0.0344
	941.03	444.32	445.132	-0.182	0.0362
II	811.90	670.92	671.217	-0.0442	0.0132
	720.20	895.000	895.052	-0.00578	0.0023
	655.22	1121.72	1117.94	0.338	0.1685
	599.49	1346.58	1353.36	-0.501	0.3023
III	555.42	1572.74	1575.58	-0.180	0.1266
	514.87	1793.62	1778.66	0.841	0.1266
	487.7	1975.68	2002.77	-1.35	1.2077
	473.20	2167.14	2152.16	0.696	0.6678
AVERAGE					0.2702



#### 2.5.2.4 SINGLE-SEGMENT NON-LINEAR REGRESSION FIT (DYNAMIC)

The same data was also fitted to a single segment polynomial. The coefficients of this polynomial are:

$$\beta_0 = 10304.1$$

$$\beta_1 = -30.8922$$

$$\beta_2 = 0.379101E-01$$

$$\beta_3 = -0.216717E-04$$

$$\beta_4 = 0.471736E-08.$$

A summary of this polynomial fit is given in Table 2-24. The coefficient of correlation for this polynomial fit is 0.999606.

#### 2.5.2.5 SUMMARY – LOX TEST RESULTS, FEBRUARY 10, 1975

From the data obtained with LOX using the breadboard RF mode counting system, the following was observed during the February 10, 1975 LOX tests:

- Changing the RF sweep speed and R-C time constants in the mode count processor will, as expected, affect the detected RF mode count. Optimization of these parameters is important.
- The average mass error (of full scale) using a best-fit multi-segment polynomial equation to calculate mass knowing mean mode count was 0.2702 percent.
- The average mass error (of full scale) using a best-fit single-segment polynomial equation to calculate mass knowing mean mode count was 0.5790 percent.



TABLE 2.24  
SUMMARY OF SINGLE SEGMENT POLYNOMIAL FIT  
(DYNAMIC DATA - FEB. 10-12, 1975)

MODES (AV)	ACTUAL MASS IN POUNDS	CALCULATED MASS IN POUNDS	DIFFERENCE IN POUNDS	% ERROR OF POINT	% ERROR OF FULL SCALE
1501.82	3.300	3.660	-0.360	-9.84	0.0165
1257.54	112.440	106.527	5.913	5.55	0.2636
1119.66	224.660	235.324	-10.664	-4.53	0.4754
941.03	444.320	444.302	0.018	0.04	0.0008
811.90	670.920	663.719	7.201	1.08	0.3210
720.20	895.000	892.566	2.434	0.27	0.1085
655.22	1121.72	1111.57	10.147	0.91	0.4525
599.49	1346.58	1349.14	-2.559	-0.19	0.1141
555.42	1572.74	1576.57	-3.834	-0.24	0.1707
514.87	1793.62	1821.88	-28.256	-1.55	1.2598
487.70	1975.68	2007.92	-32.239	-1.61	1.4373
473.20	2167.14	2114.93	52.212	2.47	2.3275
AVERAGE					0.5790



### 3.0 EMPTY TANK ORIENTATION SENSITIVITY

In the March 1974, LH<sub>2</sub> tests, it was noted that the RF system output exhibited some sensitivity to orientation of the test tank even when the tank was completely empty. This indicated that either the breadboarded RF signal processing electronics, the RF sweep oscillator, or the test tank was causing the variations. An examination of each of these parts of the test system was then conducted to ascertain the cause and to eliminate it.

#### 3.1 CAUSE OF EMPTY TANK ORIENTATION SENSITIVITY

Initial examination and test of the RF signal processing electronics and RF sweep generator indicated both were not significantly sensitive to orientation position. Orientation tests were then performed with the empty test tank utilizing the output of each respective RF probe element of the multi-element probe assembly, and also with all four probe elements operating sequentially. In each case, the test tank was pressurized with 0, 10, 20 and finally 30 psig using N<sub>2</sub> gas. X-Y plots of mode count versus angular position of the test tank for each combination are shown in Figures 3-1 thru 3-5. From these plots it was evident that:

- The mode count decreased when the tank was pressurized for all angles of orientation.
- For individual antennas there was a variance in mode count for different angles of orientation.
- In each plot it can be seen that the mode count dropped drastically when the tank was pressurized to 30 psi and the orientation angle was approximately +90°. This position corresponds to the probe assembly and hatch of the tank being straight up.
- There was also a marked drop in mode count at an orientation angle of -90° when the tank was pressurized to 30 psi.

Observations of the mode pattern as the test tank was pressurized indicated that the modes tended to merge together as pressure was applied. This indicated that the Q of the system was apparently decreasing as pressure was applied. An illustration of a segment of the mode pattern under conditions of 0 psig and 30 psig is shown in Figure 3-6.

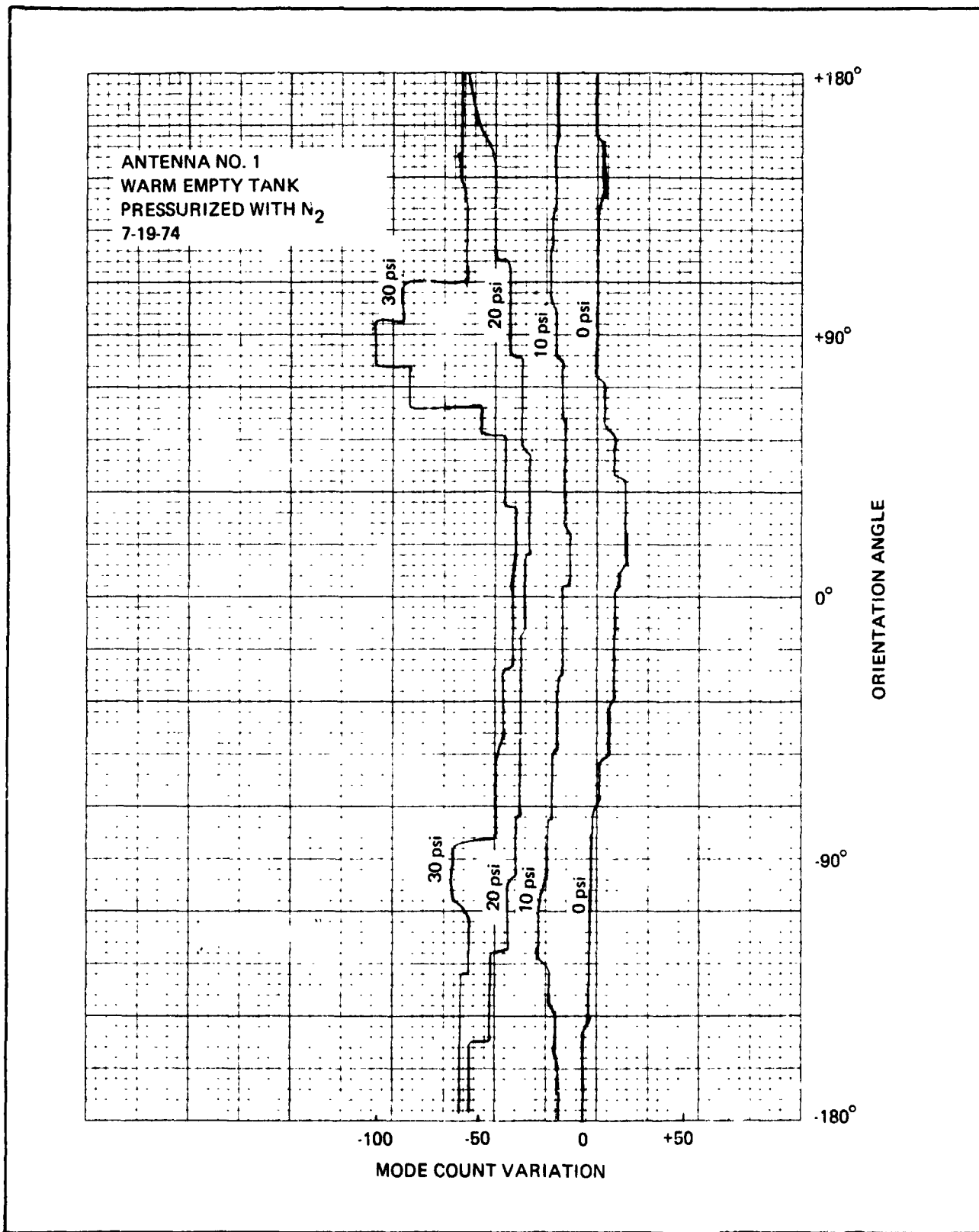
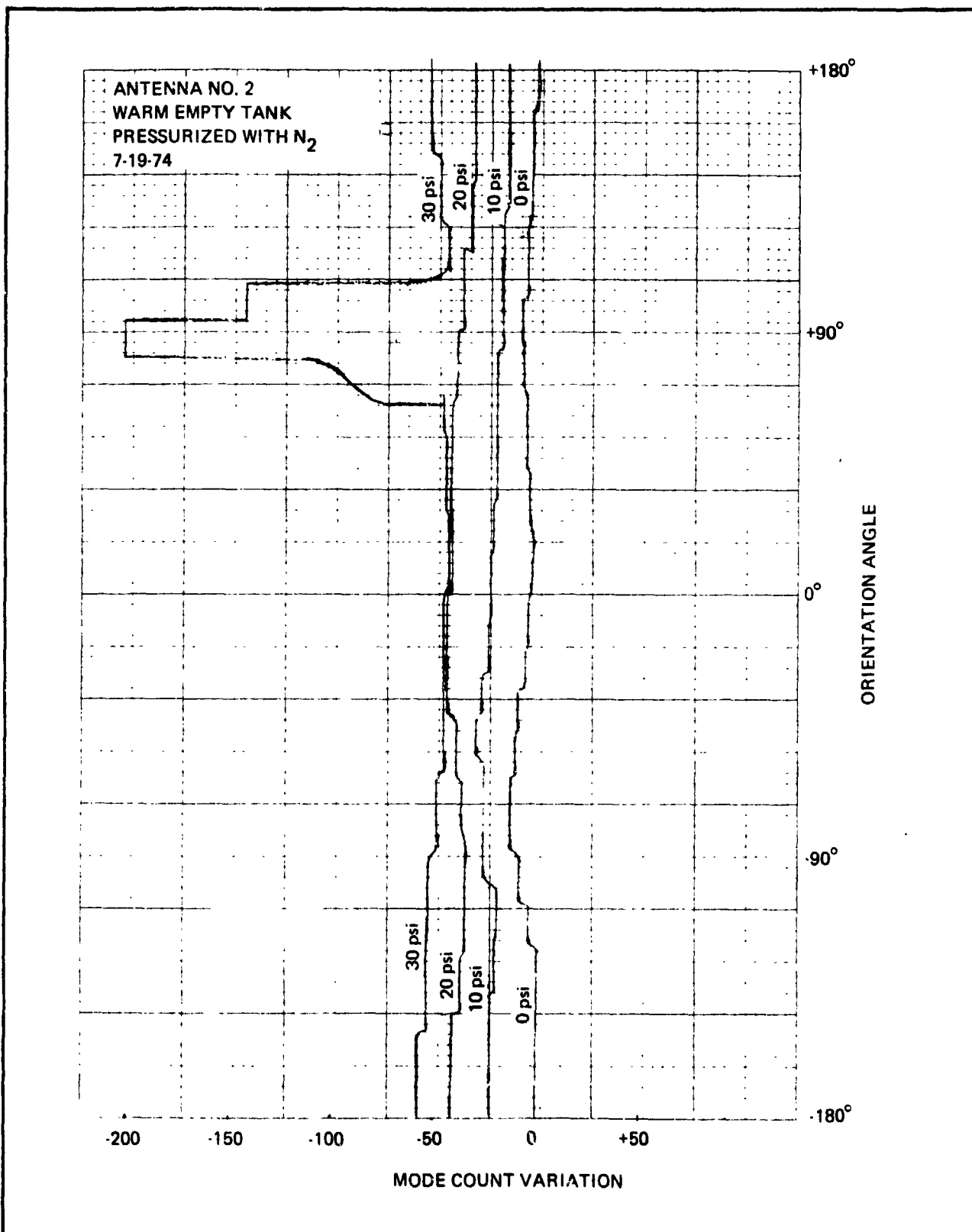


Figure 3-1



**Figure 3-2**

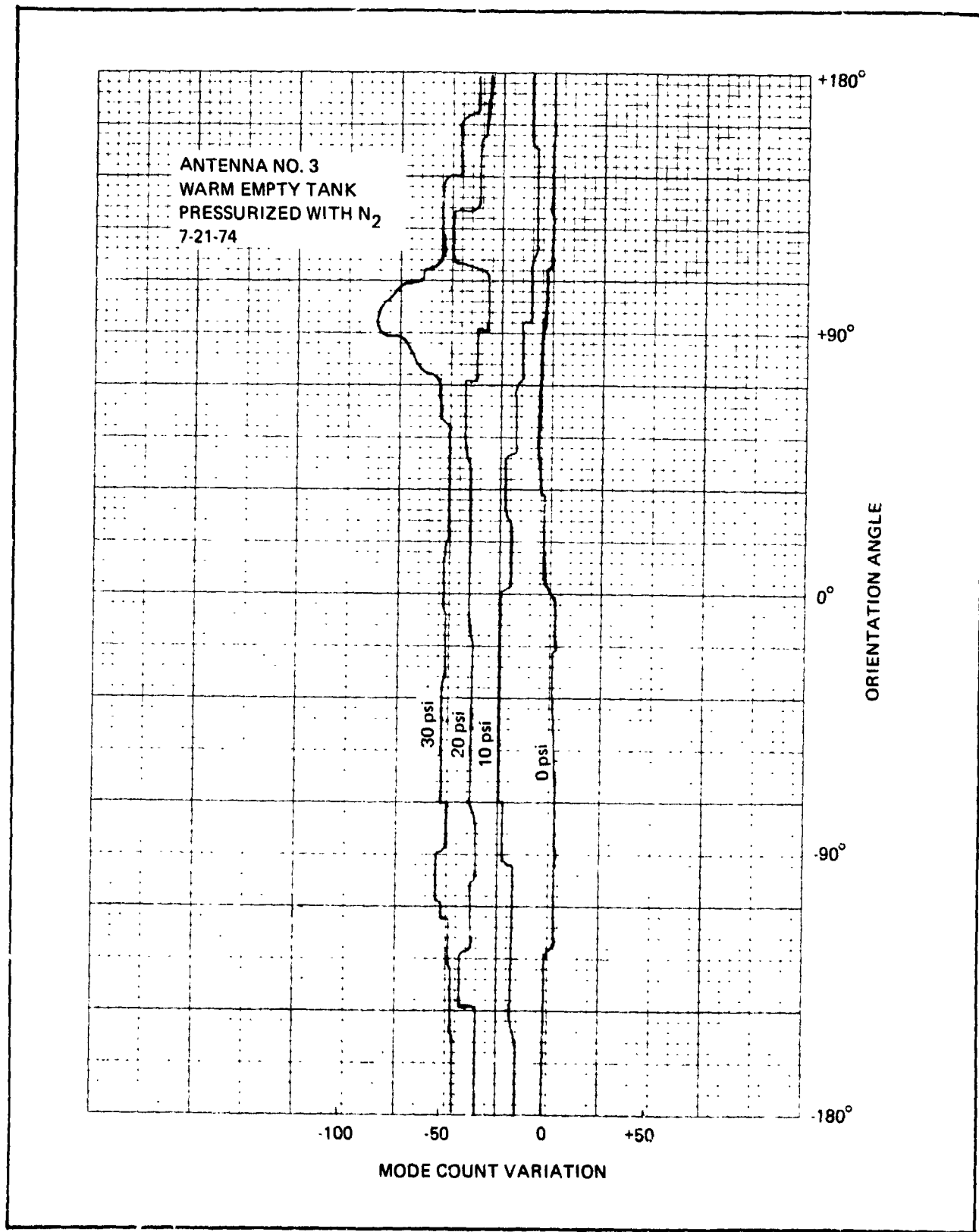
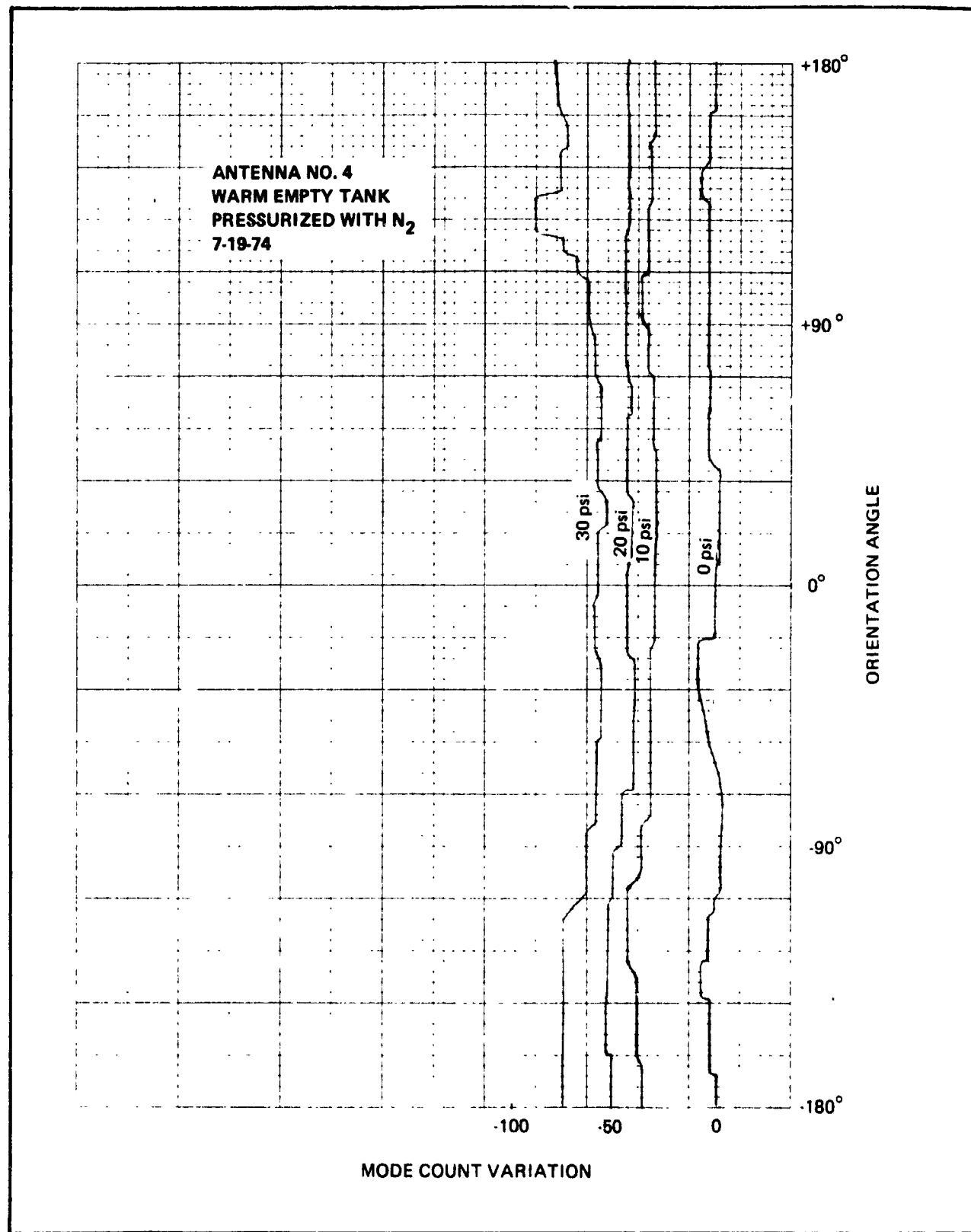


Figure 3-3



**Figure 3-4**

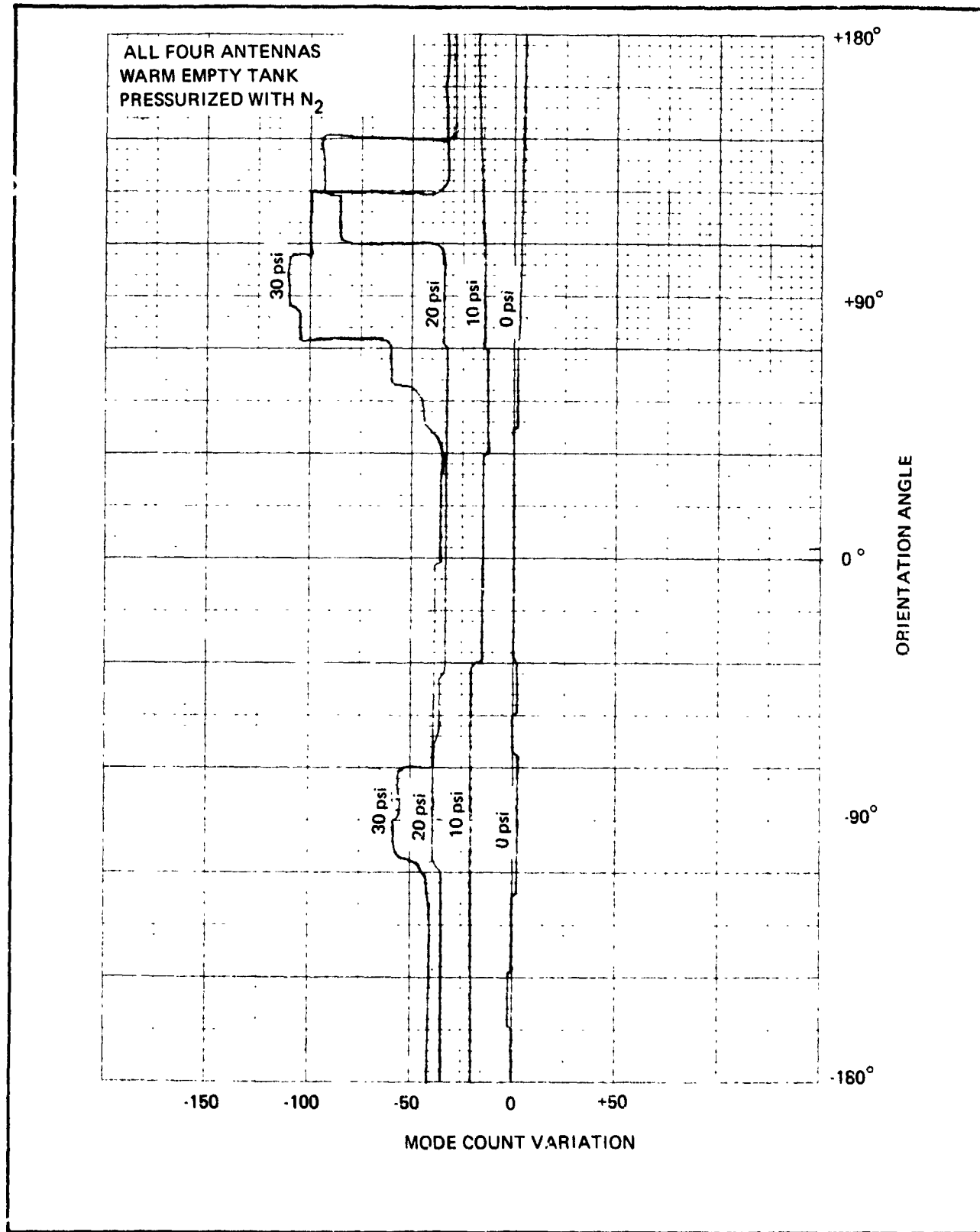


Figure 3-5

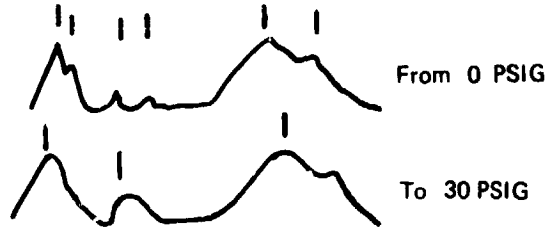


Figure 3-6  
MODE PATTERN CHANGE WITH LOW PRESSURE

From these results it was apparent that the problem was due to mechanical changes in the antenna structure or in the tank itself. To ascertain the nature of this problem, it was necessary to release the vacuum between the inner pressure vessel and the outer vessel, and to remove the outer vessel access cover (P/N 1626829). An X-Y plot of the RF mode count vs. orientation without the cover was made. The tank was oriented back and forth while pressurized with various increments of pressure ranging from 0 to 30 psig. Nitrogen gas was used as a pressurant. Figure 3-7 shows the test results, indicating a variation in mode count of up to 50 modes out of 1360 modes nominal for the empty tank.

Since the variation in mode count could be induced by pressurization of the tank, it was suspected that the pressure vessel closure and probe assembly P/N 1627189 (Figure 3-8) was moving relative to the pressure vessel fitting P/N 1626821 (Figure 3-9). Since the antenna elements are all mounted on the pressure vessel closure and probe assembly, the density of RF surface currents is relatively high in the areas around the mating threads of the closure. An opening or closing of the gap between mating threads as pressure was applied or removed could change the effective resistivity at the threaded area, and hence change the Q of the tank. This would appear as a change in the mode count. To verify if the threaded closure was indeed the problem, two tests were performed. The first involved the pressurization of the test tank from 0 to 45 psig while in a vertical position as shown in Figure 3-10. Figure 3-11 shows an X-Y plot of RF mode count vs. pressure. Note that the total excursion in mode count was approximately 75 modes. The same test was then repeated but in this case an external force was applied to the center of the

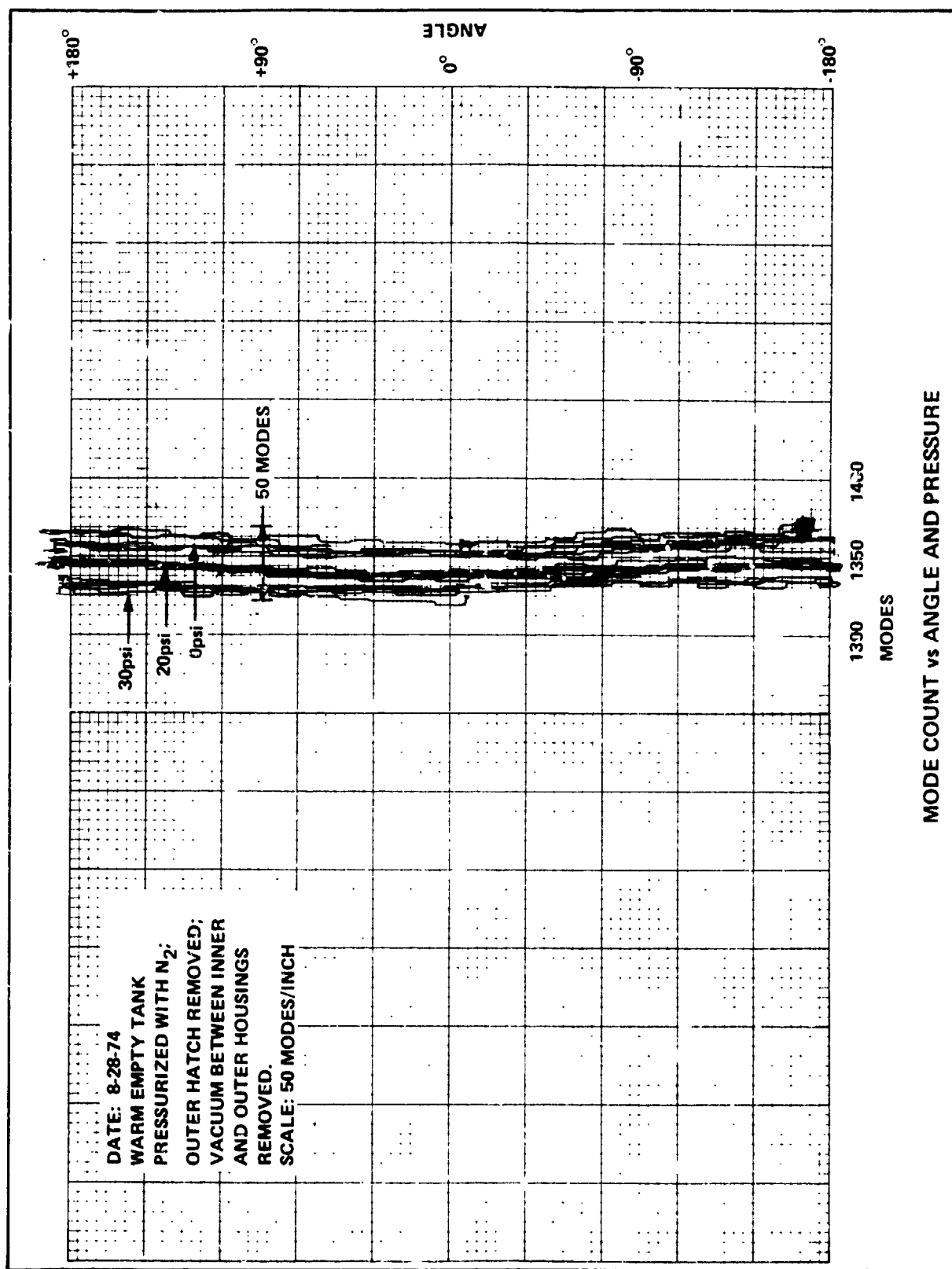


Figure 3-7

CLOSURE - PRESSURE VESSEL - ASSEMBLY

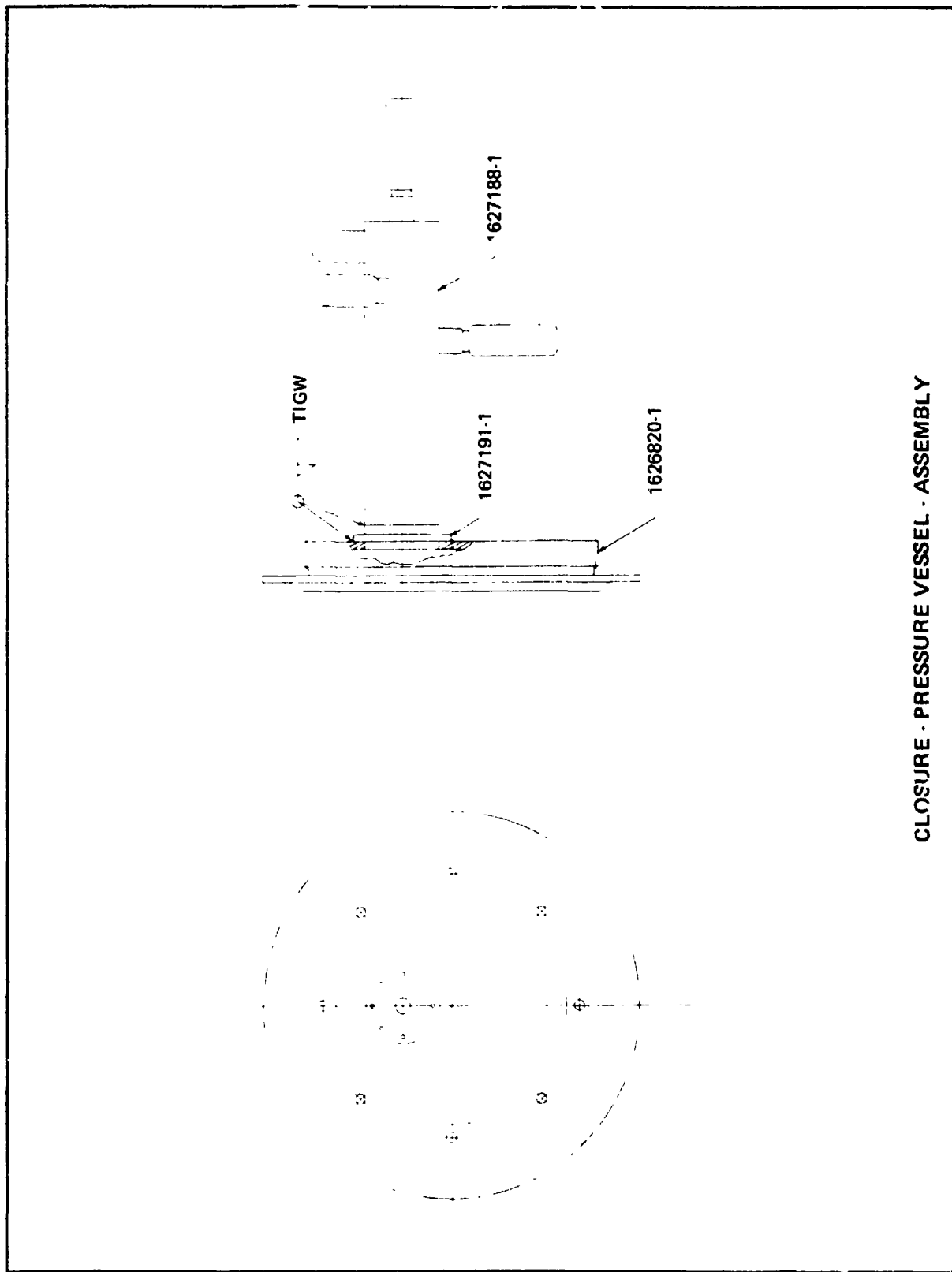
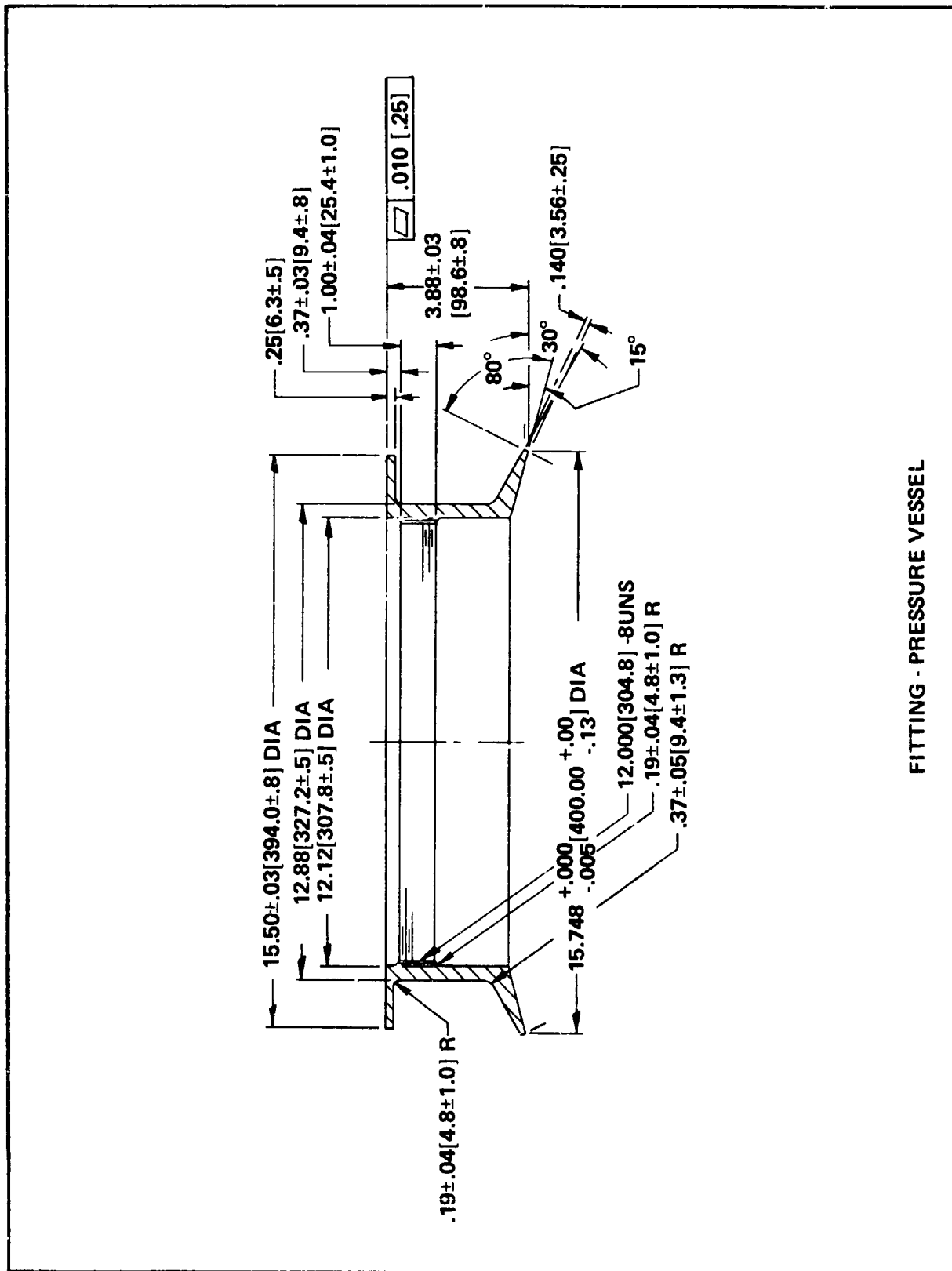


Figure 3-8



FITTING - PRESSURE VESSEL

Figure 3.9



TOP OF TEST TANK

Figure 3-10

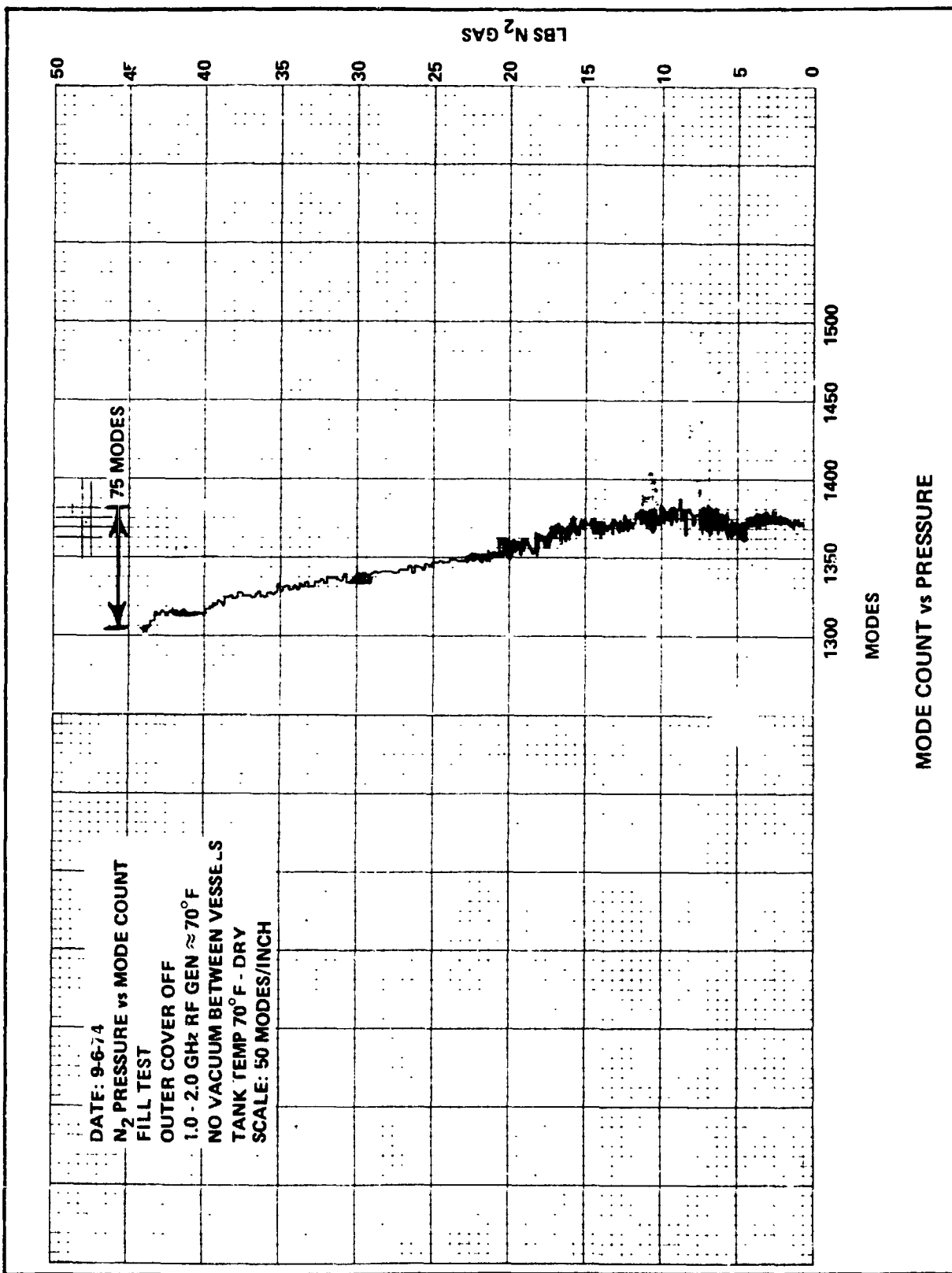


Figure 3-11

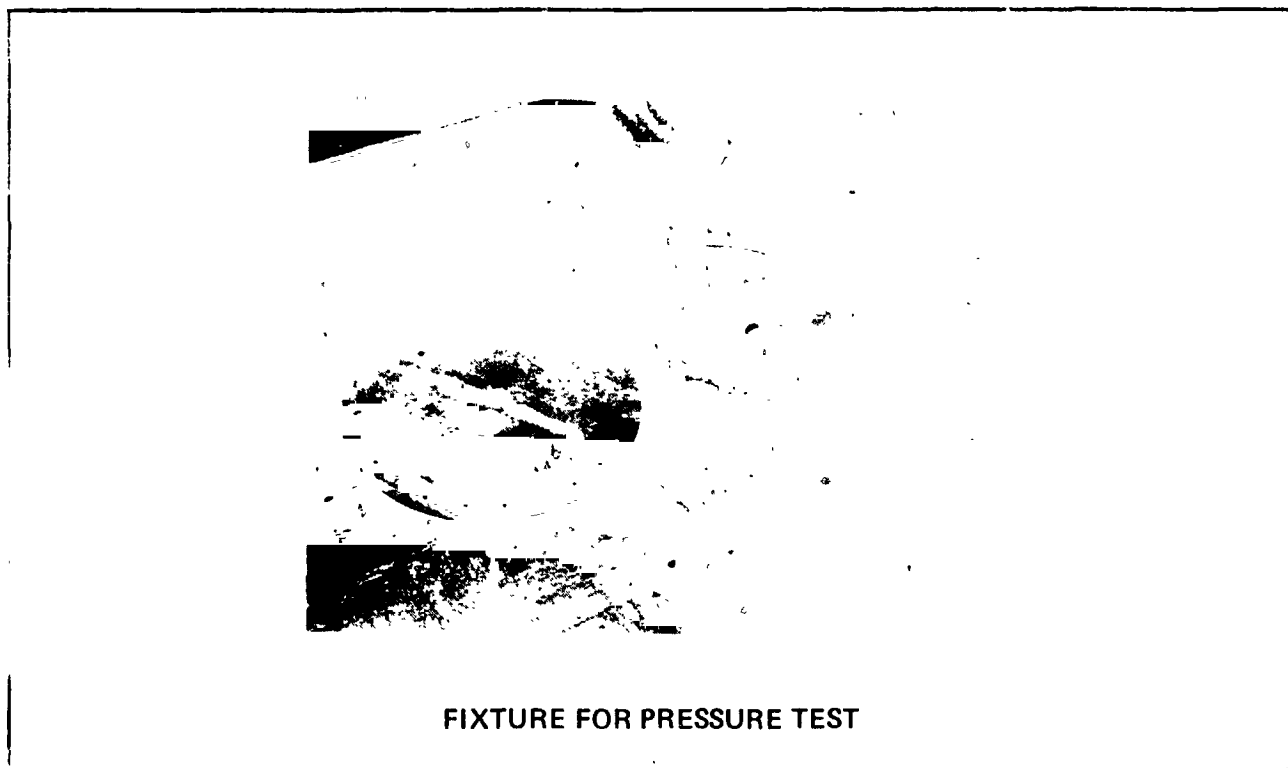


pressure vessel closure and probe assembly P/N 1627189. Applying a sufficient outside force at this position should tend to partially restrict motion due to changes in pressure. Figure 3-12 shows the fixture which was used to apply the outside counter-force. This fixture consisted of a donut shaped spacer and a thick plate cover which were bolted to the outer vessel hatch. In the center of the flat plate a large bolt was screwed into a mating threaded hole. Figure 3-13 shows the fixture mounted on the tank. The counter-force was applied by advancing the bolt. Figure 3-14 shows the X-Y plot of the RF mode count vs. pressure with the fixture in place. In this case the mode count changed by only 30 modes. These test results indicate that the empty tank orientation and pressurization problem was indeed due to a relative movement between the mating threads of the access hatch of the pressure vessel.

### 3.2 CRYOGENIC TANK RE-WORK

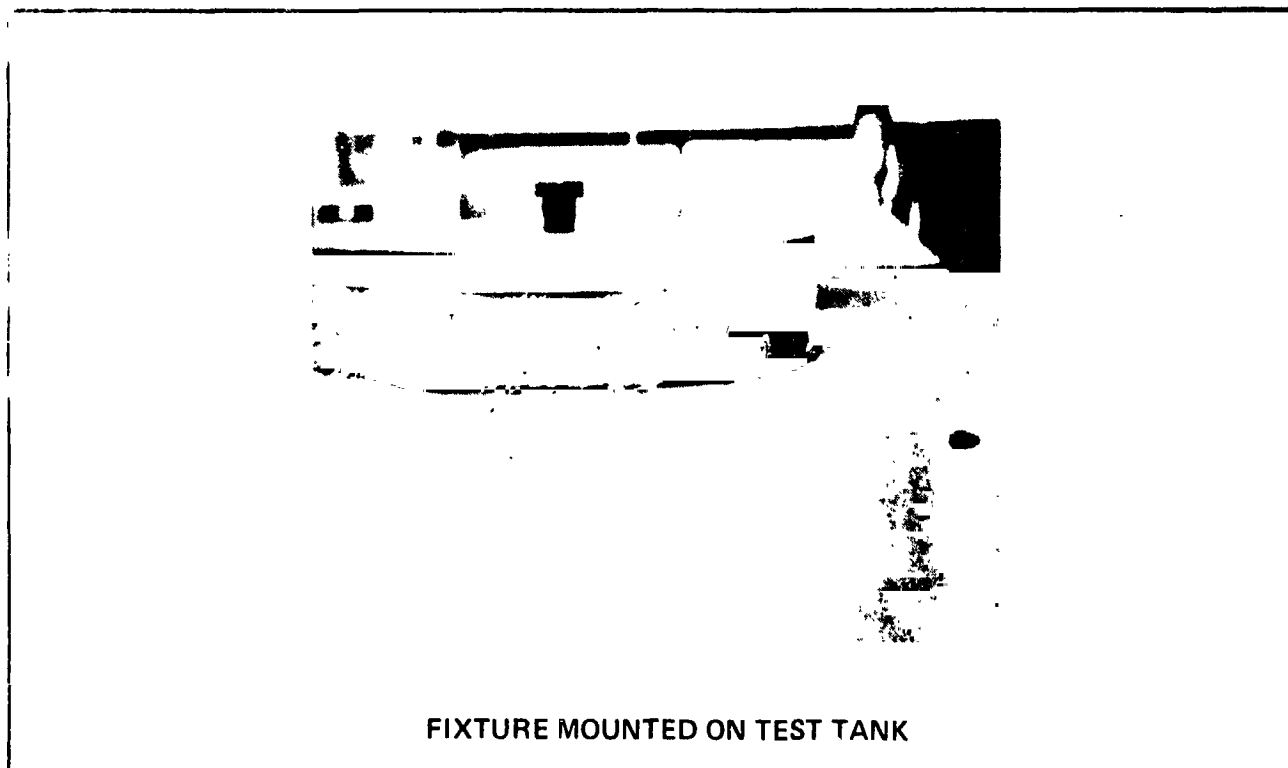
Since pressure variations and orientation of the test tank are a normal part of the testing with cryogens, an attempt was made to correct the empty tank orientation sensitivity problem by elimination of the threaded fitting. First the pressure vessel closure and probe assembly, P/N 1627189, was removed from the test tank and altered by removing the threaded section. Then the pressure vessel fitting, P/N 1626821, was altered by machining its threads off. Adapter rings were fabricated and used to adapt and secure the probe structure to the pressure vessel by welding. Figure 3-15 shows the adapter rings and probe assembly. The inner ring was bolted to the probe assembly, then inner ring, and finally the assembly was welded to the pressure vessel fitting. The welded vessel closure and probe assembly is shown in Figure 3-16. The cooling tube shown in Figure 3-16 was used to keep the back part of the fitting cool enough to prevent damage to the nylon suspension straps.

An X-Y plot of the RF mode count vs. orientation without the outer cover was made. The tank was oriented back and forth while pressurized with various increments of pressure ranging from 0 to 45 psig. Nitrogen gas was used as a pressurant. Figure 3-17 shows the test results, indicating a variation in mode count of only 15 modes out of 1392 modes, nominal for the empty tank, and approaches the variance in mode count attributed to variations in RF sweep oscillator and mode processing accuracy. This compares to a variation of approximately 75 modes noted prior to this



**Fixture for pressure test**

Figure 3-12



**Fixture mounted on test tank**

Figure 3-13

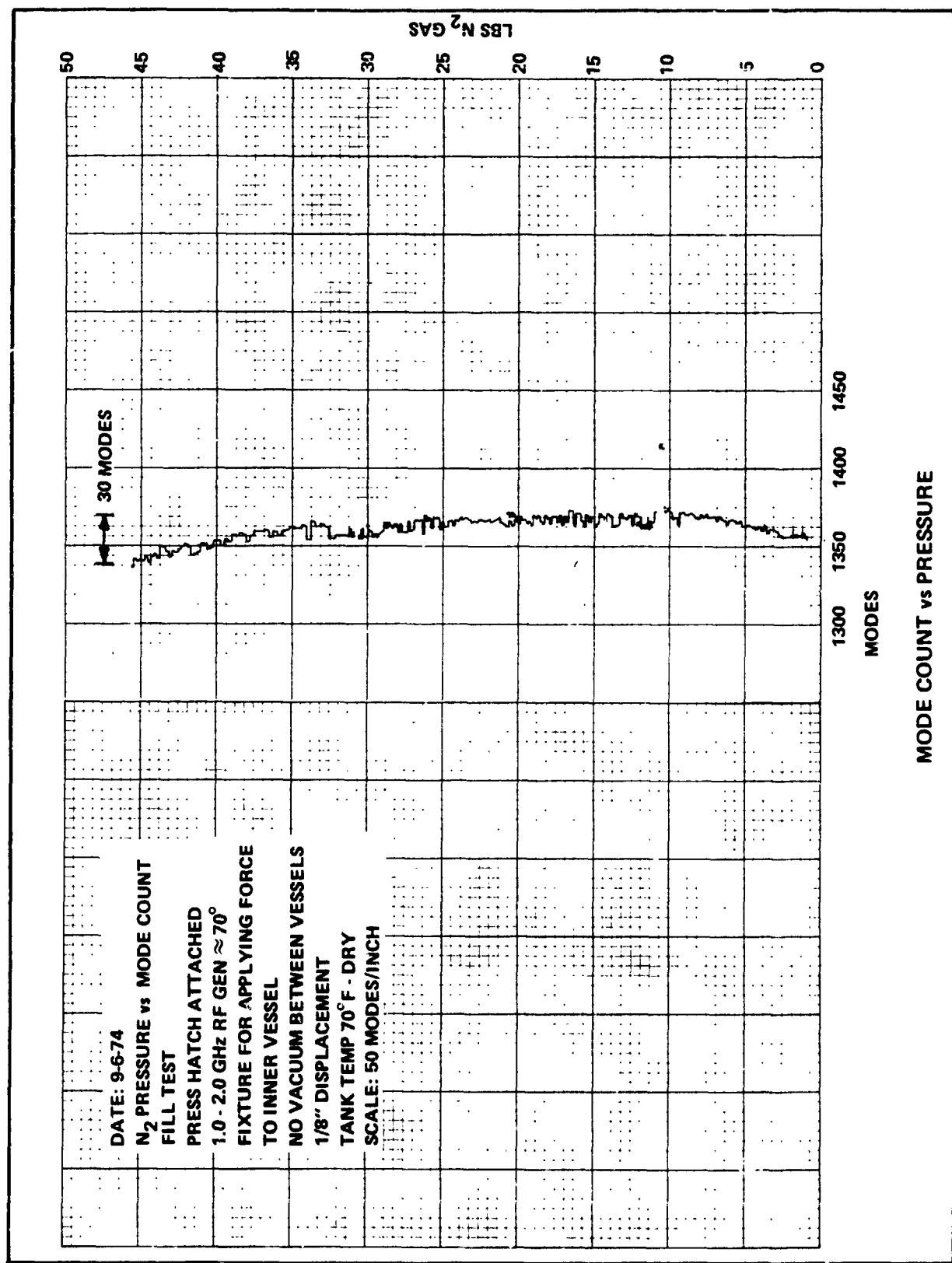
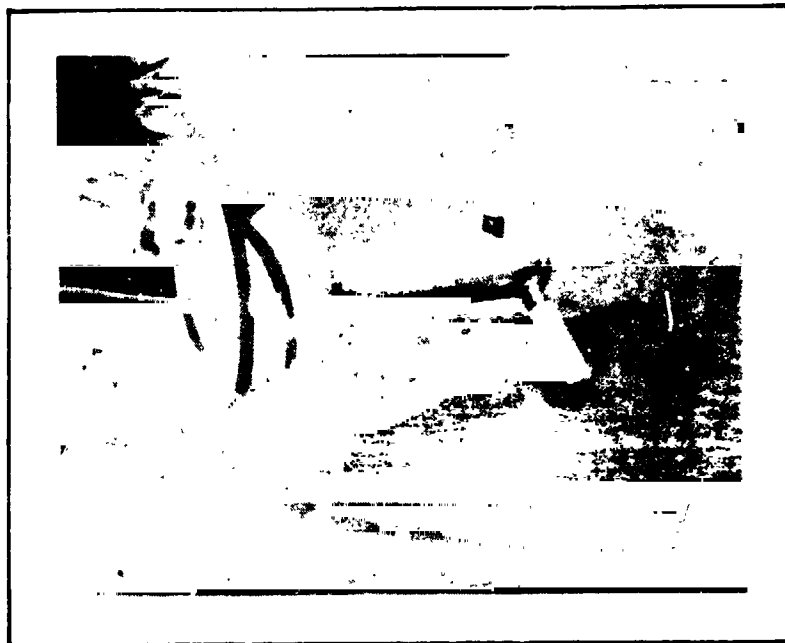


Figure 3-14



**Figure 3-15  
ADAPTER RINGS AND PROBE ASSEMBLY**

modification.

To further demonstrate the improvement made by modification, two other tests were performed. The first involved the pressurization of the test tank from 0 to 50 psig while in a vertical position. The results are shown in the X-Y plot of RF mode count vs. pressure of Figure 3-18. Note that the total excursion in mode count was approximately 13 modes. The second test was the same as the first except pressurization of the test tank was from 0 to 100 lbs. as shown in Figure 3-19. Note that the total excursion in mode count was approximately 18 modes. This represents a significant improvement over the magnitude of variations seen prior to the modification. After leak checking the welded areas the outer vessel hatch cover was replaced and the space between the inner pressure vessel and the outer vacuum shield was evacuated in preparation for the January 3, 1975 LH<sub>2</sub> tests.

### **3.3 CONCLUSIONS FROM EMPTY TANK ORIENTATION SENSITIVITY EVALUATION**

The problems experienced with the empty cryogenic test tank involving a large mode count variance with pressure or orientation was attributed to the effects of intermittent contacts in the threaded



MODIFIED CLOSURE AND PROBE ASSEMBLY

Figure 3-16

ORIGINAL PAGE IS  
OF POOR QUALITY

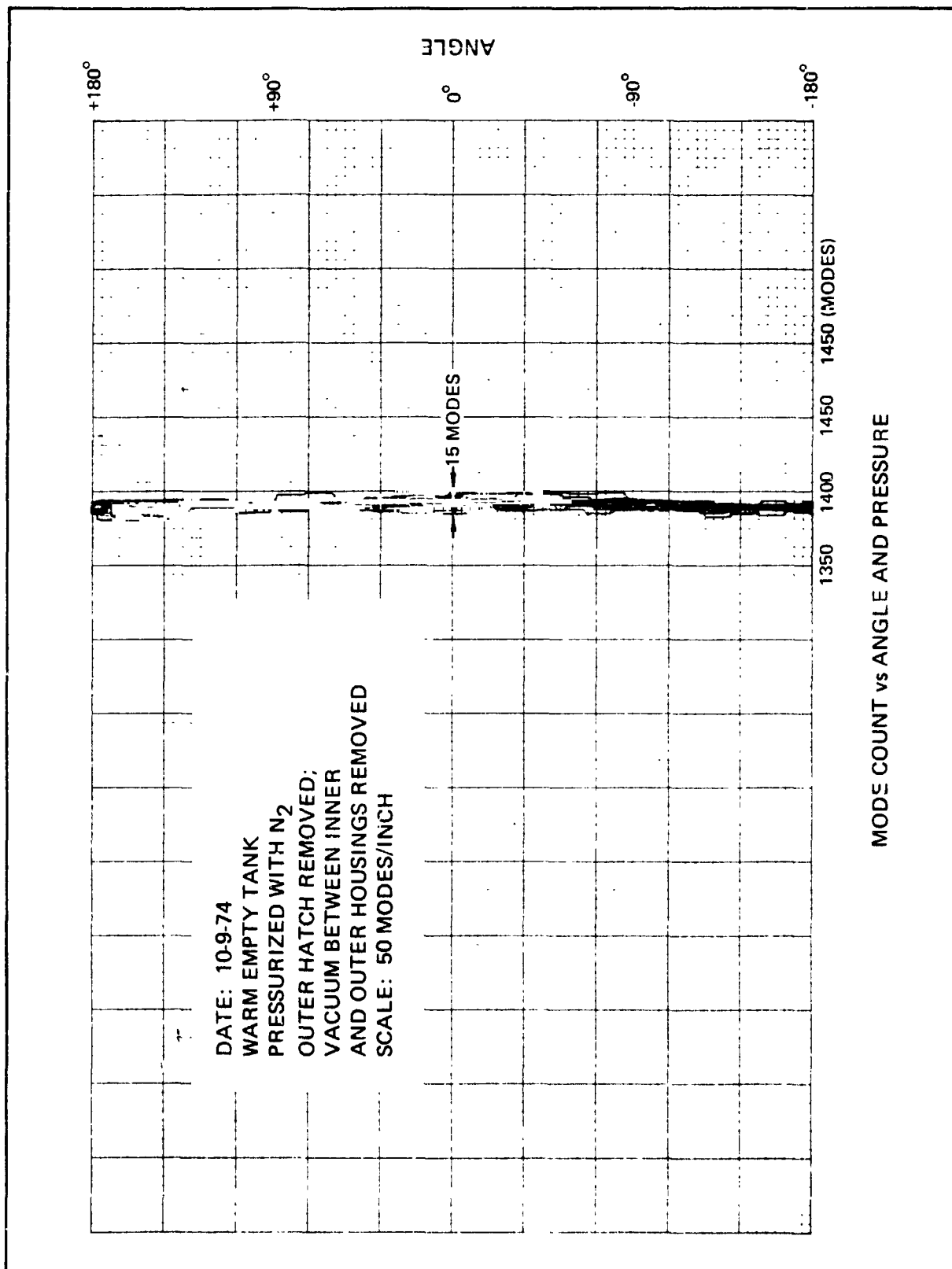


Figure 3-17

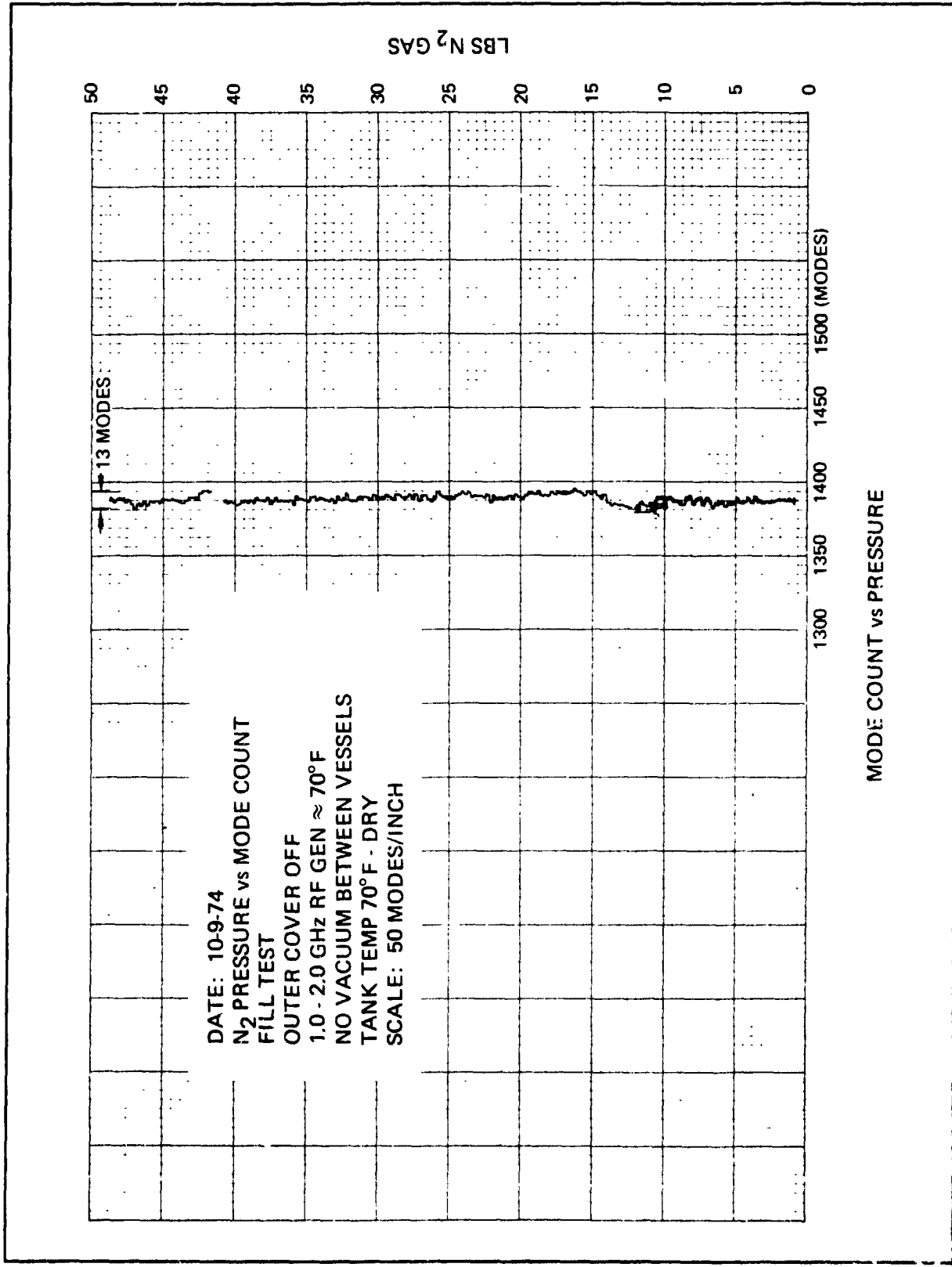


Figure 3-18

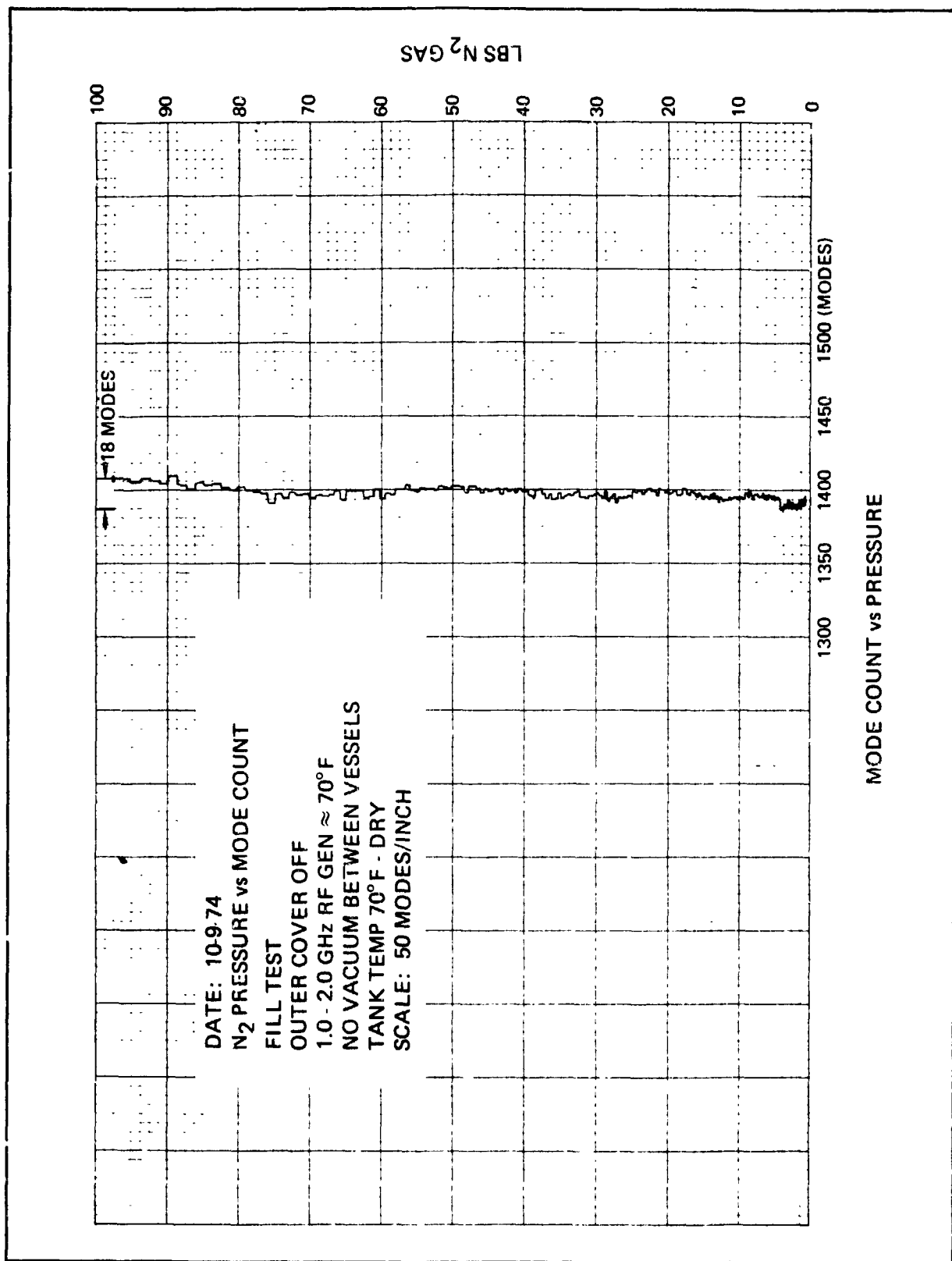


Figure 3-19



joint used to secure the probe structure at the pressure vessel access hatch. Since the size of the threaded joint (diameter of 0.296 meter) in relation to the size of the pressure vessel (diameter of 0.914 meter) was significant, the presence of the intermittent joint was very detrimental to gauging system performance as noted by sensitivity to pressure and orientation. The basic premise of a cavity whose dimensions are very large compared with the largest wavelength leads to the conclusion that changes of cavity shape or position of internal objects that do not alter the net volume of the cavity cannot affect the mode count. Therefore, rigidity (of a probe and the like) should not have to be maintained, in principle. Any detrimental effects caused by relative motion between parts such as the large threaded sections which were used to secure the probe assembly in the cryogenic test tank would be caused by the effects of the intermittent nature of the contacts of the mating threaded parts. Threaded joints are quite lossy at microwave frequencies, and even when the fit appears tight, contact may be occurring at a few well separated points. From this the following is concluded:

- Threaded joints should categorically be avoided unless the circumference of one turn of the thread is a very small fraction of the smallest wavelength.
- When access hatches are necessary, a "biting edge" contact design, with pressure applied at a multiplicity of points, is recommended.
- The rework of the cryogenic test tank did eliminate a majority of the empty tank orientation sensitivity problem. The magnitude of the mode count variations after rework of the tank was considered acceptable. Due to the physical complexity of the cryogenic test tank, further efforts to reduce sensitivity were not presently considered feasible.



## 4.0 CONFIGURATION, MULTIPLE ANTENNA, AND PRESSURE EVALUATIONS

### 4.1 CYLINDRICAL TANK EVALUATIONS

To provide an additional understanding of the need for multiple RF probe elements in conjunction with internal tank perturbations, a small cylindrical tank with protruding hemispherical ends, and a small spherical tank were fabricated and tested with RP-1 as a test fluid. The spherical tank was also used to test for the effects of pressure on the RF gauging system. The following paragraphs describe the test hardware, procedures, and results obtained in these tests.

To evaluate internal perturbation effects, it was necessary to fabricate a simple non-cryogenic test tank in which full access to its interior would be possible since modifications, i.e., the addition of perturbations would be required. As a result, the tank was designed to split into two sections. Sealing to contain liquid at pressure ranging from 0 - 20 psig was accomplished by the use of a neoprene O-ring type seal that circumscribed the entire diameter of the tank. A shallow "biting" edge was incorporated in the mating flanges that retained the O-ring to assure that the inner surfaces of the tank would maintain good electrical continuity at the separation point. The tank has an internal volume of 0.8724 cubic meters (230.5 gallons). Small threaded bosses to accommodate the RP-1 fill and vent lines, and up to four RF probe elements were incorporated in the tank walls. Figure 4-1 is a photo of one of the monopole probes used during the tests. This monopole has a teflon radome approximately 4.5 inches long and reaches into the tank a maximum of 7.0 inches. Also used were two loop probes. The loop probes were dimensionally the same as the monopoles, the only differences being the shape of the respective radiating elements inside the teflon radome.

Figure 4-2 and 4-3 show the completed test tank as adapted to the gimbaling fixture that was used with the Phase F cryogenic test tank.

Testing with the cylindrical tank involved:

- Empty tank evaluations with no internal perturbations.
- RP-1 evaluations with no internal perturbations
- Empty tank evaluations with internal perturbations.

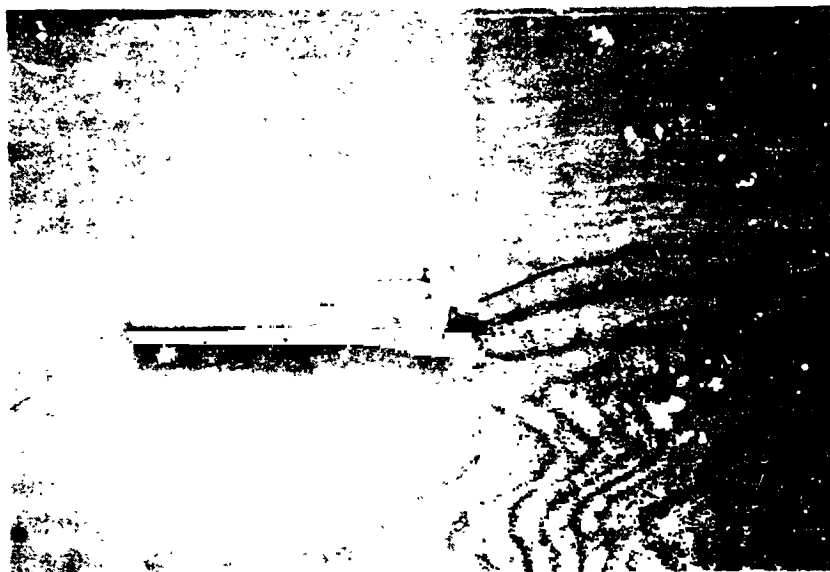


Figure 4-1  
RF MONPOLE PROBE

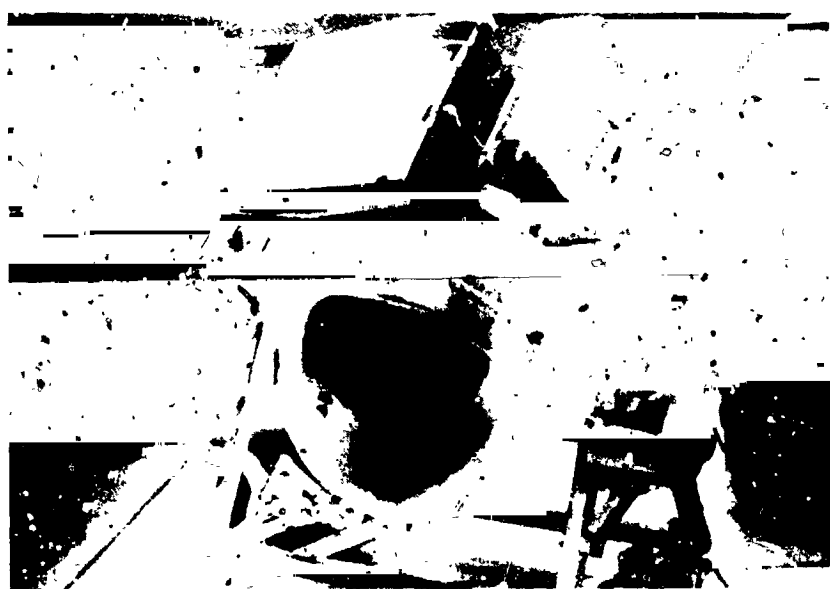


Figure 4-2  
CYLINDRICAL RP-1 TEST TANK

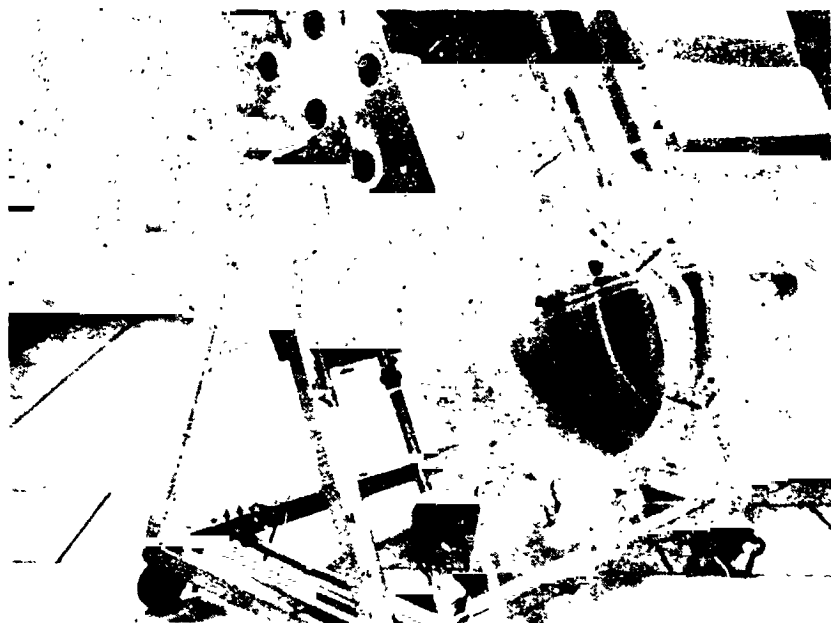


Figure 4-3  
CYLINDRICAL RP-1 TEST TANK

- RP-1 evaluations with internal perturbations.

For the tests involving the tank configuration that included internal perturbations, a number of  $\frac{1}{2}$ -inch diameter aluminum rods were randomly placed in each half of the test cavity as illustrated by one of the halves shown in Figure 4-4.

The following paragraphs summarize the tests performed with the cylindrical test tank.

#### 4.1.1 STRIP CHART DATA

As a part of the multi-probe evaluation, a series of strip chart recordings of the resonant characteristics of the 33 inch diameter cylindrical tank were taken with various combinations of monopole and loop probe elements. These tests were conducted with the cylindrical tank configured without and with internal perturbations. During the testing the unused probe ports in the tank were plugged, and when a strip chart recording of a resonant mode pattern was

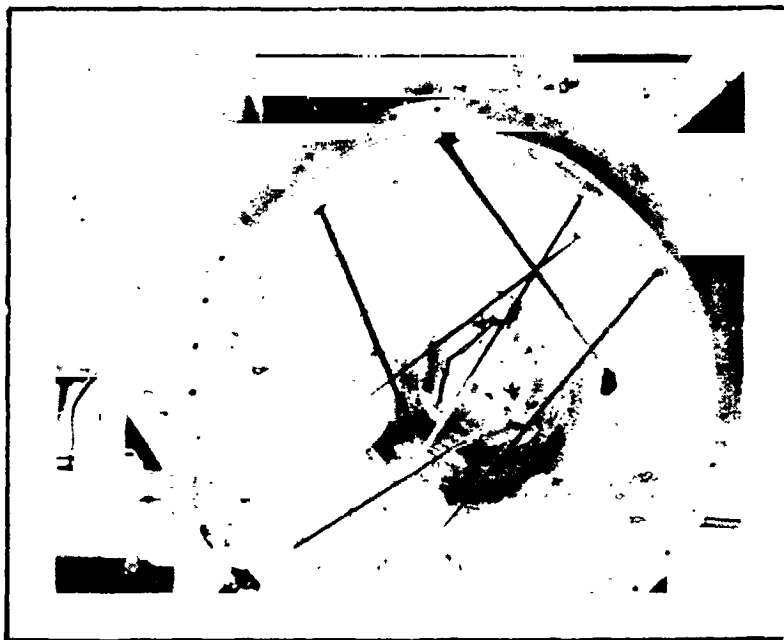


**Figure 4-4**  
**PERTURBATIONS IN CYLINDRICAL RP-1**  
**TEST TANK**

taken from a given RF probe, other RF probes were terminated with short circuits to simulate a multiplexing arrangement which used , in diode switching. A hand count of a strip chart recording provided a precise indication of the number of resonant modes which were detectable and also provided a permanent recording of the nature of that mode pattern. Table 4-1 shows a summation of the mode count for each probe combination where perturbations were not present in the test tank, and the RF frequency was swept from 1.0 to 2.0 GHz. The tank was completely empty. it is noted that, in general, the monopole probes are more effective in that they couple to a larger number of modes. Also, it is clear that as the number of probes in the tank increases, the lower the detectable number of modes. This reduction in the detectable mode count is a result of an additional lowering of the system Q with each additional RF probe (can be viewed as an additional effective parallel impedance added to the system).

It was noted from the strip charts that the distribution of the modes with frequency appears more uniform as a larger number of probes is



placed in the tank, although in general the higher the number of probes, the lower the mode count.

TABLE 4-1  
MODE COUNT FOR COMBINATIONS OF RF PROBES  
FROM STRIP CHART DATA, CYLINDRICAL TANK, 1.0-2.0 GHz  
NO PERTURBATIONS

PROBE COMBINATION NUMBER	STRIP CHART TAKEN FROM PORT #2		PORT #1	PORT #3	PORT #4
	TYPE PROBE	MODE COUNT			
1	Monopole	1386	Plug	Plug	Plug
2	Monopole	1414	Monopole	Plug	Plug
3	Monopole	1372	Monopole	Monopole	Plug
4	Monopole	1354	Monopole	Monopole	Monopole
5	Monopole	1400	Monopole	Loop	Loop
6	Loop	1298	Monopole	Monopole	Loop
7	Loop	1300	Plug	Plug	Plug

A series of strip chart recordings of the resonant characteristics of the 33-inch diameter tank with perturbations were then taken with the same combinations of monopole and loop probes. In these tests, unused probe ports in the tank were again plugged, and when a strip chart recording of a resonant mode pattern was taken from a given RF probe, other RF probes were terminated with short circuits to simulate a multiplexing arrangement which used pin diode switching. A hand count of a strip chart recording was then performed. Table 4-2 shows the mode counts obtained for each combination where the RF was swept from 1.0 to 2.0 GHz. The tank did not contain any RP-1. It was noted that the mode count was higher since the addition



of the perturbations. It was reasoned that the addition of the perturbations "brought out" many of the degenerate modes such that they could be counted. This seems to be the case as noted from the overall distribution of modes recorded on the strip charts. In the unperturbed cases, the frequency distributions of modes are seen to be concentrated in groups or clusters. In the perturbed case the frequency distribution is seen to be more uniform, and it is also noted that as the number of probes in the tank increases, the number of detectable modes decreases.

TABLE 2  
MODE COUNT FOR COMBINATIONS OF RF PROBES FROM STRIP  
CHART DATA, CYLINDRICAL TANK WITH PERTURBATIONS,  
1.0-2.0 GHz WITH PERTURBATIONS

PROBE COMBINATION NUMBER	STRIP TAKEN FROM PORT #2		PORT #1	PORT #3	PORT #4
	TYPE PROBE	MODE COUNT			
1	Monopole	1664	Plug	Plug	Plug
2	Monopole	1566	Monopole	Plug	Plug
3	Monopole	1521	Monopole	Monopole	Plug
4	Monopole	1449	Monopole	Monopole	Monopole
5	Monopole	1483	Monopole	Loop	Loop
6	Loop	1443	Monopole	Monopole	Loop
7	Loop	1633	Plug	Plug	Plug

#### 4.1.2 Q MEASUREMENTS

##### 4.1.2.1 Q MEASUREMENT TECHNIQUE

To obtain a relative figure for the average quality factor of the number of modes were examined to determine the respective Q values. This was done for combinations of RF probes with the unperturbed tank and also using a monopole probe after the perturbations were added to the tank.

The basic test setup used for determining Q is shown in Figure 4-5. A network analyzer with a phase/gain indicator (HP 8413A phase/gain indicator) is used in these measurements.

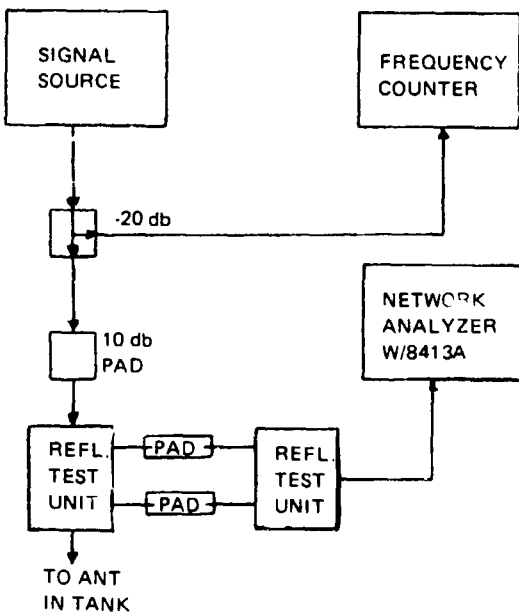


**Figure 4-5**  
**Q MEASUREMENT TEST SETUP**

The Q measurement approach is detailed in the following steps:

- 1) Set frequency to area of interest.
- 2) Place short on output of refl. test unit.
- 3) Set 8413A to 0 (center scale) on most sensitive range (3db) by varying amplitude controls of main frame.



- 4) Remove short and connect antenna to refl. test unit.
- 5) Adjust the signal source thru resonance. (Resonance occurs at furthest left meter deflection). Note reading at resonance in DB; this is  $L_0$ .
- 6) Calculate  $\rho_0$  (Resonant reflection coefficient)

$$\rho_0 = \frac{1}{\log^{-1} (.05 \times L_0)} . \quad (18)$$

- 7) Calculate  $S_0$  (VSWR at resonance)

$$S_0 = \frac{1 + \rho_0}{1 - \rho_0} \quad (19)$$

NOTE: To include the effect of coupling losses (probes, cables, etc.) on Q it is necessary to measure VSWR at points removed from resonance.

- 8) Change generator freq. in either direction slightly until further change makes little or no difference in meter reading.
- 9) Note return loss DB at this point. This is  $L_1$ .

$$10) \text{ Calculate } \rho_1 = \frac{1}{\log^{-1} (.05 L_1)} . \quad (20)$$

$$11) \text{ Calculate } S_1 = \frac{1 + \rho_1}{1 - \rho_1} . \quad (21)$$

- 12) The VSWR occurring at the half power (3 db) points is then calculated:

$$S_{1/2} = \frac{(S_0 + 1)(S_1 + 1)\sqrt{2} + \sqrt{(S_0 - 1)^2(S_1 + 1)^2 + (S_0 + 1)^2(S_1 - 1)^2}}{(S_0 + 1)(S_1 + 1)\sqrt{2} - \sqrt{(S_0 - 1)^2(S_1 + 1)^2 + (S_0 + 1)^2(S_1 - 1)^2}} \quad (22)$$

NOTE: This equation is of the form  $\frac{a + b}{a - b}$



where:

$$a = (S_0 + 1)(S_1 + 1)\sqrt{2} \quad (23)$$

and

$$b = \sqrt{(S_0 - 1)^2(S_1 + 1)^2 + (S_0 + 1)^2(S_1 - 1)^2} \quad (24)$$

$$13) \text{ Calculate } \rho_{1/2} = \frac{S_{1/2} - 1}{S_{1/2} + 1}. \quad (25)$$

$$14) \text{ Calculate } L_{1/2} \text{ (Loss in DB at half power points)}$$

$$L_{1/2} = \frac{\log \frac{1}{\rho_{1/2}}}{.05} \quad (26)$$

$$15) \text{ Vary freq. either side of } f_0 \text{ until meter reads } L_{1/2}.$$

$$16) \text{ Record } f_1 \text{ and } f_2, \text{ the frequencies where this occurs.}$$

then:

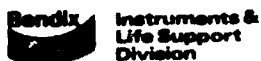
$$Q_L = \frac{f_0}{\Delta f} \quad (27)$$

$$Q_0 = Q_L \left[ \frac{(1 + S_0)(1 + S_1)}{2 S_0 + S_0 S_1 + 1} \right] \quad (28)$$

$$Q_{00} = Q_L \left[ \frac{S_1 (1 + S_0)}{1 + S_1} \right] \quad (29)$$

where:

$Q_L$  is the  $Q$  of complete system



$Q_0$  is Q of everything in cavity

$Q_{00}$  is Q of cavity excluding coupling losses.

This procedure was applied to the empty test tank under three separate configurations:

- First, measuring Q at port number 4 which contained a monopole RF probe; the other three ports contained monopole RF probes with open circuited output.
- Second, measuring Q at port number 2 which contained a monopole RF probe; each of the other ports was plugged.
- Finally, measuring Q at port number 2 which contained a loop RF probe; each of the other ports contained a monopole RF probe with open circuited outputs.

#### 4.1.2.2 Q MEASUREMENT RESULTS

Table 4-3 summarizes the Q measurement results for the un-perturbed tank at selected frequencies using the outlined Q measurement technique along with several measurements using the impedance technique previously used. It is seen that there is a fair agreement between the two Q measurement techniques. It is noted that the average System Q of Configuration III (loop type probe) is lower than that of Configuration I (monopole type probe).

To obtain a relative figure for the average quality factor of the cylindrical test tank containing the aluminum perturbations, a number of modes were examined to determine the respective Q values. The measurement technique was the same as used when measurements were taken without the perturbations. Measurements were taken at port number 2 which contained a monopole RF probe; each of the other ports was plugged. Table 4-4 summarizes the Q measurement results.

In the first tests involving the single monopole probe and no perturbations in the tank, the average values for  $Q_L$ ,  $Q_0$ , and  $Q_{0r}$  were

$$Q_L = 3.75 \times 10^4$$



**TABLE 4-3**  
**Q MEASUREMENT DATA - EMPTY CYLINDRICAL TANK - NO PERTURBATIONS**  
**(PHASE/GAIN APPROACH AND IMPEDANCE APPROACH TO Q MEASUREMENT)**

CONFIGURATION	MODE FREQ / SYSTEM Q		Q OF CAVITY Q <sub>0</sub>		Q OF CAVITY - NO COUPLING LCSS Q <sub>00</sub>	
	f <sub>0</sub> (GHz)	Q <sub>L</sub>	Phase/Gain	Impedance	Phase/Gain	Impedance
I. MONOPOLE, MULTIPLE	1.020291	—	1.87 x 10 <sup>3</sup>	—	3.44 x 10 <sup>3</sup>	—
	1.021609	—	2.98 x 10 <sup>3</sup>	—	3.38 x 10 <sup>3</sup>	—
	1.037356	—	1.6 x 10 <sup>4</sup>	—	2.26 x 10 <sup>4</sup>	—
	1.577042	1.38 x 10 <sup>4</sup>	1.56 x 10 <sup>4</sup>	1.56 x 10 <sup>4</sup>	2.43 x 10 <sup>4</sup>	3.11 x 10 <sup>4</sup>
	1.579690	5.27 x 10 <sup>4</sup>	5.1 x 10 <sup>4</sup>	6.72 x 10 <sup>4</sup>	1.22 x 10 <sup>5</sup>	1.58 x 10 <sup>5</sup>
	1.583620	2.2 x 10 <sup>4</sup>	9.9 x 10 <sup>4</sup>	8.2 x 10 <sup>4</sup>	1.22 x 10 <sup>5</sup>	2.87 x 10 <sup>5</sup>
	Averages =	3.46 x 10 <sup>4</sup>	3.11 x 10 <sup>4</sup>	5.63 x 10 <sup>4</sup>	4.96 x 10 <sup>4</sup>	1.59 x 10 <sup>5</sup>
II. MONOPOLE, SINGLE	.560025	4.87 x 10 <sup>3</sup>	—	5.5 x 10 <sup>3</sup>	—	3.34 x 10 <sup>4</sup>
	.681072	1.45 x 10 <sup>4</sup>	—	2.03 x 10 <sup>4</sup>	—	4.37 x 10 <sup>4</sup>
	.908717	2.02 x 10 <sup>4</sup>	—	2.84 x 10 <sup>4</sup>	—	5.44 x 10 <sup>4</sup>
	1.764474	7.06 x 10 <sup>4</sup>	—	1.02 x 10 <sup>5</sup>	—	3.55 x 10 <sup>5</sup>
	1.910966	5.79 x 10 <sup>4</sup>	—	7.14 x 10 <sup>4</sup>	—	1.2 x 10 <sup>5</sup>
	1.914770	6.18 x 10 <sup>4</sup>	—	8.53 x 10 <sup>4</sup>	—	1.09 x 10 <sup>5</sup>
	1.963161	3.27 x 10 <sup>4</sup>	—	5.00 x 10 <sup>4</sup>	—	2.73 x 10 <sup>4</sup>
III. LOOP, MULTIPLE	Averages =	3.75 x 10 <sup>4</sup>	—	5.18 x 10 <sup>4</sup>	—	1.13 x 10 <sup>5</sup>
	1.143397	7.89 x 10 <sup>3</sup>	—	1.22 x 10 <sup>4</sup>	—	1.91 x 10 <sup>4</sup>
	1.514971	1.32 x 10 <sup>4</sup>	—	1.51 x 10 <sup>4</sup>	—	7.26 x 10 <sup>4</sup>
	1.881580	285 x 10 <sup>4</sup>	—	3.92 x 10 <sup>4</sup>	—	2.76 x 10 <sup>4</sup>
Averages =		1.65 x 10 <sup>4</sup>	—	2.22 x 10 <sup>4</sup>	—	5.64 x 10 <sup>4</sup>



$$Q_0 = 5.18 \times 10^4$$

$$Q_{00} = 1.13 \times 10^5$$

From these measurements it is reasoned that the addition of the aluminum rods in the cylindrical test tank did not reduce the average Q values. However, a word of caution is appropriate. Ideally, to establish the average values for  $Q_L$ ,  $Q_0$ , and  $Q_{00}$  one would like to measure a large number of modes.

With the monopole probes, a majority of the modes are undercoupled, a number of them are overcoupled, and a few approach critical coupling. With the Q measurement technique used, the greatest accuracy is obtained when measuring overcoupled modes. To make a large number of Q measurements and to include all three cases of coupling is not practical with the available equipment. As a result, these Q measurement results can be considered only as "relative" indications of Q.

TABLE 4-4  
Q MEASUREMENT DATA - EMPTY CYLINDRICAL TANK  
(WITH PERTURBATIONS, SINGLE MONPOLE PROBE)

MODE FREQ. $f_0$ (GHz)	SYSTEM Q $Q_L$	Q OF CAVITY $Q_0$	Q OF CAVITY - NO COUPLING LOSS $Q_{00}$
1.763962	$1.23 \times 10^4$	$1.88 \times 10^4$	$2.23 \times 10^4$
1.7665059	$1.18 \times 10^4$	$1.41 \times 10^4$	$5.10 \times 10^4$
1.911863	$5.17 \times 10^4$	$6.83 \times 10^4$	$1.36 \times 10^5$
1.913077	$8.70 \times 10^4$	$1.05 \times 10^5$	$1.55 \times 10^5$
1.9142262	$5.17 \times 10^4$	$6.76 \times 10^4$	$1.00 \times 10^5$
1.964133	$1.23 \times 10^4$	$1.29 \times 10^4$	$7.51 \times 10^4$
AVERAGES	$3.78 \times 10^4$	$4.78 \times 10^4$	$8.99 \times 10^4$



#### 4.1.3 VSWR DATA

As a further examination of the sampling of the modes in the empty cylindrical test tank, the VSWR at resonance and far from resonance can be examined. Table 4-5 summarizes the VSWR data taken for several resonant modes, as obtained in the unperturbed cylindrical tank. It is noted that for each configuration the coupling loss factor is similar and that in general the average is 0.727.

Likewise, for the cylindrical test tank after the aluminum perturbations were added, at a number of resonant modes, the VSWR at resonance and far from resonance was examined using a single monopole probe. Table 4-6 summarizes this data. It is noted that the average coupling loss factor is 0.752. The average for the single monopole without perturbation in the tank was 0.709, which is not significantly different considering the size of the sample and the fact that it is not possible to be 100% certain that the identical modes were measured.

#### 4.1.4 RP-1 FUEL PROPERTIES

The available RP-1 for performing tests was found to be contaminated with water and small solid particles. As a result, the barrels of RP-1 were set aside to permit the bulk of water and heavy particles to settle to the bottom. The RP-1 was then siphoned off and continuously cycled through filtering and drying equipment. After completion of this cleaning process, measurement of the dielectric constant and the loss tangent of the RP-1 was made to assure that the water and other contamination were indeed removed.

In order to obtain the dielectric constant  $\epsilon'$ , the real part of the complex permittivity, and the loss tangent  $\delta$ , the ratio of the imaginary and real parts of the complex permittivity of a liquid, the experimental setup shown in Figure 4-6 is used to measure the following parameters:

$f_0$ Empty - Resonant frequency of the empty cavity

$f_0$ Full - Resonant frequency of the cavity when filled with the liquid under test

$f_1$ Full - Lower Half-power frequency of the cavity when filled with the liquid under test



Instruments &  
Life Support  
Division

TABLE 4-5  
VSWR READINGS FOR EMPTY CYLINDRICAL TANK  
(NO PERTURBATIONS)

CONFIGURATION	FREQUENCY $f_0$ (GHz)	VSWR AT RESONANCE ( $S_C$ )	VSWR FAR FROM RESONANCE ( $S_1$ )	COUPLING LOSS FACTOR $\frac{S_0(1+S_1)}{S_1(1+S_0)}$
I. MONOPOLE, MULTIPLE	1.577042	1.51	8.72	.671
	1.579690	1.76	5.85	.747
	1.583620	3.44	8.72	.864
II. MONOPOLE, SINGLE	.560025	6.05	34.8	.883
	.681072	2.10	34.8	.697
	.908717	1.87	15.8	.693
	1.764474	1.11	5.0	.631
	1.910966	1.58	4.03	.764
	1.914770	1.17	4.42	.661
	1.963161	1.50	17.4	.634
III. LOOP, MULTIPLE	1.143397	1.53	21.7	.633
	1.514971	4.77	21.7	.865
	1.881530	1.92	13.4	.707

TABLE 4-6  
VSWR READINGS FOR EMPTY CYLINDRICAL TANK  
(WITH PERTURBATIONS)

MODE FREQ $f_0$ (GHz)	VSWR AT RESONANCE ( $S_0$ )	VSWR FAR FROM RESONANCE ( $S_1$ )	COUPLING LOSS FACTOR $\frac{S_0(1+S_1)}{S_1(1+S_0)}$
.963645	1.92	34.7	.676
1.763962	1.09	6.49	.602
1.7665059	3.57	17.3	.826
1.911663	1.92	9.18	.729
1.913077	1.38	3.00	.773
1.9142252	1.38	4.42	.711
1.964133	5.77	9.18	.945
Average Coupling Loss Factor			.752

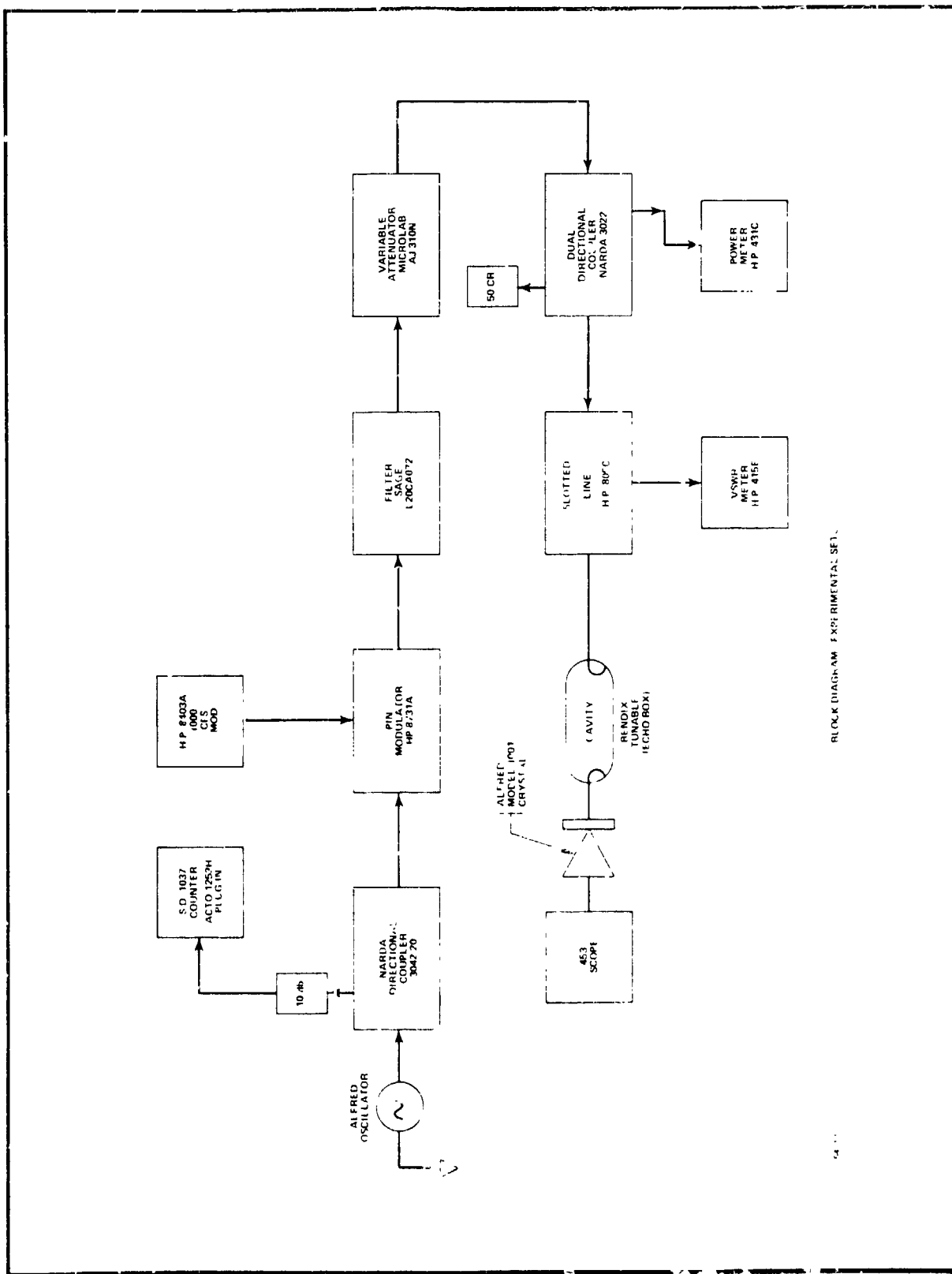


Figure 4-6



$f_2^{\text{Full}}$  - Upper Half-power frequency of the cavity when filled with the liquid

VSWR - Voltage standing wave ratio of filled cavity input port

The dielectric constant  $\epsilon'$  is obtained directly from the equation:

$$\epsilon' = \left( \frac{f_0^{\text{Empty}}}{f_0^{\text{Full}}} \right)^2$$

The loss tangent is defined as:

$$\tan\delta = \frac{\epsilon'}{\epsilon''} \cdot \frac{1}{Q_0}$$

where

$\epsilon'$  is the real part of the complex permittivity or dielectric of a fluid

$\epsilon''$  is the imaginary part of the complex permittivity

$Q_0$  is the selectivity factor of the filled cavity

The selectivity factor  $Q_0$  is obtained from the cavity loaded Q or ratio of total reactance to total loss obtained from the relationship:

$$Q_L = \frac{f_0^{\text{Full}}}{f_2^{\text{Full}} \cdot f_1^{\text{Full}}}$$

and the VSWR of the filled cavity from:

$$Q_0 = Q_L \cdot \left( 1 + \frac{2}{VSWR} \right)$$



Table 4-7 shows the frequency and VSWR data taken with samples of RP-1 from each barrel, and Table 4-8 summarizes the results for  $\epsilon'$  and the Loss Tangent. These readings are quite close to previous data taken for RP-1, indicating that the RP-1 is relatively pure, and more importantly, defined.

#### 4.1.5 RP-1 TEST RESULTS WITH CYLINDRICAL TEST TANK

The cylindrical test tank was placed in the test cell as illustrated in Figure 4-7. It is positioned on a load cell platform to permit an accurate determination of RP-1 weight during testing. The data acquisition system and orientation controls used during the cryogenic testing were adapted to the RP-1 test setup. Data was recorded automatically on IBM cards. The RP-1 fluid handling system consisted of a reservoir tank, heater, heat exchanger, motor and pump, interconnecting plumbing, and various manual and electrically activated valves. The RP-1 reservoir tank was contained in an insulated shelter to isolate the RP-1 from the outside ambient temperature. Figure 4-8 shows the RP-1 reservoir tank with heat exchanger secured to its side. Also shown is the motor and pump used in the transfer of the RP-1 between the reservoir tank and the test tank. Figure 4-9 shows the heater and air ducting used to supply heat to the heat exchanger. When cooling is necessary, a  $\text{LN}_2$  supply is utilized instead of the heater.

Using the 1.0-2.0 GHz RF band with the RP-1 cylindrical test tank, the following combinations of tank configuration and probe configurations were tested.

- 4 Monopole probe elements, no perturbations.
- 1 Monopole probe element, no perturbations.
- 2 Monopole and 2 Loop probe elements, no perturbations.
- 4 Monopole probe elements, with perturbations.
- 1 Monopole probe element, with perturbations.
- 2 Monopole and 2 Loop probe elements, with perturbations.

For each of the six test configurations the following data was obtained:



**TABLE 4-7**  
**VSWR DATA FOR RP-1**

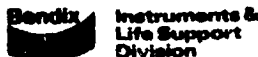
$f_0$ (GHz)	$f_1$ (GHz)	$f_2$ (GHz)	VSWR	POWER METER	COMMENTS
1.969069	1.968821	1.968297			
1.969071	1.968826	1.968298			(Empty Tank)
1.969068	1.968822	1.968284			
1.969072	1.968819	1.968299			
1.969075	1.968826	1.968297			
1.969075	1.968823	1.968295			Average
1.366652	1.365781	1.367981			
1.366651	1.365736	1.367971			
1.366657	1.365770	1.367976			
1.366659	1.365776	1.367974			
1.366656	1.365772	1.367977			
1.366655	1.365777	1.367975			Average
1.366407	1.365260	1.368072			
1.366424	1.365259	1.368079			
1.366441	1.365259	1.368078			
1.366443	1.365265	1.368085			
1.366331	1.365274	1.368088			
1.366410	1.365263	1.368082			Average
1.365971	1.364402	1.367316			
1.365026	1.364410	1.367284			
1.365944	1.364413	1.367323			
1.365935	1.364360	1.367352			
1.365894	1.364421	1.367352			
1.365754	1.364401	1.367325			Average
1.364673	1.363531	1.366745			
1.364680	1.363573	1.366757			
1.364671	1.363569	1.366754			
1.364690	1.363575	1.366750			
1.364694	1.363572	1.366761			
1.364681	1.363564	1.366755			Average
1.365566	1.364513	1.367515			
365544	1.364524	1.367530			
1.365527	1.364500	1.367532			
1.365547	1.364489	1.367470			
1.365561	1.364499	1.367499			
1.365546	1.364501	1.367509			Average
1.366184	1.365106	1.367977			
1.366242	1.365149	1.367991			
1.366193	1.365098	1.367980			
1.366190	1.365113	1.367986			
1.366196	1.365131	1.367990			
1.366201	1.365119	1.267985			Average
1.366984	1.365870	1.368656			
1.366980	1.365866	1.368659			
1.366979	1.365828	1.368653			
1.366977	1.365877	1.368663			
1.366980	1.365876	1.368671			
1.366980	1.365873	1.368660			Average
1.363747	1.362585	1.365788			
1.363739	1.362587	1.365786			
1.363734	1.362590	1.365789			
1.363753	1.362589	1.365787			
1.363747	1.362586	1.365794			
1.363744	1.362587	1.365789			Average
1.365423	1.364272	1.367189			
1.365371	1.364261	1.367161			
1.365366	1.364258	1.367137			
1.365333	1.364262	1.367148			
1.365377	1.364257	1.367148			
1.365374	1.364262	1.367163			Average

ORIGINAL PAGE IS  
OF POOR QUALITY



TABLE 4-8  
ELECTRICAL PROPERTIES OF RP-1  
RP CAVITY SETTING 20.8

Barrel No.	$\epsilon'$	TAN $\delta$ (10 <sup>-3</sup> )	$Q_L$	$Q_0$	$\epsilon''$ (10 <sup>-3</sup> )	Comment
1.	2.07588	1.24280	621.770	804.63	2.57990	*Sample 1 cavity not full
2.	2.06434	1.78812	427.660	559.246	3.69120	
3.	2.059741	1.77994	434.128	561.814	3.66621	
4.	2.076625	1.60463	484.714	623.196	3.33214	
5.	2.06172	1.69506	453.971	589.948	3.49474	
6.	2.07861	1.86519	467.084	600.530	3.46000	
7.	2.05742	1.55908	490.484	641.400	3.20768	
1.	2.06223	1.55805	472.284	629.710	3.27492	(Sample 1 rerun)
1.	2.06718	1.81431	425.904	594.627	3.48467	(Sample No. 2)
Average	2.06598	1.68305	457.029	594.627	3.48467	Except barrel 1 sample 1
Theoretical	2.08000	1.60000			3.32000	



- RP-1 loading data (IBM cards and analog X-Y plots of modes versus mass).
- Dynamic orientation data at every 10% RP-1 mass increment from 100% thru 0%. Approximately 100 data frames were recorded directly on IBM cards at each 10% loading condition. (Approximately 1100 data frames per test configuration).
- Static orientation data at 80% and 20% RP-1 loading increments. At each RP-1 loading, approximately 20 data frames were recorded for each tank position at angular increments of 45 degrees from 0-360 degrees, i.e., approximately 180 data frames at each loading. (Approximately 360 data frames per configuration).

Figures 4-10 thru 4-15 contain the X-Y plots of the analog RF system output versus the RP-1 mass obtained during the RP-1 loading tests with each of the six test configurations. The dynamic orientation data obtained during each of the six test configurations were analyzed by establishing for each mass loading:

- Minimum mode count
- Maximum mode count
- Mean mode count
- Variance in mode count
- Standard deviation of mode count.

Table 4-9 contains the results obtained with each of the three probe configurations using the uncluttered, unperturbed test tank. It is noted that the variance and standard deviation mode count at each mass % loading is clearly lower with the 4-monopole configuration. The probe configuration containing two monopoles and two loops clearly does not offer any significant advantage over a single monopole probe, even though the X-Y loading curves would seem to indicate that it might. In comparing the results, averages of the calculated standard deviations in mode count for each test

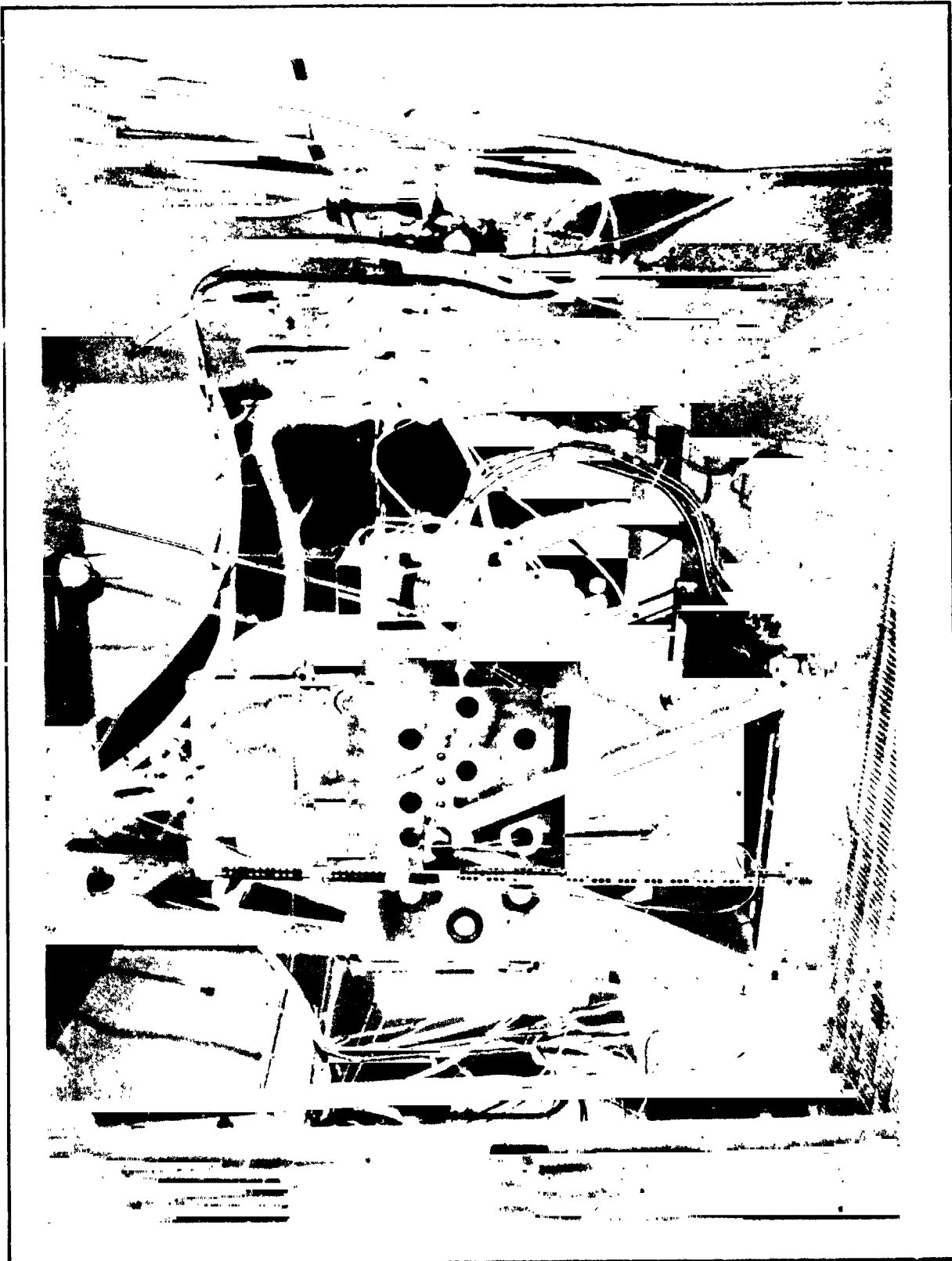


Figure 4-7

**Bendix** Instruments &  
Life Support  
Division

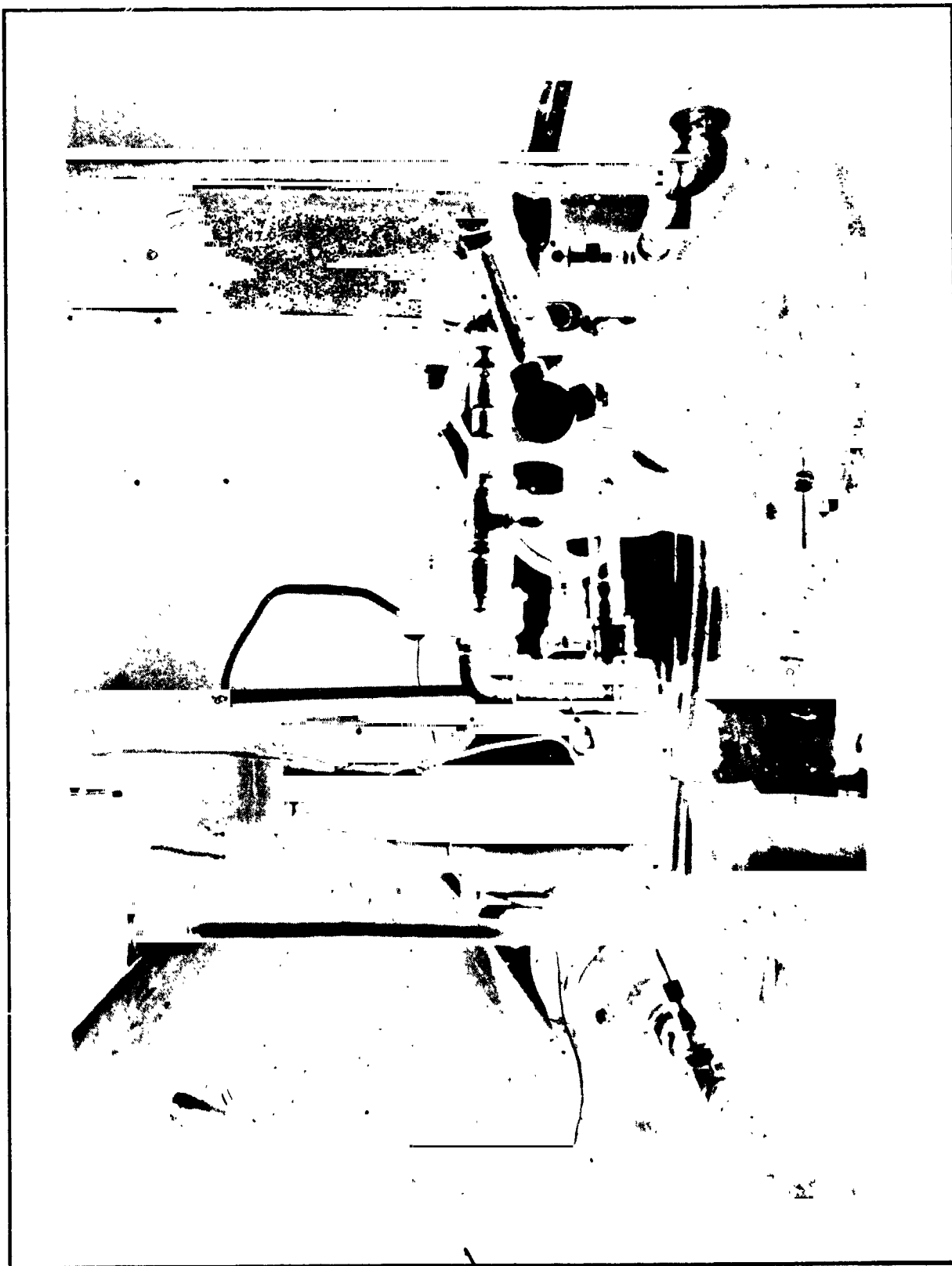


Figure 4-8



Figure 4-9

ORIGINAL PAGE IS  
OF POOR QUALITY



configuration confirms the conclusion that four monopole probes provide better gauging accuracy in a small tank that does not contain any perturbations.

Table 4-10 contains the results obtained with each of the three probe configurations, after the aluminum rod perturbations were added to the test tank. Again it is noted that the 4-monopole probe configuration provides a lower variance and standard deviation in mode count, and that the 2-monopole & 2-loop probe configuration does not offer any advantage over the single monopole probe configuration. It is further noted that in comparing the results of Table 4-9 with those of Table 4-10, the variance and standard deviation is the lowest in the test configuration where four monopole probes were used and perturbations were added to the test tank. These results are consistent with the understanding of mode degeneracies.

For tank configurations with symmetry about one or more axes, mode degeneracies exist, and the modes that can be counted tend to be grouped together and are fewer than the number that actually exist. In small tanks whose dimensions are only a few times greater than the smallest wavelength, introducing symmetry-destroying perturbations does tend to "break-up" the mode groupings and provide a more uniform distribution of the modes with frequency, and subsequently cause less variance in mode count. This is dramatically illustrated by the RP-1 loading curves shown in Figures 4-11 and 4-14, and by the calculated variances and standard deviations for the single monopole test configurations. With tanks whose dimensions are very large compared with the smallest wavelength, the situation is quite different. The mode density is very high and the spacing between most modes is small and relatively uniform. This was observed on the strip charts taken during some of the large tank tests in Phases A and B. Any perturbation capable of resolving a degeneracy by frequency shifting one of two modes would tend to shift it into superposition with some other nearby mode. As a result, solution of the "degeneracy problem" through deliberate introduction of deformations or other physical perturbations into a truly large cavity would probably be pointless.

Table 4-11 provides a comparison of the dynamic and static RP-1

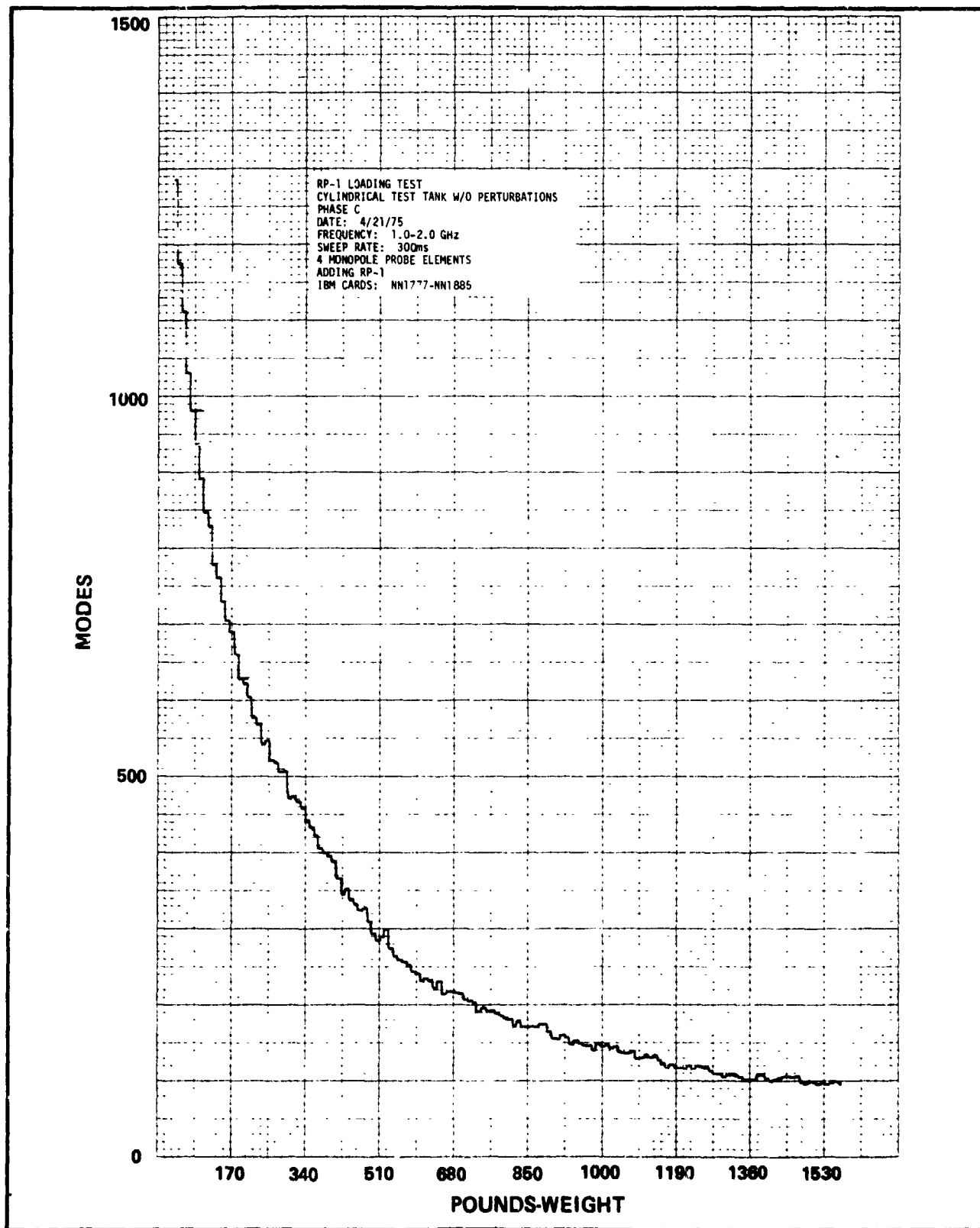


Figure 4-10

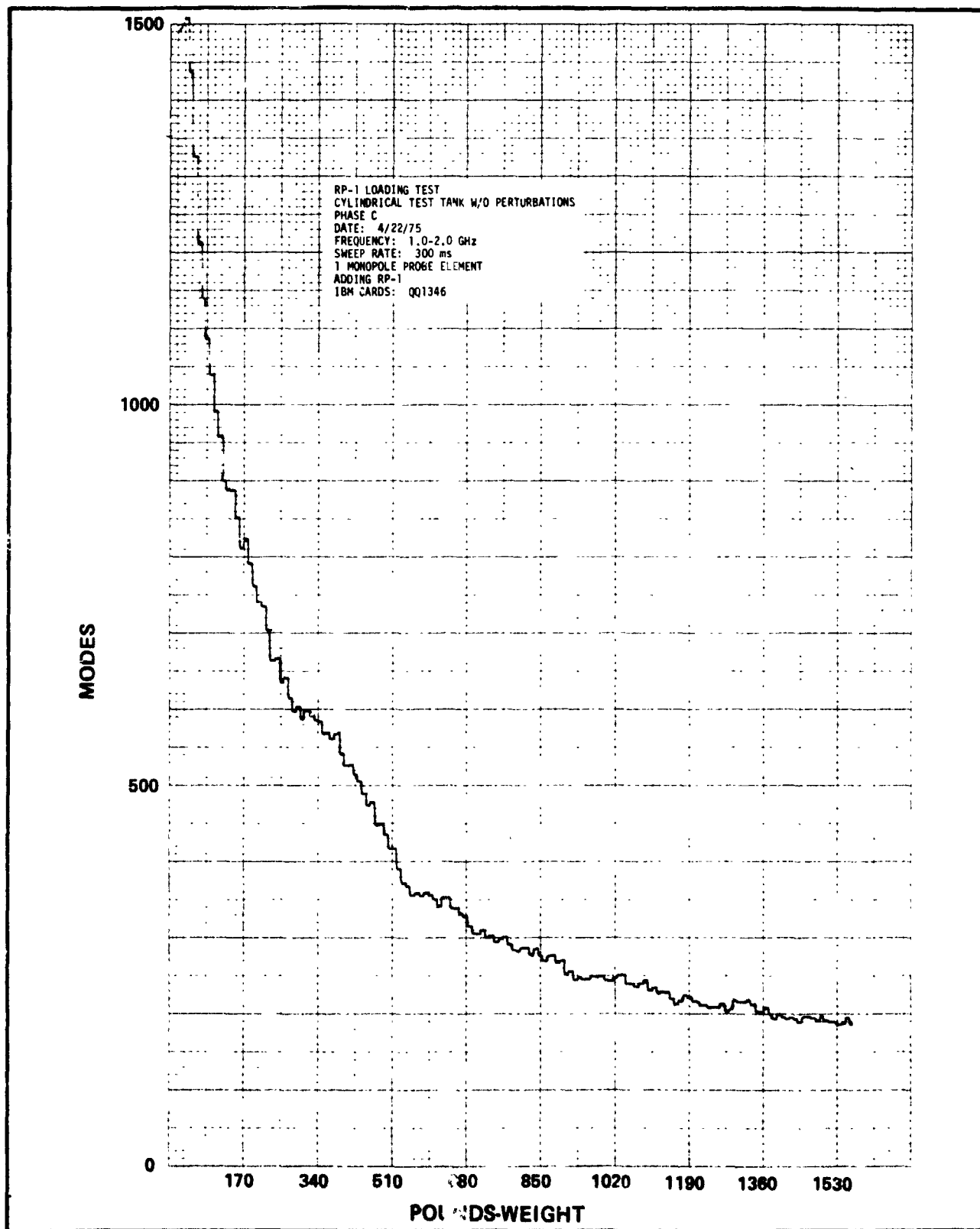


Figure 4-11

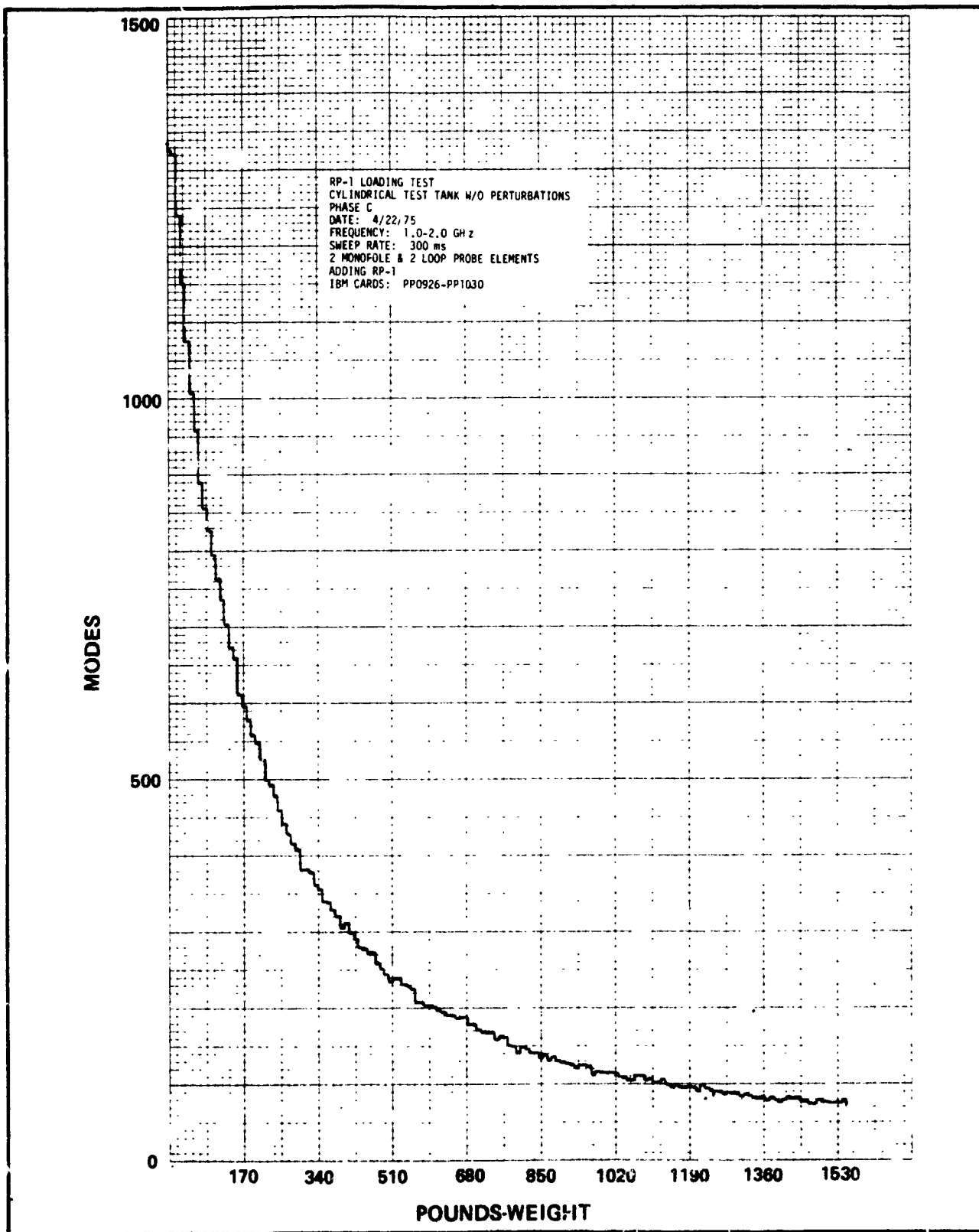


Figure 4-12

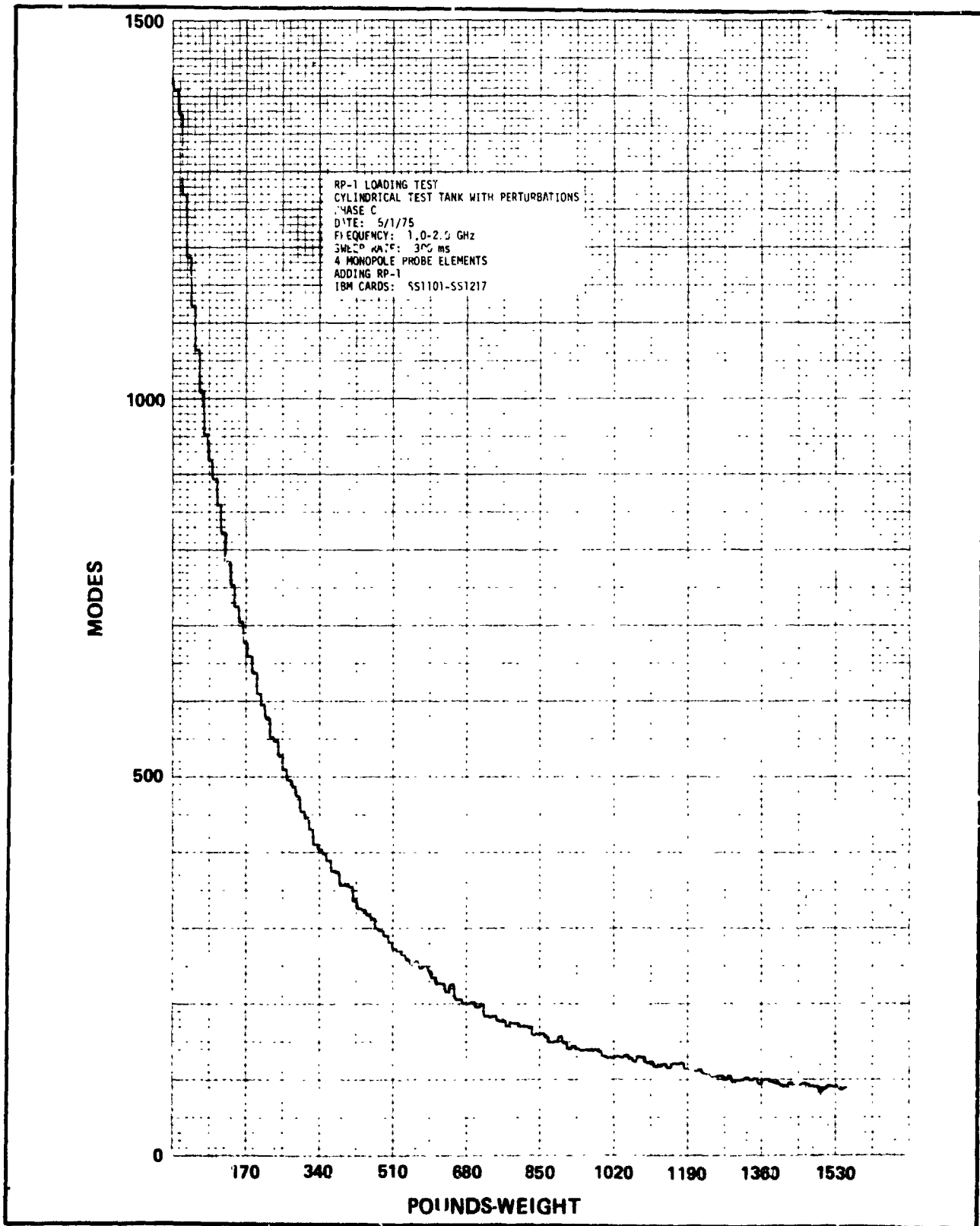


Figure 4-13

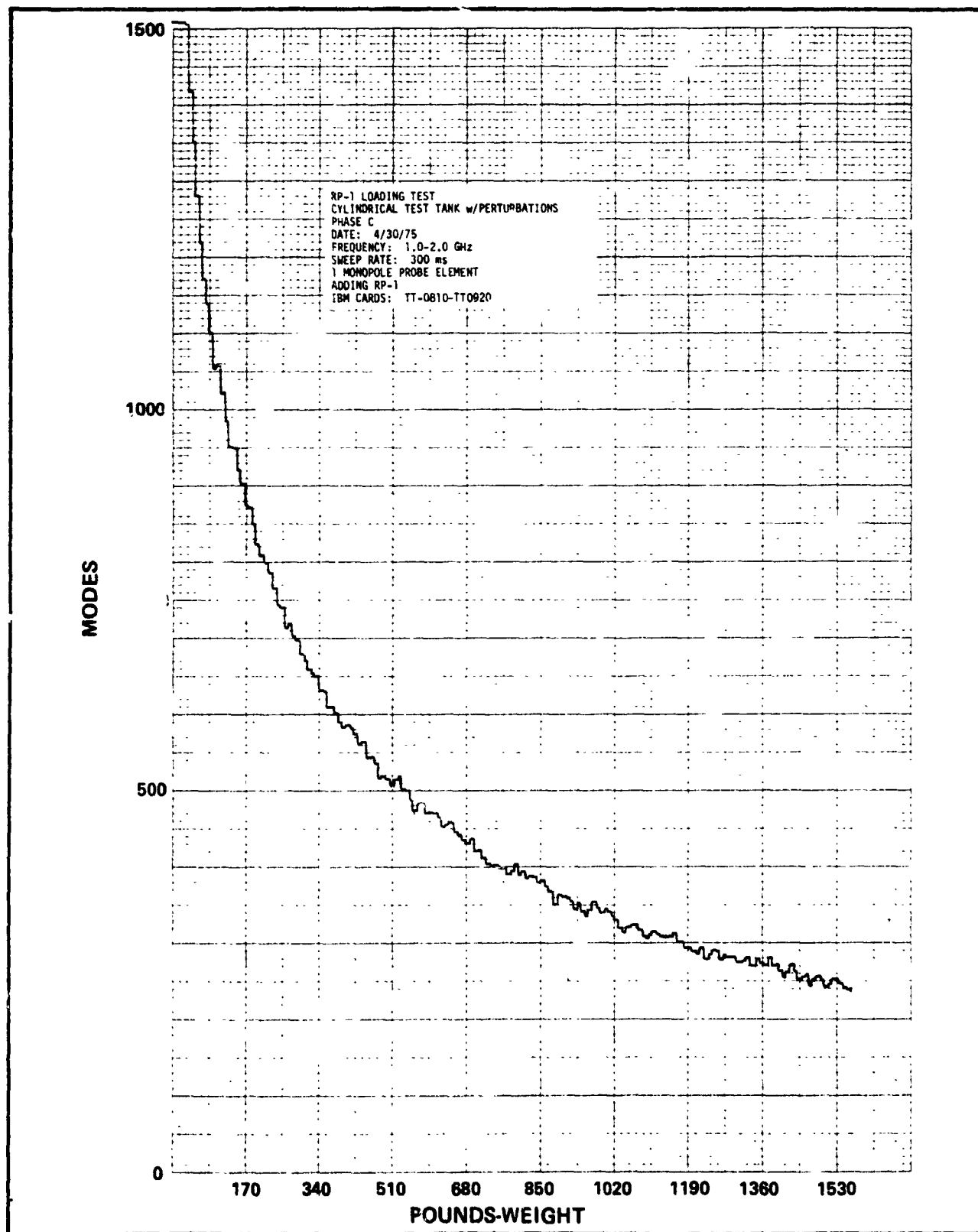


Figure 4-14

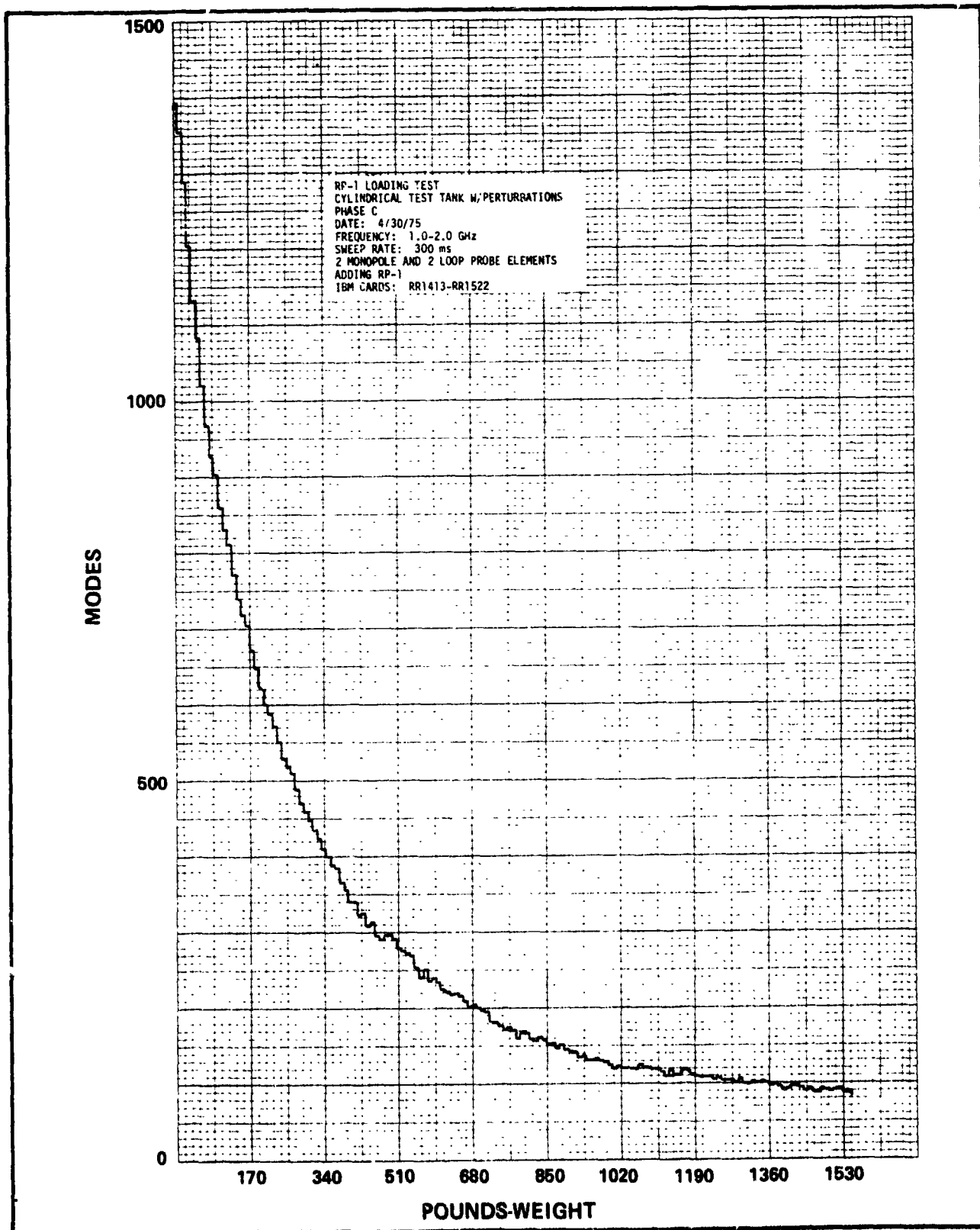


Figure 4-15

TABLE 4-9  
RANGE, MEAN, VARIANCE, AND STANDARD DEVIATION OF  
MODE COUNT DATA: RP-1 DYNAMIC ORIENTATION TESTS - CYLINDRICAL  
TEST TANK (NO PERTURBATIONS)

Mass % Loading	Probe Configuration 4 Monopole Elements						Probe Configuration 1 Monopole Element						Probe Configuration 2 Loop & 2 Monopole Elements											
	Range		Mean		Var		Range		Mean		Var		S.D.		Range		Mean		Var		S.D.			
	Min	Max	Mean	S.D.	Min	Max	Mean	S.D.	Min	Max	Mean	S.D.	Min	Max	Mean	S.D.	Min	Max	Mean	S.D.	Min	Max		
100	76	82	77.97	1.21	1.10	138	175	156.22	72.09	8.49	50	55	52.73	6.88	0.94									
90	75	92	83.57	10.47	3.24	150	180	168.07	28.20	5.31	41	61	53.74	16.90	4.11									
80	87	105	94.61	9.96	3.16	170	198	184.84	34.64	5.89	50	74	61.55	28.17	5.31									
70	99	122	111.14	18.18	4.26	189	231	209.50	52.66	7.26	57	86	72.75	47.79	6.91									
60	118	142	131.30	20.13	4.49	218	260	242.70	72.99	8.54	76	103	90.74	44.23	6.65									
50	147	172	161.65	25.97	5.10	255	303	283.99	105.61	10.28	94	135	114.72	60.04	7.75									
40	190	219	202.40	34.77	5.90	302	369	342.26	201.43	14.19	127	177	153.99	90.83	9.53									
30	257	299	276.24	88.59	9.41	387	459	428.86	259.68	16.11	195	257	223.58	133.41	11.55									
20	392	445	413.97	120.63	10.98	524	610	568.31	435.10	20.86	336	389	361.42	164.56	12.83									
10	614	684	656.11	149.25	12.22	725	876	820.61	1724.48	41.53	571	658	617.55	232.09	15.23									
0	1356	1383	1371.16	34.27	5.85	2203	2258	2224.52	126.79	11.26	1314	1345	1329.55	35.17	5.93									
			Average S.D.	5.97						Average S.D.	13.6					Average S.D.	7.88							

**TABLE 4-10**  
**RANGE, MEAN, VARIANCE, AND STANDARD DEVIATION OF**  
**MODE COUNT DATA: RP-1 DYNAMIC ORIENTATION TESTS - CYLINDRICAL**  
**TEST TANK (WITH PERTURBATIONS)**

Mass % Loading	Probe Configuration 4 Monopole Elements					Probe Configuration 1 Monopole Element					Probe Configuration 2 Loop & 2 Monopole Elements				
	Range		Mean	Var	S.D.	Range		Mean	Var	S.D.	Range		Mean	Var	S.D.
	Min	Max				Min	Max				Min	Max			
100	69	74	71.95	0.83	0.91	217	224	219.82	2.87	1.69	61	66	62.64	1.39	1.18
90	72	89	81.64	12.05	3.47	220	256	243.36	31.28	5.59	58	82	73.75	31.01	5.57
80	85	102	94.36	13.52	3.68	237	281	264.68	112.94	10.63	67	99	86.10	59.11	7.69
70	102	120	110.04	14.24	3.77	274	311	293.60	106.74	10.33	79	109	92.65	56.35	7.51
60	119	143	131.68	21.09	4.59	306	349	326.23	114.44	10.70	98	132	112.70	61.53	7.84
50	150	176	163.12	20.59	4.54	353	392	371.33	104.10	10.20	115	167	143.27	92.10	9.60
40	199	222	209.82	21.69	4.66	412	449	427.48	71.41	8.45	168	204	191.17	68.82	8.30
30	274	302	287.63	35.97	6.00	497	538	514.04	57.12	7.56	248	290	271.19	118.11	10.87
20	408	459	429.14	82.46	9.08	626	660	644.58	66.22	8.14	392	449	416.33	138.42	11.77
10	670	720	690.96	95.69	9.78	878	908	889.82	36.87	6.07	650	713	685.32	136.88	11.70
0	1425	1443	1433.33	14.44	3.80	1765	1796	1776.33	38.83	6.23	1378	1399	1389.07	25.18	5.02
Average S.D.				4.86	Average S.D.				7.78	Average S.D.				7.91	



orientation test data for each of the tank and probe configurations. It is seen that in general the variance and standard deviation of mode count data is lower in the case of dynamic orientation where the test fluid is in motion relative to the interior of the test tank. It is also noted that the mean mode count for both the dynamic and static orientation testing is in relatively close agreement, although in general the mean mode count obtained during the dynamic orientation is slightly lower than that obtained during the static orientation. This is attributed to the fact that the RF sweep speed during the dynamic tests was slow relative to the very rapid dynamic changes in the positioning of the RP-1 within the tank. Note that the differences in mean mode count for the 80% mass loadings is smaller than for the 20% mass loadings. This follows from the fact that the motion of the liquid is much more restricted at the 80% mass loading.

## 4.2 SPHERICAL TANK EVALUATIONS

To provide additional configuration evaluations and a test vessel for RP-1 pressurization tests, a small spherical test tank was designed for use with RP-1. This tank has an internal diameter of 0.857 meters and a volume of 0.330 cubic meters. Figure 4-16 shows this tank mounted in the orientation test fixture. Since RP-1 pressure tests were to be performed in this tank, the two hemispherical half shells were welded together at the mating surfaces. Aluminum rod perturbations were placed in each hemisphere as shown in Figure 4-17 just prior to welding together each half. The final configurations of RP probes used during the RP-1 tests included the same four monopole probes that were used during the cylindrical tank tests.

Testing with the spherical tank included empty tank strip charts with various combinations of RF probes, loading and orientation tests, and pressurization tests. The following paragraphs describe this testing.

### 4.2.1 STRIP CHART DATA

An examination of strip charts with various combinations of monopole and loop probe elements was performed with the spherical test tank with an RF frequency band of 1.0 to 2.0 GHz. Table 4-12 summarizes the mode count obtained for each probe combination. Again it is seen that as the number of probes increases, the detectable mode count decreases. The advantages of using multiple probes in terms of improved performance with orientation must be weighed

**TABLE 4-11**  
**COMPARISON OF RANGE, MEAN, VARIANCE, AND STANDARD DEVIATION**  
**OF MODE COUNT DATA OBTAINED DURING STATIC AND**  
**DYNAMIC ORIENTATION: RP-1 CYLINDRICAL TEST TANK**

Tank Configuration	Probe Configuration	Mass % Loading	Dynamic Orientation						Static Orientation					
			Range		Mean	Var.	S.D.	Range		Mean	Var.	S.D.		
			Min	Max				Min	Max					
No Perturbations	4 Monopole	80	87	105	94.61	9.96	3.16	89	102	96.23	9.54	3.09		
	4 Monopole	20	392	445	413.97	120.63	10.98	386	451	406.67	293.13	17.12		
	1 Monopole	80	170	198	184.84	34.64	5.89	170	210	187.48	90.31	9.50		
	1 Monopole	20	524	610	568.31	435.10	20.86	536	610	571.47	309.71	17.60		
	2 Monopole & 2 Loop	80	50	74	61.55	28.17	5.31	51	78	63.25	51.41	7.17		
	2 Monopole & 2 Loop	20	336	389	361.42	164.56	12.83	331	398	356.92	262.88	15.21		
With Perturbations	4 Monopole	80	85	102	94.36	13.52	3.68	90	101	95.49	5.42	2.33		
	4 Monopole	20	408	452	429.14	82.46	9.08	413	445	430.26	55.19	7.43		
	1 Monopole	80	237	281	264.68	112.94	10.63	236	294	268.34	220.69	14.86		
	1 Monopole	20	626	660	644.58	66.22	8.14	634	700	653.73	185.96	13.64		
	2 Monopole & 2 Loop	80	67	99	86.10	59.11	7.69	71	97	85.34	48.90	6.99		
	2 Monopole & 2 Loop	20	392	449	416.33	138.42	11.77	395	423	407.36	40.65	6.38		



**Figure 4-16**  
**SPHERICAL RP-1 TEST TANK**

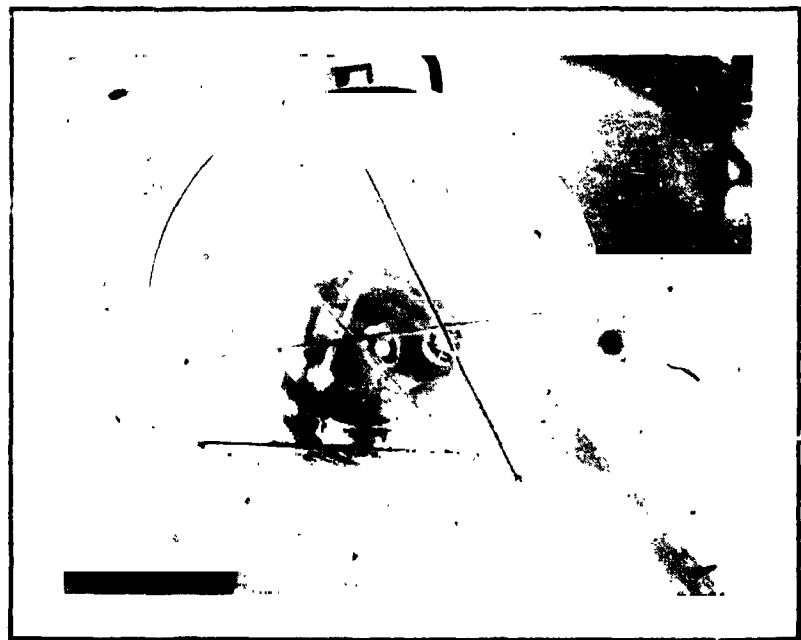


**Figure 4-17**  
**HEMISPHERE WITH PERTURBATIONS**



against the lower Q and subsequently lower mode count. From the evaluations with the cylindrical test tank it is clear that the advantages of using a multiple probe are significant enough to support its use. It is also noted that the loop probes do not offer any advantage over the monopole type probes.

TABLE 4-12  
MODE COUNT FOR COMBINATIONS OF RF PROBES  
FROM STRIP CHART DATA, SPHERICAL TANK, 1.0-2.0 GHz

PROBE COMBINATION NUMBER	STRIP CHART TAKEN FROM PORT #2		PORT #1	PORT #3	PORT #4
	TYPE PROBE	MODE COUNT			
1	Monopole	686	Plug	Plug	Plug
2	Monopole	634	Monopole	Plug	Plug
3	Monopole	600	Monopole	Monopole	Plug
4	Monopole	595	Monopole	Monopole	Monopole
5	Monopole	602	Monopole	Loop	Loop
6	Loop	561	Monopole	Monopole	Loop
7	Loop	666	Plug	Plug	Plug

#### 4.2.2 RP-1 TEST RESULTS

The spherical test tank was moved to the test cell and interfaced with the fluids and data acquisition systems. Using an RF range of 1.0-2.0 GHz an X-Y plot of the systems analog output versus mass of RP-1 was taken as illustrated in Figure 4-18. Using the 1.0-2.0 GHz RF frequency band with RP-1 and four monopole probes, the following orientation data was obtained:

- Dynamic orientation data at every 10% RP-1 mass increment from 100% thru 0%. Approximately 100 data frames were



recorded directly on IBM cards at each 10% loading condition. (Approximately 1100 data frames).

- Static orientation data at 80% and 20% RP-1 loading increments. At each RP-1 loading, approximately 20 data frames were recorded for each tank position at angular increments of 45 degrees from 0-360 degrees, i.e., approximately 180 data frames at each loading. (Approximately 360 data frames).

The dynamic orientation data obtained during the test was analyzed by establishing for each mass loading:

- Minimum mode count
- Maximum mode count
- Mean mode count
- Variance in mode count
- Standard deviation of mode count.

Table 4-13 contains the results obtained during the dynamic orientation tests, indicating an average standard deviation of 4.59 modes for all fill levels. Table 4-14 shows a comparison of the test results obtained for the dynamic and static orientations with 80% and 20% RP-1 mass loadings. It is noted that the mean mode count for the dynamic and static orientation are in close agreement.



TABLE 4-13  
RANGE, MEAN, VARIANCE, AND STANDARD DEVIATION OF  
MODE COUNT DATA: RP-1 DYNAMIC ORIENTATION TESTS  
SPHERICAL TEST TANK – MAY 14, 1975

MASS % LOADING	RANGE		MEAN	VAR	S.D.
	MIN	MAX			
100	73	78	75.34	1.34	1.16
90	94	110	102.69	11.11	3.33
80	104	121	112.50	12.07	3.47
70	119	137	127.14	14.22	3.77
60	133	150	140.66	17.46	4.18
50	150	170	161.08	19.29	4.39
40	177	208	192.53	37.81	6.15
30	229	258	242.63	47.11	6.86
20	293	334	313.62	56.03	7.49
10	394	426	411.11	46.02	6.78
0	629	643	636.61	8.64	2.94
Average S.D.					4.59

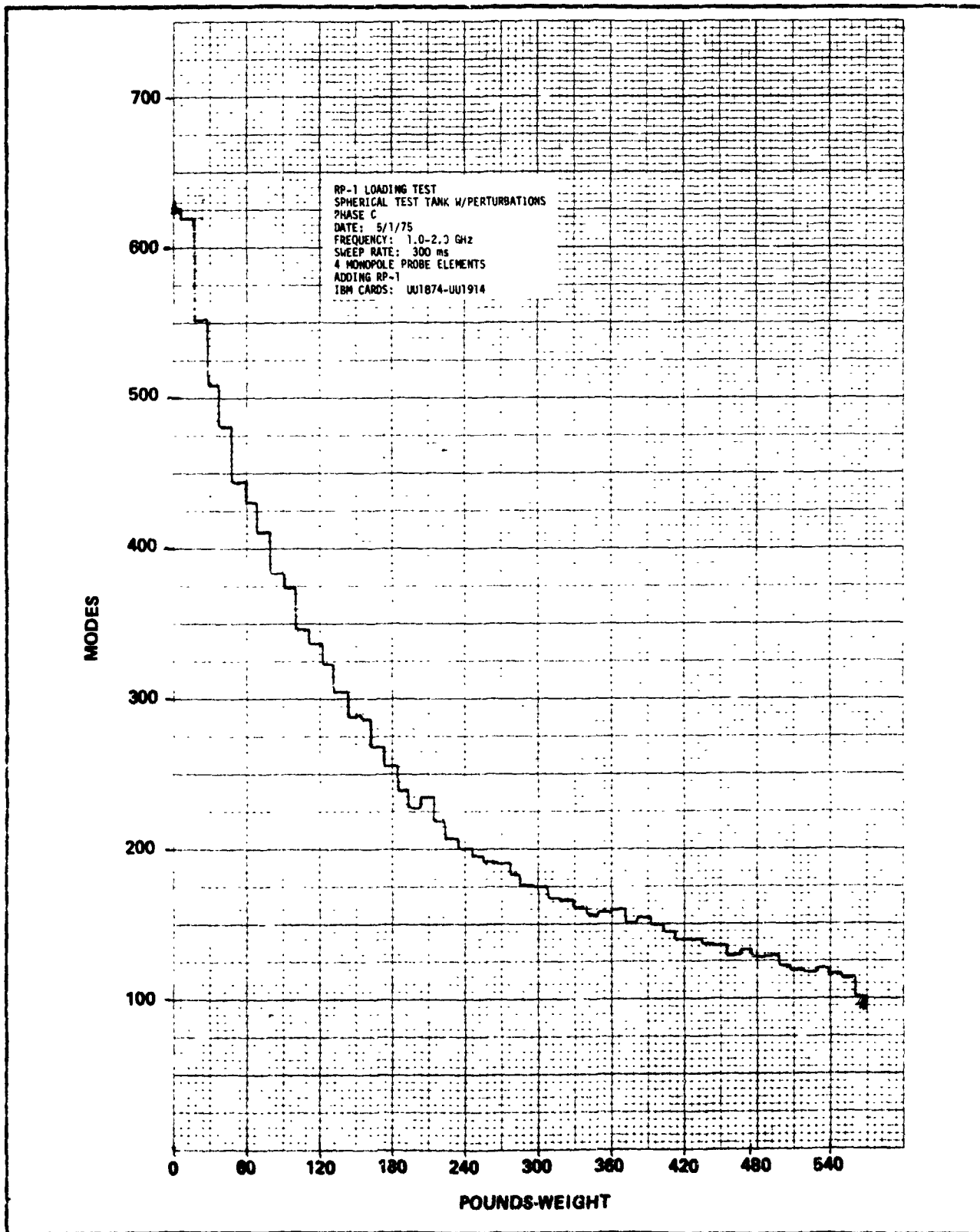


Figure 4-18



**TABLE 4-14**  
**COMPARISON OF RANGE, MEAN, VARIANCE, AND STANDARD DEVIATION**  
**OF MODE COUNT DATA OBTAINED DURING STATIC AND**  
**DYNAMIC ORIENTATION: RP-1 SPHERICAL TANK**

MASS % LOADING	DYNAMIC ORIENTATION					STATIC ORIENTATION				
	RANGE		MEAN	VARIANCE	S.D.	RANGE		MEAN	VARIANCE	S.D.
	MIN	MAX				MIN	MAX			
80	104	121	112.50	12.07	3.47	107	121	112.61	12.58	3.55
20	293	334	313.62	56.03	7.49	304	322	314.08	27.79	5.27

#### 4.2.3 PRESSURIZATION TESTS

A pressurization test using the spherical RP-1 test tank was performed to determine the effect on the RF gauging system output under conditions of pressure. Theory would demand that if the volume of the tank is not changed and if the electrical characteristics of the RF probes are not altered by the pressure conditions, the RF mode count will not change.

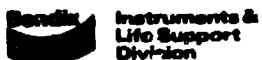
##### 4.2.3.1 VOLUME CHANGE WITH PRESSURE

The volume of the test tank does, however, change with pressure. To estimate the amount of volume change anticipated with the application of 200 psig internal pressure, for the purposes of simplicity, the following can be assumed about the spherical RP-1 test tank:

- It is an ideal sphere, i.e. no welds, holes, etc.
- Made from T-6061 aluminum
- Average thickness;  $t = 0.390$  inches
- Nominal internal radius;  $r = 16.88$  inches.

The tank volume at 0 psig would be

$$V = \frac{4}{3}\pi R^3 = \frac{4}{3}\pi (16.88)^3 \quad (34)$$



$$V = 20146.8 \text{ in}^3 (0.3302 \text{ m}^3).$$

At 200 psig, an estimated volume can be determined by noting that for an ideal sphere the change in radius is

$$\Delta R = \frac{R\sigma}{E} (1 - \nu) \quad (35)$$

where

$R$  = radius (16.88 inches)

$\sigma$  = unit stress

$E$  = modulus of elasticity ( $10.0 \times 10^6$  psi)

$\nu$  = Poisson's ratio (0.30)

and

$$\sigma = \frac{pR}{2t} \quad (36)$$

where

$p$  = pressure (200 psig)

$t$  = thickness (0.390 inch).

Combining equation 35 and 36, and solving for  $\Delta R$

$$\Delta R = \frac{pR^2}{2tE} (1 - \nu)$$

$$\Delta R = \frac{(200)(16.88)^2(1 - 0.3)}{(2)(0.39)(10.0 \times 10^6)} = .0051 \text{ inch (.00013m).} \quad (37)$$

The new volume would then be

$$V = \frac{4}{3}\pi(16.8851)^3 = 20165.06 \text{ in}^3 (.3305 \text{ m}^3).$$



This indicates that an increase in volume of approximately 18.26 in<sup>3</sup> (.003m<sup>3</sup>), i.e., approximately 0.09% increase.

For the empty tank, considering the maximum theoretical number of modes possible based on the volume dependency relationship,

$$N = \frac{8\pi V}{3 C^3} \left( f_2^3 - f_1^3 \right) \quad (38)$$

it would be expected for a 200 psig pressure increase that the maximum number of modes would increase in proportion to the increase in tank volume, i.e. by only 0.09%.

#### 4.2.3.2 PROOF PRESSURE TESTING

A proof pressure test of 600 psig with water was planned prior to beginning the RP-1 pressurization tests. Pressure was gradually increased during the proof pressure test until at 525 psig, the girth weld of the test tank failed. Figures 4-19 and 4-20 illustrate this failure in the weld. The test tank was reworked by machining away the welded area and then again welding together each hemisphere. A proof pressure test was then repeated with a maximum pressure of 325 psig.

#### 4.2.3.3 RP-1 PRESSURIZATION TESTS

For the pressurization tests, twenty IBM data frames of RF mode count and pressure were taken at each 50 psig increments of pressure from 0 to 200 psig for each 10% fill level of RP-1 from 0 to 100%. An X-Y plot of RF mode count versus pressure was also recorded at each RP-1 loading. The IBM recordings at each pressure increment were taken on a static basis where data was first taken at the lowest pressure increment, and then at each successive pressure increment. The X-Y plots at each fill level are continuous recordings which were taken as the pressure was relieved from the test tank.

Table 4-15 is a summary of the average mode count obtained for each combination of pressure and RP-1 loading level. Figures 4-21 thru 4-26 show the X-Y plot recording of 0% (dry), 100%, 90%, 80%, 70%, and the 60% RP-1 loadings. It is noted that at the 60% loading the RF output as seen on the X-Y plot became very irregular. The X-Y plots for the 50%, 40%, 30%, 20%, 10%, and 0% Wet RP-1 loading also showed a very irregular variation in mode count. After

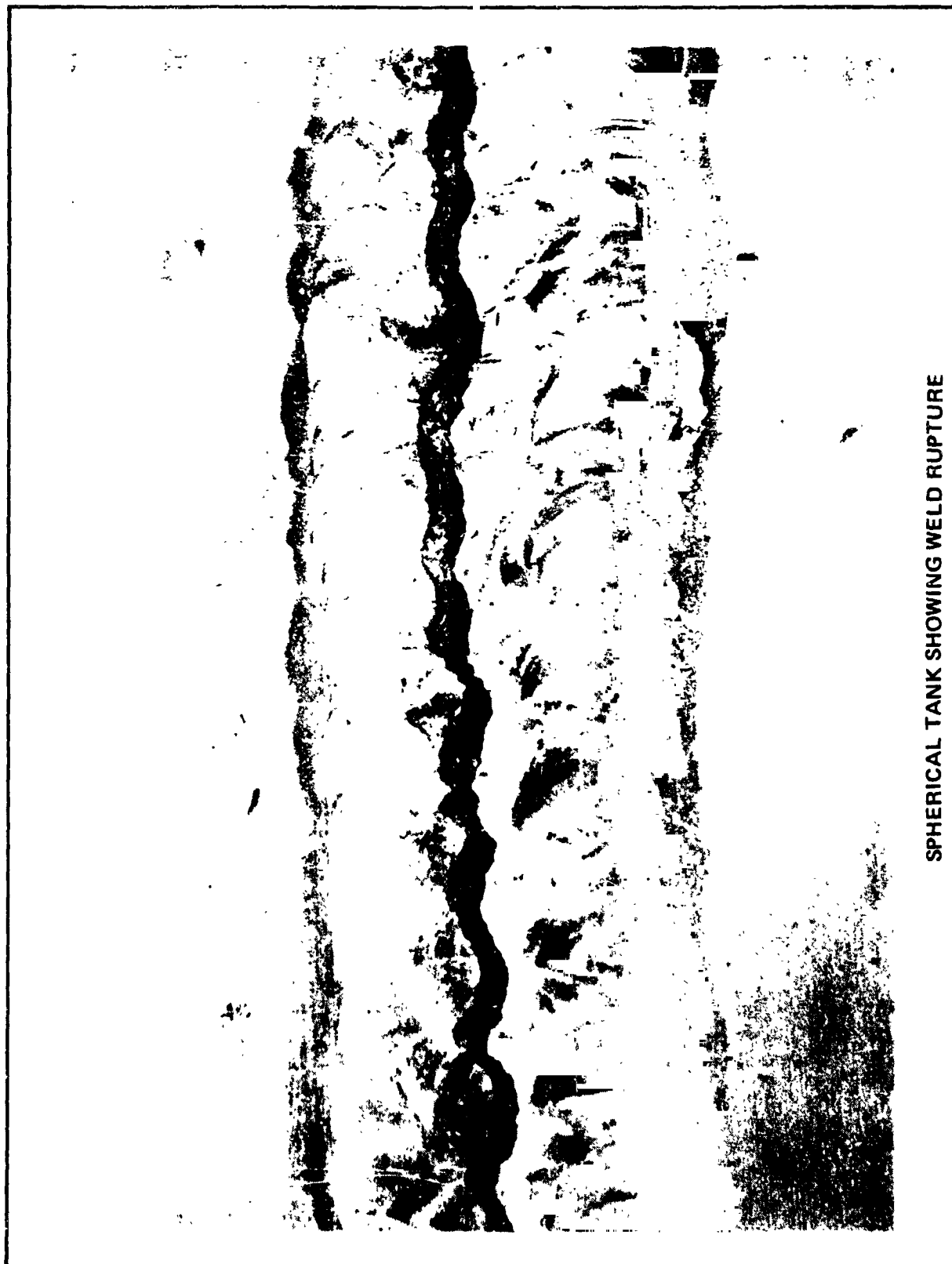
Figure 4-19

SPHERIC VL TANK SHOWING WELD RUPTURE



ORIGINAL PAGE IS  
OF POOR QUALITY

Figure 4-20



SPHERICAL TANK SHOWING WELD RUPTURE

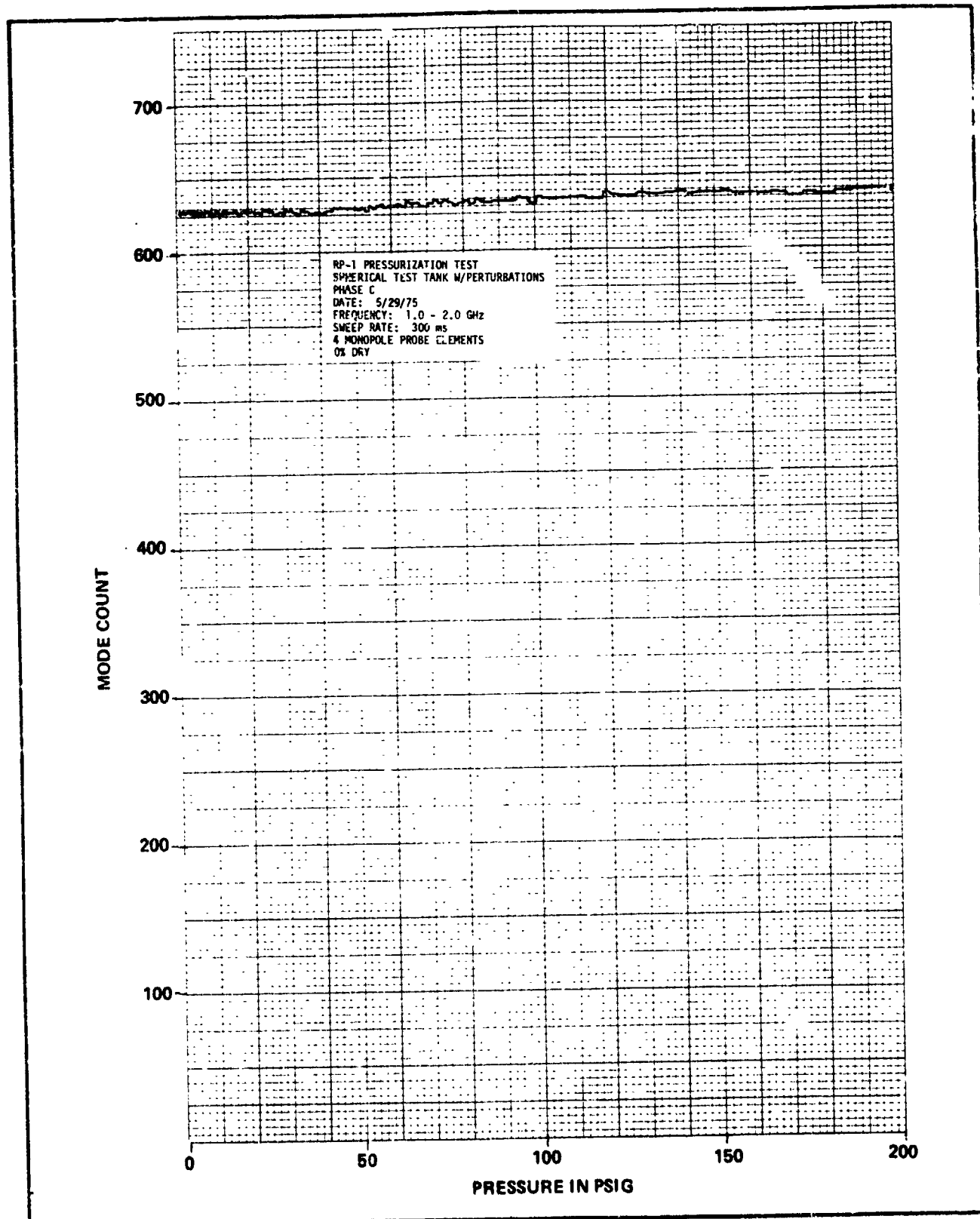


Figure 4-21

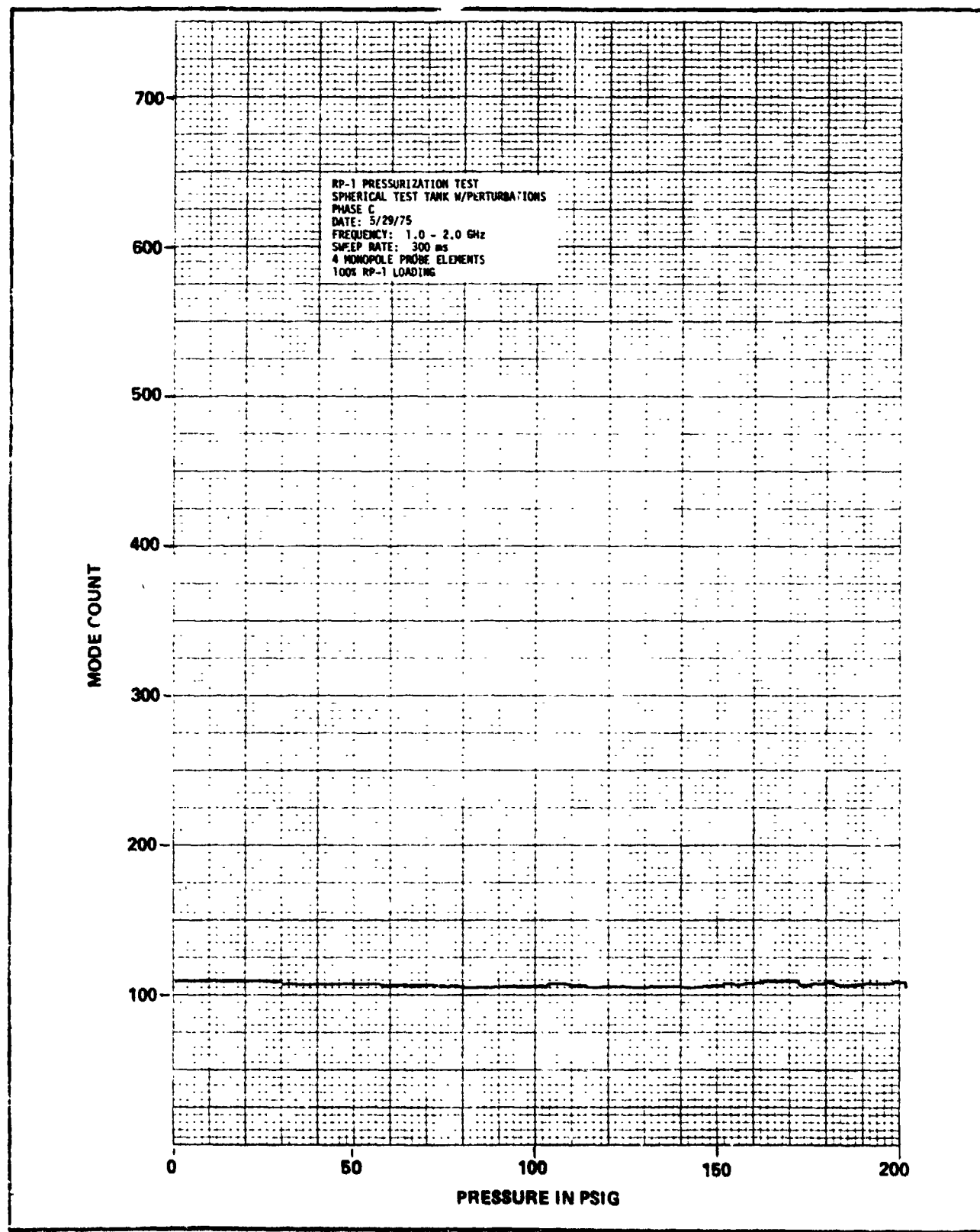


Figure 4-22

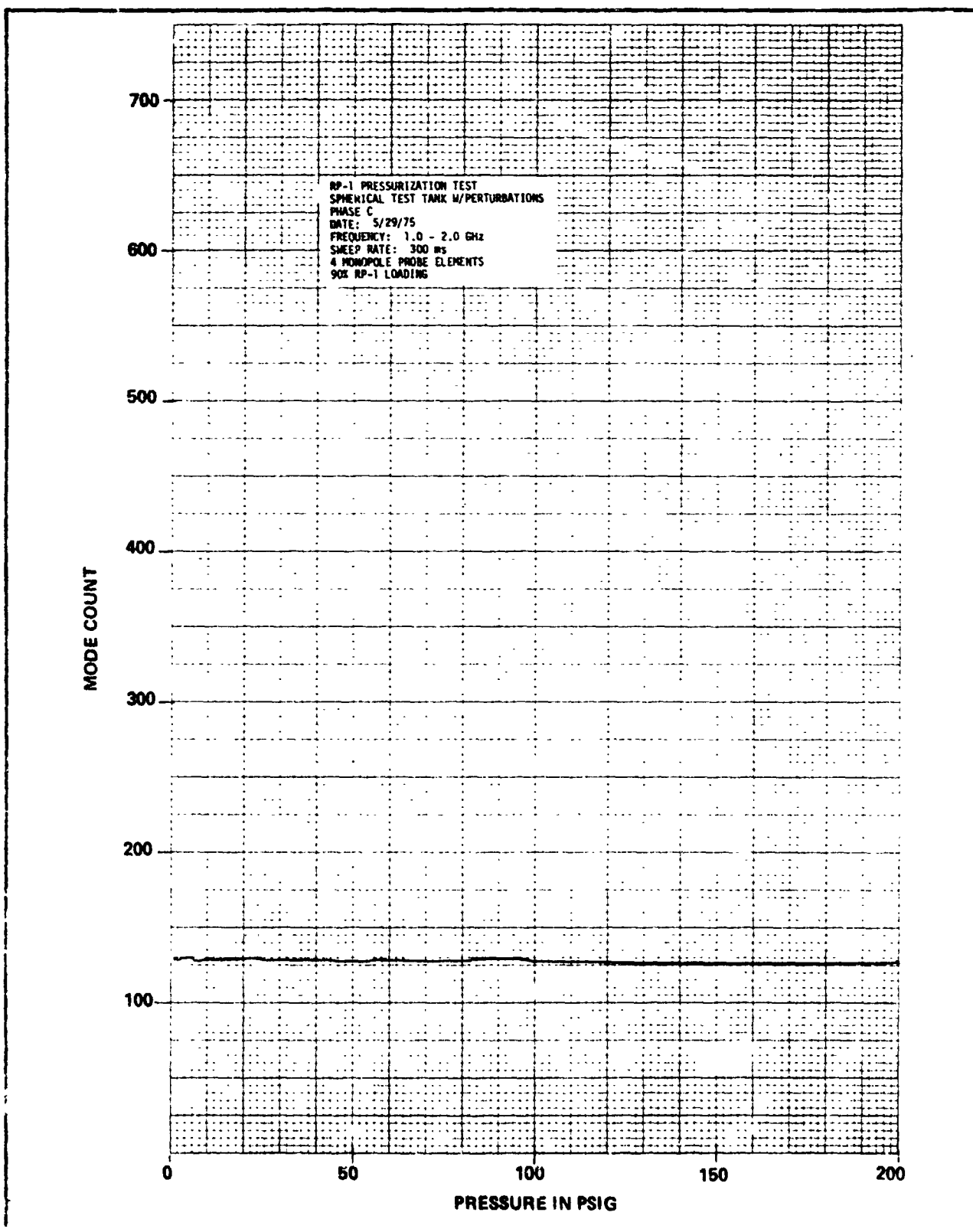


Figure 4-23

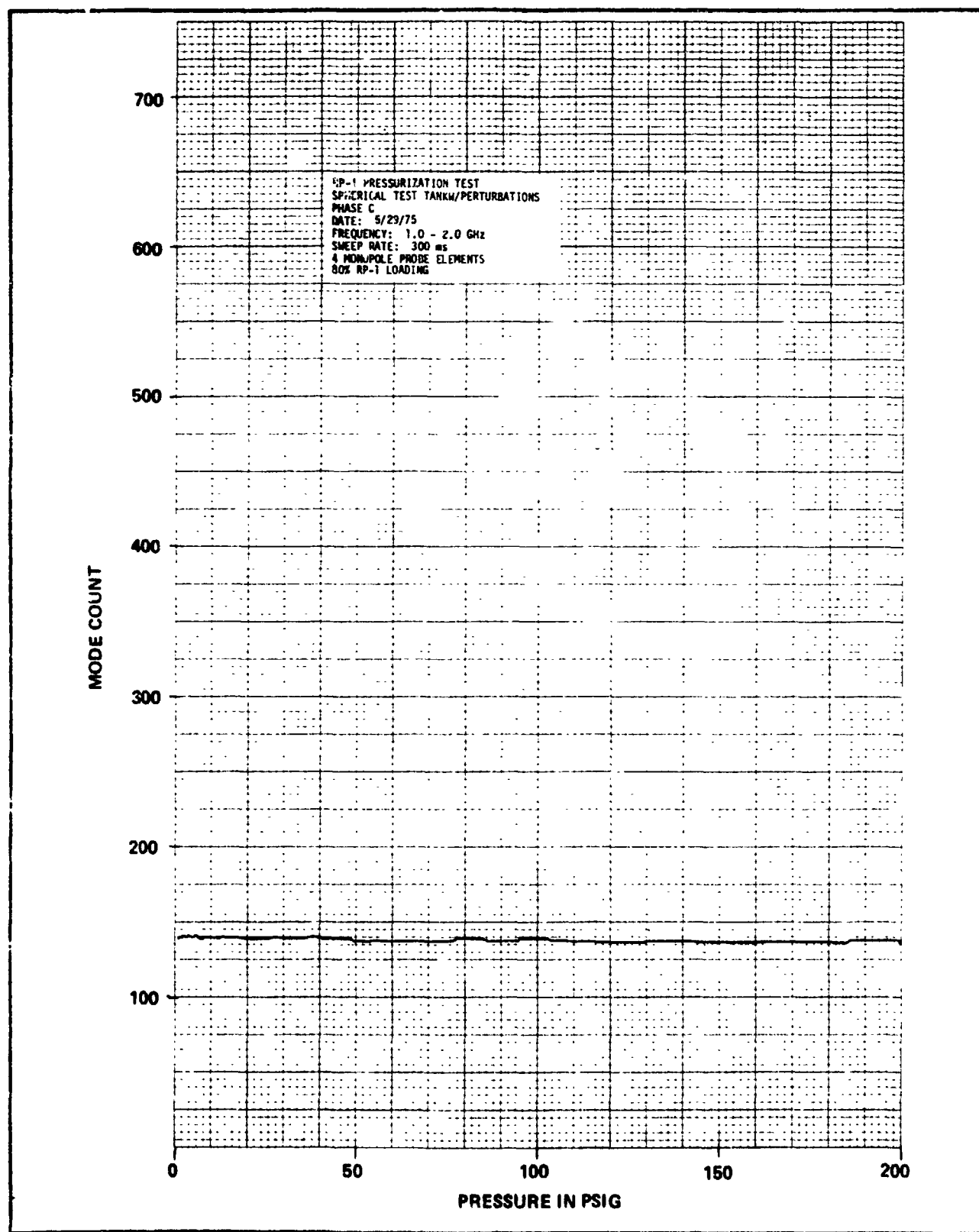


Figure 4-24

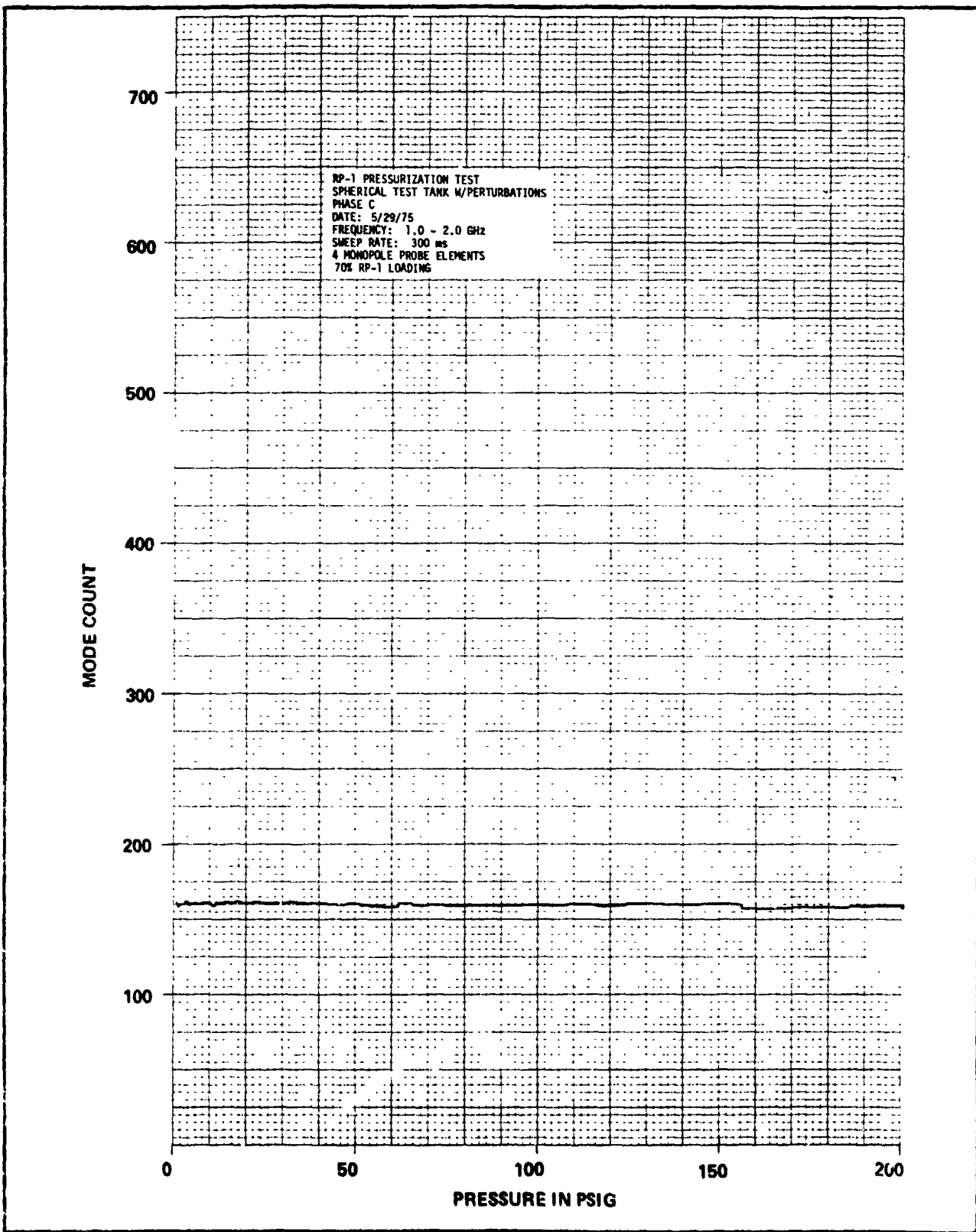


Figure 4-25

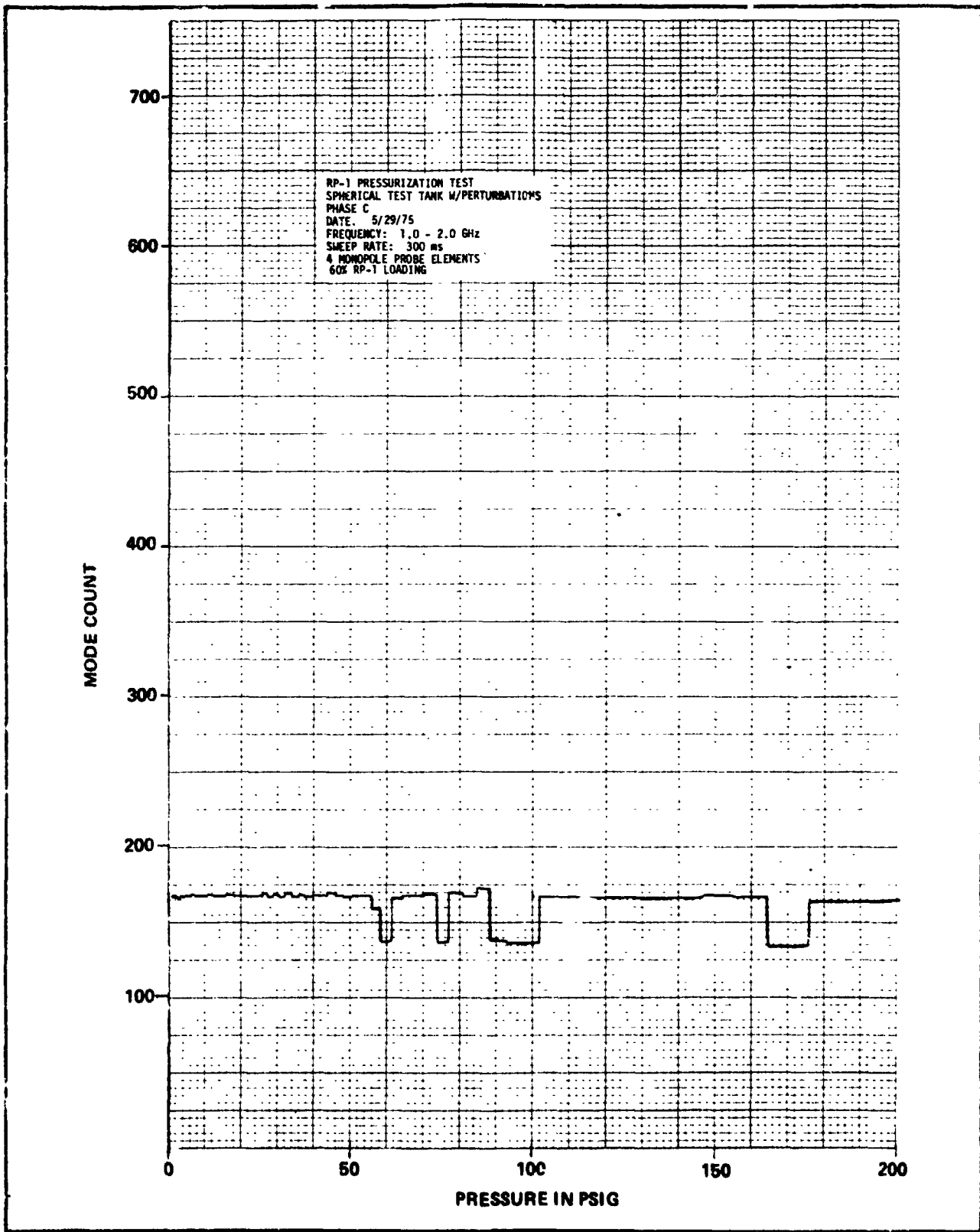


Figure 4-26

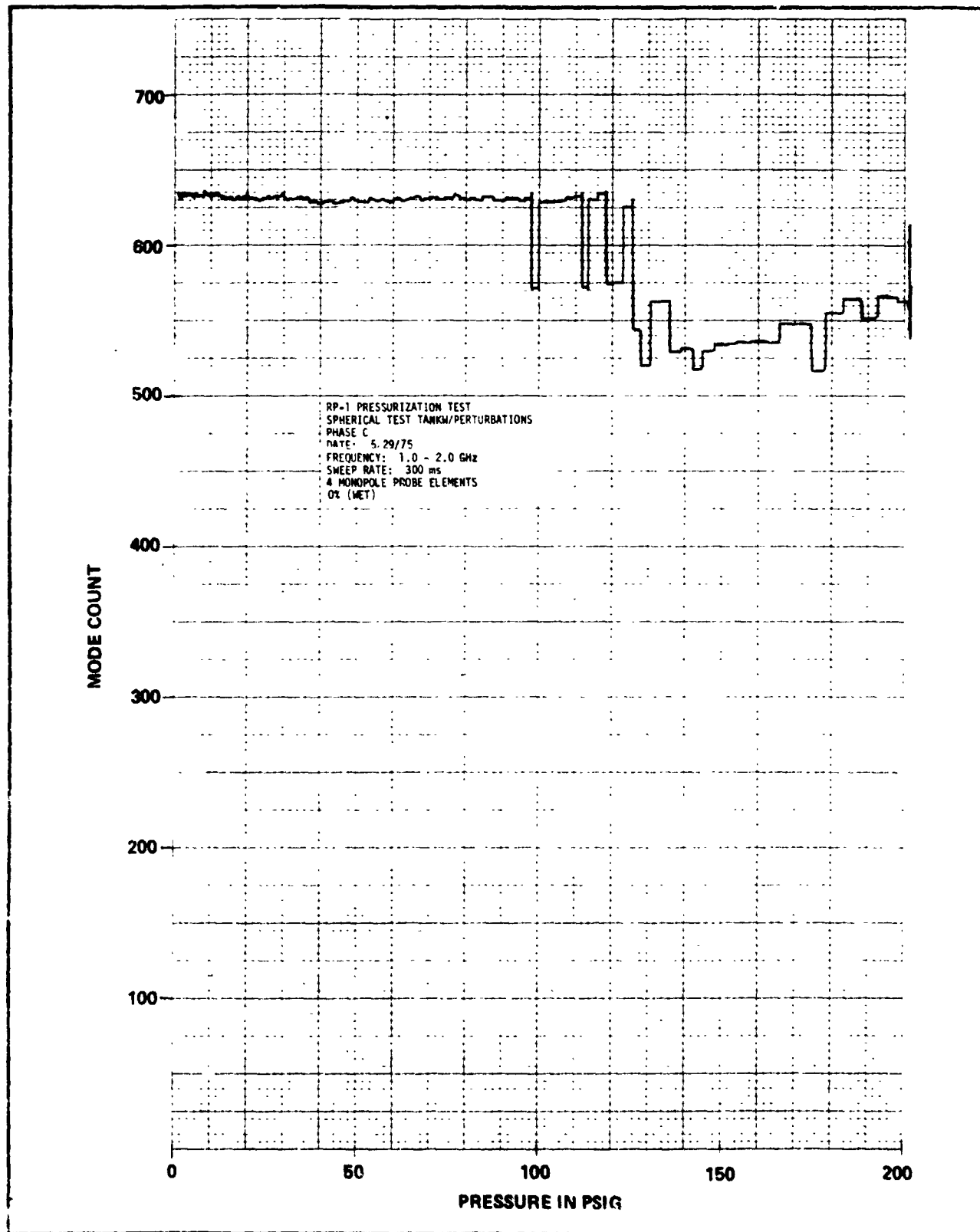
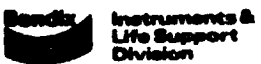


Figure 4-27



the testing, the RF probes were removed from the test tank and the radomes removed. It was noted that RP-1 had leaked into the probes and that in one of the probes the pressure had pushed the radome such that it physically caused the radiation element to short out against the outer conductor of the semi-rigid coax. It was apparent that this was causing an intermittent electrical short during the pressurization. The highlighted data in Table 4-15 are clearly data in which such shorting out of the RF probe was occurring. The remaining data is sufficient to illustrate that there is no significant variation in RF mode count as a function of pressure with RP-1 as the test fluid. A slight increase in mode count in the dry empty tank was noted, and exceeded any increase that could possibly be caused by an increasing tank volume. Figure 4-27 shows the empty tank X-Y plot of mode count versus pressure that was performed after all RP-1 fill levels were tested. It is interesting to note that at the lower increments of pressure there is no such increase in mode count as the pressure was increased. The same is noted from Table 4-15.

An insulating spacer was then fabricated and inserted in each probe to assure that the radiation element would not short out regardless of any collapsing or movement in the radome. It was, however, not feasible to make further modifications to ruggedize or prevent RP-1 from entering the probes. Nonetheless, the pressurization tests were repeated and the results are summarized in Table 4-16. Figures 4-28 thru 4-38 show the X-Y plots of the 100%, 90%, 80%, 70%, 60%, 50%, 40%, 30%, 20%, 10%, and 0% RP-1 loadings. These plots recorded the analog RF output as the pressure in the tank was relieved from 200 psig. It is clear that the addition of the insulating spacers in the RF probes minimized variations with pressure. A more rigid radome would undoubtedly be advantageous to further minimize possible effects due to the probes. One additional test with a 100% RP-1 loading was performed where the tank was pressurized to 300 psig. Figure 4-39 shows the X-Y plot of mode count versus pressure as the pressure was released. There was no detectable change in mode count over the span of 300 psig.



TABLE 4-15  
MODE COUNT VS. PRESSURE  
RP-1 PRESSURE TEST – MAY 29, 1975

APPROX. % RP-1 LOADING	N <sub>2</sub> PRESSURE IN PSIG				
	0	50	100	150	200
DRY EMPTY TANK	614.0	620.9	623.9	627.1	629.9
100	92.2	91.3	88.4	88.7	90.75
90	112.1	111.35	110.5	109.8	109.0
80	124.1	121.2	120.2	119.25	118.5
70	141.9	141.6	140.3	140.5	138.7
60	151.1	150.6	148.0	42.6	142.0
50	172.3	174.2	170.5	141.4	169.1
40	199.5	198.1	178.0	163.2	193.5
30	248.4	49.0	245.4	201.5	201.7
	310.8	307.8	308.1	249.5	278.9
10	415.3	414.0	415.5	378.1	354.65
0 (wet)	618.4	611.5	614.3	618.3	547.7

TABLE 4-16  
MODE COUNT VS. PRESSURE  
RP-1 PRESSURE TEST – JUNE 2, 1975

APPROX. % RP-1 LOADING	N <sub>2</sub> PRESSURE IN PSIG				
	0	50	100	150	200
100	75.6	83.1	84.3	84.6	85.9
90	108.1	108.3	108.6	108.1	107.4
80	124.5	124.8	122.5	120.6	120.6
70	133.1	134.2	133.4	135.0	134.4
60	145.7	148.7	146.0	144.6	146.2
50	167.0	165.5	166.8	169.7	168.8
40	208.4	206.8	205.0	204.4	203.2
30	252.3	251.7	253.0	250.6	246.4
20	316.5	314.0	314.1	317.4	322.3
10	401.7	407.6	410.7	410.4	411.8
0 (Wet)	628.3	630.7	631.8	628.2	630.8

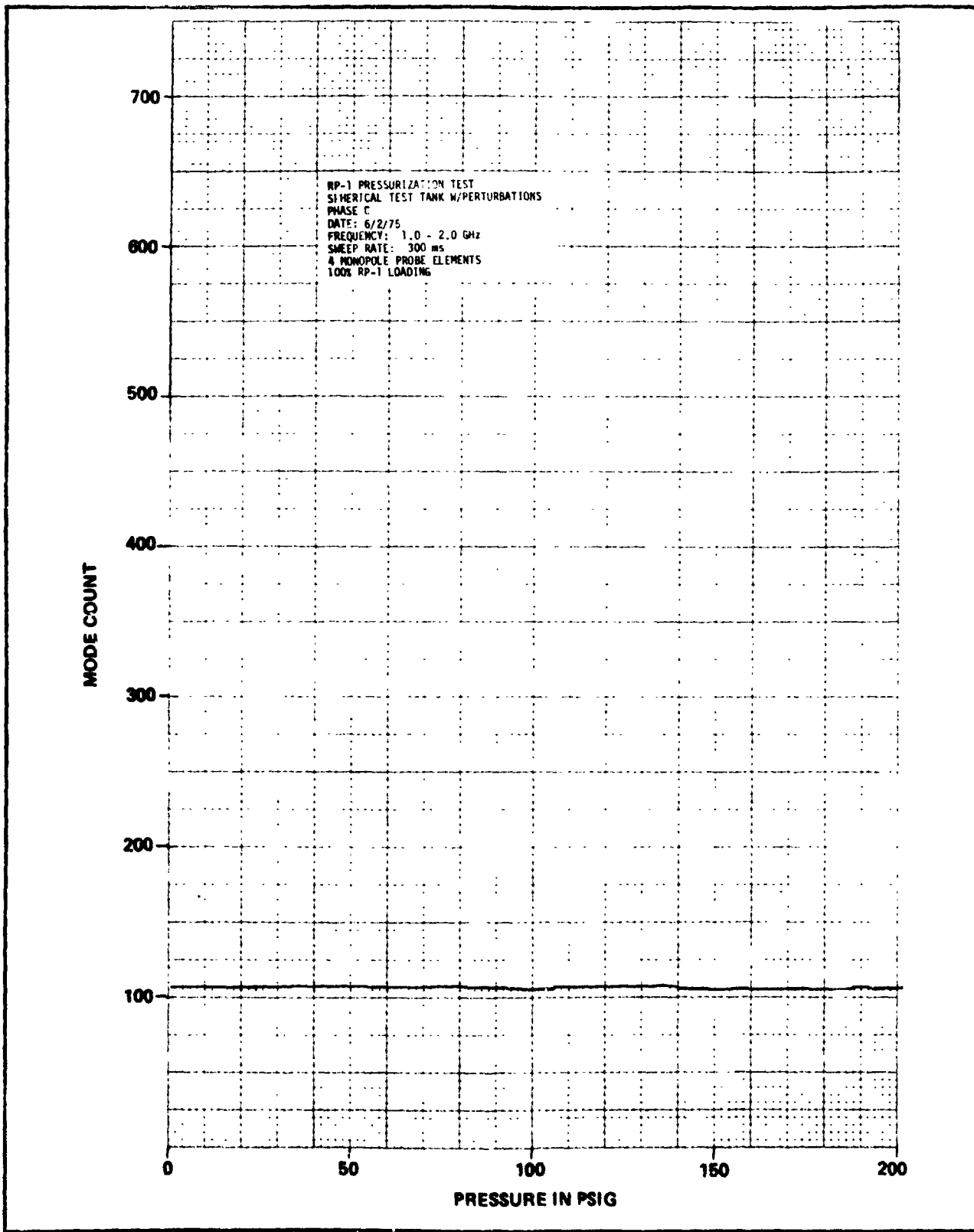


Figure 4-28

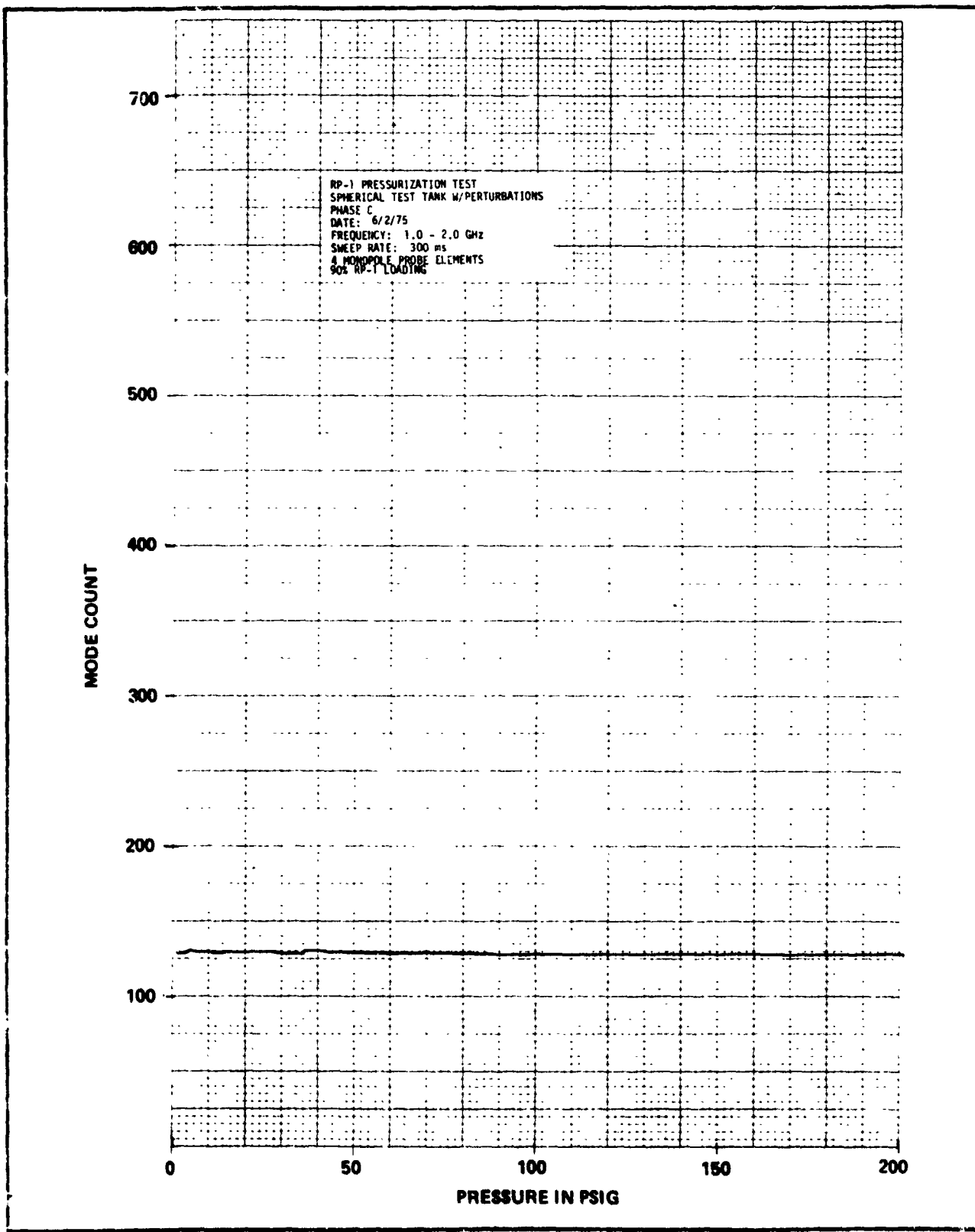


Figure 4-29

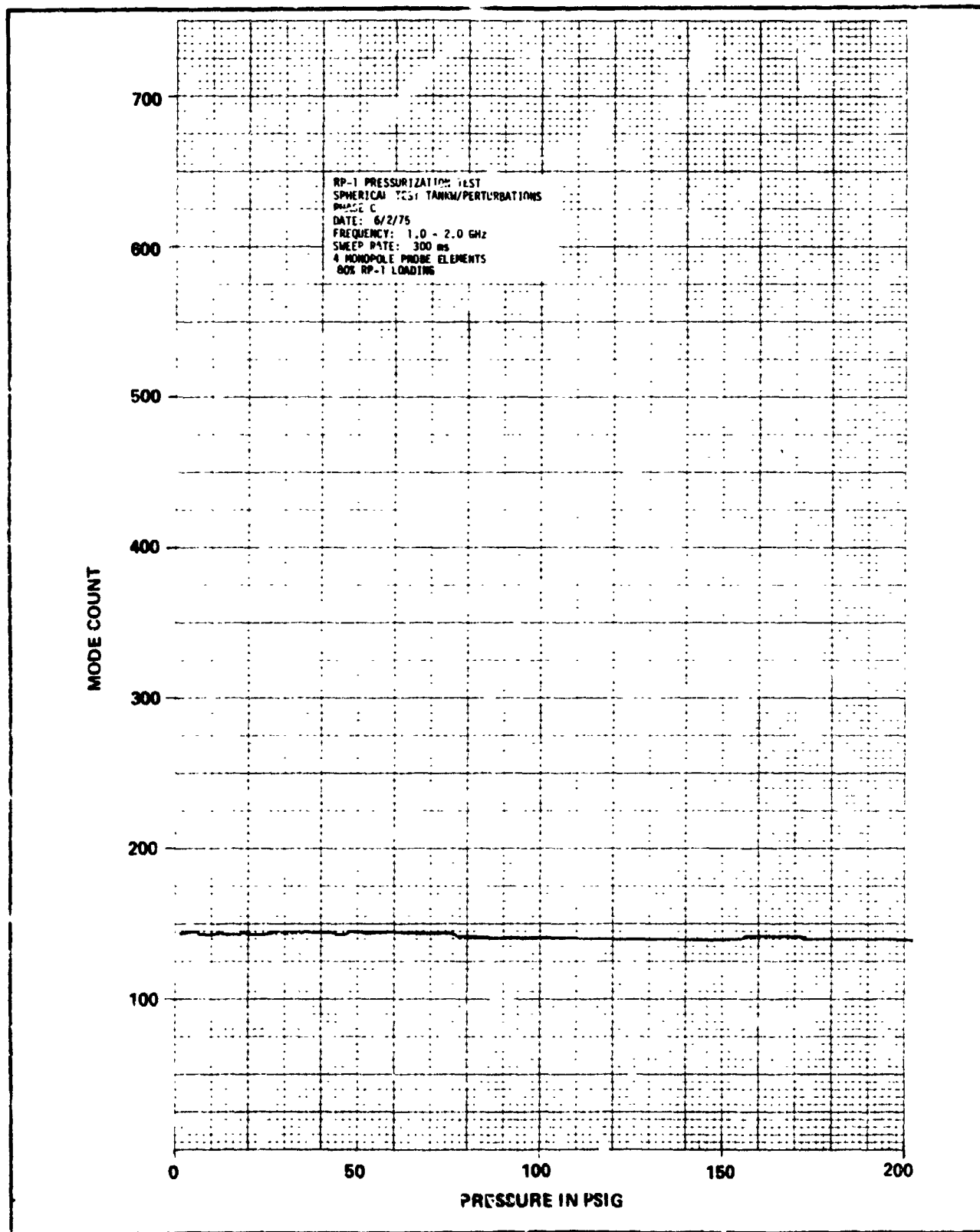


Figure 4-30

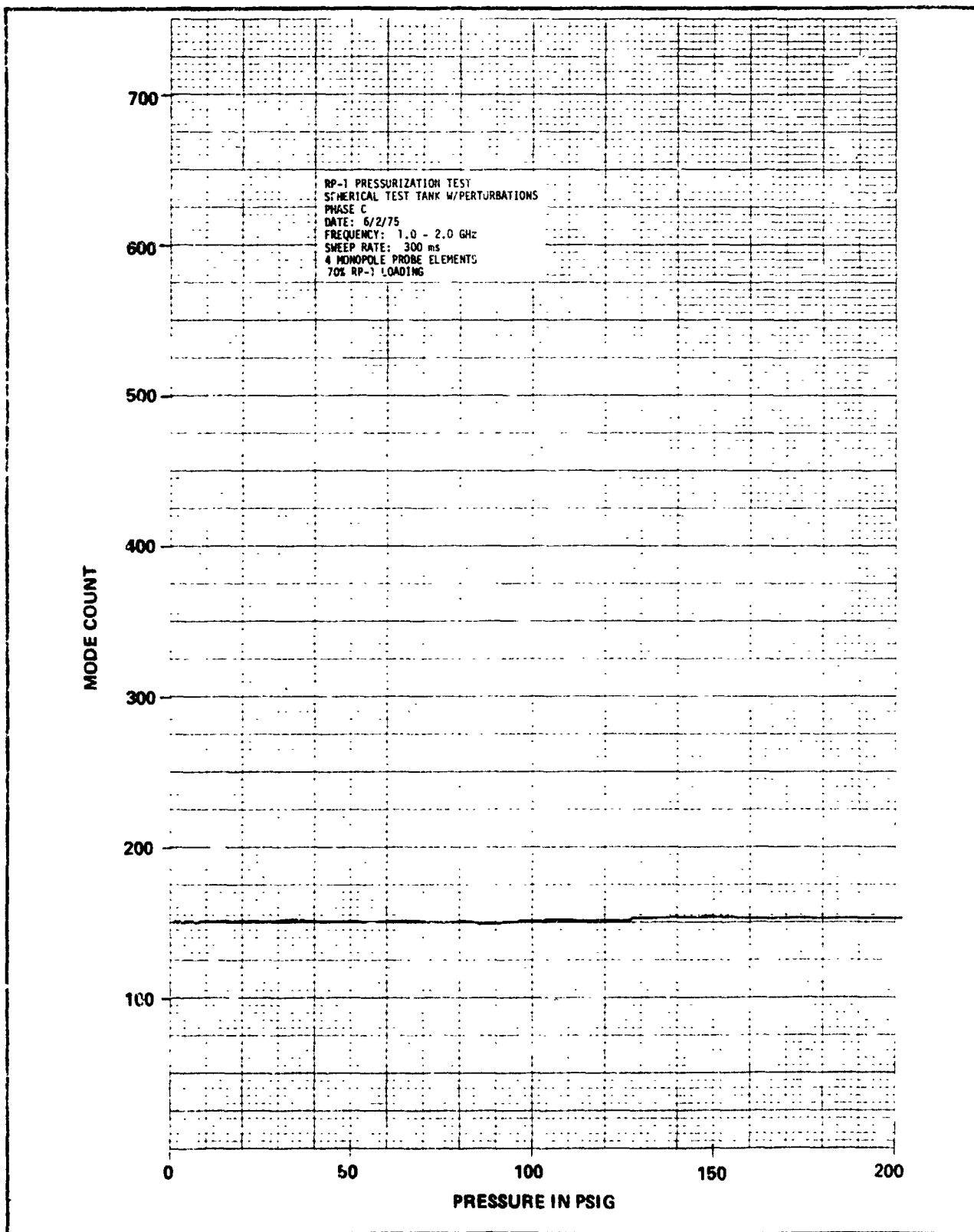


Figure 4-31

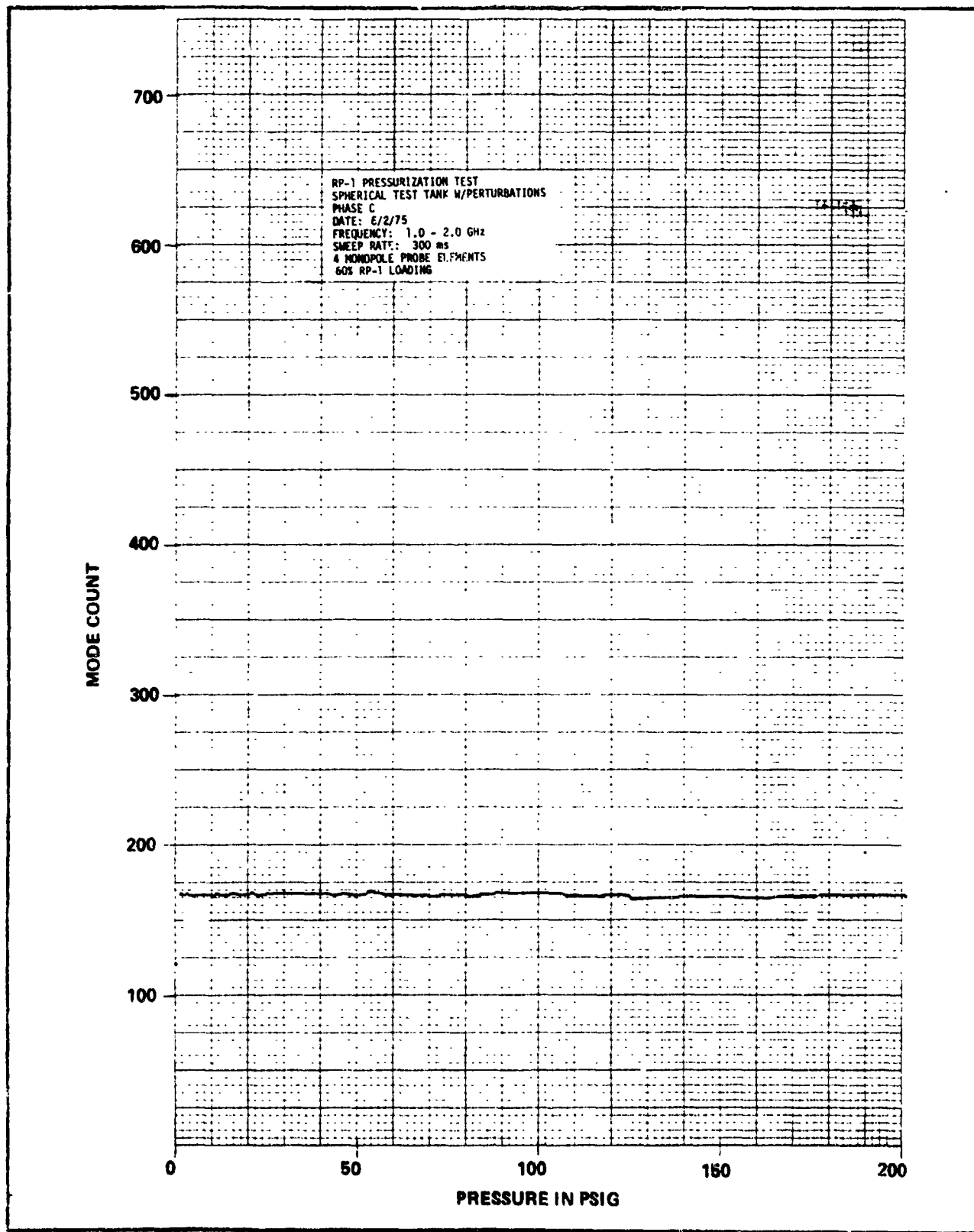


Figure 4-32

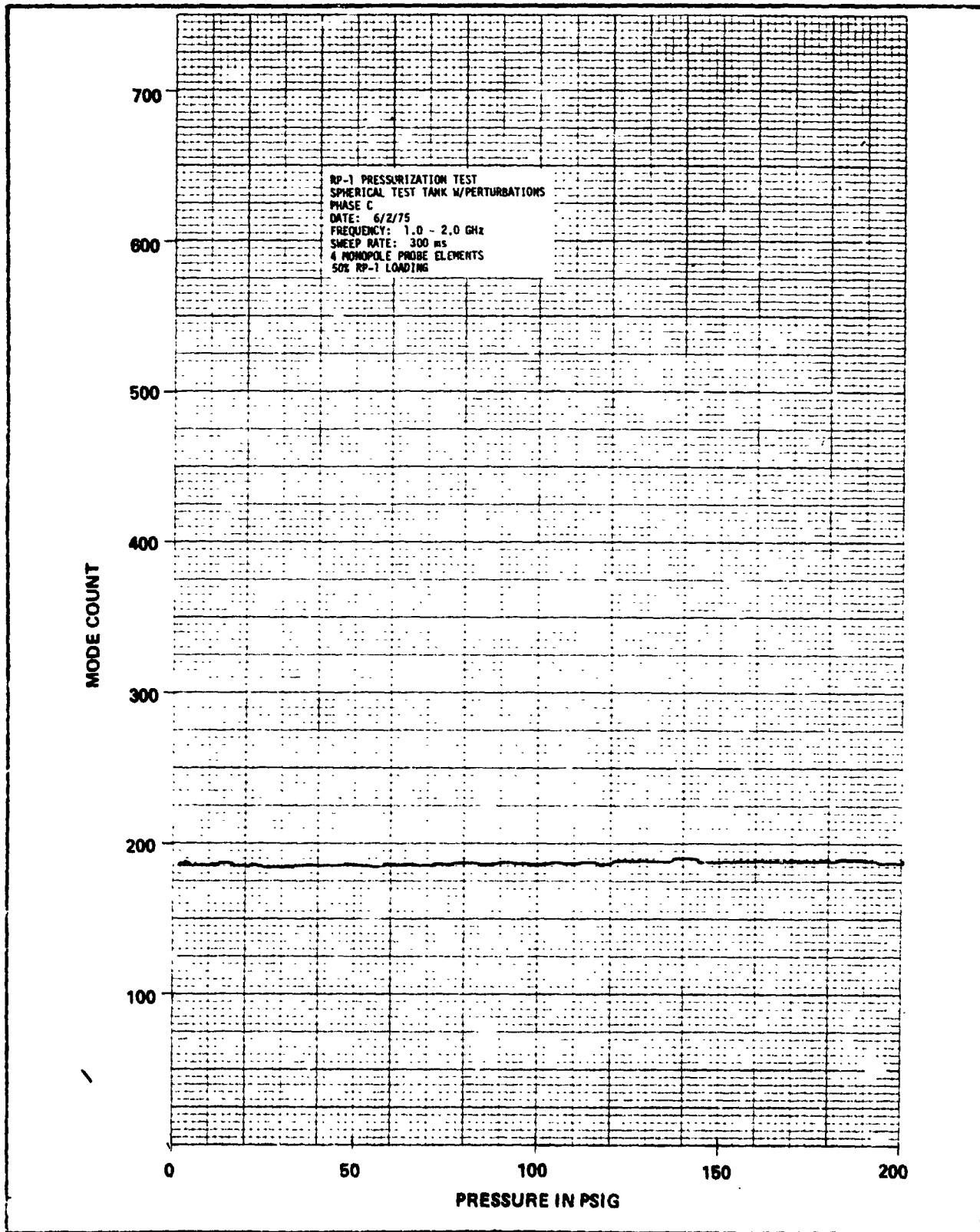


Figure 4-33

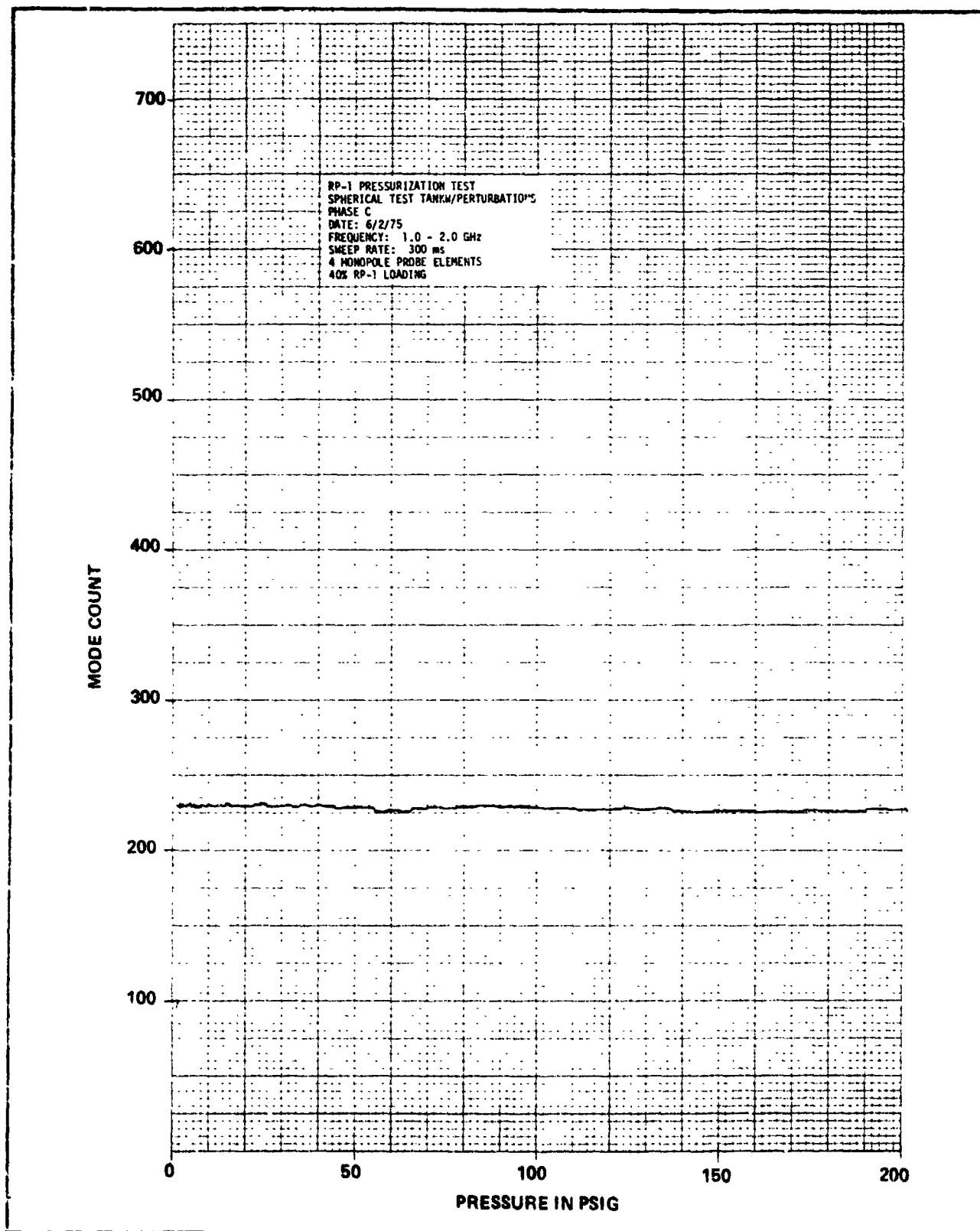


Figure 4-34

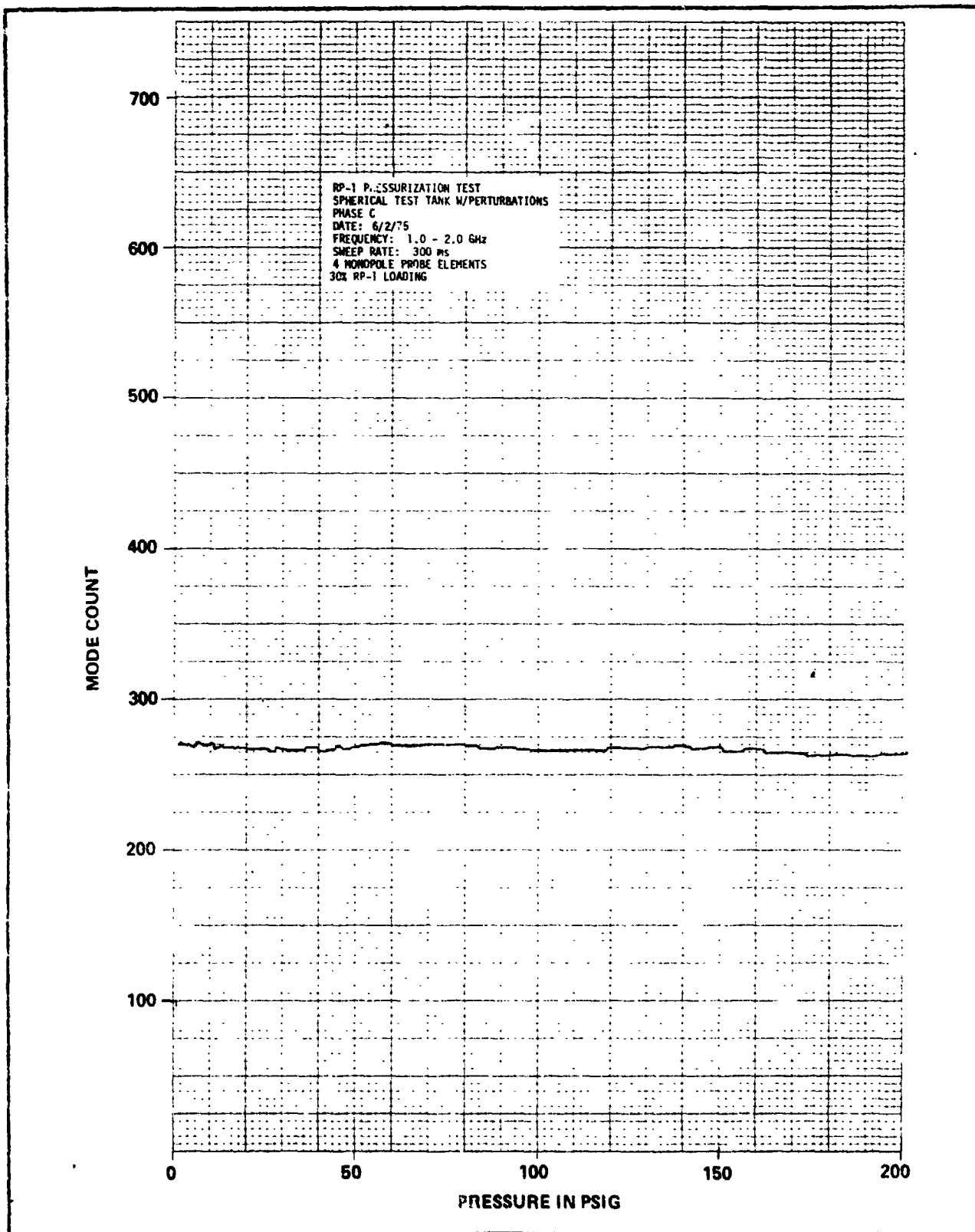


Figure 4-35

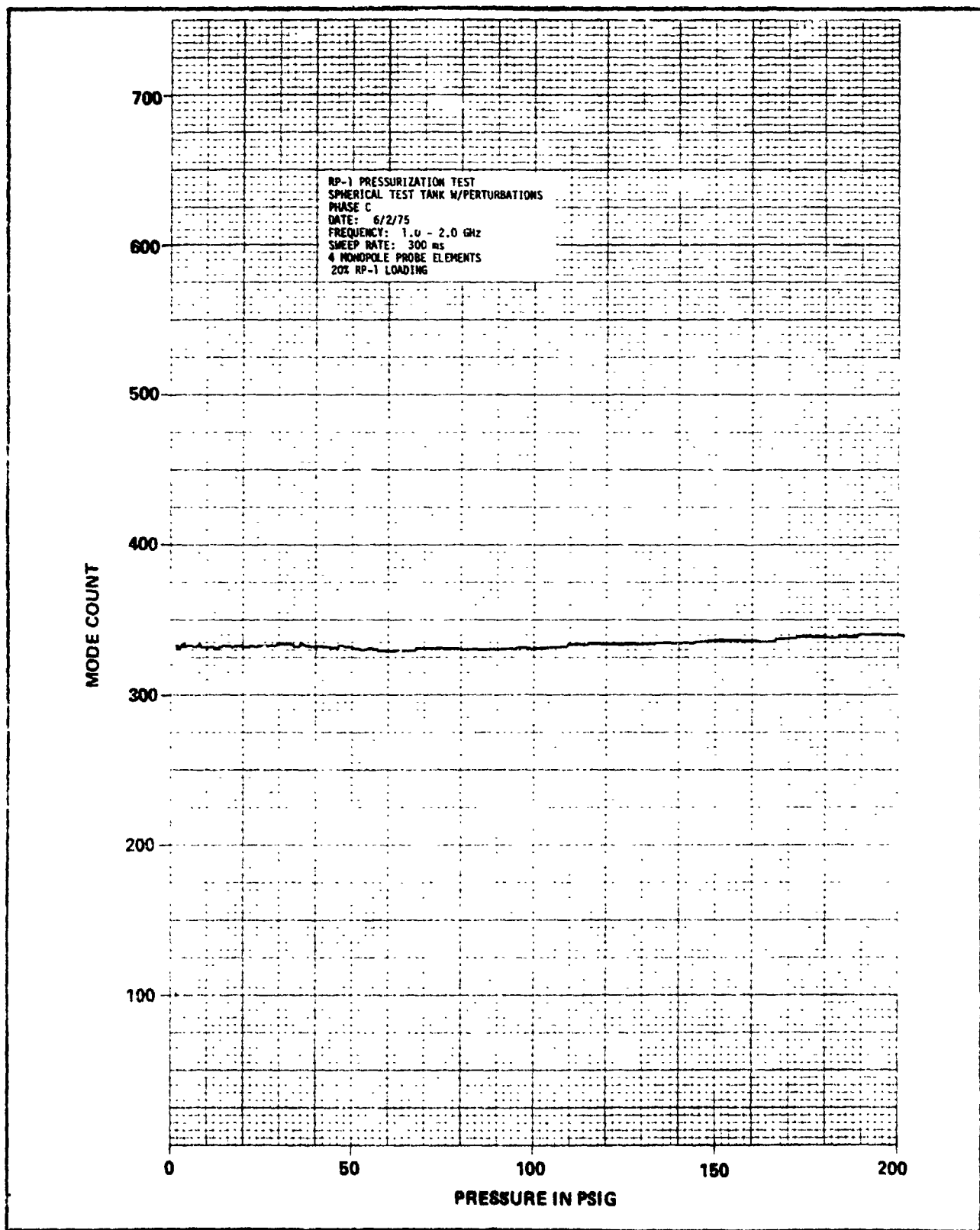
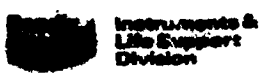


Figure 4-36

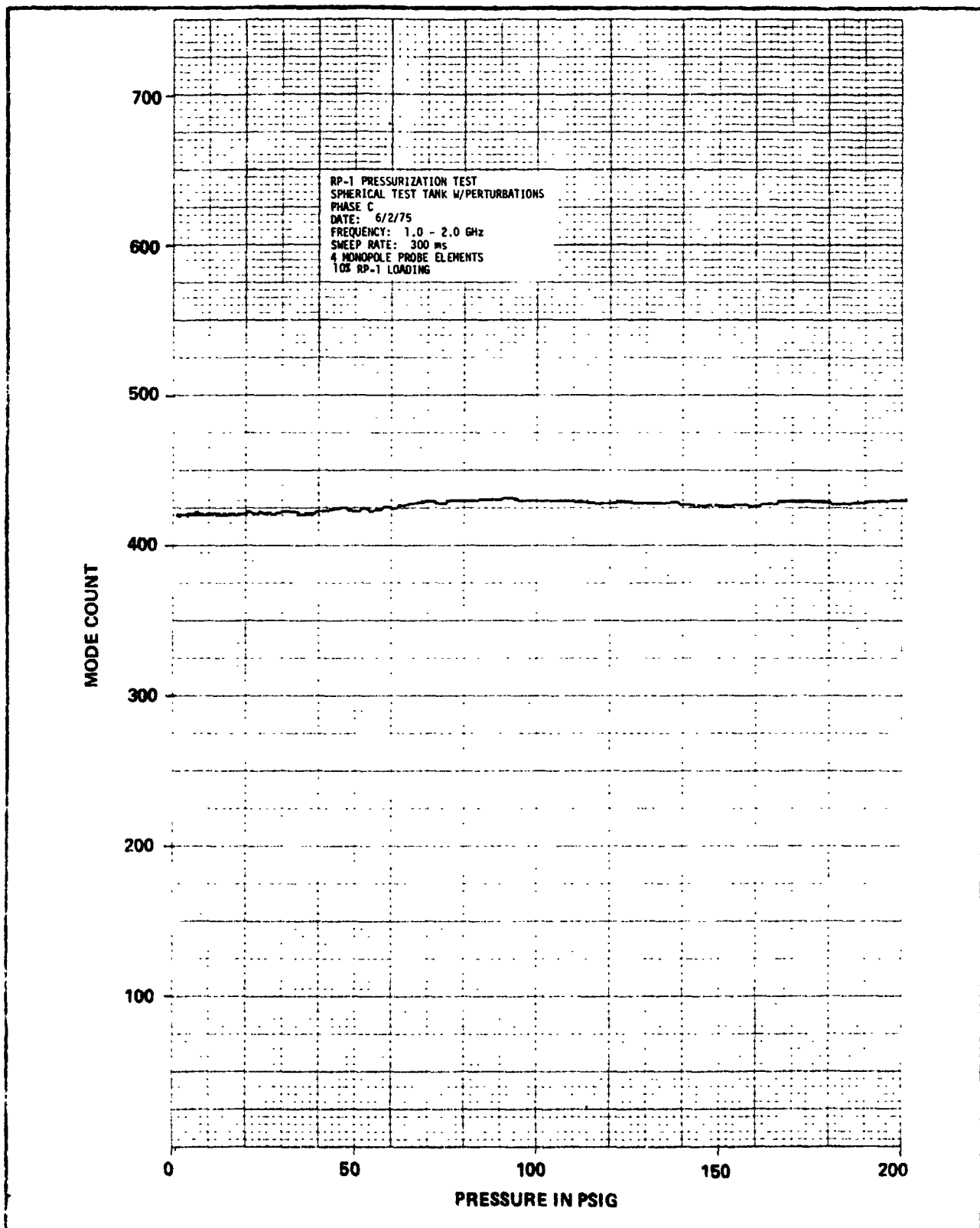


Figure 4-37

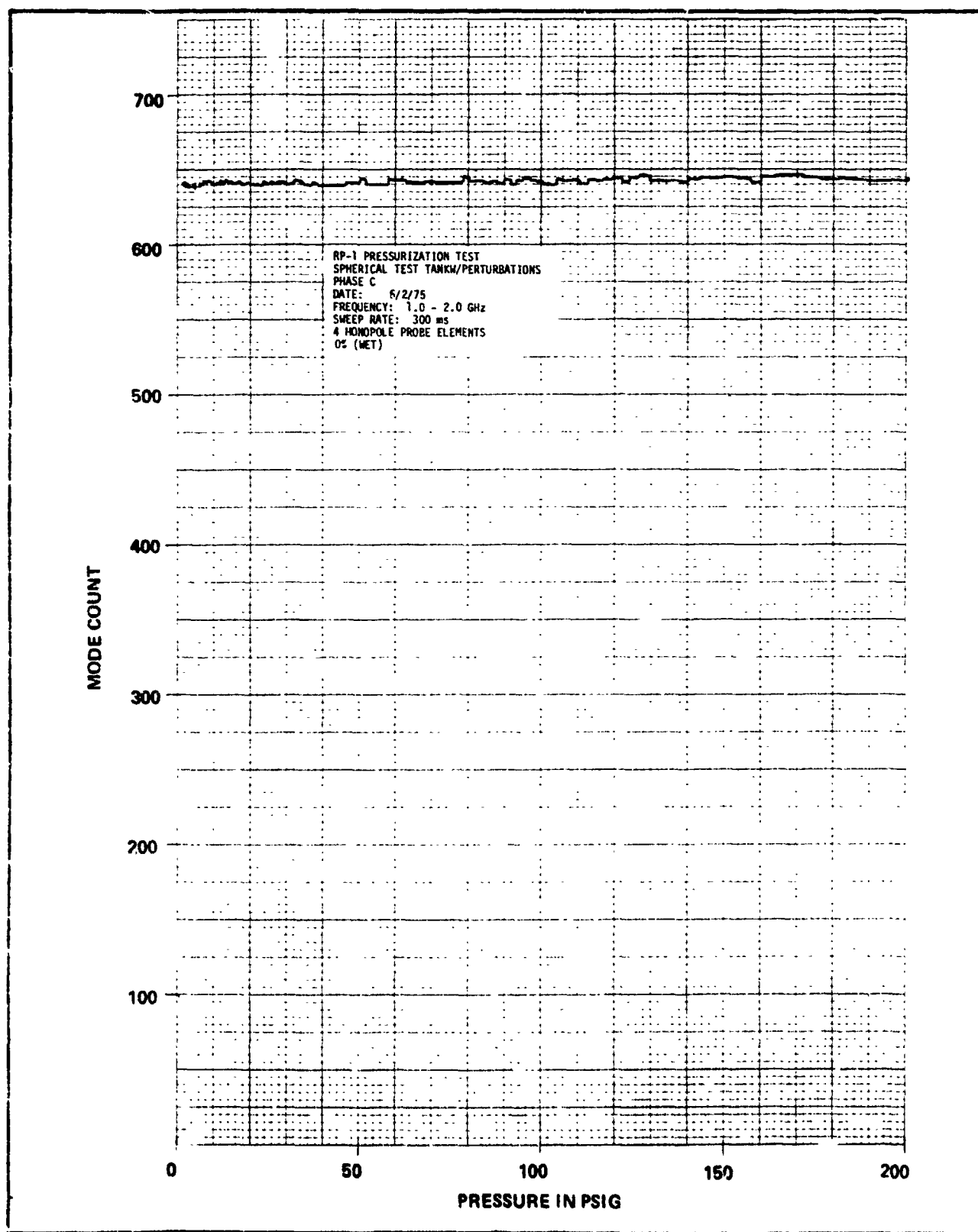


Figure 4-38

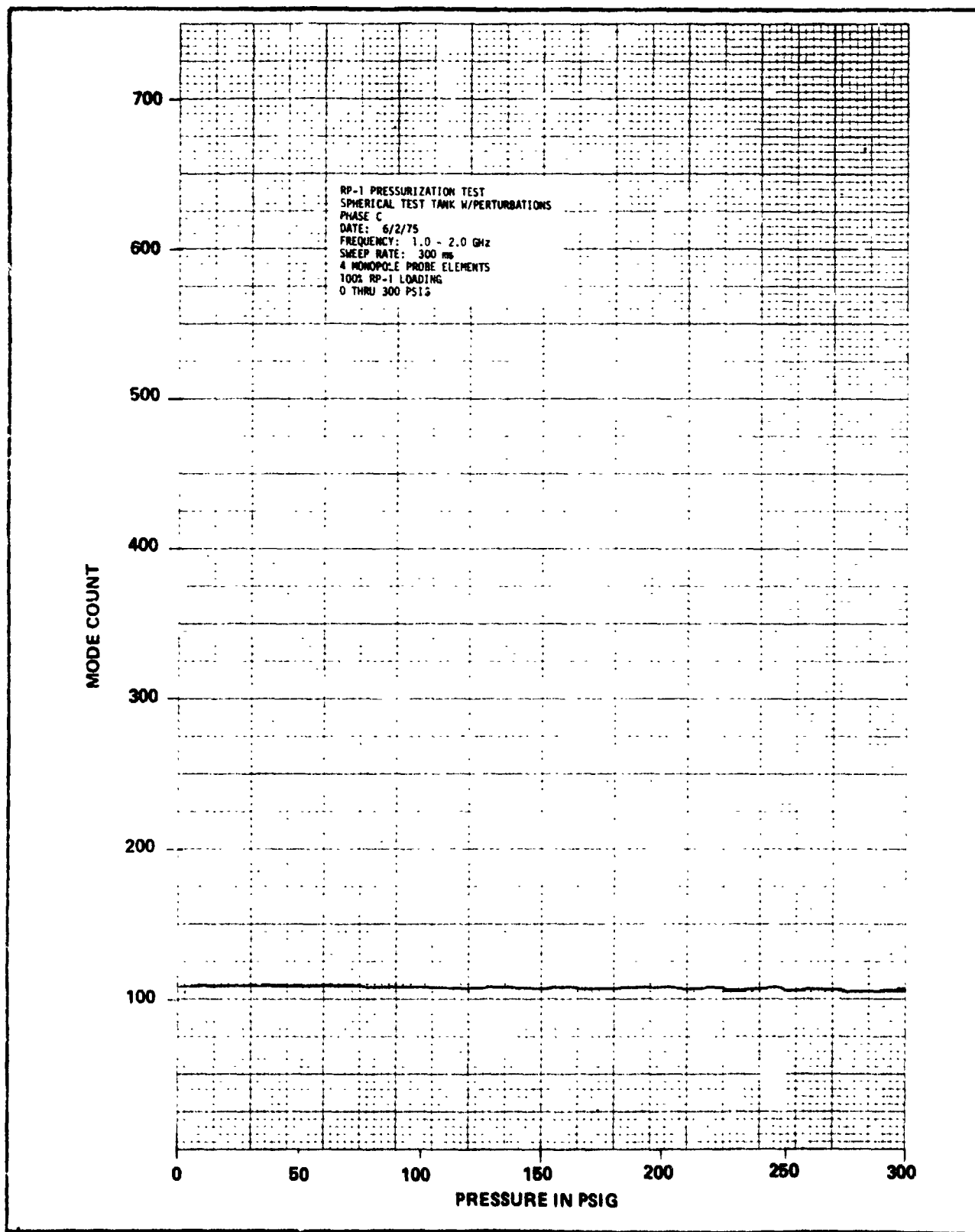


Figure 4-39



#### 4.3 SUMMARY OF CONFIGURATION, MULTIPLE PROBE, AND PRESSURE EVALUATIONS

The evaluation of configuration and multiple probes in the cylindrical and spherical RP-1 test tanks has provided an additional understanding of the effect perturbations and multiple probes have on RF gauging performance. From this effort we can conclude the following:

- Multiple 'space-diversity' probes provide better coupling to the resonant modes than utilization of a single probe element. This was clearly demonstrated by comparing the variances in mode count in the test case of the four monopole probe elements and that of the test case involving only one monopole probe element.
- The use of loop type probe elements does not offer any real advantages over the monopole type probe elements.
- With small tankage, the presence of internal hardware or other perturbing structural members need not be a detriment to gauging performance, and in fact can greatly enhance gauging performance. This was clearly demonstrated by the comparative tests performed with RP-1. This improvement in performance is attributed to a reduction in symmetry which effectively "breaks up" mode degeneracies and provides in effect a more uniform distribution of modes as a function of frequency.
- It is noted that in the case of large tanks; i.e., tanks whose dimensions are very large compared with wavelength, mode density and spacing between modes is small and in effect tends to inherently provide uniform distribution of modes as a function of frequency. Therefore the introduction of a perturbation capable of breaking up mode degeneracies by frequency shifting one of two grouped modes would, with equal likelihood, shift it into superposition with some other nearby mode. Hence, the introduction of perturbations in a truly large tank will not be expected to be either detrimental or beneficial to gauging performance.

From the pressurization testing using the spherical RP-1 test tank, the following can be concluded:

- Pressurization with up to 200 psig  $N_2$  gas in the empty spherical tank caused no appreciable change in mode count.
- Pressurization with up to 300 psig in the spherical tank containing RP-1 caused no appreciable change in mode count.



- Examination of the RF probes after the pressurization tests revealed that RP-1 had leaked into the probe. A long term pressurization with RP-1 could force RP-1 into the semi-rigid coax line and eventually out at the probes terminating connector. To prevent this, a more ruggedized radome and/or hermetic seal would be required for high pressure or flight applications.

## 5.0 ANALOG PROCESSING ELECTRONICS

The present method of detecting mode pulses is through the use of a time delay-differentiator-comparator scheme shown in Figure 5-1. In this scheme the incoming mode pattern is compared to the same pattern which has been delayed in time. At each resonant peak the difference between the delayed and undelayed mode pattern changes sign causing the comparator to change state. The Laplace transfer function for this circuit can be described as follows, assuming an ideal amplifier with gain of A:

$$\frac{E_1}{E_{in}} = \frac{1}{1+RCs} ; \frac{E_2}{E_{in}} = 1 \quad (39)$$

$$\frac{E_0}{E_{in}} = A \left( \frac{E_1}{E_{in}} - \frac{E_2}{E_{in}} \right)$$

$$= A \left( \frac{1}{1+RCs} - 1 \right)$$

$$= A \frac{1 - 1 - RCS}{1 + RCS}$$

$$= A \left( \frac{2 RCS}{1 + RCS} \right) = A \left( \frac{RCs}{1 + \frac{s}{1/RC}} \right)$$

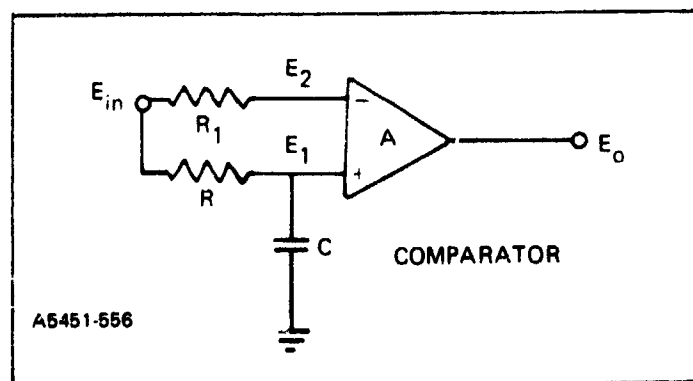


Figure 5-1  
ANALOG MODE DETECTOR

The circuit is therefore band limited with the limits being determined by the RC network as well as the non-ideal characteristics of the operational amplifier.

If R and C are chosen as  $1\text{ k}\Omega$  and  $1500\text{ pf}$  respectively and a  $\mu\text{A715}$  amplifier with a gain of 31,600 is assumed, representative bandwidths can be calculated from the Laplace transfer function. When this is done using the above values, it is found that the gain of the circuit is greater than 1 above approximately 3.5 Hz and that above approximately 400 KHz the network phase shift becomes  $180^\circ$  resulting in instability. The calculated bandwidth for this circuit is therefore from 3.5 Hz to 400 KHz.

One way to assure that the rise time of the fastest modes is not faster than the maximum detector response frequency is to sweep slower through fast modes while retaining a fast sweep through slower modes. This can be accomplished using a feedback scheme in which a signal which is proportional to the rise time of a mode is used to control the sweep rate of the RF generator.

A possible implementation of such a scheme is shown in Figure 5-2 in block diagram form. In this circuit the incoming modes signal is differentiated resulting in a voltage which is proportional to the rise time of the mode pulse. This signal is retained in a peak detector which gives a fast "attack," slow decay control signal. This signal, after amplification, is used to tune (decrease the frequency) of a voltage controlled oscillator (VCO). The signal from this VCO is digitally counted continuously in a 12 bit binary up-down counter. The digital contents of the counter are continually converted to an analog signal of from 0 to 10 volts. With no control voltage applied to the VCO the output of the Digital-to-Analog Converter is a sawtooth wave of 0 to 10 volts. The slope (and period) of the sawtooth is controlled by the VCO frequency such that the sweep rate is decreased when a fast rise time mode is detected (the VCO frequency is decreased). A schematic diagram of the circuit is shown in Figure 5-3.

This circuit was built and tested as a sweep source for the solid state RF VCO which sweeps 1 to 2 GHz. The sweep rate was adjusted to approximately 20 seconds and strip charts were made of the mode

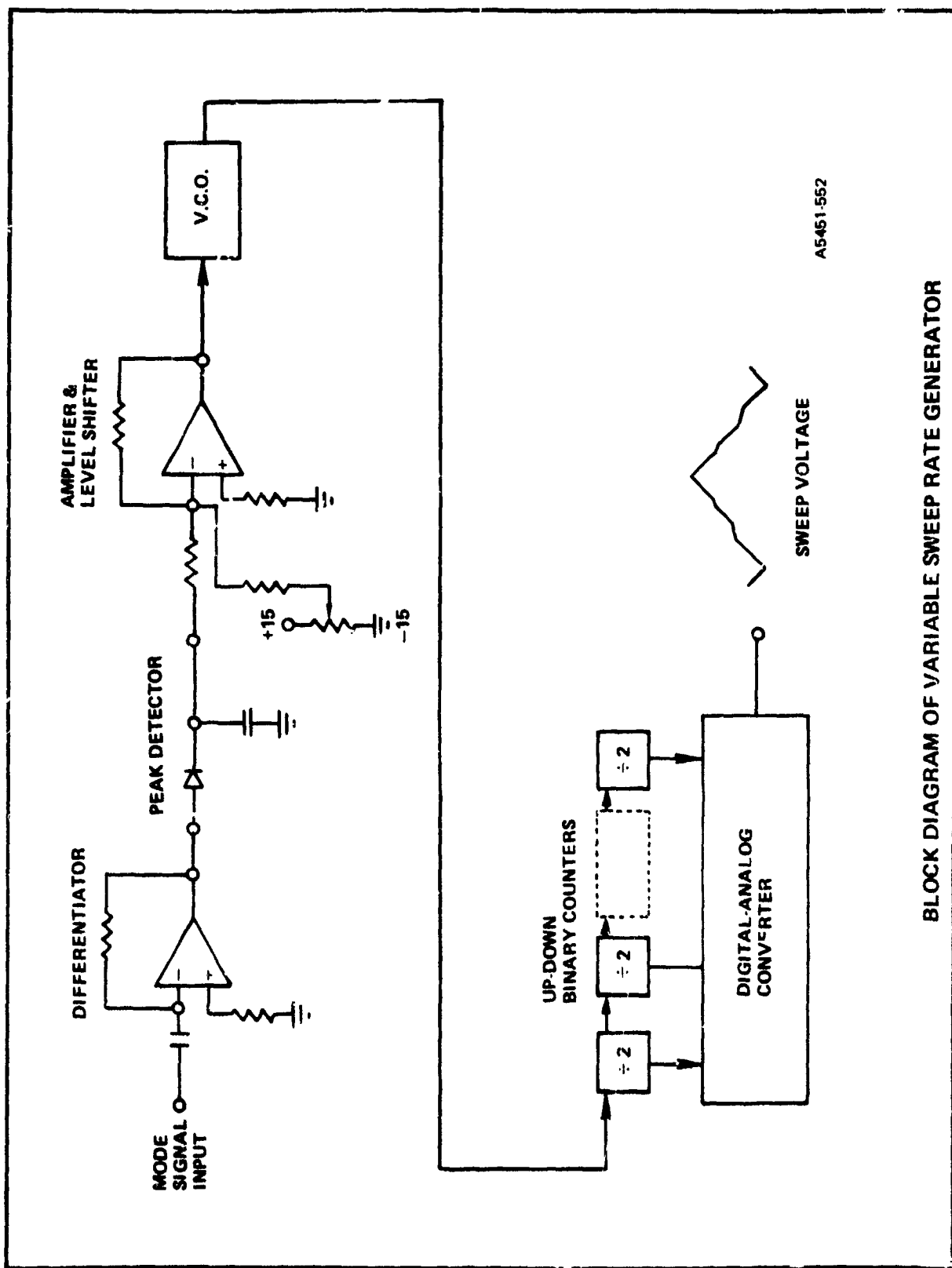


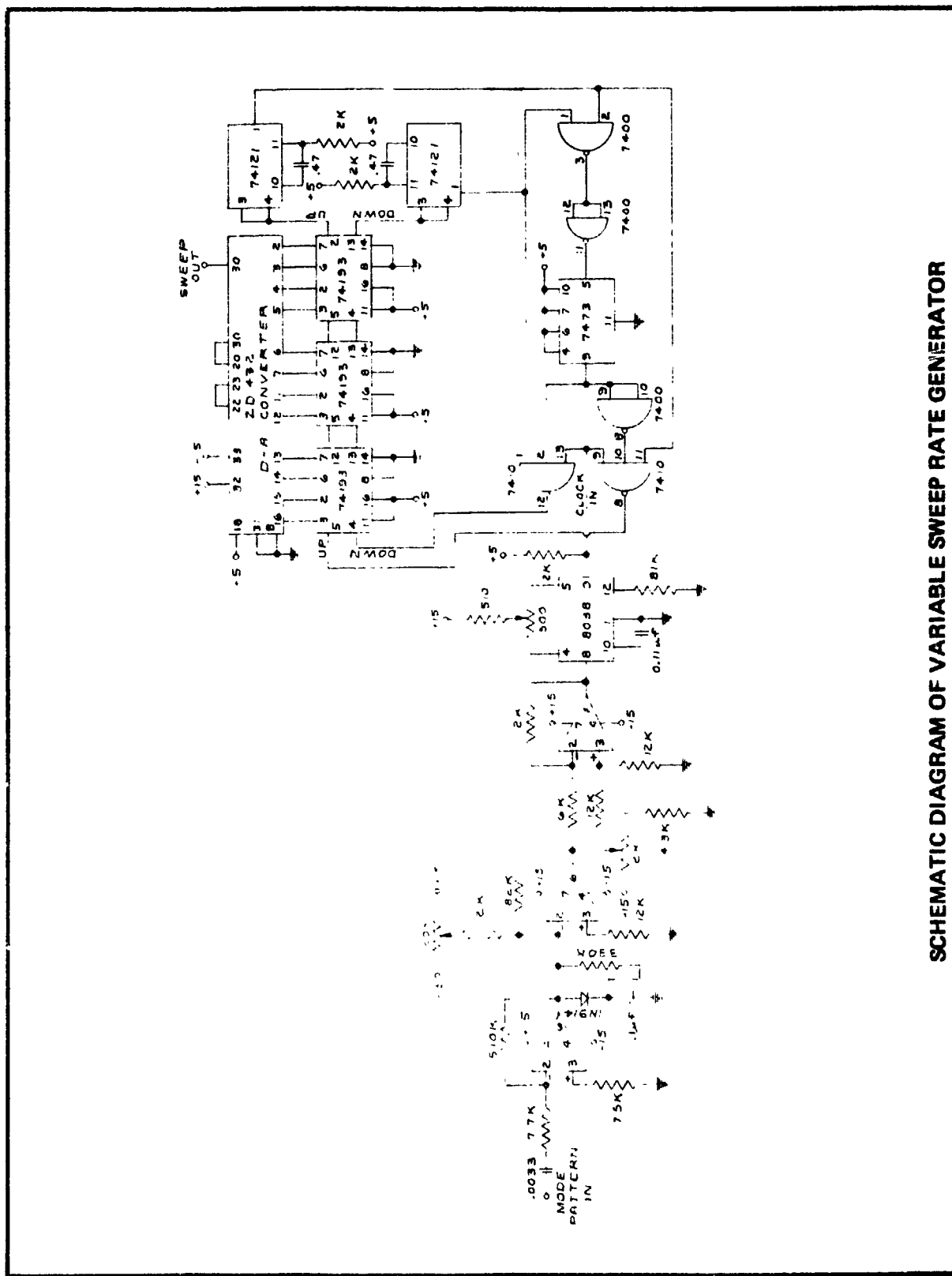
Figure 5-2



pattern and the sweep voltage to establish that the scheme was working. Extracts of these strip charts for the same frequency band are shown in Figures 5-4 and 5-5. Both graphs were made with the chart speed and vertical sensitivity the same. The first graph, Figure 5-4 was made with the feedback loop open so that the VCO was free running. The second graph, Figure 5-5, was made with the feedback loop closed so that the VCO frequency was decreased during fast rise time modes. Note that the sweep voltage of the first graph is linear while that of the second is not linear, but has a slope which decreases with each fast mode and then increases again after the mode. These graphs make several facts apparent.

First, it will be noted that the distribution of modes in the graph produced with the feedback loop closed is much more uniform with much less "dead" space between mode pulses. Also, the detail available is much improved when several modes of nearly equal frequency are merged into apparently one mode. Since the detail is needed only during a mode and not in the dead space between modes, more efficient use is made of the time during the sweep. This occurs because the RF source is swept more rapidly through dead areas than is normally possible with a constant frequency sweep, but more slowly through rapid modes than is likewise possible with a constant sweep.

Not immediately apparent on the graph is the fact that the high frequency content of the mode pattern is considerably reduced when the feedback loop is closed. This is the desired result from the circuit, which with further refinement should enhance the detectability of modes and minimize errors due to mode processing.



Eigene E-3

**ORIGINAL PAGE IS  
OF POOR QUALITY**

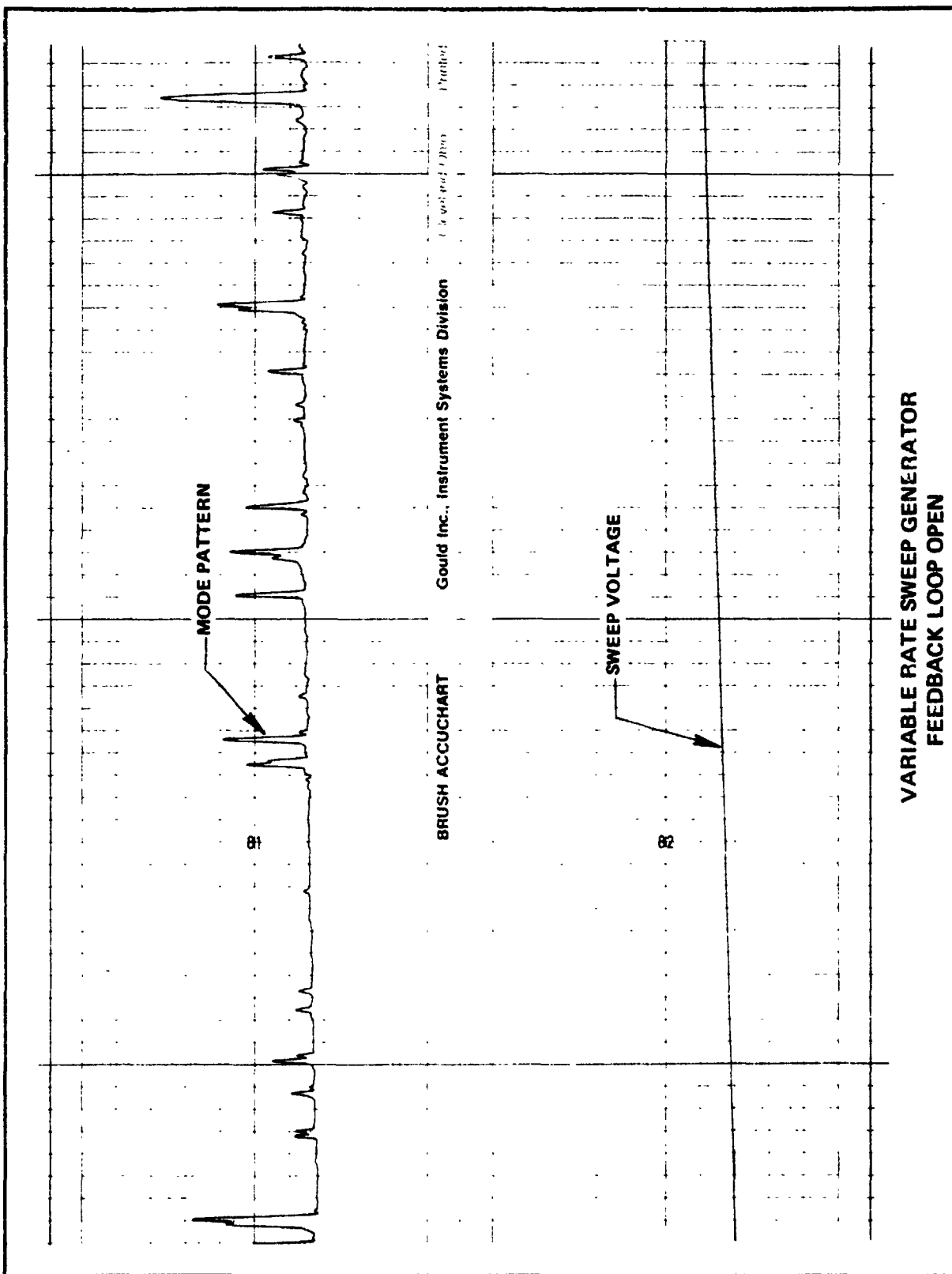


Figure 5-4

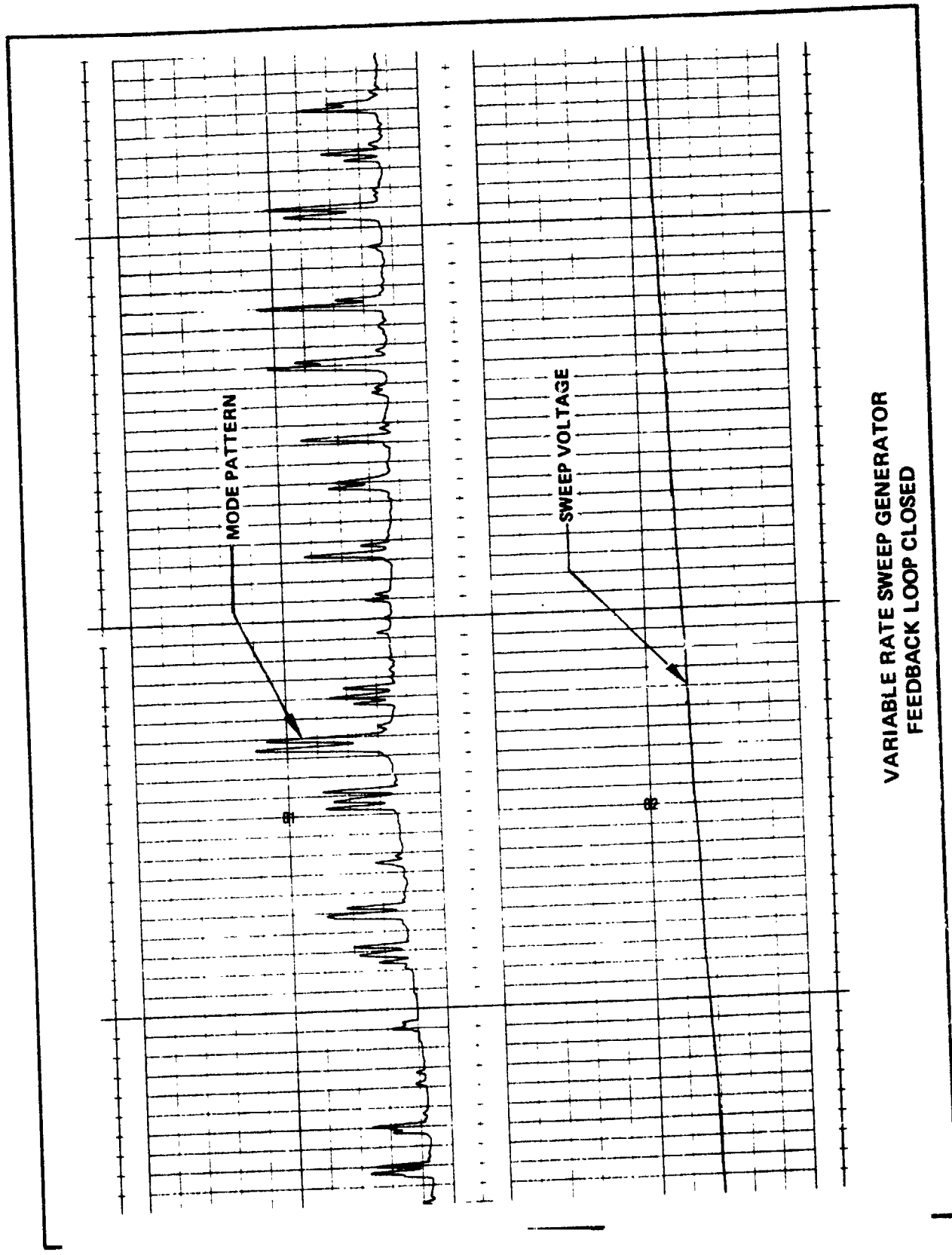


Figure 5-5

## 6.0 DIGITAL PROCESSING ELECTRONICS

Another method of detecting resonant mode pulses is through the use of digital comparison techniques. A block diagram illustrating this technique is shown in Figure 6-1. As shown the circuit employs a four phase clock to implement a sample, compare, sample, compare sequence. The sequential operation of the circuit is described in Table 6-1. Simply stated, the mode processing is accomplished by comparing a sample of the mode pattern with a previously attained sample. The comparator output will change state at each comparison until a resonant peak is detected. When the comparator output fails to change as the result of a comparison, the post comparator logic detects the failure to change and the output changes state. This mode detection scheme is also band limited. All of the following have an influence on the bandwidth of the circuit: the threshold voltage of the comparator, the input signal amplitude, the sample rate, and the acquisition time of the sample-hold. For ease of calculation a sine wave will be used in the analysis:

$\omega_L$  - Low radian frequency limit

$f_L$  - Low frequency limit

$t_1$  - time of first sample

$t_2$  - time of second sample

V - Threshold voltage of comparator

A - Amplitude of sine wave input

$f_H$  - High frequency limit

$f_s$  - Sampling frequency

The relationship between the sampling frequency ( $f_s$ ) and the low frequency limit, ( $f_L$ ) is derived using the equation

$$A (\sin \omega_L t_1 - \sin \omega_L t_2) = \pm V. \quad (40)$$

This equation states that the magnitude of the sample taken at  $t_1$ ,  $A \sin \omega_L t_1$ , minus the magnitude of the sample taken at  $t_2$ ,  $A \sin \omega_L t_2$ ,

**DIGITAL MODE PROCESSING APPROACH**

Figure 6-1

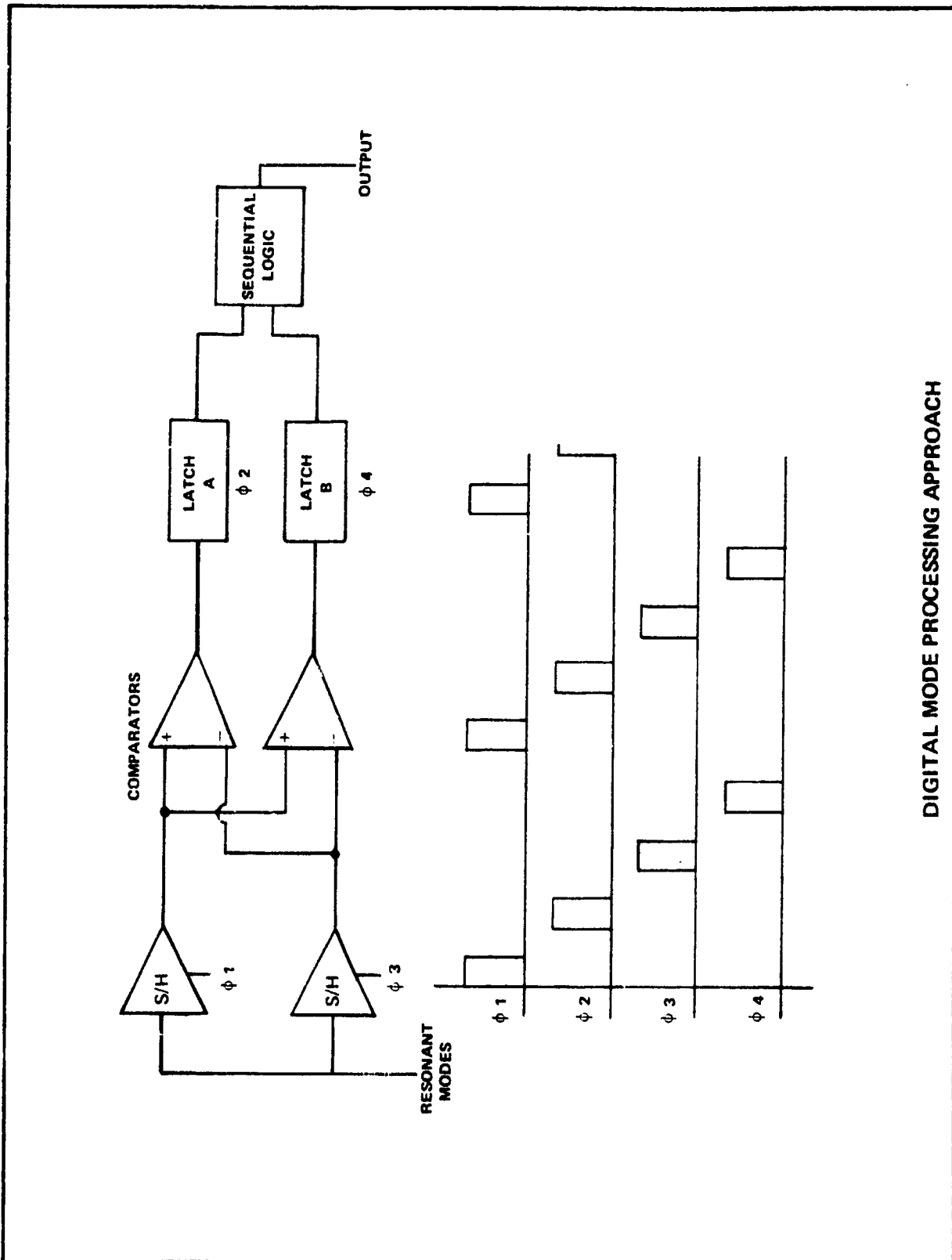




TABLE 6-1  
DIGITAL MODE PROCESSING SCHEME

Clock Pulse No.	Operation S - Sample C - Compare	Description
1	S	First sample is taken.
2	C	Compare sample 1 with 0 volts - Latch A goes high; output goes high
3	S	Take a sample
4	C	Compare previous 2 samples - Latch B goes high; output remains high
1	S	Take a sample
2	C	Compare previous 2 samples - Latch A remains high; output remains high
3	S	Take a sample
4	C	Compare previous 2 samples - Latch B goes low; output goes low
1	S	Take a sample
2	C	Compare previous 2 samples - Latch A goes low; output remains low, etc.

$\omega_L t_2$ , must be greater than or equal to the threshold voltage of the comparator for an input signal with a radian frequency of  $\omega_L$ . If this equation is satisfied, mode pulses corresponding to frequencies greater than  $\omega_L$ . If this equation is satisfied, mode pulses corresponding to frequencies greater than  $\omega_L$  will be sensed, and those below  $\omega_L$  will go by undetected. Returning to the above equation

$$A (\sin \omega_L t_1 \cdot \sin \omega_L t_2) \geq \pm V$$

$$A (\sin 2\pi f_L t_1 \cdot \sin 2\pi f_L t_2) \geq \pm V.$$

Zero time is chosen as a starting point so  $t_1$  is set equal to 0

$$A (-\sin 2\pi f_L t_2) \geq \pm V$$

$$A \sin 2\pi f_L t_2 \geq V$$

$$\sin 2\pi f_L t_2 \geq V/A$$

$$t_2 \geq \frac{\arcsin(V/A)}{2\pi f_L}$$

$t_2$  is the time between successive samples, so the sampling frequency is

$$f_s \geq \frac{1}{t_2} \geq \frac{2\pi f_L}{\arcsin(V/A)}$$

From this equation it can be seen that the sampling frequency is dependent upon the lowest frequency to be processed, the threshold voltage of the op amp, and the amplitude of the incoming signal.

According to sampling theory, a signal must be sampled twice every cycle, at the minimum, to get an accurate representation of the signal. In this case, to insure accuracy, the signal being processed will be sampled at a minimum of 4 times per cycle. Now a relationship can be given for the upper frequency limit.

$$f_h = \frac{f_s}{4} = \frac{2\pi f_L}{f_r \arcsin(V/A)}$$

$$f_R = \text{Sampling Rate} \geq 4$$

Using realistic values in the equations derived, a bandwidth for this circuit can be computed.

For V, the threshold voltage of the comparator, 5 mV has been selected and the amplitude of the sine wave input, A, is taken to be 1 volt. The low frequency limit of 25 Hz will be used,

$$f_h = \frac{f_s}{4} = \frac{2\pi f_L}{4 \arcsin(V/A)} = \frac{2\pi(25)}{4 \arcsin \left( \frac{.005}{1} \right)} = 7.85 \text{ KHz.}$$

A common approximation is that  $\arcsin \theta = 0$  for  $\theta \leq 0.1$ , it can therefore be seen that the high frequency limit is inversely proportional to the threshold voltage of the comparator and directly proportional to the low frequency limit.

Therefore to increase the upper frequency limit it is necessary to use a comparator with the lowest possible threshold voltage and to operate with the highest possible low frequency limit.

The circuit was built and tested with a sine wave input signal to simulate the mode pattern. For a sample frequency of 500 KHz the maximum and minimum frequencies were 170 KHz and 38 KHz respectively. These values are considerably poorer than anticipated. The poor low frequency response is apparently due to both the large threshold voltage of the comparator used and noise problems associated with comparator indecision at the lower frequencies. No further attempts were made to further improve the response of the digital mode processor. It is concluded that although the digital mode processing approach does offer some conceptual advantages over the analog mode processing approach, at present the analog approach is simpler, has been proven by demonstration in gauging tests, and hence is the choice for a processing approach.



## 7.0 CONCLUSIONS

From the experimental results of the tests conducted during Phase C, the following conclusions may be made:

- The feasibility of the RF Gauging mode counting technique has again been demonstrated for gauging liquid hydrogen and liquid oxygen under all altitude conditions.
- With LH<sub>2</sub>, it has been demonstrated under dynamic fluid conditions, in which the fluid assumes (with time) ever changing positions within the tank, that the RF Gauging technique on the average provides a very good indication of mass. The average percent of error mass from the best fit linear-regression curve for all fill levels was 1.17 percent.
- With LOX, it has been demonstrated under dynamic fluid conditions, in which the fluid assumes (with time) ever changing positions within the tank, that the RF Gauging technique on the average provide a very good indication of mass. The average mass error using a single-segment polynomial equation to calculate mass knowing mean mode count was 0.8576 percent of full scale.
- It is significant to note that the distribution of the mode count data at each fill level during dynamic LH<sub>2</sub> and LOX orientation testing does approach a statistical normal distribution.
- Multiple 'space-diversity' probes provide better coupling to the resonant modes than utilization of a single probe element. This was clearly demonstrated by comparing the variances in mode count in the test case of the four monopole probe elements and that of the test case involving only one monopole probe element.
- With small tankage, the presence of internal hardware or other perturbing structural members need not be a detriment to gauging performance, and in fact can greatly enhance gauging performance. This was clearly demonstrated by the comparative tests performed with RP-1. This improvement in performance is attributed to a reduction in symmetry which effectively "breaks up" mode degeneracies and provides in effect a more uniform

distribution of modes as a function of frequency. It is, however, noted that in the case of large tanks, i.e. tanks whose dimensions are very large compared with wavelength, mode density and spacing between modes is small and in effect tends to inherently provide a uniform distribution of modes as a function of frequency. Therefore the introduction of a perturbation capable of breaking up mode degeneracies by frequency shifting one of two grouped modes would, with equal likelihood, shift it into superposition with some other nearby mode. Hence, the introduction of perturbations in a truly large tank will not be expected to be either detrimental or beneficial to gauging performance.

- Pressurization with up to 200 psig N<sub>2</sub> gas in the empty spherical tank caused no appreciable change in mode count.
- Pressurization with up to 300 psig in the spherical tank containing RP-1 caused no appreciable change in mode count.
- The variable sweep rate generator technique provides a more uniform mode versus time distribution for processing. Signal processing using the analog mode processing technique and the variable sweep rate concept is recommended for implementation in Phase D.



**APPENDIX A**  
**COMPUTER PLOTS OF**  
**FREQUENCY OF OCCURRENCE VS. MODE COUNT**  
**AND**  
**MODE COUNT VS. ORIENTATION ANGLE**  
**JANUARY 15, 1975 LH<sub>2</sub> TESTS**

**PRECEDING PAGE BLANK NOT FILMED**



## APPENDIX A

### TABLE OF CONTENTS

COMPUTER PLOT	PAGE NO.
FREQUENCY OF OCCURENCE VS. MODE COUNT (DYNAMIC ORIENTATION)	
• 0% LH <sub>2</sub> LOADING .....	A-1
• 5% LH <sub>2</sub> LOADING .....	A-2
• 10% LH <sub>2</sub> LOADING .....	A-3
• 20% LH <sub>2</sub> LOADING .....	A-4
• 30% LH <sub>2</sub> LOADING .....	A-5
• 40% LH <sub>2</sub> LOADING .....	A-6
• 50% LH <sub>2</sub> LOADING .....	A-7
• 60% LH <sub>2</sub> LOADING .....	A-8
• 70% LH <sub>2</sub> LOADING .....	A-9
• 80% LH <sub>2</sub> LOADING .....	A-10
• 90% LH <sub>2</sub> LOADING .....	A-11
• 95% LH <sub>2</sub> LOADING .....	A-12
MODE COUNT VS. ORIENTATION ANGLE (DYNAMIC ORIENTATION)	
• 0% LH <sub>2</sub> LOADING .....	A-13
• 5% LH <sub>2</sub> LOADING .....	A-14
• 10% LH <sub>2</sub> LOADING .....	A-15
• 20% LH <sub>2</sub> LOADING .....	A-16
• 30% LH <sub>2</sub> LOADING .....	A-17
• 40% LH <sub>2</sub> LOADING .....	A-18
• 50% LH <sub>2</sub> LOADING .....	A-19
• 60% LH <sub>2</sub> LOADING .....	A-20
• 70% LH <sub>2</sub> LOADING .....	A-21
• 80% LH <sub>2</sub> LOADING .....	A-22
• 90% LH <sub>2</sub> LOADING .....	A-23
• 95% LH <sub>2</sub> LOADING .....	A-24
FREQUENCY OF OCCURENCE VS. MODE COUNT (STATIC ORIENTATION)	
• 0% LH <sub>2</sub> LOADING .....	A-25
• 5% LH <sub>2</sub> LOADING .....	A-26



## COMPUTER PLOT

PAGE NO.

● 10% LH <sub>2</sub> LOADING .....	A-27
● 20% LH <sub>2</sub> LOADING .....	A-28
● 30% LH <sub>2</sub> LOADING .....	A-29
● 40% LH <sub>2</sub> LOADING .....	A-30
● 50% LH <sub>2</sub> LOADING .....	A-31
● 60% LH <sub>2</sub> LOADING .....	A-32
● 70% LH <sub>2</sub> LOADING .....	A-33
● 80% LH <sub>2</sub> LOADING .....	A-34
● 90% LH <sub>2</sub> LOADING .....	A-35
● 95% LH <sub>2</sub> LOADING .....	A-36

## MODE COUNT VS. ORIENTATION ANGLE (STATIC ORIENTATION)

● 0% LH <sub>2</sub> LOADING .....	A-37
● 5% LH <sub>2</sub> LOADING .....	A-38
● 10% LH <sub>2</sub> LOADING .....	A-39
● 20% LH <sub>2</sub> LOADING .....	A-40
● 30% LH <sub>2</sub> LOADING .....	A-41
● 40% LH <sub>2</sub> LOADING .....	A-42
● 50% LH <sub>2</sub> LOADING .....	A-43
● 60% LH <sub>2</sub> LOADING .....	A-44
● 70% LH <sub>2</sub> LOADING .....	A-45
● 80% LH <sub>2</sub> LOADING .....	A-46
● 90% LH <sub>2</sub> LOADING .....	A-47
● 95% LH <sub>2</sub> LOADING .....	A-48

LW2 OCC DYNAMICS NET

JAN 15 1975.

PRECEDING PAGE BLANK NOT FILMED

PRECEDING

1.45E+01

1.20E+00

1.00E+01

8.00

6.00

2.00

0.00

1.51E+03

MODE COUNT

4

1.54E+03 1.54E+03 1.54E+03 1.55E+03 1.55E+03 1.56E+C3 1.56E+C3 1.56E+C3 1.57E+C3 1.57E+C3

0 2 1

A-1

FREQUENCY

LH2 +5% DYNAMIC ORT

JAN 15 1975

6.45

5.60

4.05

3.20

2.40

1.60

SOURCE=01  
1.58E+03 1.59E+03 1.60E+03 1.61E+03 1.62E+03 1.63E+03 1.64E+03 1.65E+03 1.66E+03  
MODE COUNT

A-2

FREQUENCY

LW2 10X DYNAMIC CRT

JAN 15 1975

4.5C

4.0C

3.5C

3.0C

2.5C

2.0C

1.5C

1.0C

1.60E+03 1.61E+03 1.62E+03 1.63E+03 1.64E+03 1.65E+03 1.66E+03 1.67E+03 1.68E+03 1.69E+03 1.70E+03

MODE COUNT

A3

FREQUENCY

1.MHz 2CX DYNAMIC CAT

JAN 15 1975

4.50

4.00

3.50

3.00

2.50

2.00

1.50

1.00

MODE COUNT

A4

1.66E+03

1.67E+03

1.68E+03

1.69E+03

1.70E+03

1.71E+03

1.70E+03

1.71E+03

1.72E+03

1.73E+03

1.74E+03

1.75E+03

1.76E+03

1.77E+03

1.78E+03

1.79E+03

1.70E+03

1.71E+03

1.72E+03

1.73E+03

1.74E+03

1.75E+03

1.76E+03

1.77E+03

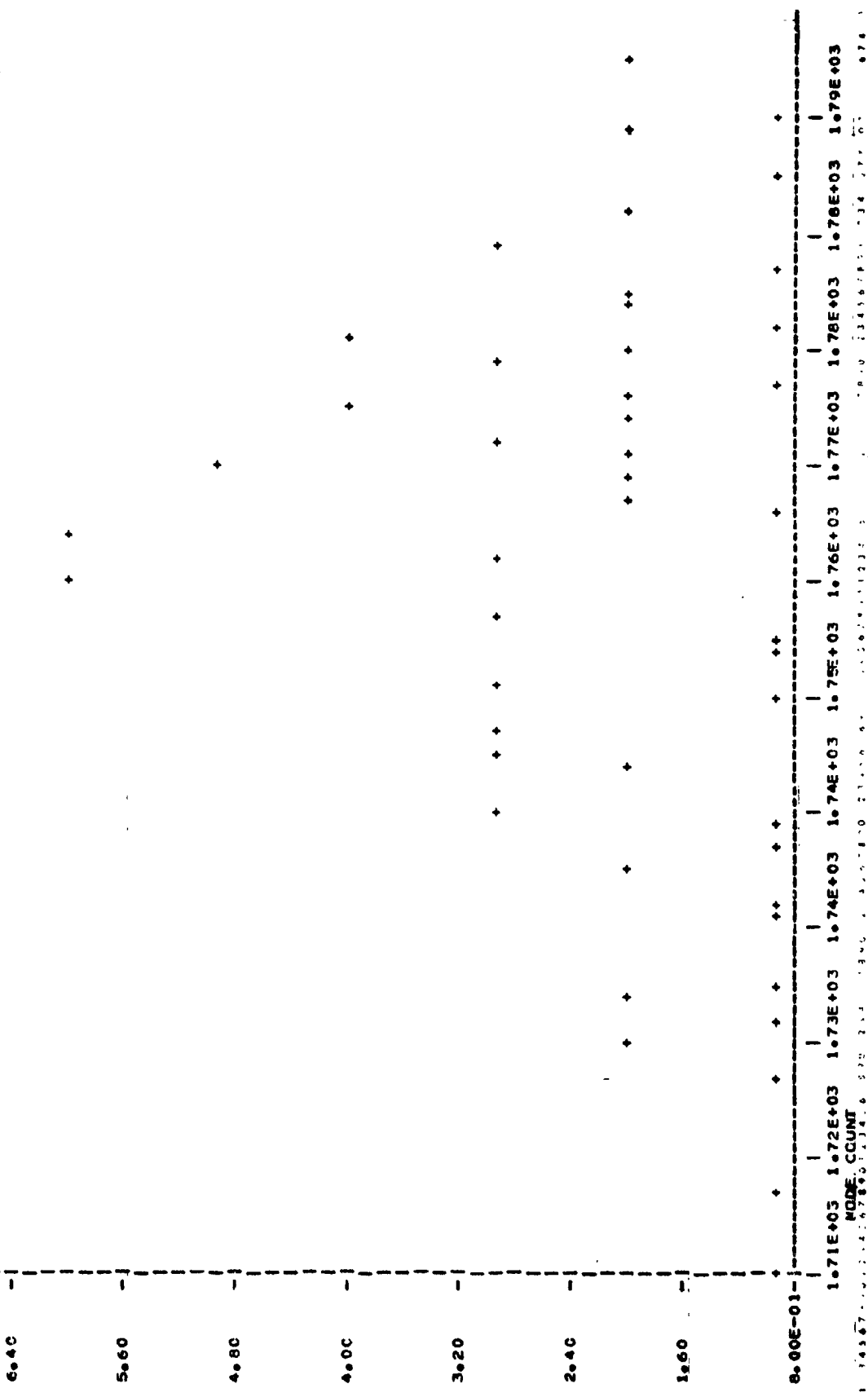
1.78E+03

1.79E+03

FREQUENCY

LH2 30X DYNAMIC ORT

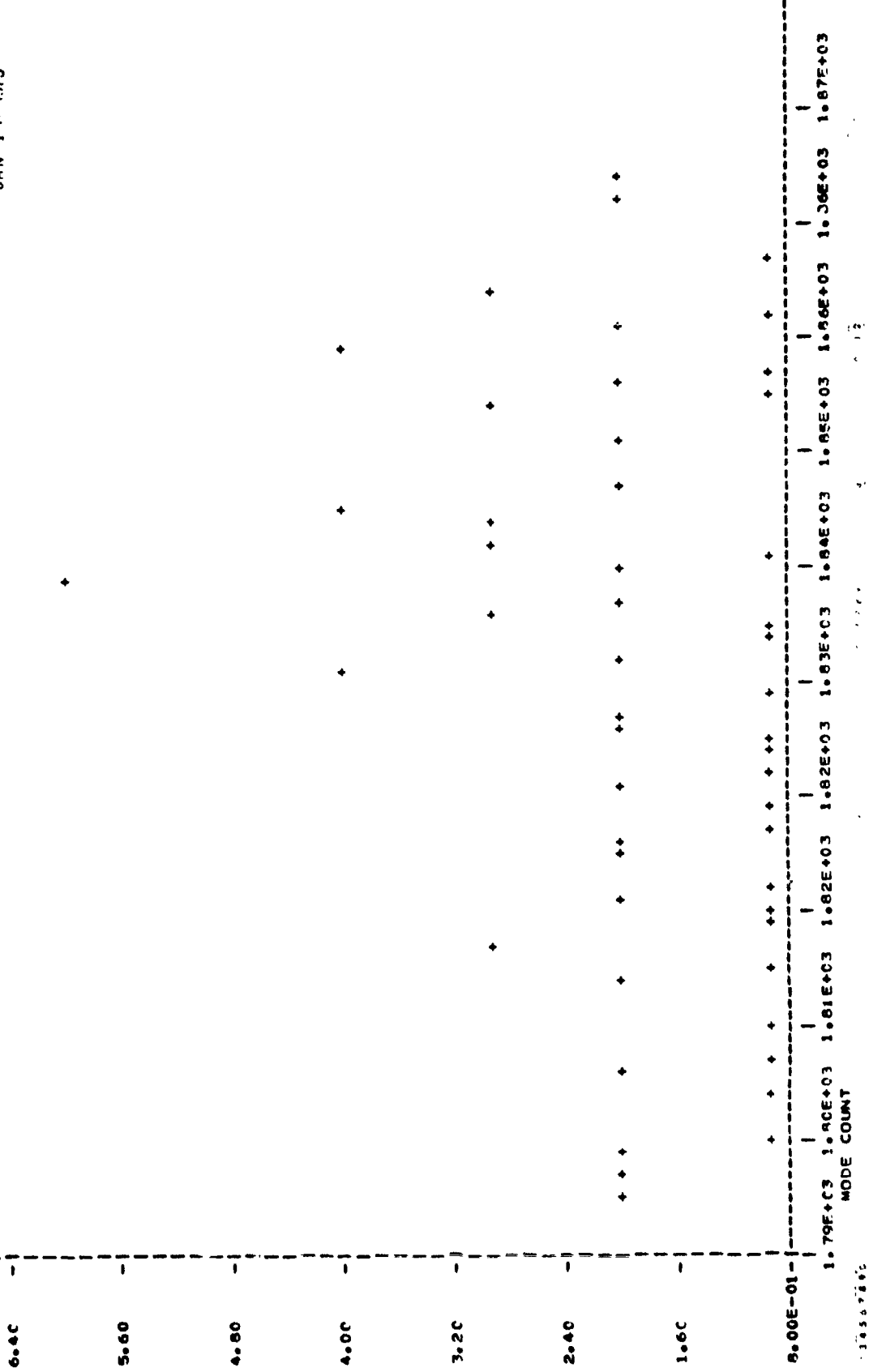
JAN 15 1975



FREQUENCY

LH2 & CX DYNAMIC ORT

JAN 15 1975



FREQUENCY

-Hz SRS DYNAMIC NET

JAN 15 1975

8.00

7.00

6.00

5.00

4.00

3.00

2.00

1.00

0.00

1.00

1.00

1.00

1.00

1.00

1.00

1.00

1.00

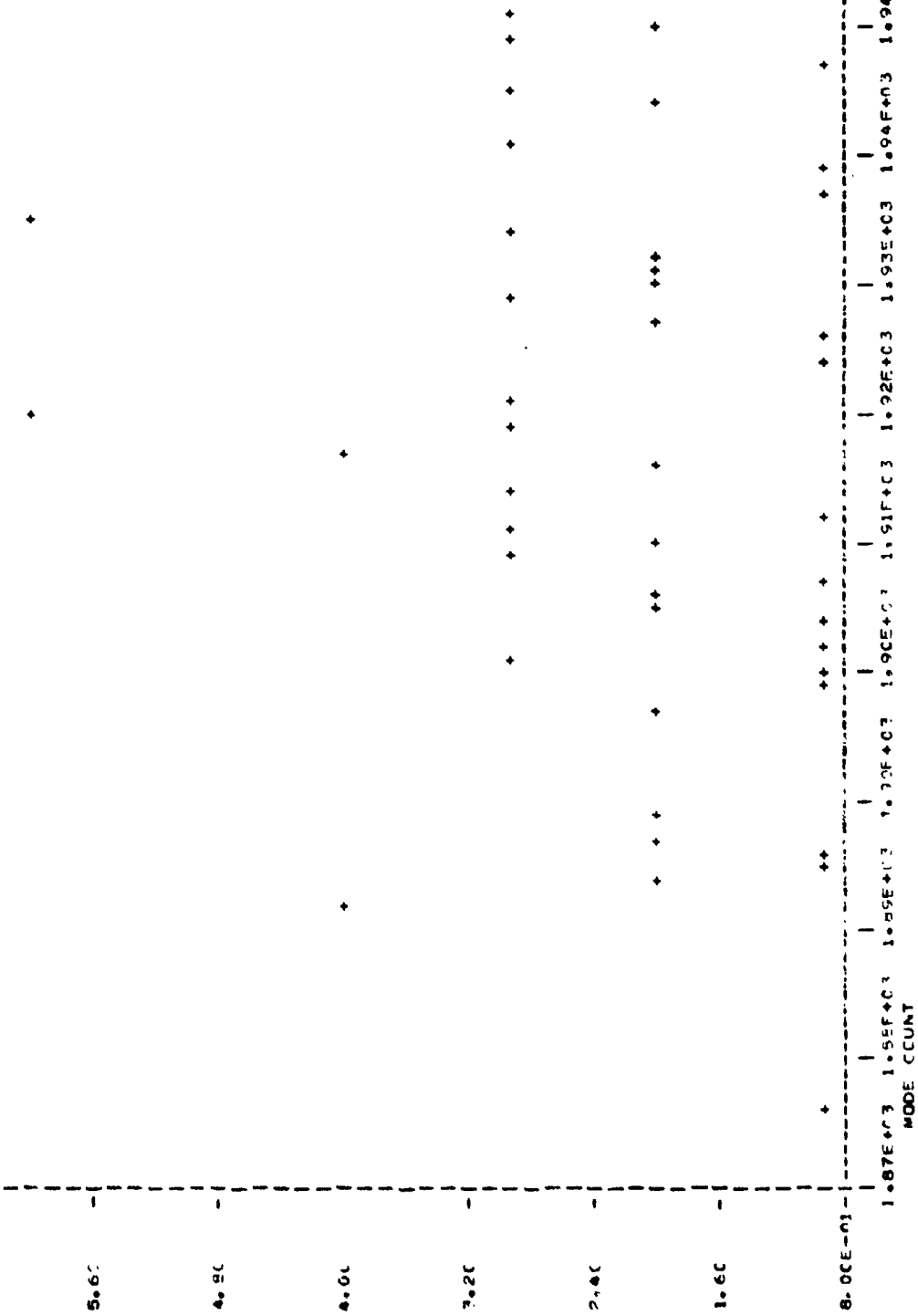
1.82E+03 1.83E+03 1.84E+03 1.85E+03 1.86E+03 1.86E+03 1.87E+03 1.88E+03 1.89E+03 1.90E+03  
MODE COUNT 3.6

A.7

፩፻፭፻፮፯

LHP ECK DYNAMIC CHT

JAN 4 2 1975



8

F=ECOUNT

LH2 7CX DYNAMIC CRT

C, AR

S, EC

4, EC

2, EC

2, 2C

2, 4C

1, EC

3.0CF  
1.34F+2 1.24E+01 1.95E+03 1.96F+02 1.07E+03 1.98E+03 1.99E+03 2.00E+03 2.01E+03 2.02E+03

A.9

FREQUENCY

LH2 BOX DYNAMIC OFF

JAN 15 1975

$\epsilon - \Delta \epsilon$

$S_0, \epsilon r$

$A_0, BC$

$A_0, CC$

$3 \times 2r$

$2 \times 4C$

$1 \times 6C$

$-8.0CE-01$

$2.02E+C3$

$2.02F+C3$

$2.03E+03$

$2.04E+03$

$2.05E+03$

$2.06E+03$

$2.07E+03$

$2.08E+03$

$2.09E+03$

$2.10E+03$

$2.00E+03$

$2.01E+03$

$2.02E+03$

$2.03E+03$

$2.04E+03$

$2.05E+03$

$2.06E+03$

$2.07E+03$

$2.08E+03$

$2.09E+03$

$2.10E+03$

A-8C

A-10

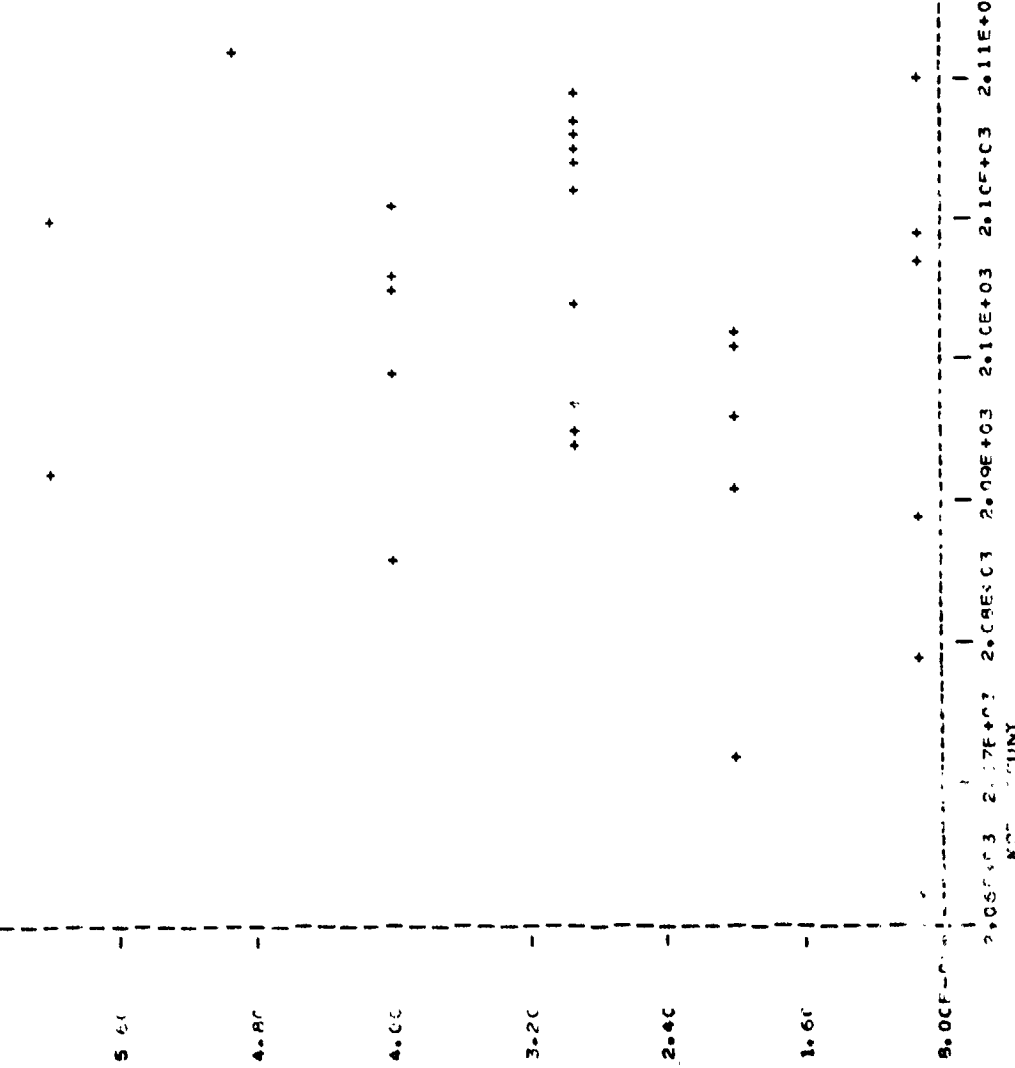
MODE COUNT

FREQUENCY

L-1P 9CX DYNAMIC DFT

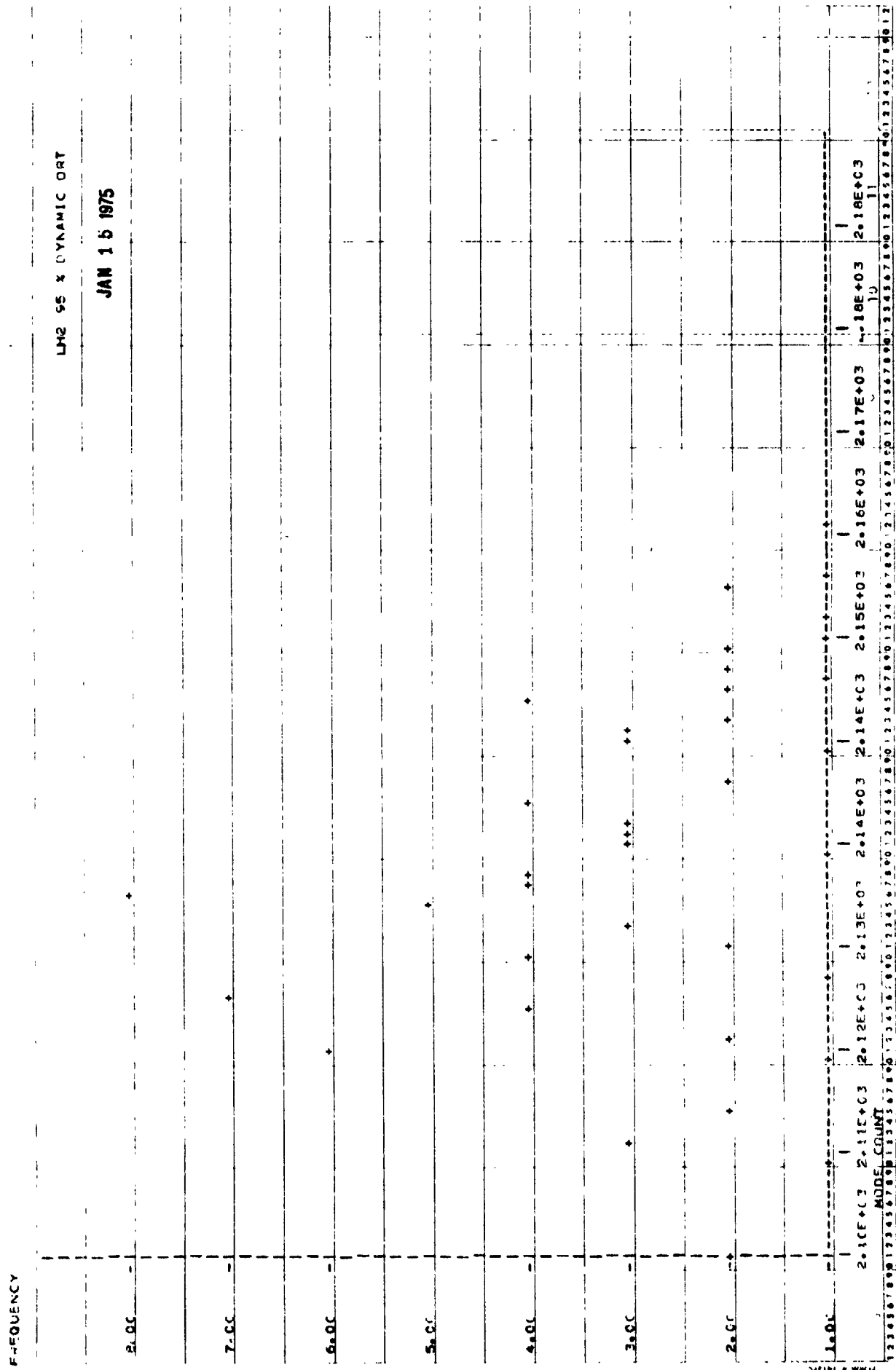
JAN 15 1975

6-4r



THE DYNAMIC STATE

JAN 15 1975



13

MODE CT

LH2 OCC DYNAMIC ORT

JAN 15 1975

1.57E+03-

1.56E+03-

1.55E+03-

1.54E+03-

1.53E+03-

1.52E+03-

1.51E+03-

1.50E+03-

1.49E+03-

1.48E+03-

1.47E+03-

1.46E+03-

1.45E+03-

1.44E+03-

1.43E+03-

1.42E+03-

1.41E+03-

1.40E+03-

1.39E+03-

1.38E+03-

1.37E+03-

1.36E+03-

1.35E+03-

1.34E+03-

A-13

MODE CT

LH2 CSX DYNAMIC ORT

1.07E+03-  
1.08E+03-

1.066E+03-

1.064E+03-

1.062E+03-

1.060E+03-

1.056E+03-

-2.000E+02 -1.66E+02 -1.20E+02 -8.00E+01 -4.00E+01  
C.C0 4.00E+01 8.00E+01 1.020E+02 1.600E+02 2.000E+02  
ORIENTATION

A14

WDDC CT

LNC 10% DYNAMIC CAT

JAN 15 1975

1.079E+02-

1.072E+03-

1.075E+02-

1.066E+02-

1.064E+03-

1.062E+03-

1.061E+03-

1.060E+02

-2.00E+02 -1.60E+02 -1.20E+02 -8.00E+01 -4.00E+01 0.00 4.00E+01 8.00E+01 1.020E+02 1.060E+02 2.00E+02  
ORIENTATION ORIENTATION

A-15

NODE C1

L42 3DX DYNAMIC FST

JAN 15 1975

1.90E+02-

1.78E+03-

1.74E+03-

1.72E+03-

1.70E+03-

1.68E+03-

1.66E+03-

1.64E+03-

-2.0CE+02 -1.6CE+02 -1.0CE+02 -8.0CE+01 -4.00E+01 0.00  
ORIENTATION

A-16

1.20E+02 8.00E+01 1.02E+02 1.60E+02 2.0CE+02

0.00

MODE C

LH2 30X DYNAMIC DAT

JAN 15 1975

1.0 34E+02-

1.0 82E+02-

1.0 8CE+C2-

1.0 76E+C7-

1.0 7CE+C3-

1.0 74E+C3-

1.0 72E+C3-

1.0 7CF+C7-  
1.0 6CE+C2 -1.0 6CE+C2  
-2.0 CCE+C2 -8.0 CCE+C2 -8.0 CCE+C2 -4.00E+01  
C.CC 4.0 CE+C1 8.0 CE+C1 1.20E+02 1.60E+02 2.00E+02  
ORIENTATION

MODE CT

LHE 45% DYNAMIC CEF

JAN 15 1975

1.0E6+C3-

1.0E5E+C3-

1.0E4E+03-

1.0E3E+03-

1.0E2E+03-

1.0E1E+03-

1.0E0E+C3-

1.0E0E+C2 -1.0E0E+C2 -1.0E0E+02 -8.0E+01 -4.0E+01 C.00  
4.0E0E+01 8.0E0E+01 1.0E0E+C2 1.0E0E+C2 2.0E0E+02  
-2.0E0E+C2 CRIEATIUN

A-18

CODE CT

LH<sub>2</sub> SO<sub>4</sub>X DYNAMIC TEST

JAN 15 1976

卷之二

卷之三

卷之三

1.27E+02 -

卷之三

10853 • J. CLIN.

1087

-3-  
10824

四

MOORE CTR

20 CIV + C3-

10585 + 52-0

1096

1094 E + C 3 -

-23432601

10903402

1.088E+32

1086

四  
A-2

LH2 60% DYNAMIC 32T

JAN 15 1975

卷之三

MODE CT

LM2 70X DYNAMIC ORT

JAN 15 1975

2.01E+C2-

2.00E+03-

1.99E+03-

1.98E+03-

1.97E+03-

1.96E+03-

1.95E+C3-

1.94E+03-

-2.0CE+C2 -1.60E+02 -1.2CE+02 -8.00E+01 -4.00E+01 0.0C

ORIENTATION

7.14

0.C

7.14

0.C

7.14

0.C

7.14

0.C

7.14

0.C

7.14

0.C

7.14

A-21

CODE CT

LH2 BOX DYNAMIC ORBIT

卷之三

JAN 15 1975

20 C7E + 03 -

2006F+02-

- -

2.CSE-03

2-04 E+C3-1

2. C2E + C3 -

2. C2- + C3-

--20 CCCE-<sup>n</sup>2 -11-60E +C'2  
ORIENTATION

१५८

MODE CT

LH2 9CX DYNAMIC GRT

JUN 15 1975

2.13E+03-

2.12E+03-

2.11E+03-

2.10E+03-

2.09E+03-

2.08E+03-

2.07E+03-

2.06E+03-  
-2.05E+02 -1.60E+02 -8.00E+01 -4.00E+01 0.CC  
ORIENTATION

A-23

MODE CT

LH2 95 % DYNAMIC ORT

JAN 15 1975

2.16E+03-

2.15E+C3-

2.14E+C3-

2.13E+C3-

2.12E+03-

2.11E+03-

2.1CF+C3-  
-2.0CE+C2 -1.6CE+02 -1.20E+C2 -8.00E+01 -4.00E+01 0.00  
ORIENTATION

A-24

FREQUENCY

LHD CCW STATIC DEF

JAN 15 1975

2.8CE+01-

2.49E+01-

2.0CE+C1-

1.6CE+C1-

1.20E+C1-

8.0C

4.0CC

0.0C

1.52E+03 1.52E+03 1.53E+03 1.53E+03 1.54E+03 1.54E+03 1.55E+03 1.55E+03 1.56E+03 1.56E+03 1.56E+03 1.56E+03 1.57E+03 1.57E+03

40DE COUNT

A-25

FREQUENCY

LH2 EX STATIC GET

JAN 15 1975

1.04CE+01

1.026E+01

1.011E+01

8.00

6.00

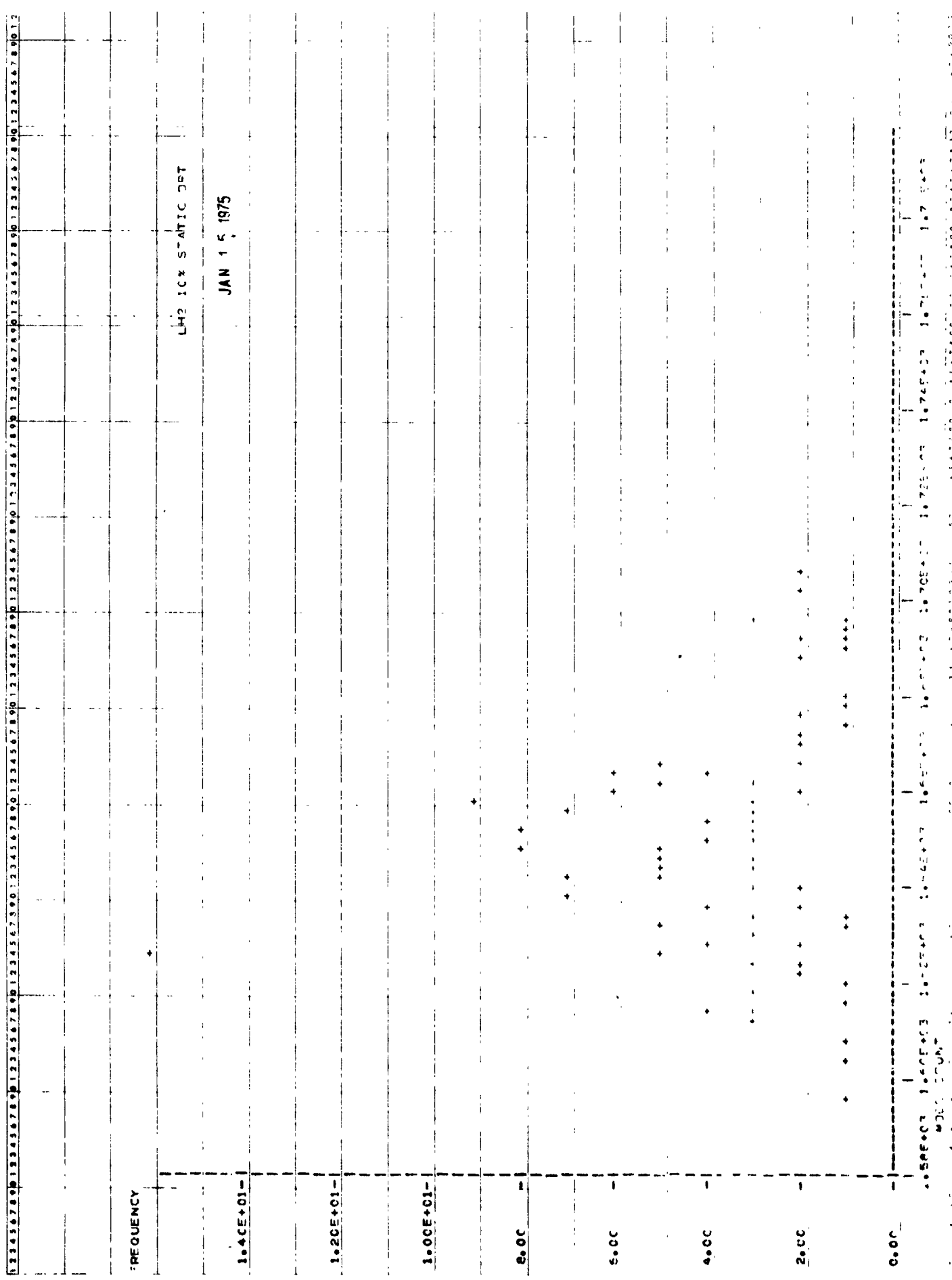
4.00

2.00

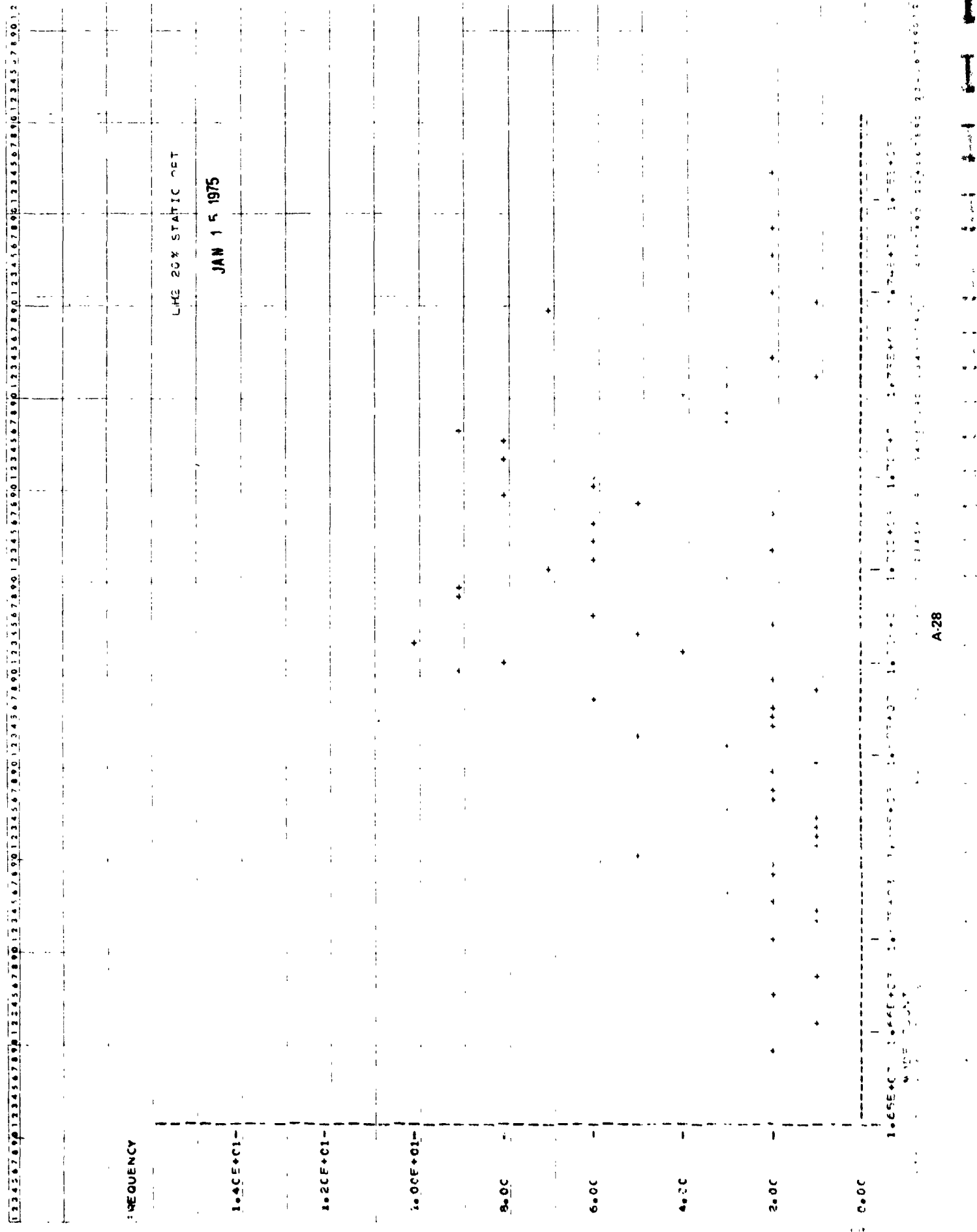
0.00

1.0EE+02 1.04E+03 1.07E+03 1.062E+03 1.0625E+03 1.064E+03 1.0645E+03 1.065E+03 1.0655E+03 1.066E+03 1.0665E+03  
M2DF COUNT

A26



۸۳



C  
W

FREQUENCY

JAN 15 1975

1.4CE+C1-

1.2CE+C1-

1.0CE+C1-

8.0C

6.0C

4.0C

2.0C

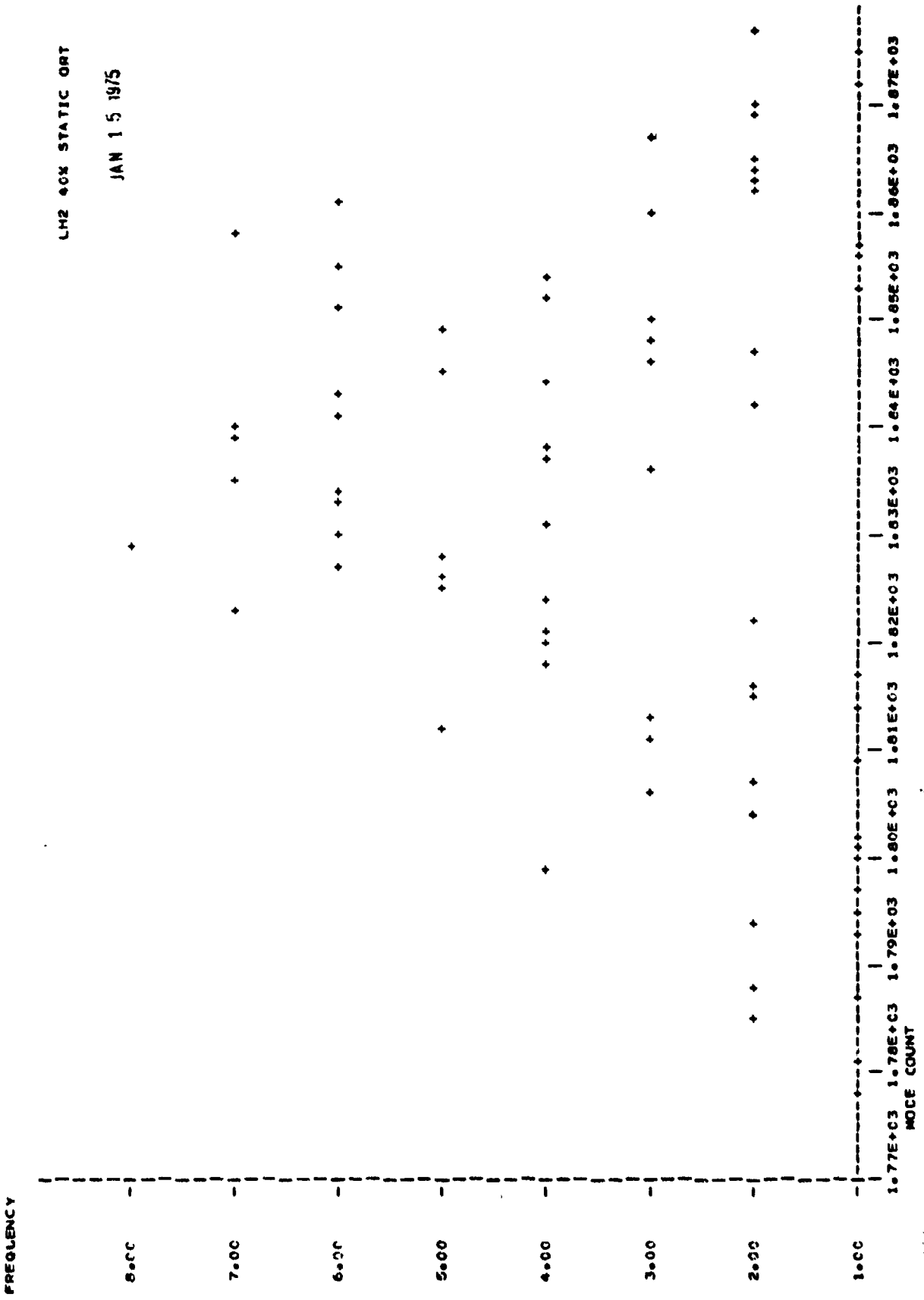
0.0C

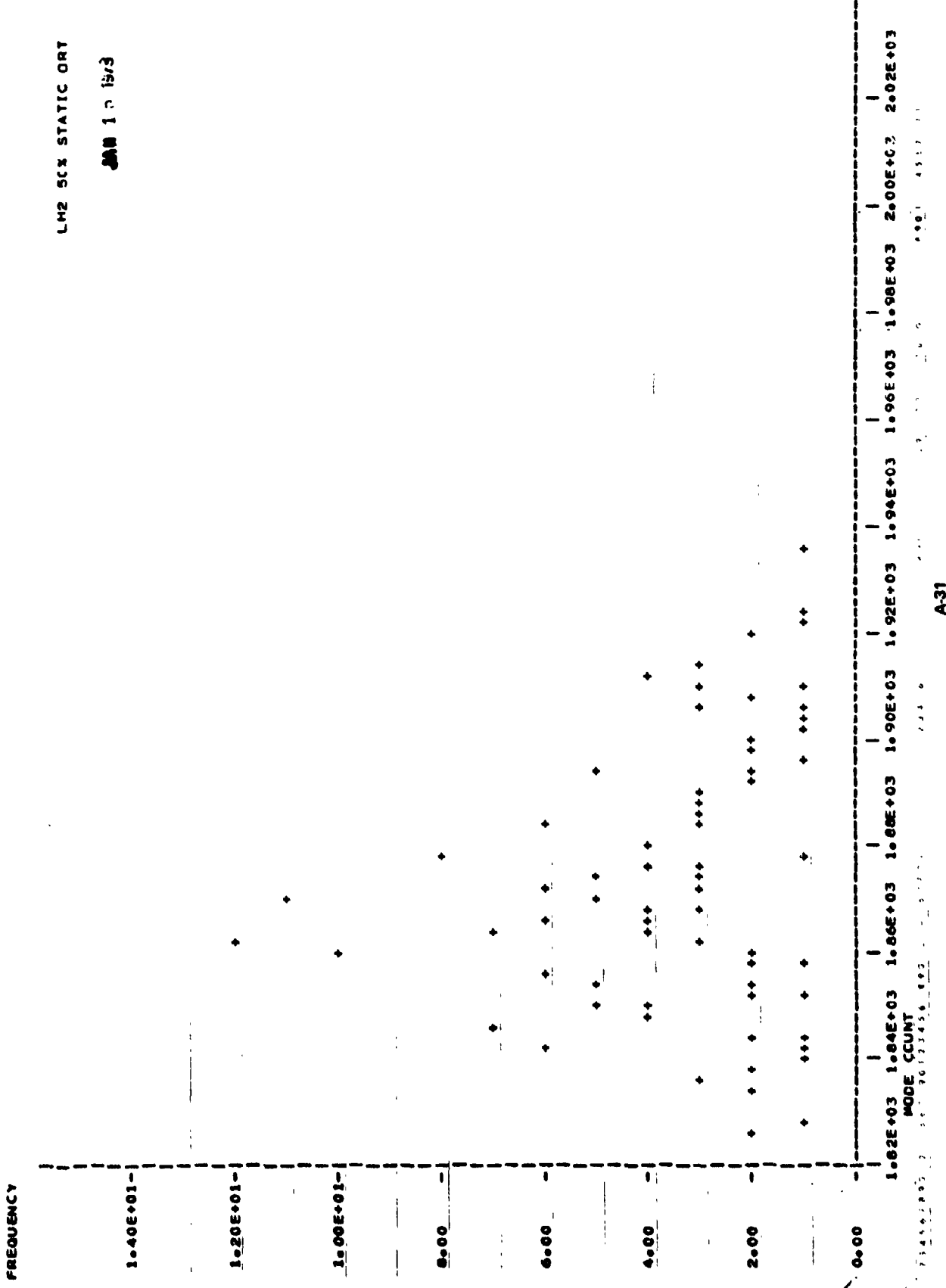
1.7CE+C3 1.7CE+C7 1.74E+C7 1.76E+C5 1.78E+C5 1.8CE+C3 1.82E+C7 1.84E+C7 1.86E+C7 1.88E+C7  
MCDF COUNT

A-29

LHZ4CX STATIC ORT

JAN 15 1975





FREQUENCY

LH2 60x STATIC ORT

JUN 15 1975

8.0C

7.00

6.00

5.0C

4.00

3.00

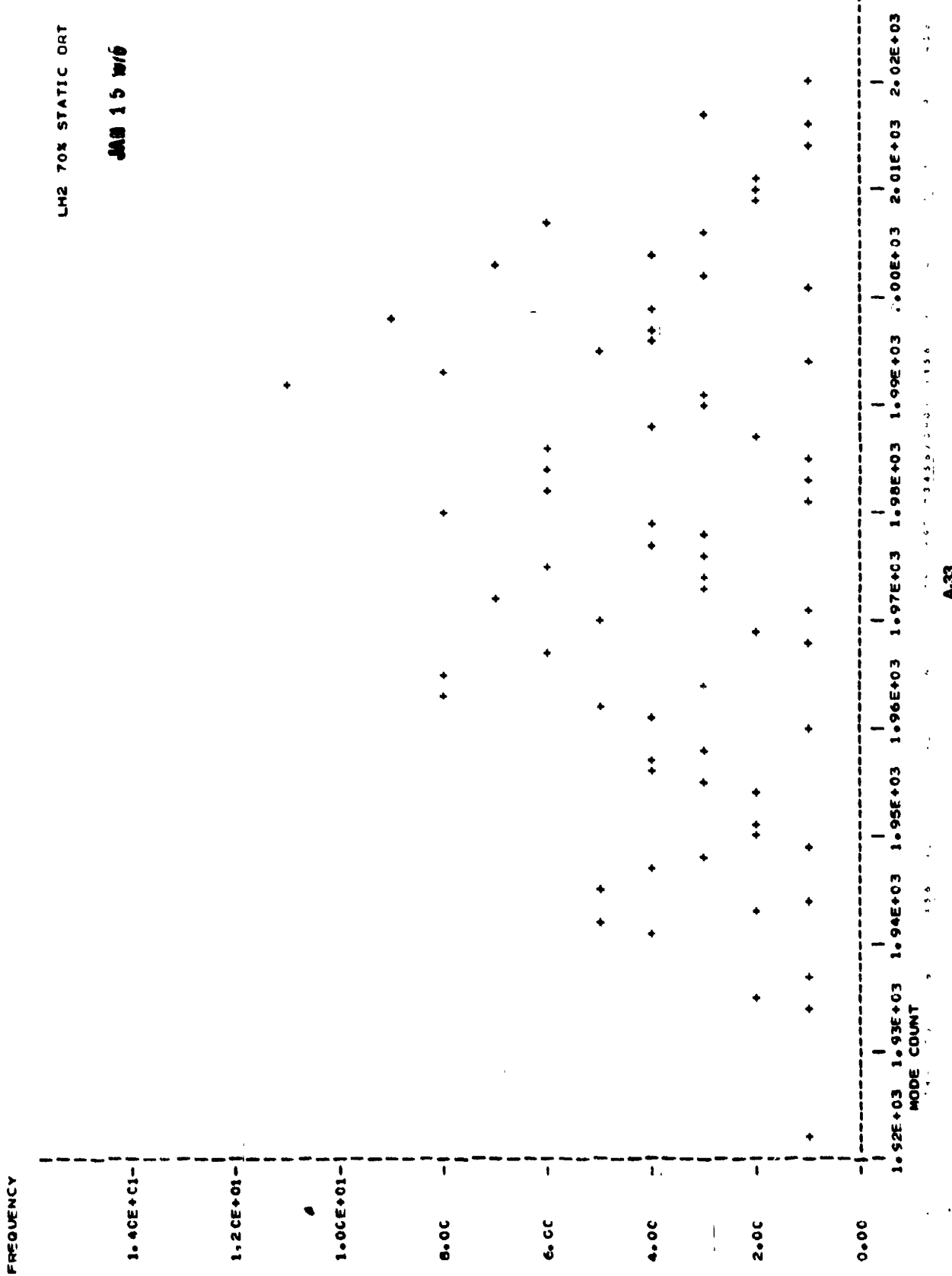
2.0C

1.0C

1.86E+03 1.88E+03 1.90E+03 1.92E+03 1.94E+03 1.96E+03 1.98E+03 2.00E+03 2.02E+03 2.04E+03 2.06E+03

MODE COUNT

A-32



FREQUENCY

LH2 SCK STATIC ORY

JAN 1 = 1975

1.40E+01

1.20E+01

1.00E+01

0.00

0.00

0.00

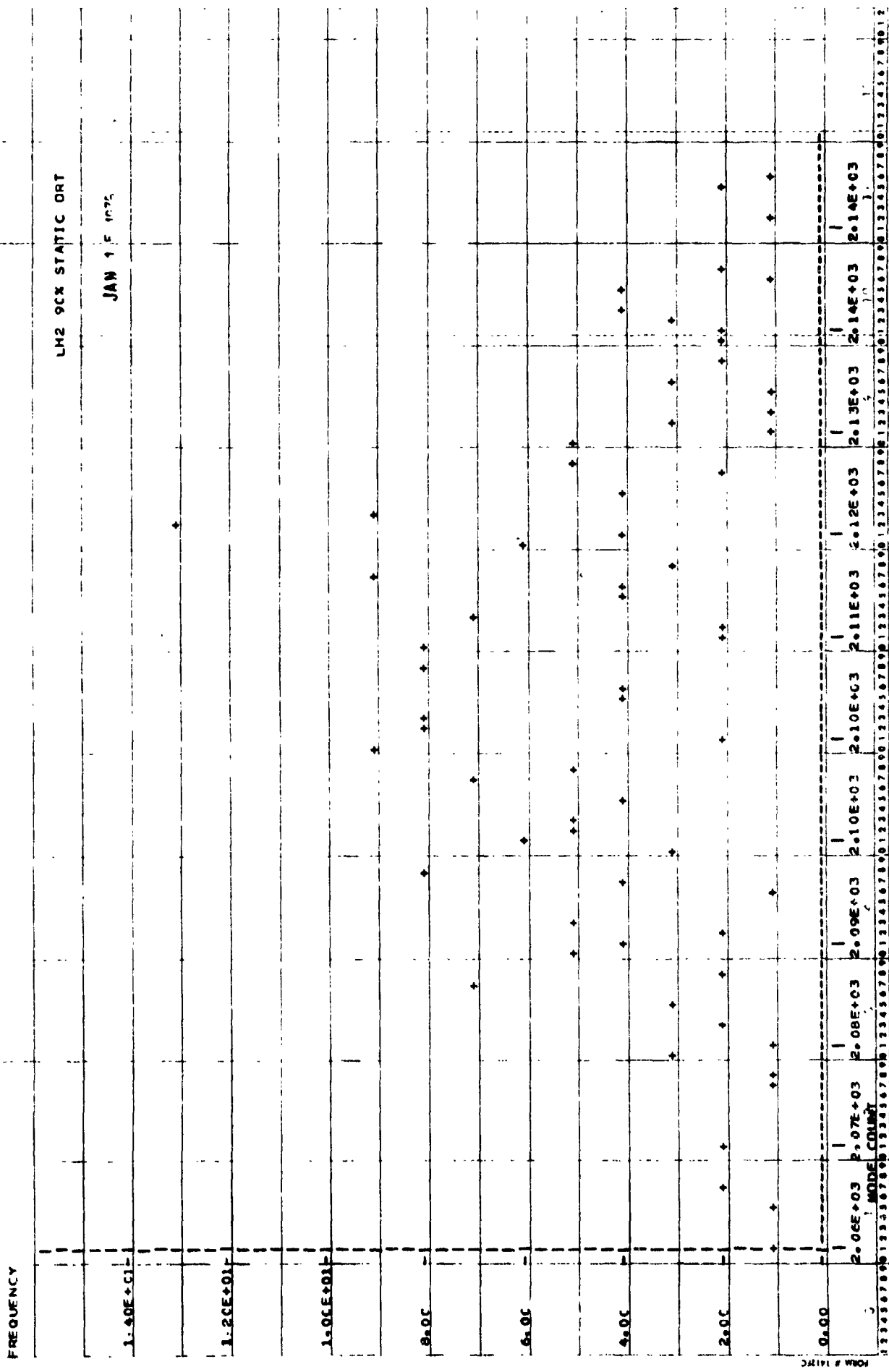
0.00

0.00

MODE COUNT

1.96E+03 1.98E+03 2.00E+03 2.02E+03 2.04E+03 2.06E+03 2.08E+03 2.10E+03 2.12E+03 2.14E+03 2.16E+03 2.18E+03

A34



四

FREQUENCY

LH2 95 X STATIC CRNT

JAN 15 1975

1.40E+01

1.20E+01

1.00E+01

0.00

0.00

0.00

2.00

0.00

2.09E+03 2.10E+03 2.11E+03 2.12E+03 2.13E+03 2.14E+03 2.15E+03 2.16E+03 2.17E+03

MODE COUNT

A-36

MODE C1

1.57E+03-

1.56E+03-

1.55E+03-

1.54E+03-

1.54E+03-

1.52E+03-

1.51E+03-

-2.00E+02 -1.60E+02 -1.20E+02 -8.00E+01 -4.00E+01 0.00  
ORIENTATION

A-37

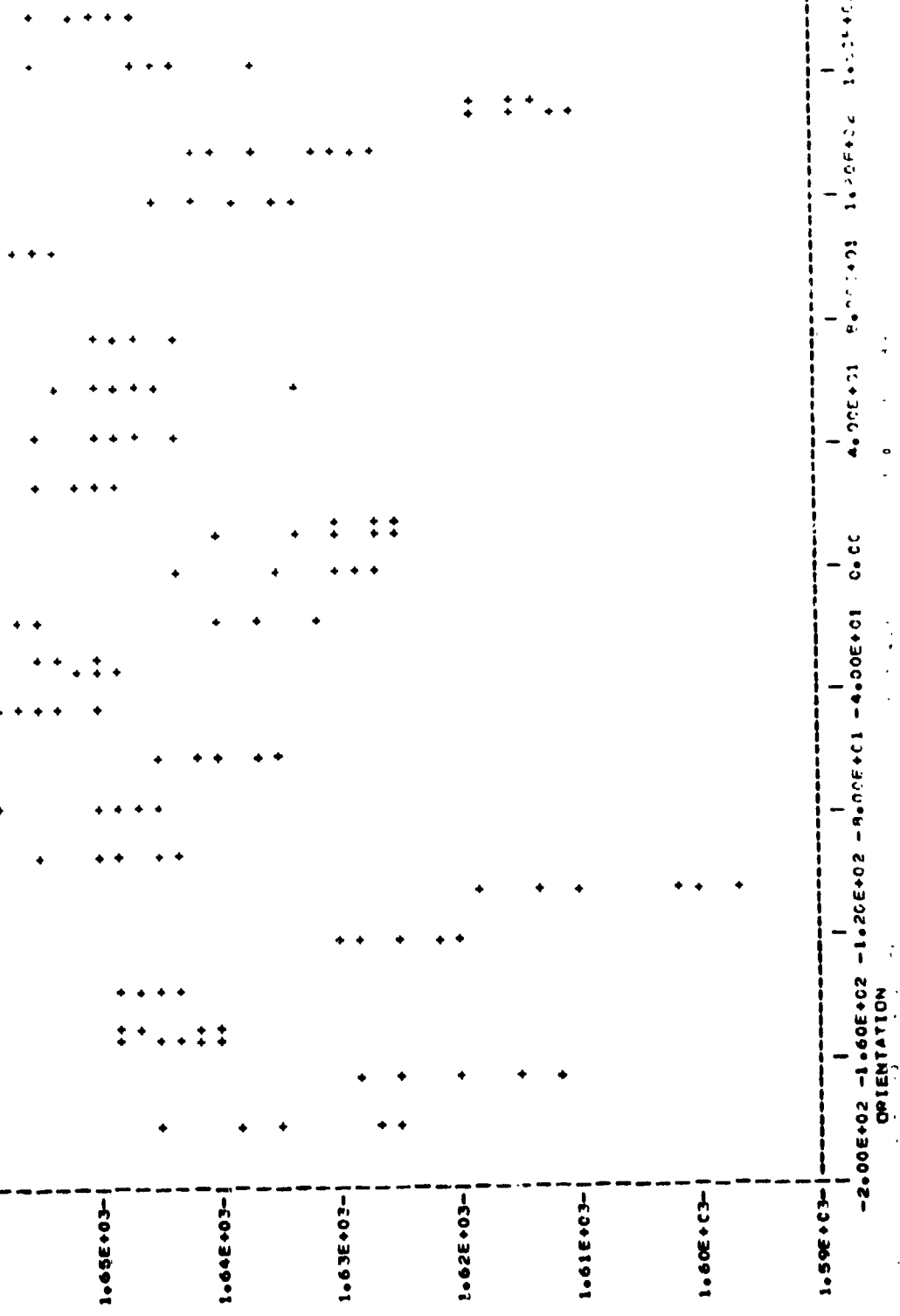
LH2 OCC STATIC CRT

JAN 14, 1975

MODE C1

LHS = STDEV

JAN 15 1975



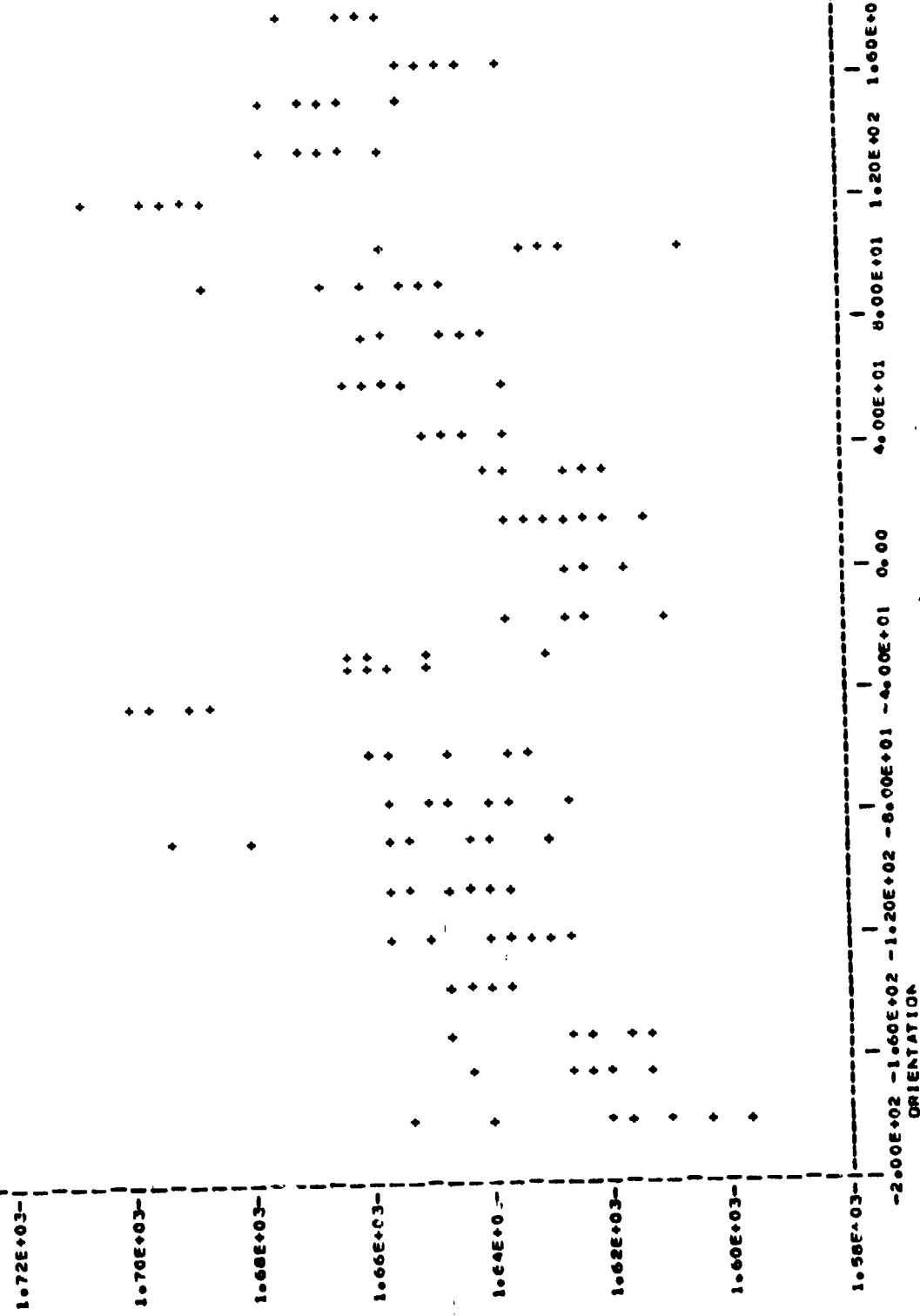
A-38

-2.00E+02 -1.60E+02 -1.60E+02 -1.60E+02 -1.60E+02 -1.60E+02 -1.60E+02  
ORIENTATION

MODE CT

LW2 1CX STATIC CRT

JAN 15 1975



A30

WINE CT

LH2 2CX STATIC TRT

JAN 15 1975

1.70E+03-

1.74E+03-

1.72E+03-

1.70E+03-

1.68E+03-

1.66E+03-

1.64E+03-

-2.00E+02 -1.50E+02 -0.50E+01 -4.00E+01 0.00 4.00E+01 8.00E+01 1.020E+02 1.60E+02 2.00F+02

ORIENTATION

A-40

NODE CT

LH2 30% STATIC ORT

JAN 15 1975

1.84F+C3-

1.82E+C3-

1.8CF+C3-

1.78E+C3-

1.74E+C3-

1.72E+C3-

1.7CF+C3-  
-2.0CF+C2 -1.60F+C2 -1.20E+C2 -8.00E+C1 0.0C  
ORIENTATION

A41

WDF 57

L12 ACC STATIC NOT

JAN 15 1975

1.09E+07-

1.09E+07-

1.08E+07-

1.05E+07-

1.03E+07-

1.03E+07-

1.07E+02-

1.07E+03-

A-22

-2.30E+02 -1.05E+02 -1.07E+02 -8.03E+01 -4.05E+01 3.03E+01 4.05E+01 9.00E+01 1.20E+02 1.60E+02 2.00E+02  
CENTRATION

MCODE CT

LH2 SCX STATIC ORT

جامعة مصر

18 56E+03-

1094E+03-1

1-92E+03-1

1-50E+G-3-

1088E+C3-1

186E+03

1084E+03

1.082E+03-1

1

三

343

LHS & RHS STATIC JAT

JAN 15 1975

2. COE + 03 -

1-98E+C 3-

1e 96E+03

1054 E + C 3

1092E+03-

190502

卷之三

100

~~-42.00E+02 -1.60E+02 -1.20E+02 -8.00E+01 -4.00E+01 C+C 4.00E+01 8.00E+01 1.20E+02 1.60E+02 2.00E+02~~

NODE CT

2. CCE+C3-

LH2 7CX STATIC ORT

JAN 15 1975

2.0CF+C3-

1.98E+03-  
1.96E+03-  
1.94E+03-  
1.92E+03-  
-2.00E+C2 -1.60E+C2 -6.00E+C1 -4.00E+01 0.00  
ORIENTATION

MODE CT

LHM BCK STATIC GR

JAN 15 1975

2.10E+03-

2.0EE+03-

2.06E+03-

2.02E+03-

2.00E+03-

1.98E+03-

1.96E+03-

-2.00E+02 -1.63E+02 -1.20E+02 -8.00E+01 -4.00E+01 0.0C  
ORIENTATION

A-46

CODE CT

LITZ 90% STATIC ORT

JAN 15 1973

202CE+COM-1

10

一一

2010E+03-1

1

1

2016 ECA

100

三

2014EEC3-1

104

十一

2, 12E + C2-

104

1

2.1ICE+C3

104

1

卷之三

104

100

22 CEE + GZ -

-2-

卷之三

2

### ORIENTATION

MODE CT

LH2 95 % STATIC ORNT

IN 15 1975

2.022E+03-

2.020E+03-

2.018E+03-

2.016E+03-

2.014E+03-

2.012E+03-

2.010E+03-

2.008E+03-

-2.00E+02 -1.60E+02 -1.20E+02 -8.00E+01 -4.00E+01 0.00 4.00E+01 8.00E+01 1.20E+02 1.60E+02 2.00E+02  
ORIENTAT DDN

A48



**APPENDIX B**  
**COMPUTER PLOTS OF**  
**FREQUENCY OF OCCURRENCE VS. MODE COUNT**  
**AND**  
**MODE COUNT VS. ORIENTATION ANGLE**  
**FEBRUARY 3, 1975 LOX TESTS**



## APPENDIX B

### TABLE OF CONTENTS

COMPUTER PLOT	PAGE NO.
---------------	----------

#### FREQUENCY OF OCCURENCE VS. MODE COUNT (DYNAMIC ORIENTATION)

● 0% LOX LOADING .....	B-1
● 5% LOX LOADING .....	B-2
● 10% LOX LOADING .....	B-3
● 20% LOX LOADING .....	B-4
● 30% LOX LOADING .....	B-5
● 40% LOX LOADING .....	B-6
● 50% LOX LOADING .....	B-7
● 60% LOX LOADING .....	B-8
● 70% LOX LOADING .....	B-9
● 80% LOX LOADING .....	B-10
● 90% LOX LOADING .....	B-11
● 95% LOX LOADING .....	B-12

#### MODE COUNT VS. ORIENTATION ANGLE (DYNAMIC ORIENTATION)

● 0% LOX LOADING .....	B-13
● 5% LOX LOADING .....	B-14
● 10% LOX LOADING .....	B-15
● 20% LOX LOADING .....	B-16
● 30% LOX LOADING .....	B-17
● 40% LOX LOADING .....	B-18
● 50% LOX LOADING .....	B-19
● 60% LOX LOADING .....	B-20
● 70% LOX LOADING .....	B-21
● 80% LOX LOADING .....	B-22
● 90% LOX LOADING .....	B-23
● 95% LOX LOADING .....	B-24

#### FREQUENCY OF OCCURENCE VS. MODE COUNT (STATIC ORIENTATION)

● 0% LOX LOADING .....	B-25
● 5% LOX LOADING .....	B-26



## COMPUTER PLOT

## PAGE NO.

● 10% LOX LOADING .....	B-27
● 20% LOX LOADING .....	B-28
● 30% LOX LOADING .....	B-29
● 40% LOX LOADING .....	B-30
● 50% LOX LOADING .....	B-31
● 60% LOX LOADING .....	B-32
● 70% LOX LOADING .....	B-33
● 80% LOX LOADING .....	B-34
● 90% LOX LOADING .....	B-35
● 95% LOX LOADING .....	B-36

## MODE COUNT VS. ORIENTATION ANGLE (STATIC ORIENTATION)

● 0% LOX LOADING .....	B-37
● 5% LOX LOADING .....	B-38
● 10% LOX LOADING .....	B-39
● 20% LOX LOADING .....	B-40
● 30% LOX LOADING .....	B-41
● 40% LOX LOADING .....	B-42
● 50% LOX LOADING .....	B-43
● 60% LOX LOADING .....	B-44
● 70% LOX LOADING .....	B-45
● 80% LOX LOADING .....	B-46
● 90% LOX LOADING .....	B-47
● 95% LOX LOADING .....	B-48

LOCK IN FREQUENCY

Feb 3 1975

FREQUENCY

9.00

7.00

5.00

3.00

1.00

2.00

1.00

1.05E+07 1.05E+07 1.05E+07 1.05E+07 1.05E+07 1.05E+07 1.05E+07 1.05E+07

"DE COUNT

B-1

1.0E+00

0.8E+

0.6E+

0.4E+

0.2E+

0.E+

-0.2E+

-0.4E+

-0.6E+

B2

LINX 5X DYNAMIC CCT

FEB 9 1997



FREQUENCY

LOCK ICX DYNAMIC OPT

FEB 3 1975

7.00

6.00

4.00

2.00

1.00

0.00

-1.00

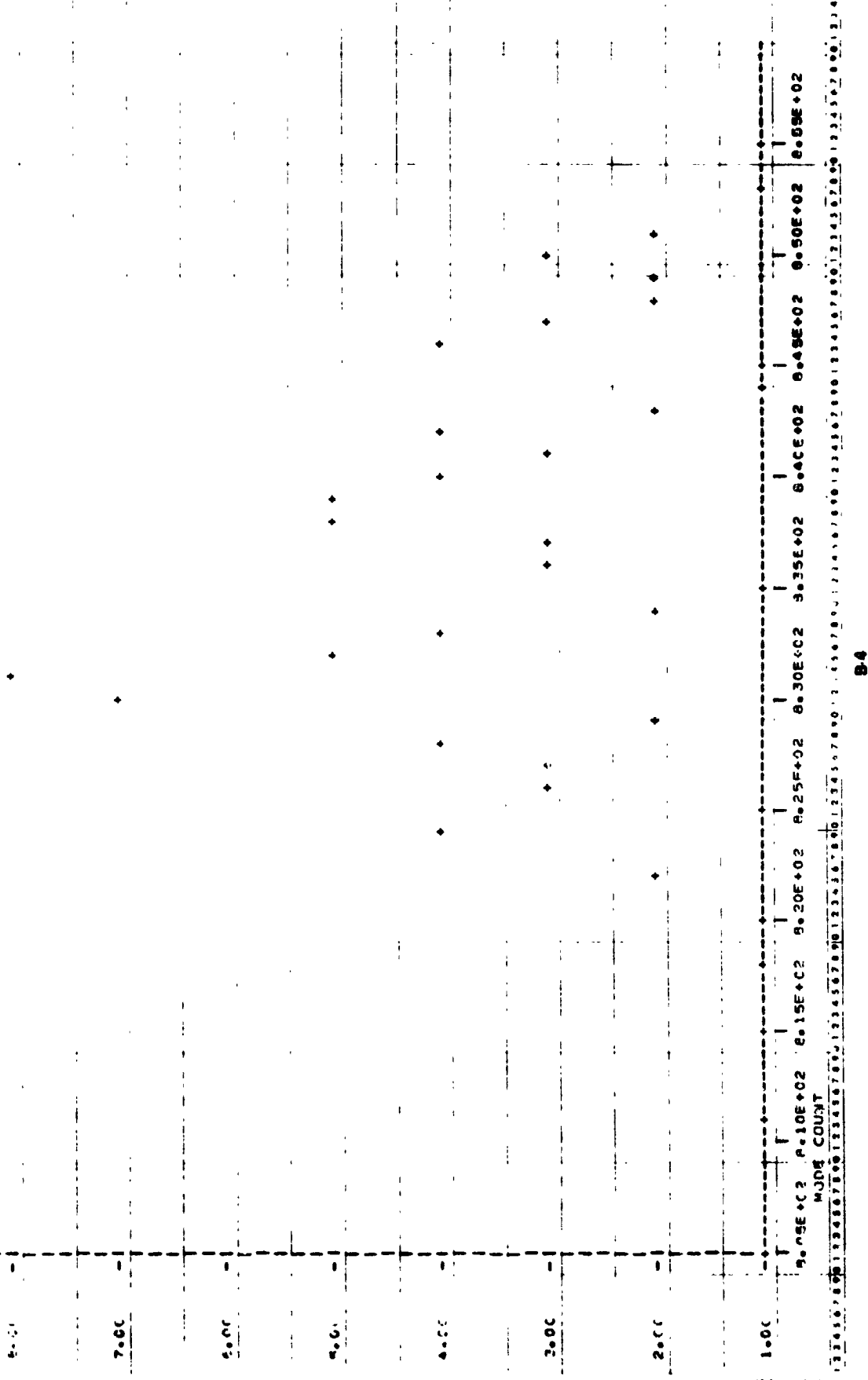
NOCE COUNT

1.0E+03 1.05E+03 1.09E+03 1.07E+03 1.06E+03 1.03E+03 1.09E+03 1.11E+03 1.13E+03

B-3

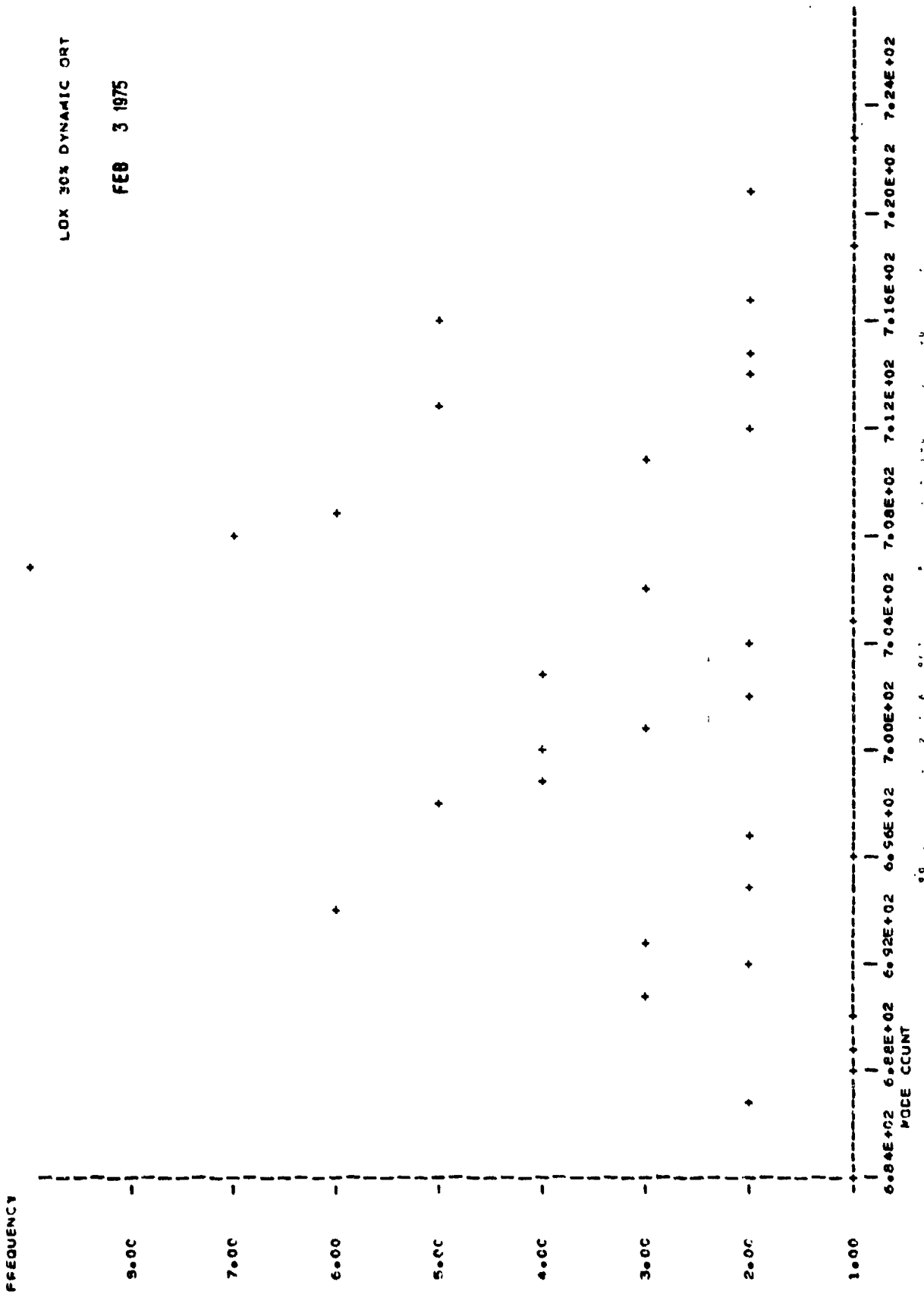
אנו שרים

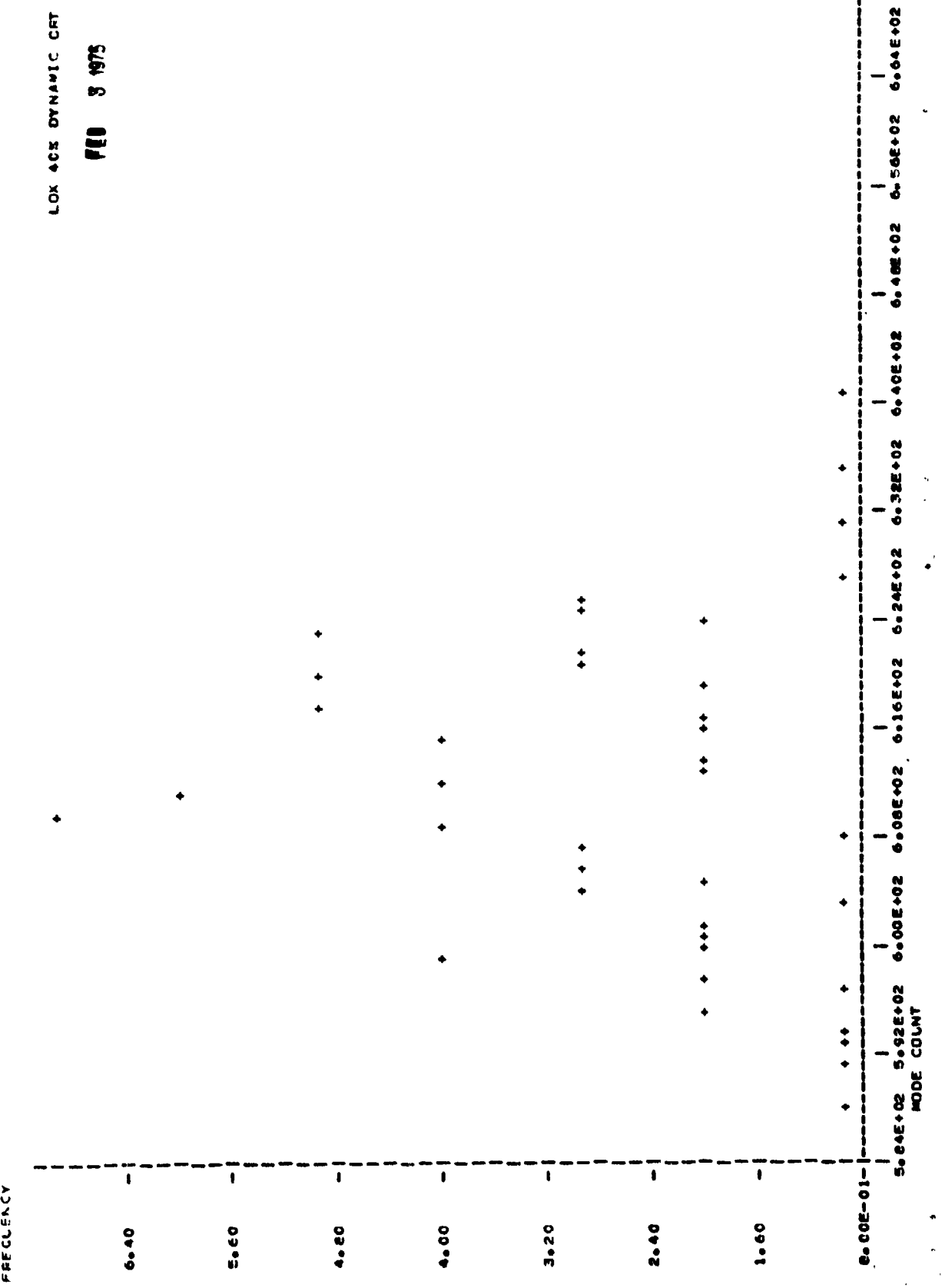
LOX 22CX DYNALINE DRAFT FEBRUARY 3, 1978



LOX 30X DYNAMIC ORT

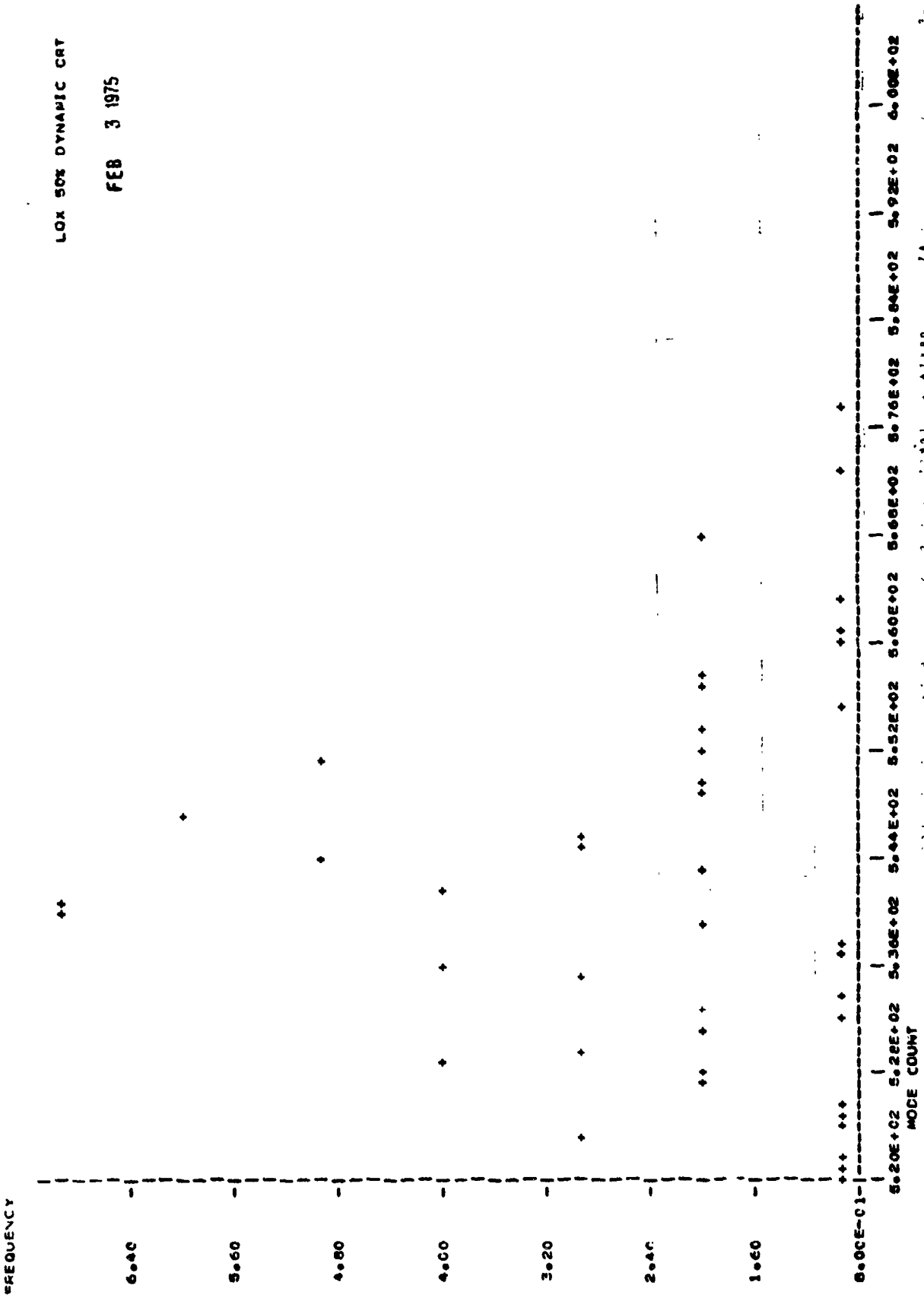
FE8 3 1975





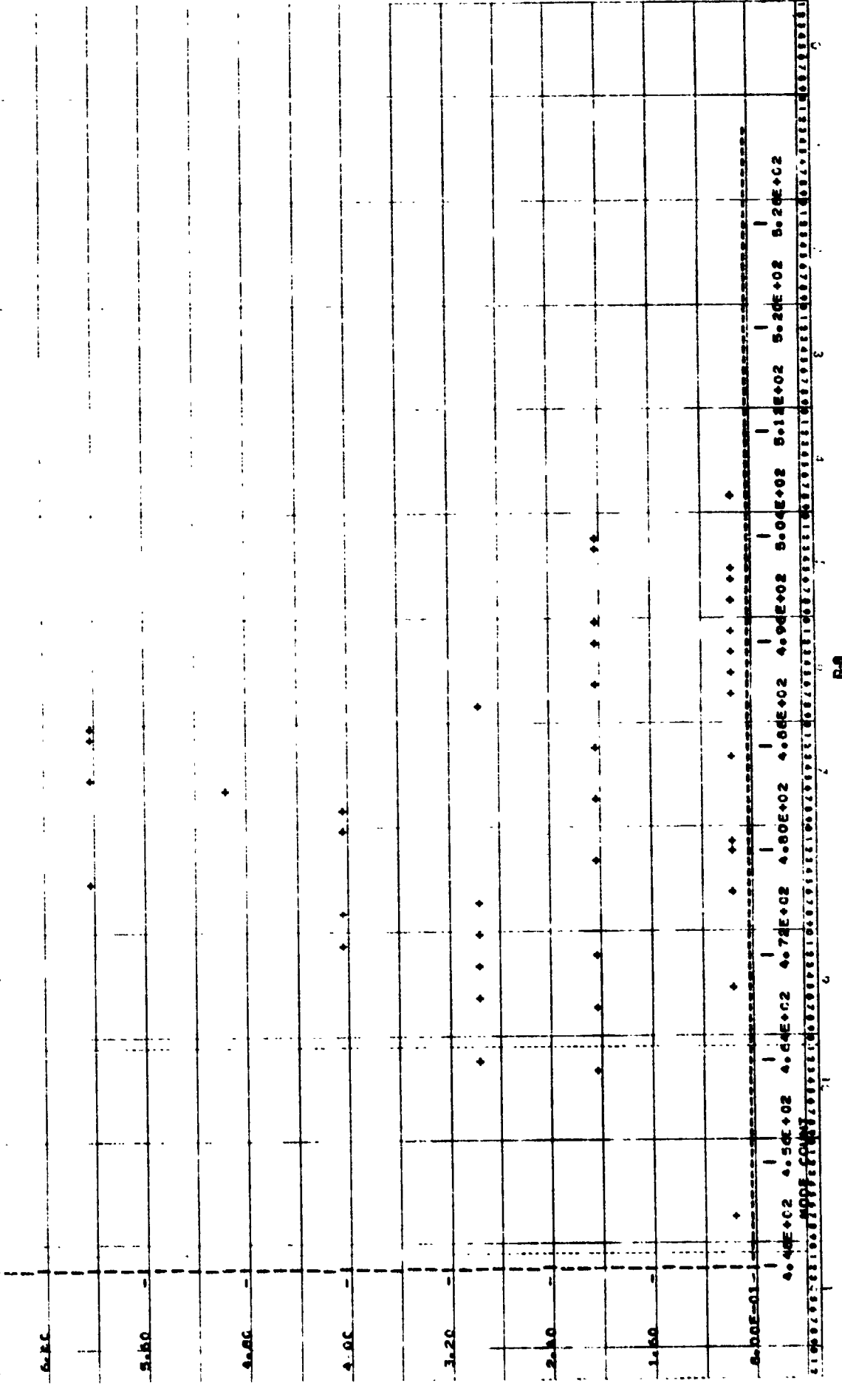
LOX 50X DYNAMIC CRT

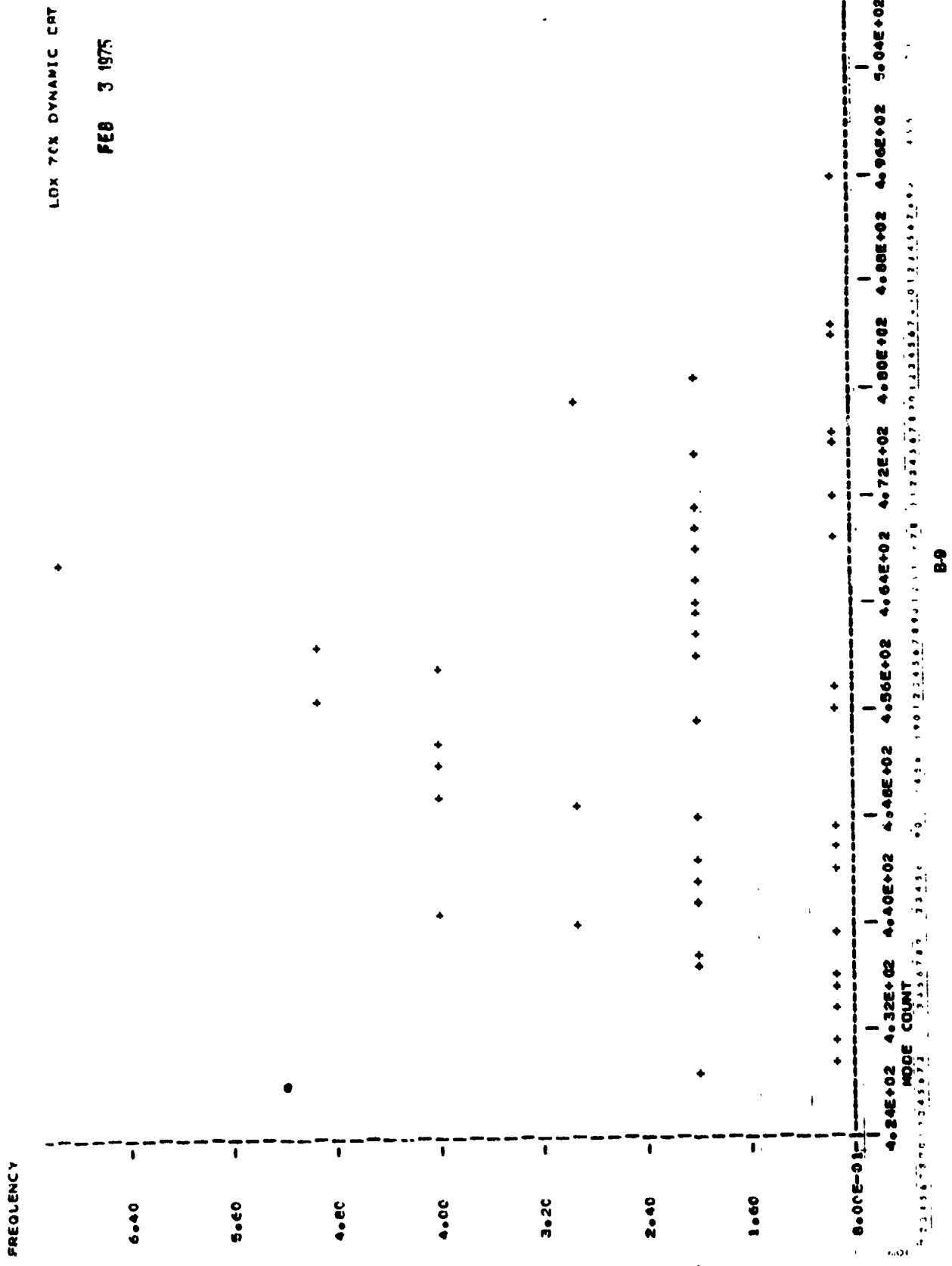
FEB 3 1975



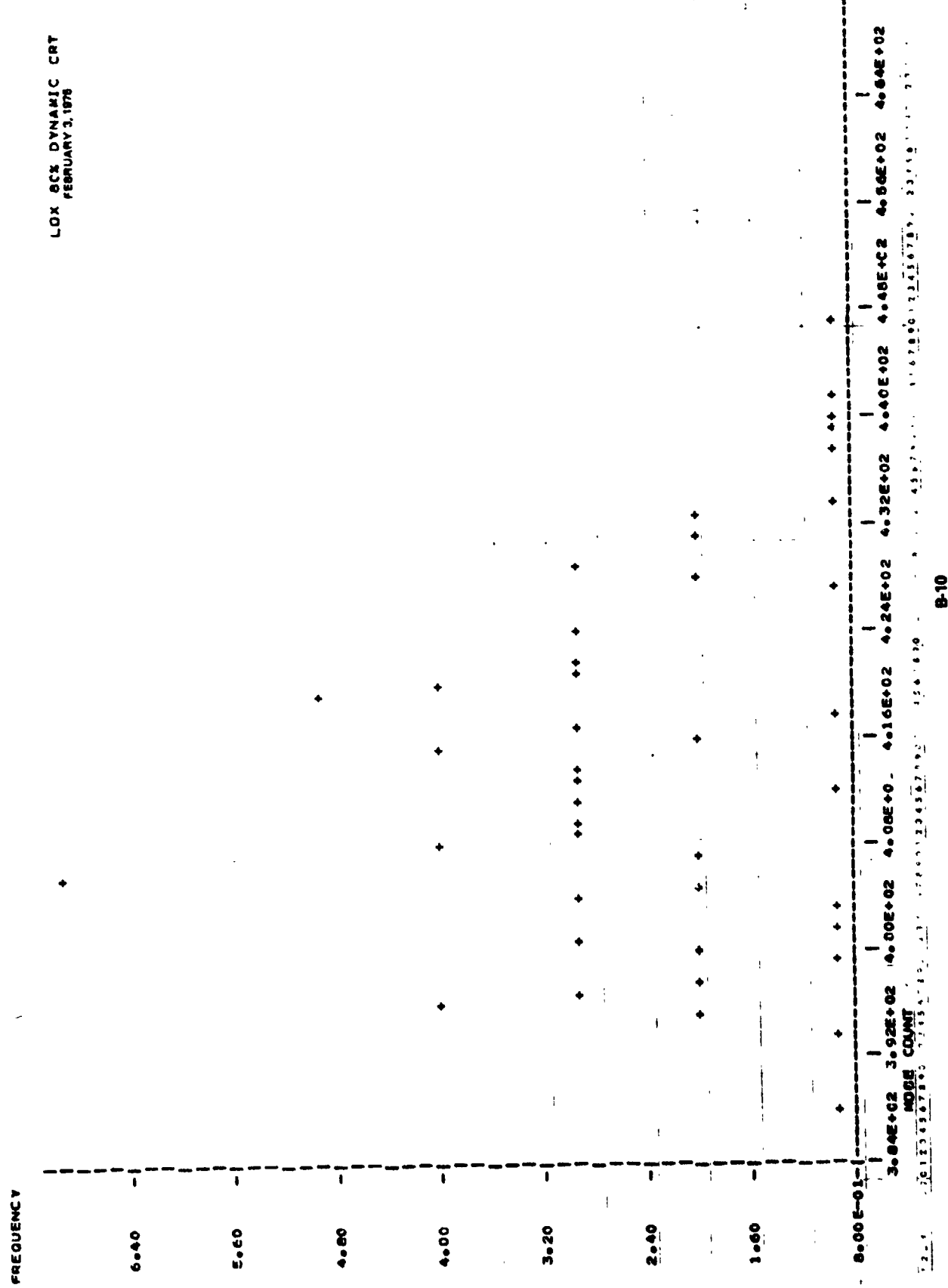
FREQUENCY

LOX 6C X DYNAMIC DATA  
FEBRUARY 3, 1976





LOCK STOCK DYNAMIC CART FEBRUARY 3, 1986



FEB 23 1975

FFA 2 1075

LOX 95% DYNAMIC OFF

9.0r

7.0r

5.0r

3.0r

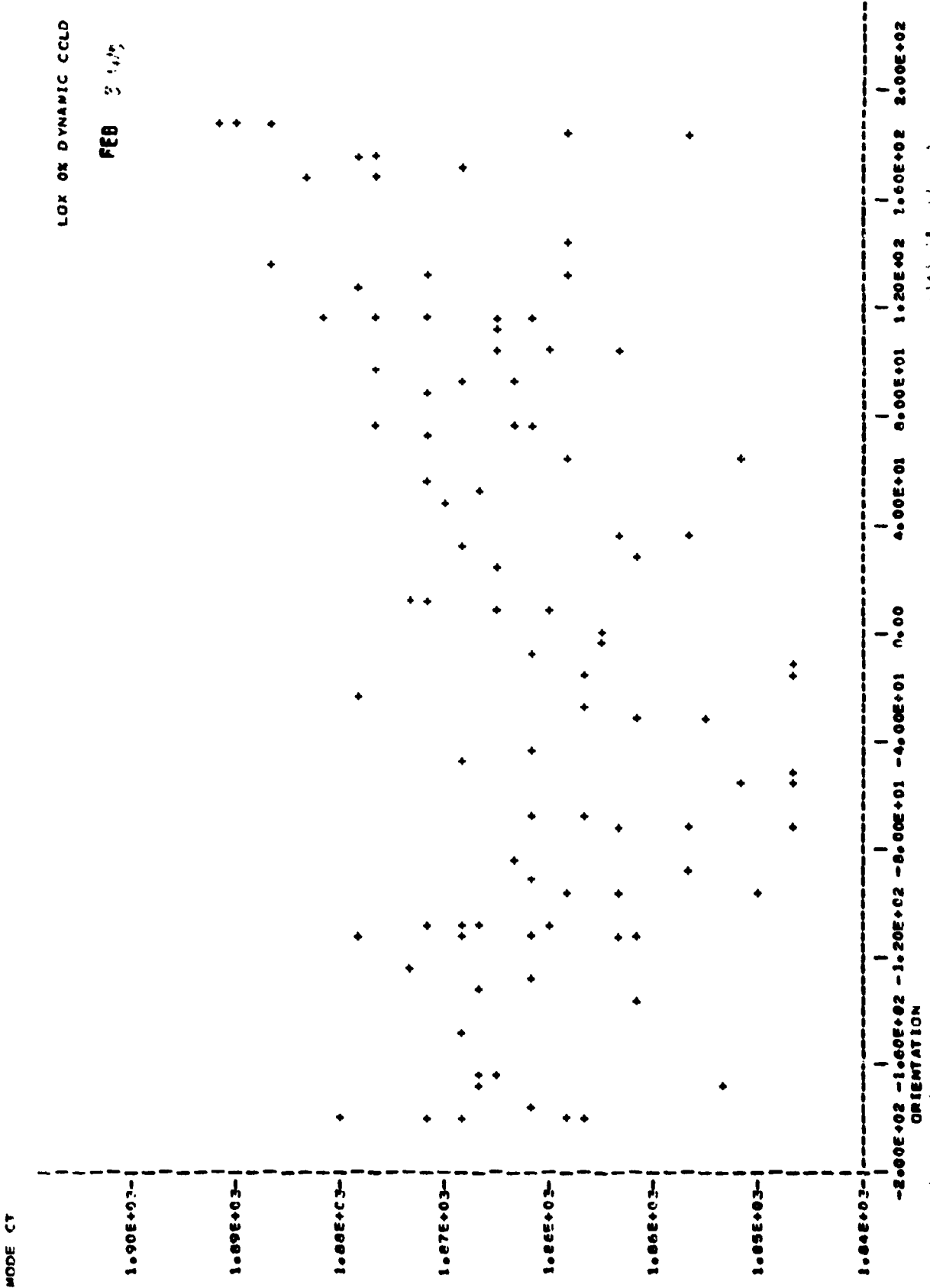
1.0r

2.0r

1.0r

1.0r

B-12  
3.48E+02 3.52E+02 3.56E+02 3.60E+02 3.64E+02 3.68E+02 3.72E+02 3.76E+02 3.80E+02 3.84E+02 3.88E+02 3.92E+02 3.96E+02 4.00E+02



MCDF CRT

LUX EX PLASTIC JFT

FEB 3 1975

1.02E+02-

1.037E+02-

1.0366E+01-

1.035E+03-

1.034E+02-

1.033E+02-

1.022E+02-

-2.00E+02

-1.00E+02

-1.025E+02

-0.00E+01

0.00E+01

1.020E+02

1.025E+02

B-14

ORIENTATION  
X 1.0000000000000000E+00 Y 1.0000000000000000E+00 Z 1.0000000000000000E+00

node C T

LOG-WEAK DYNAMIC SIST.

E 39 1975

१०१ चैत्र + चृष्ण-

1000 + 25

100000

一九四四年

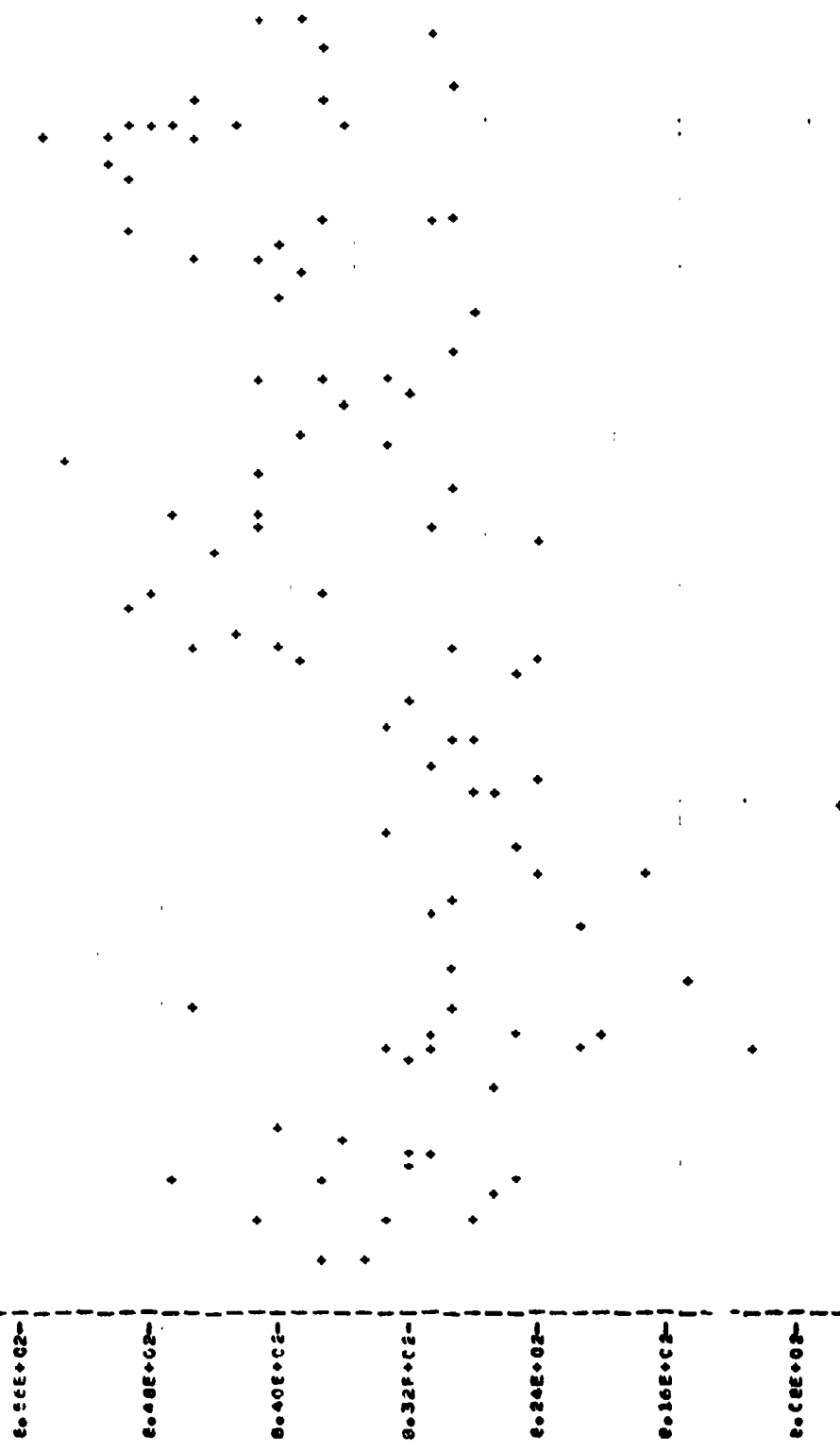
100000

LOGO C

15

•CCE CT

LGX 2CX DYNAMIC ORT  
FEBRUARY 3, 1976



-2.00E+02 -1.60E+02 -8.00E+02 -4.00E+01 0.00E+01 4.00E+01 8.00E+01 1.20E+02 1.60E+02 2.00E+02  
ORIENTATION  
B-16

WCCF CT

7.36E+02-

7.28E+02-

7.20E+02-

7.12E+02-

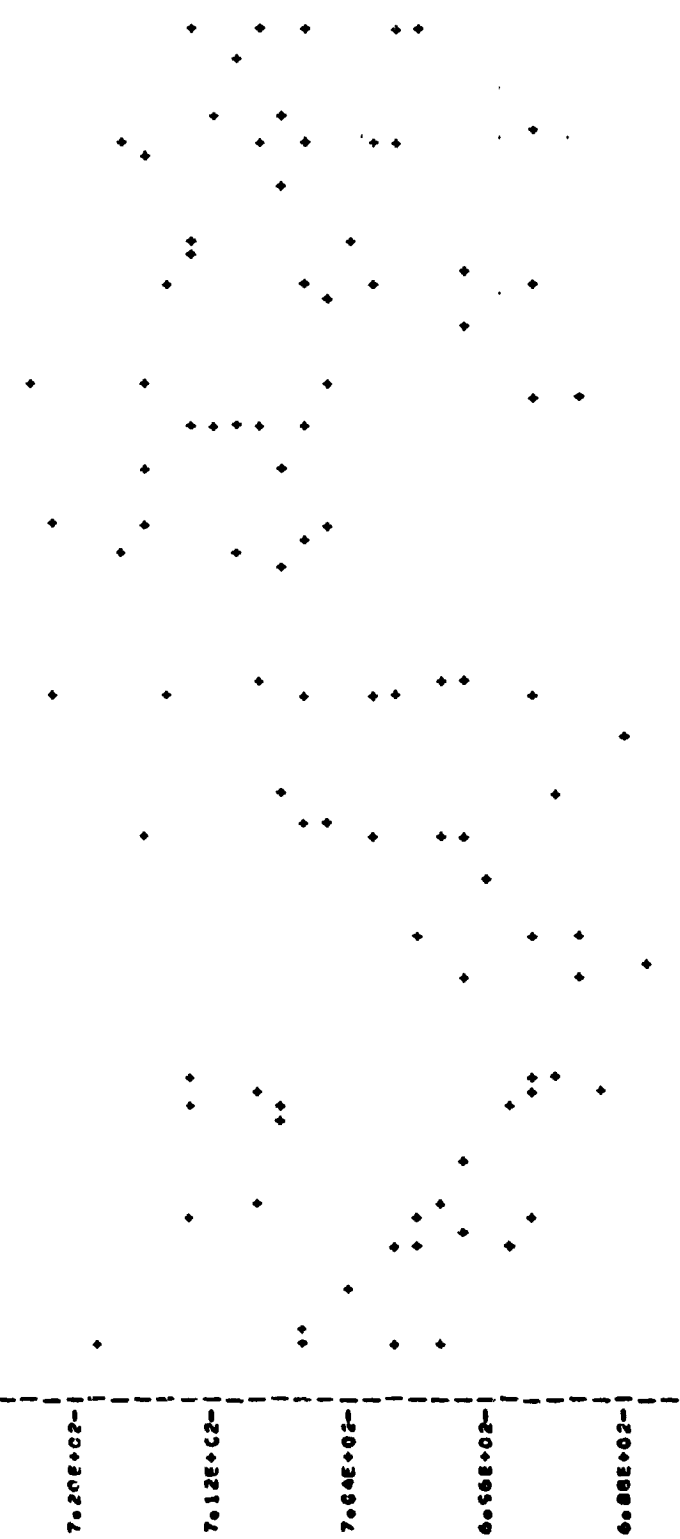
7.04E+02-

6.96E+02-

6.88E+02-

LCCX TCA DYNAMIC GCR

FEB 2 1974

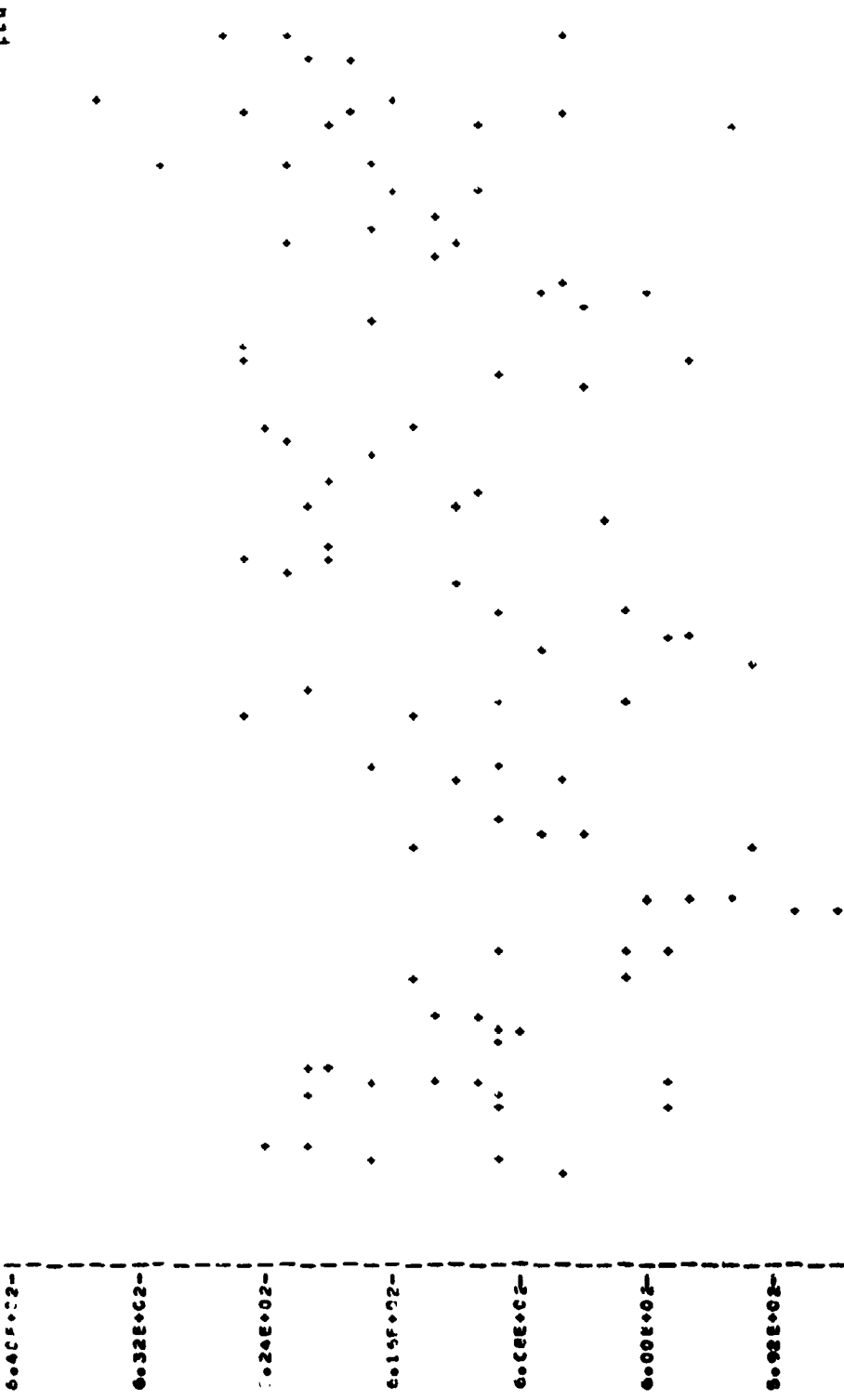


-2.00E+02 -1.60E+02 -1.20E+02 -8.00E+01 0.00 4.00E+01 8.00E+01 1.20E+02 1.60E+02 2.00E+02  
CEIMENTATIJA

MCDF CR

LIA ARX DYNAMIC CRV

FCA = 1075



-2.00E+02 -1.60E+02 -1.20E+02 -8.00E+01 -4.00E+01 0.00 4.00E+01 8.00E+01 1.20E+02 1.60E+02 2.00E+02  
ORIENTATION

B-18

NAME CT

S• 76F+C2-

S• 18F+C2-

S• 6CE+C2-

S• 52F+02-

S• 44F+C2-

S• 36F+C2-

S• 2AF+C2-

S• 27F+C2-

1.0rF+C2 -1.60E+02 -8.0nE+01 -4.0CE+01 C.CC 4.00E+01 1.00E+01 1.20E+02 1.6CE+02 2.0CE+02  
ORIENTATION

NAME CRT

LOX 60% DYNAMIC TEST  
FEBRUARY 3, 1976

5.04E+02-

4.04E+02-

4.03E+02-

4.02E+02-

4.01E+02-

4.00E+02-

4.05E+02-

4.06E+02-

-2.00E+02

B-20

-1.60E+02

C-20

-1.20E+02

C-10

-8.00E+01

C-0

-4.00E+01

C+0

0.00

C+10

4.00E+01

C+20

8.00E+01

C+30

1.20E+02

C+40

1.60E+02

C+50

2.00E+02

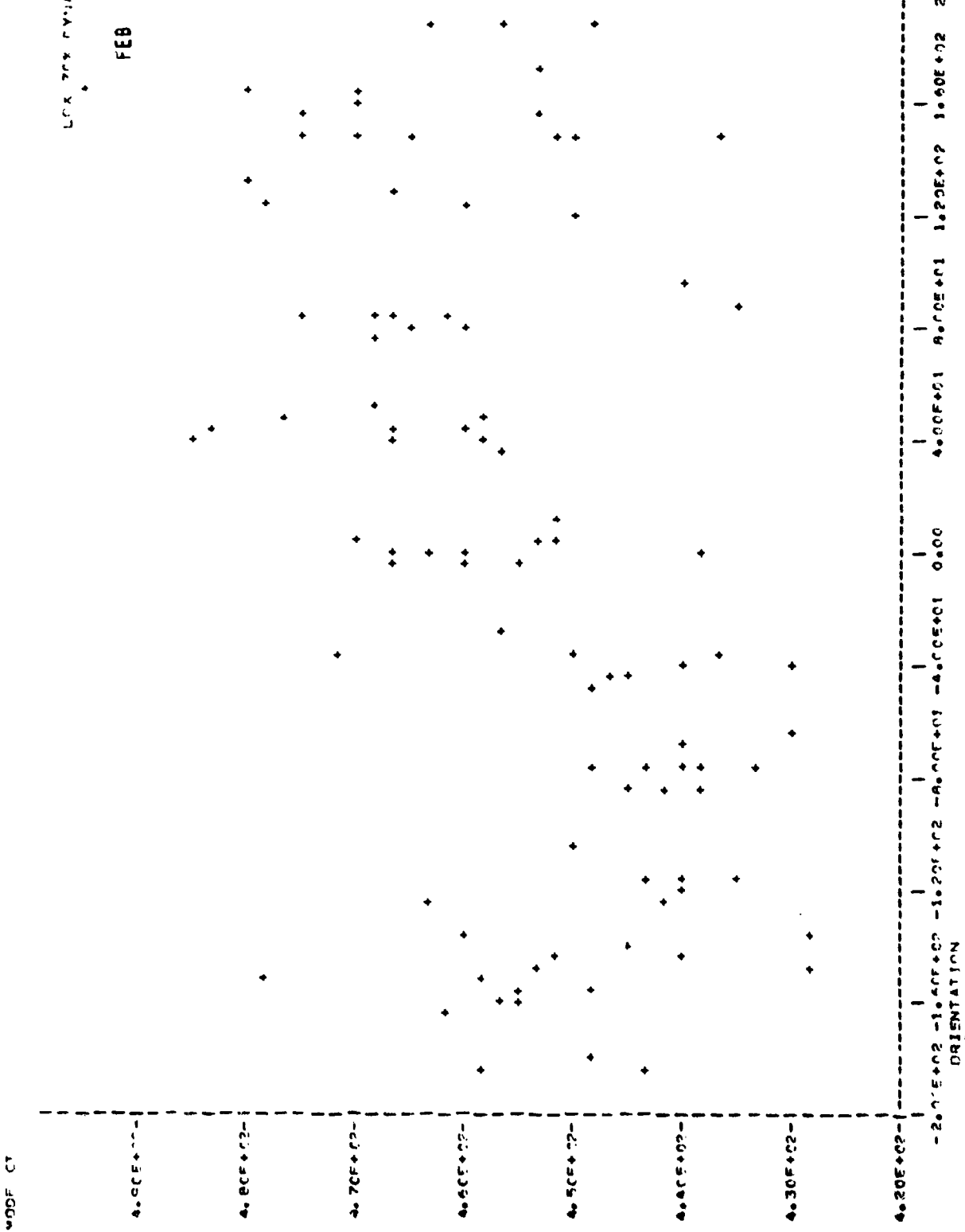
C+60

1.00E+01 1.00E+01 1.00E+01 1.00E+01 1.00E+01 1.00E+01 1.00E+01 1.00E+01 1.00E+01 1.00E+01

CRIENTATION

לראתך רוחני נברא

FE8 3 1975



YRPNCE RT

LNX 8CX DYNAMIC ORT  
FEBRUARY 3, 1975

4.00E+02-

4.00E+02-

4.00E+02-

4.00E+02-

4.00E+02-

3.92E+02-

3.84E+02-

-2.00E+02 -1.65E+02 -1.20E+02 -8.70E+01 -4.00E+01 0.00  
DRIFTATION

4.00E+02 4.00E+01 4.00E+00 1.20E+02 1.60E+02 2.00E+02

WEDGE CT

LOX 90% DYNAMIC ORT

4.0E+02-

4.0CF+02-

3.02E+02-

3.08E+02-

3.07E+02-

3.068E+02-

3.06E+02-

3.052E+02-

FFB 3.0E+02

-2.00E+02 -1.60E+02 -1.20E+02 -8.00E+01 -4.00E+01 0.00 4.00E+01 8.00E+01 1.20E+02 1.60E+02 2.00E+02 ORIENTATION

8-23

LINE C

LOX 95% DYNAMIC ORT

FEB 3 1975

3.85E+02-

3.8CE+02-

3.75E+02-

3.7CE+02-

3.65E+02-

3.6CE+02-

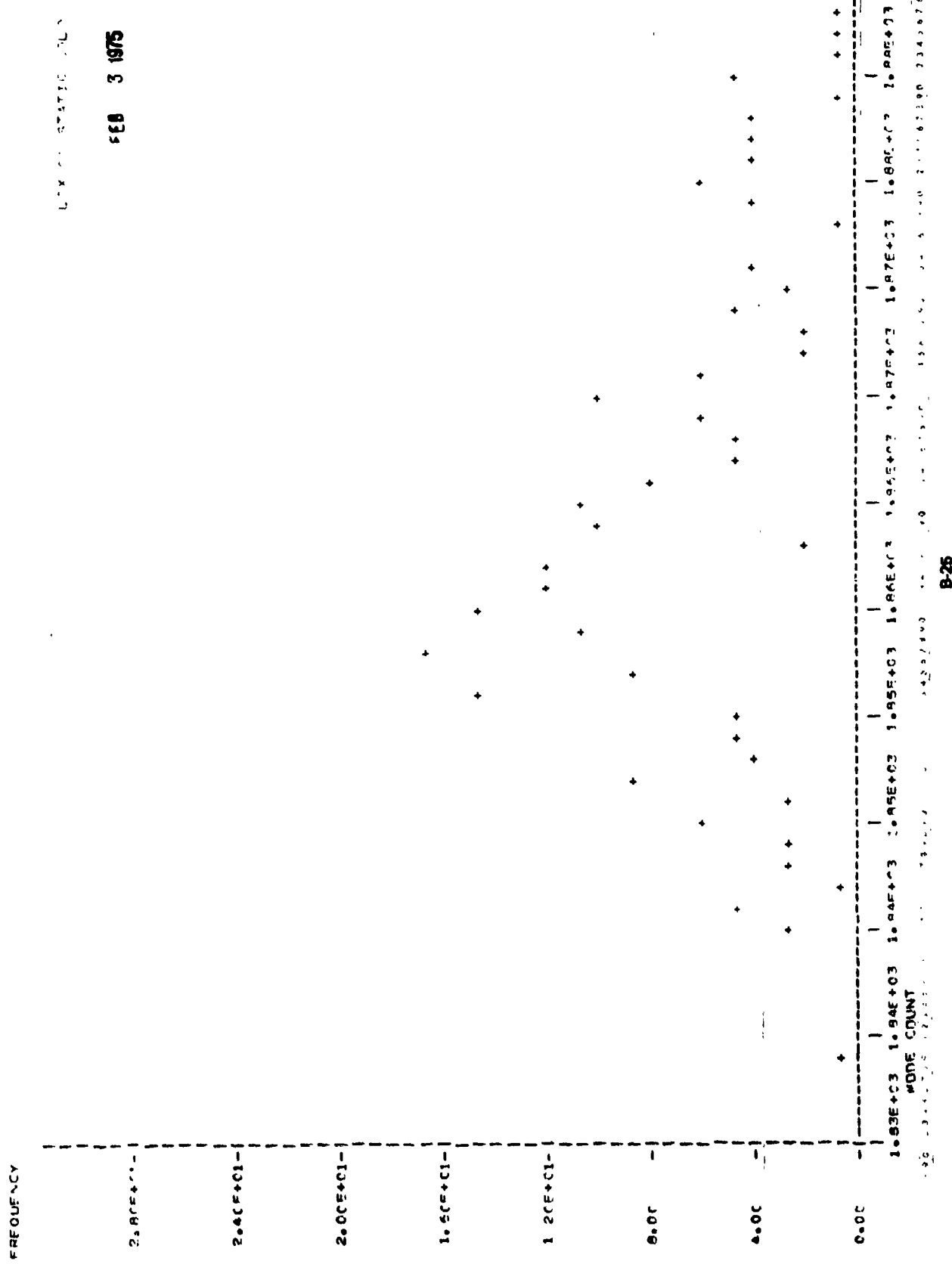
3.5CE+02-

3.50E+02-

-2.00E+02 -1.60E+02 -1.20E+02 -8.00E+01 -4.00E+01 0.00 4.00E+01 8.00E+01 1.20E+02 1.60E+02 2.00E+02

ORIENTATION

B-24



EFFECTIVENESS

LINK L=0.0000000000000000

1.4E+01  
1.2CE+C1-  
1.0CE+C1-

FE8 3 1075

8.00

6.00

4.00

2.00

0.00

1.32E+3 1.33E+03 1.34E+03 1.34E+03 1.35E+03 1.36E+03 1.37E+03 1.38E+03 1.39E+03 1.40E+03

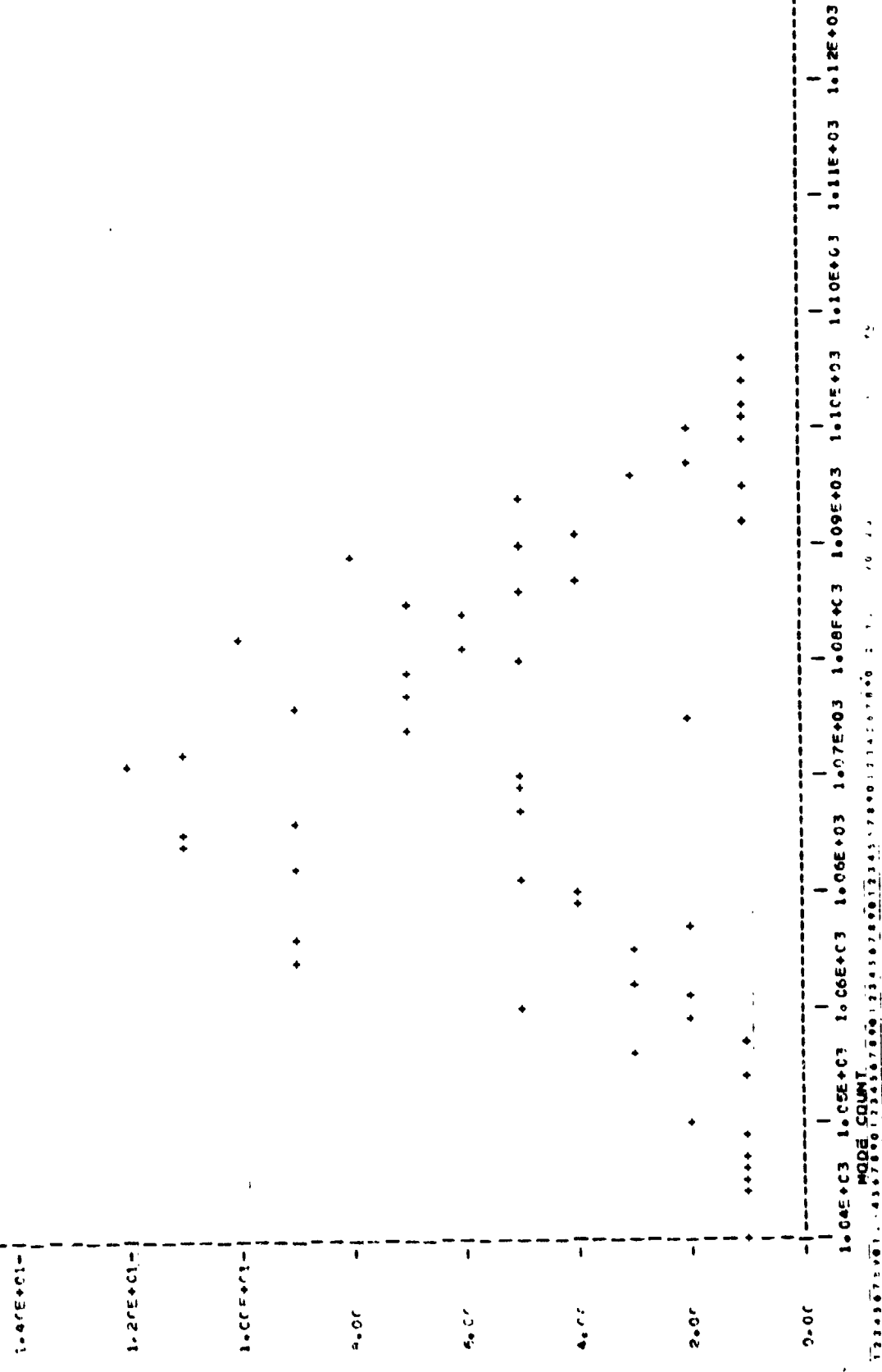
MODE COUNT

B26

FREQUENCY

LOX 1CX STATIC ORT

FEB 3 1975



REQUETE

LOX 20% STATIC OUT  
FEBRUARY 3, 1976

20 95 E + C -

2005-01-2

200CE+J=

1-505-017

1-29E+01 =

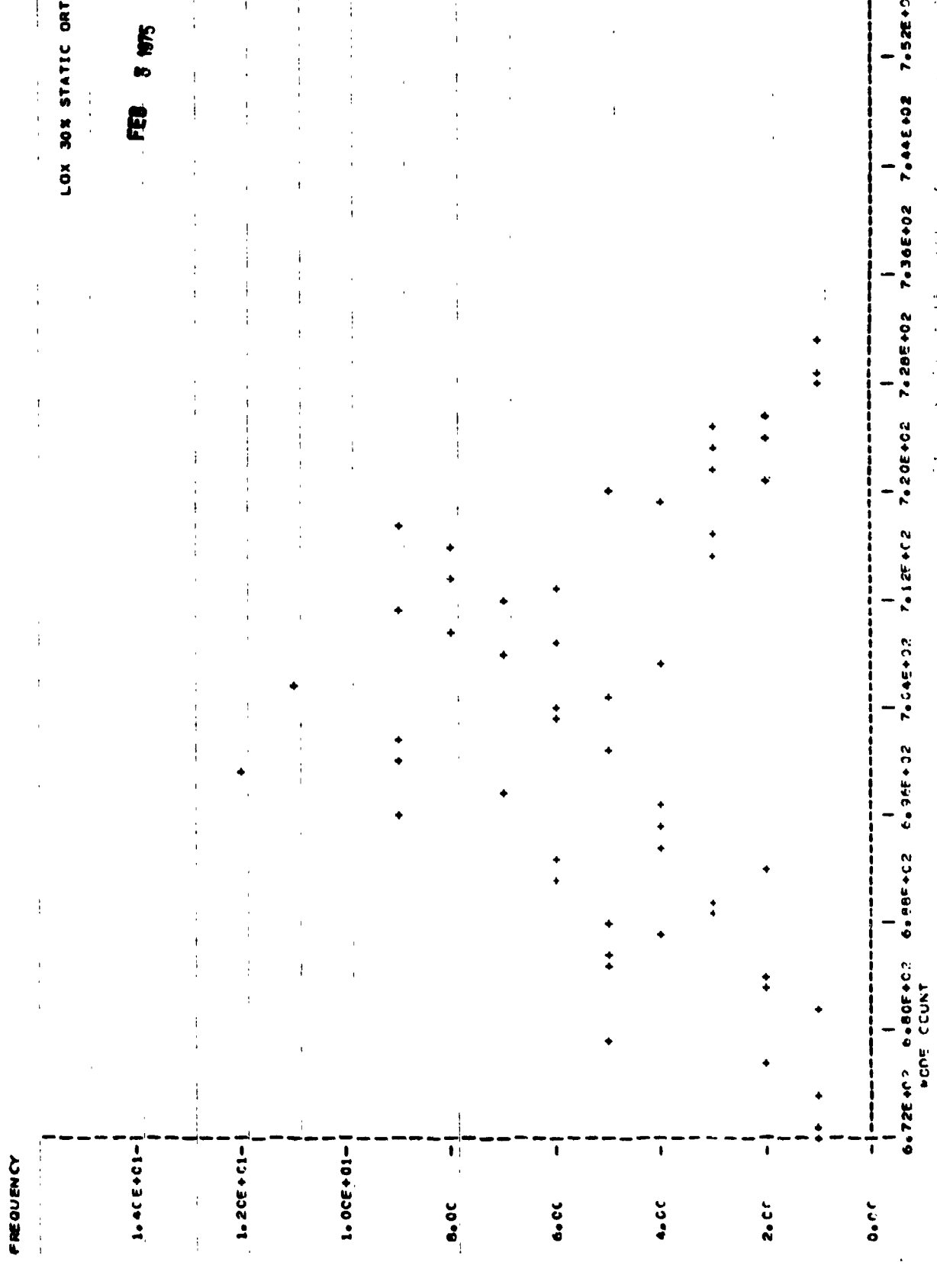
808

一一

10

1

1



B-29

1

LOX 40% STATIC ORT

FREQUENCY

FREQUENCY

1.40E+01

1.20E+01

1.00E+01

8.0E

6.0E

4.0E

2.0E

0.0E

5.0E+02  
4.0E+02  
3.0E+02  
2.0E+02  
1.0E+02  
0.0E+02

-30

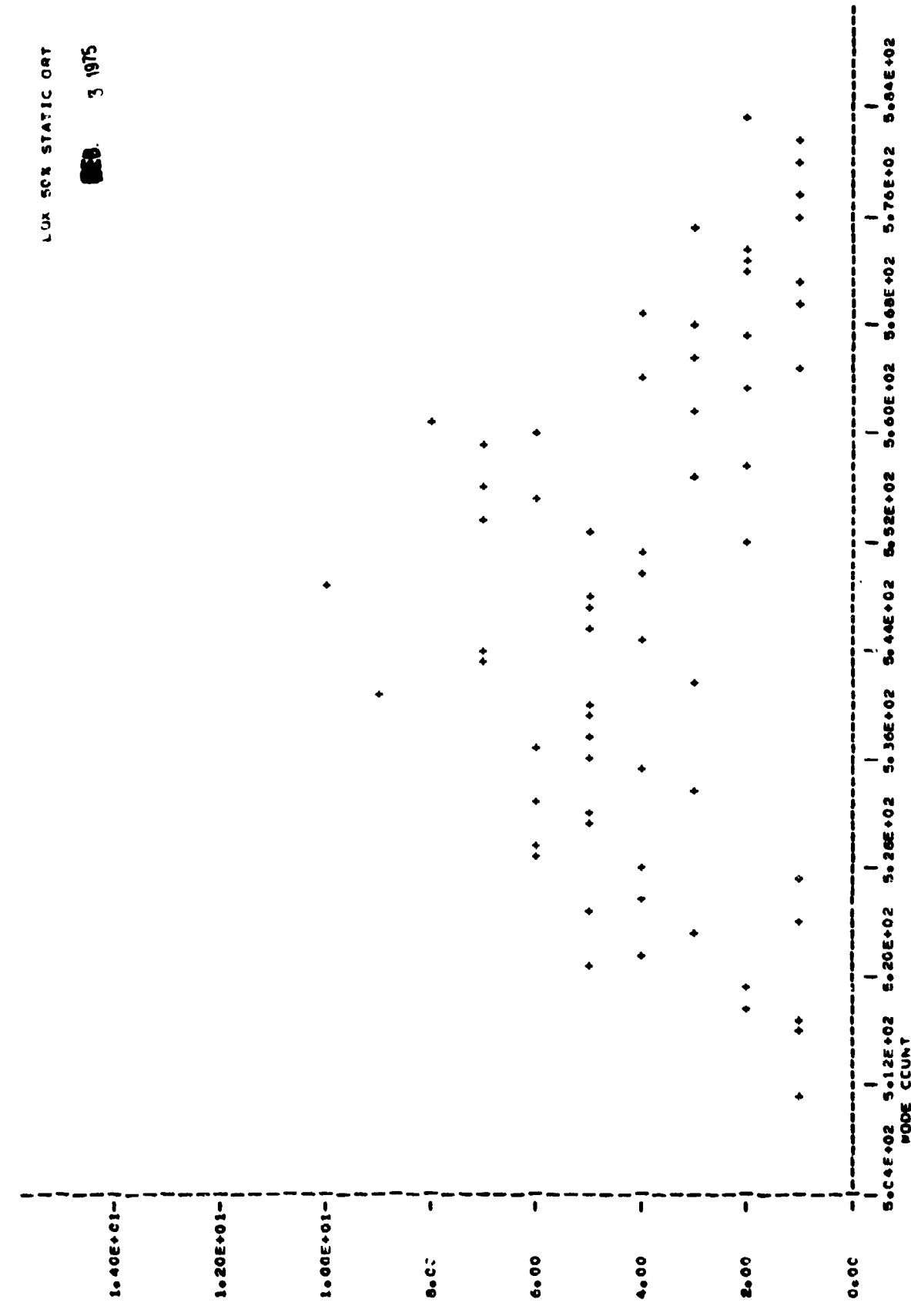
8.0E+02  
5.0E+02  
3.0E+02  
1.0E+02  
0.0E+02

MODE COUNT

FREQUENCY

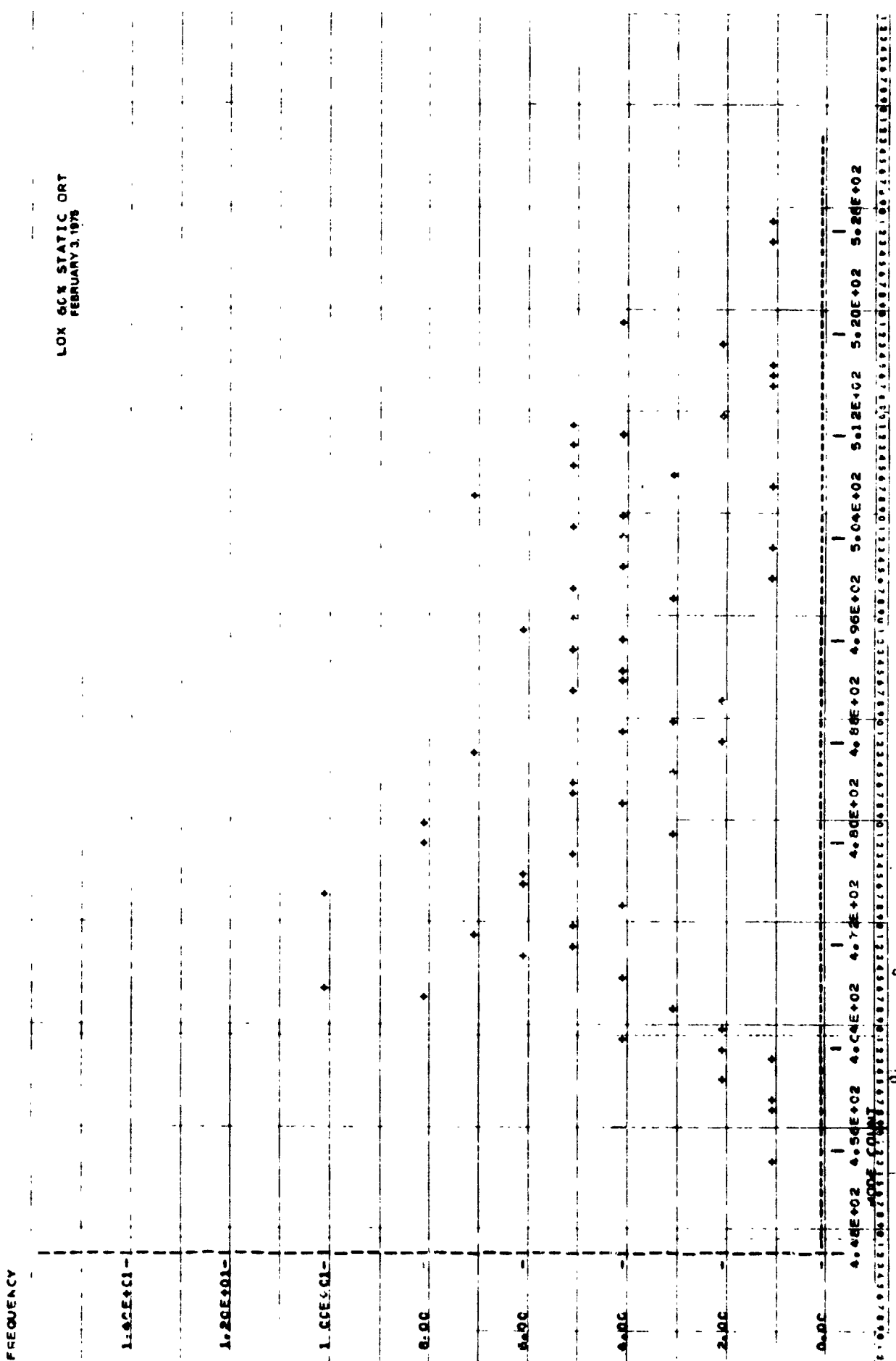
LUX SEC STATIC ORT

3 1975



B-31

332



LOG ECEG-1 vs FREQUENCY

FREQUENCY

LOG TCX STATIC CPT

FEB 3 1975

1.4CE+01-

1.2CE+C1-

1.0CE+01-

9.0C

6.0C

4.0C

2.00

0.0C

MOLE COUNT

4.10E+02 4.20E+02 4.30E+02 4.40E+02 4.50E+02 4.60E+02 4.70E+02 4.80E+02 4.90E+02 5.00E+02 5.10E+02

B-33

FREQUENCY

LOX BOX STATIC ORT  
FEBRUARY 3, 1975

1.40E+01

1.20E+01

1.00E+01

6.00

4.00

2.00

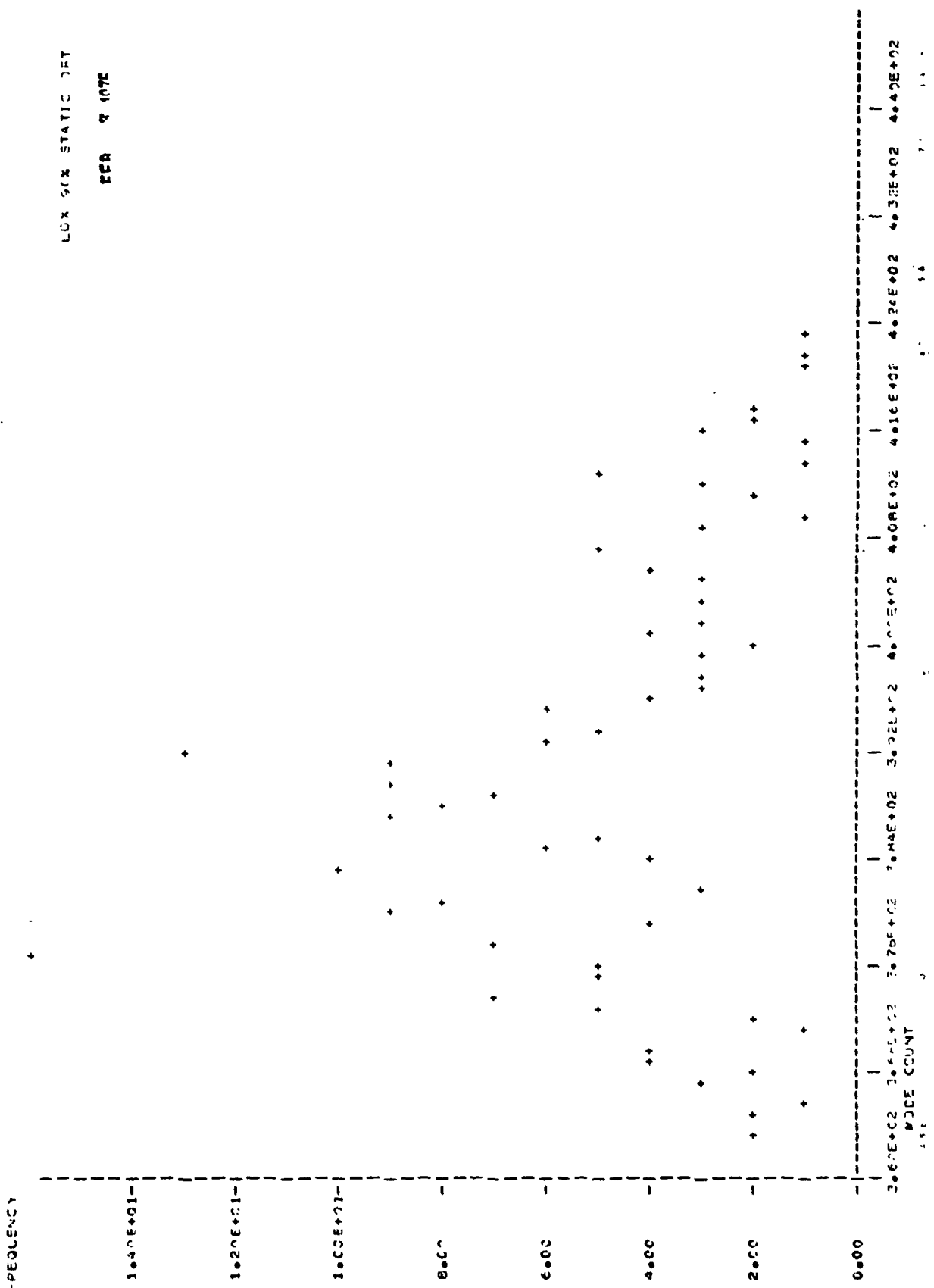
0.00

3.00E+02 3.90E+02 4.00E+02 4.10E+02 4.20E+02 4.30E+02 4.40E+02 4.50E+02 4.60E+02 4.70E+02 4.80E+02

MODE COUNT

23

B-34



FREQUENCY

LOX 55% STATIC DRT

FFR 3 1975

1.44E+01

1.20E+01

1.00E+01

8.00

6.00

4.00

2.00

0.00

3.36E+02 3.44E+02 3.52F+02 3.62E+02 3.68E+02 3.76E+02 3.84E+02 3.92E+02 4.00E+02 4.08E+02 4.16E+02  
NODE COUNT

B-36

WCD E CT

LIX CX STATIC COLD

1.89E+07-

1.8BF+C3-

1.87E+C3-

1.86E+07-

1.85E+07-

1.84E+07-

1.83E+C3-

1.82E+C2-

1.81E+C2-

1.80E+C2-

MODE CT

L0X \*\* STATIC DR

FEB 3 1975

1.35E+02-  
1.36E+03-  
1.37E+03-  
1.36E+03-  
1.35E+03-  
1.34E+03-  
1.33E+03-  
1.32E+03-  
-1.6CE+02 -1.20E+E2 -8.0CF+C1 -4.0NE+C1 0.0C  
4.00E+01 E.0CE+C1 1.2CE+C2 1.60E+02 2.00E+02  
CR IDENTATION  
B-38

四

四百三

LOX 20X STATIC OF T  
FEBRUARY 3, 1975

四庫全書

90 CEE & CEE

E. 555 + 23 -

一〇四

पृष्ठा ३८८

一

四百一十一

8.00E+02 -1.00E+02 -1.00E+02 -1.00E+01 -4.00E+01 0.00 4.00E+01 8.00E+01 1.020E+02 1.60F+02 2.00F+02

CODE C7

LOX TCC STARTUP TEST

FFB 3 1975

7.02EF+02-

7.02CE+02-

7.012F+02-

7.01AF+02-

6.96EF+02-

6.88FE+02-

6.72F+02-

ORIENTATION

B41

-2.00E+02 -1.60E+02 -1.20E+02 -8.00E+01 -4.00E+01 0.00

4.00F+01 8.00E+01 1.02CE+02 1.6CF+02 2.0CE+02

1.02CE+02 1.6CF+02 2.0CE+02

WIND C7

LOX 4-4 START -

FFR 2 1975

7.00E+02 -

6.00E+02 -

6.00E+02 -

6.00E+02 -

6.00E+02 -

6.00E+02 -

6.00E+02 -

5.00E+02 -  
-2.00E+02 -1.00E+02 -8.00E+01 -4.00E+01 corr  
1.00E+01 2.00E+01 1.00E+02 1.60E+02 2.00E+02

ORIENTATION

B-42

NAME: C\*

LINX CCRX STATIC MAT

S<sub>0</sub> RCF+C2-

S<sub>0</sub> TCF+C2-

S<sub>0</sub> SRF+C2-

S<sub>0</sub> CCE+C2-

S<sub>0</sub> 3CF+C2-

S<sub>0</sub> 2CF+C2-

S<sub>0</sub> 1CF+C2-

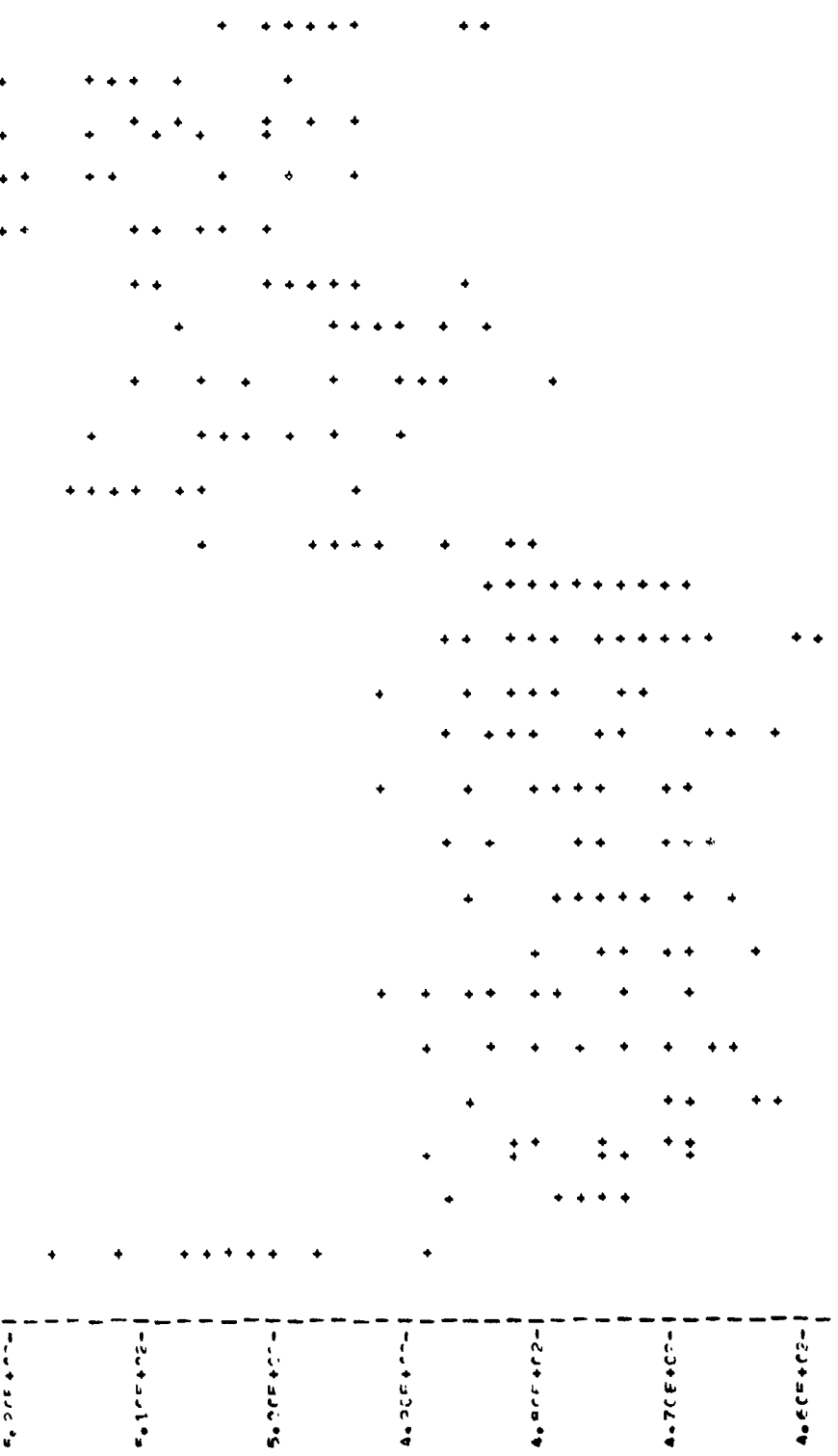
-2.0CF+C2 -1.6CF+C2 -1.2CF+C2 -8.20F+91 -4.00E+21 3.0F  
DEFINITION

B-43

4EB

L9X+6CX STATIC FFT  
FEBRUARY 3, 1976

WME RT



## LOX 7CX STATIC OPT

3.675

WCODE CT

5.00E+02-

5.20E+02-

5.00E+02-

4.80E+02-

4.60E+02-

4.40E+02-

4.20E+02-

4.00E+02  
 $-2.00E+02 -1.60E+02 -1.20E+02 -8.00E+01 -4.00E+01 0.00$   
 ORIENTATION

B45

LOX BOX STATIC ORT  
FEBRUARY 3, 1975

MODE CRT

5.2E+02-

5. CCE+C2-

4. BCF+C2-

4. BCF+C2-

4. CCF+C2-

4. CCE+C2-

4. CCE+C2-

3. BCF+C2-  
-2.00E+02 -1.60E+02 -1.20E+02 -8.00E+02 -4.00E+01 0.00  
ORIENTATION

B-46

MODE C7

+ LOX 90x STATIC ORT

FEB 3 1975

4.16E+02-

4.0RE+02-

0CE+02-

3.92E+02-

3.84E+02-

3.76E+02-

3.68E+02-

3.60E+02-  
-2.0E+02 -1.60E+02  
-1.20E+02 -8.00E+01  
-4.00E+01 0.0C  
4.00E+01 8.00E+01  
1.20E+02 1.60E+02  
2.00E+02  
ORIENTATION  
7.9

B-47

MODERATOR

LOG AND STATIC DATA

FFA 2 1975